University of Technology Sydney
Faculty of Engineering and Information Technology
School of Electrical and Data Engineering

Enabling Secure and Reliable Wireless Services With Intelligent Reflecting Surfaces

Monir Abughalwa

A Thesis Submitted
in Fulfillment of the
Requirements for the Degree

Doctor of Philosophy

under the supervision of

A/Prof. Diep N. Nguyen
A/Prof. Dinh Thai Hoang
Prof. Eryk Dutkiewicz

Sydney, Australia

August 2025

CERTIFICATE OF ORIGINAL AUTHORSHIP

I, MONIR ABUGHALWA declare that this thesis, is submitted in fulfillment of the requirements for the award of DOCTOR OF PHILOSOPHY, in the Faculty of Engineering and Information Technology at the University of Technology Sydney.

This thesis is wholly my own work unless otherwise referenced or acknowledged. In addition, I certify that all information sources and literature used are indicated in the thesis.

This document has not been submitted for qualifications at any other academic institution.

This research was supported by an Australian Government Research Training Program (RTP) Scholarship doi.org/10.82133/C42F-K220.

Signature: Production Note: Signature removed prior to publication.

Date: 06/01/2026

ABSTRACT

Enabling Secure and Reliable Wireless Services With Intelligent Reflecting Surfaces

by

Monir Abughalwa

The forthcoming sixth-generation (6G) mobile networks are expected to deliver ultra-fast, low-latency, and highly reliable connectivity, supporting applications in smart cities, healthcare, transportation, and industry. However, 6G systems face major challenges, including extremely low latency, high reliability, and security requirements. Intelligent reflecting surfaces (IRS) have emerged as a promising technology to improve user data rates and secrecy by enhancing the received signal of legitimate users while limiting eavesdroppers' interception. This thesis investigates IRS-assisted secure communication through joint optimization of the transmitter beamforming vector and the IRS programmable reflecting elements (PREs), considering practical constraints such as low-resolution IRS, imperfect channel state information (CSI), and different eavesdropper CSI assumptions (perfect, imperfect, or unknown).

First, we study data rate maximization in a downlink IRS-aided system under the finite blocklength regime (FBR), where a base station serves multiple single-antenna users. Since achievable rates in the FBR are intricate functions of beamforming and IRS phase shifts, we propose a joint optimization framework that maximizes the geometric mean of user rates. A computationally efficient algorithm based on closed-form approximations is developed, and simulations confirm its effectiveness.

Second, we address users' secrecy in long blocklength (LBR) IRS-aided systems with low-resolution IRS. The objective is to maximize the minimum secrecy rate among *all users* under different CSI conditions. The resulting nonconvex problem is

tackled by linearizing its objective function and then decomposing it into a series of tractable subproblems. For imperfect CSI, we use the successive convex approximation (SCA) method, and $\mathcal{S}$-procedure to tackle the problem. Extensive simulations under practical settings validate the efficacy of the proposed framework.

Finally, we extend the study to users' secrecy in FBR-IRS-aided systems, where enhancing users' secrecy is more challenging due to latency and reliability FBR constraints. We formulate problems to maximize both the minimum and sum secrecy rates while satisfying FBR constraints, by jointly optimizing the beamform and the IRS PREs. We address the nonconvex problems using linearization and the SCA technique. Extensive simulations under practical conditions demonstrate that, when it is feasible, the proposed framework can reliably ensure secure communications for *all users* under FBR constraints.

In conclusion, this thesis develops robust and scalable optimization frameworks for data rate maximization and secrecy provisioning in IRS-aided 6G networks under both LBR and FBR regimes. The proposed methods provide scalable solutions to practical settings with large IRSs, enabling secure, reliable, and high-rate communication in future 6G systems.

Dedication

To my parents, my wife, my sons, my daughter, my brothers and sisters, and my whole family.

Acknowledgements

First and foremost, I would like to express my sincere gratitude to my supervisors, A/Prof. Diep N. Nguyen, A/Prof. Dinh Thai Hoang, and Prof. Eryk Dutkiewicz for all the guidance, encouragement, and enduring patience. All my supervisors have taught me a lot on both the scientific and personal sides of the research journey. Their guidance and support go far beyond this thesis, and I have been greatly fortunate to be supervised by them. I would also like to express my sincere gratitude to Prof. Hoang D. Tuan for his invaluable guidance and support at the early stages of this work, which laid a strong foundation for the development of this thesis.

Furthermore, many thanks to all the staff from the School of Electrical and Data Engineering, Faculty of Engineering and Information Technology, University of Technology Sydney (UTS), and UTS Library for the various forms of help they gave me. Special thanks to UTS for giving me the rare opportunity to study at this prestigious university in Australia, and the Australian Government Research Training Program Scholarship.

To my homeland, Palestine, for instilling in me the spirit of resilience, motivation, and inspiring my journey. And to my second home, Australia, for providing the opportunity and support to pursue and complete my degree.

Last but most importantly, my deepest gratitude, love, and respect are offered to my whole family, who have been supporting me through all difficult times during this long journey. Without their infinite love, inspiration, and patience, this work could never have been accomplished.

Contents

List of Publications

Journal Papers

J-1. **M. Abughalwa**, H. D. Tuan, D. N. Nguyen, H. V. Poor and L. Hanzo, "Finite-Blocklength RIS-Aided Transmit Beamforming," in IEEE Transactions on Vehicular Technology, vol. 71, no. 11, pp. 12374-12379, Nov. 2022, doi: 10.1109/TVT.2022.3193443. `https://ieeexplore.ieee.org/document/9839546`. (Corresponding to Chapter 2).

J-2. **M. Abughalwa**, D. N. Nguyen, Dinh Thai Hoang, Thang X. Vu, Eryk Dutkiewicz, and Symeon Chatzinotas, Secure Communications for All Users in Low-Resolution IRS-aided Systems Under Imperfect and Unknown CSI. Submitted to *IEEE Transactions on Cognitive Communications and Networking, under review.* `https://arxiv.org/abs/2504.05048`. (Corresponding to Chapter 3).

J-3. **M. Abughalwa**, D. N. Nguyen, Dinh Thai Hoang, Dinh Thai Hoang, Van-Dinh Nguyen, Ming Zeng, Quoc-Viet Pham, and Eryk Dutkiewicz. "Security for Everyone" in Finite Blocklength IRS-aided Systems With Perfect and Imperfect CSI. Submitted to *IEEE Transactions on Wireless Communications*, under review. `https://arxiv.org/abs/2504.05067`. (Corresponding to Chapter 4).

J-4. **M. Abughalwa**, Nguyen Van Huynh, D. N. Nguyen, Dinh Thai Hoang, and Eryk Dutkiewicz, Secrecy Sum-Rate Maximization in Finite Blocklength IRS-aided Systems With Perfect and Imperfect CSI, under revision for *IEEE Internet of Things Journal.* (Corresponding to Chapter 5).

Conference Papers

J-1. **M. Abughalwa**, D. N. Nguyen, D. T. Hoang and E. Dutkiewicz, "Multi-User Secrecy Rate Maximization in IRS-aided Systems," IEEE Global Communications Conference (GLOBECOM 2024), Cape Town, South Africa, 2024, pp. 2491-2496, doi: 10.1109/GLOBECOM52923.2024.10901599. `https://ieeexplore.ieee.org/document/10901599`. (Corresponding to Chapter 3)

J-2. **M. Abughalwa**, D. N. Nguyen, Dinh Thai Hoang, and Eryk Dutkiewicz, "Multi-user Secrecy Rate Maximization in Finite Blocklength IRS-aided Systems." Accepted by IEEE Global Communications Conference (GLOBECOM 2025), Taipei, Taiwan. (Corresponding to Chapters 4 & 5).

List of Figures

List of Tables

Abbreviation

6G	The sixth generation technology standard for cellular networks
AN	Artificial Noise
AWGN	Additive White Gaussian Noise
BER	Bit Error Rate
BS	Base Station
CPS	Continuous Phase Shift
CSI	Channel State Information
DPS	Discrete Phase Shift
FBL	Finite Blocklength
FBR	Finite Blocklength Regime
ICSI	Imperfect Channel State Information
IEEE	Institute of Electrical and Electronics Engineers
IRS	Intelligent Reflecting Surface
KKT	Karush-Kuhn-Tucker
LBL	Long Blocklength
LBR	Long Blocklength Regime
LMI	Linear Matrix Inequality
LTE	Long-Term Evolution
MEC	Multi-Access Edge Computing
MIMO	Multiple Input Multiple Output
MISO	Multiple Input Single Output
MMSE	Minimum Mean Square Error
mMTC	Massive Machine Type Communication
MSE	Mean Square Error
OFDM	Orthogonal Frequency Division Multiplexing

OFDMA	Orthogonal Frequency Division Multiple Access
PCCP	Penalty Convex-Concave Procedure
PLS	Physical Layer Security
PRE	Passive Reflective Element
PSE	Phase Shift Error
QPSE	Quantized Phase Shift Error
RCG	Riemannian Conjugate Gradient
RIS	Reconfigurable Intelligent Surface
SCA	Successive Convex Approximation
SDP	Semidefinite Programming
SDR	Semidefinite Relaxation
SINR	Signal-to-Interference-plus-Noise Ratio
SNR	Signal-to-Noise Ratio
SSR	Secrecy Sum Rate
UE	User Equipment
UMC	Unit Modules Constraint
URLLC	Ultra-Reliable Low-Latency Communication
WSSR	Weighted Sum Secrecy Rate

List of Symbols by Chapter

Chapter 2: Finite-Blocklength IRS-Aided Transmit Beamforming

Symbol	Definition
M	Number of base-station antennas.
K	Number of single-antenna users.
N	Number of IRS reflecting elements.
$\tilde{H}_{\text{B-R}}$	BS-to-IRS channel.
$\tilde{h}_{\text{R-}k}$	IRS-to-user k channel.
$\beta_{\text{B-R}}$	Large-scale fading of BS-to-IRS link.
$\beta_{\text{R-}k}$	Large-scale fading of IRS-to-user k link.
$H_{\text{B-R}}$	BS-to-IRS channel (small-scale).
$h_{\text{R-}k}$	IRS-to-user k channel (small-scale).
s_k	Information symbol for user k.
$\mathbf{w}_k$	Beamforming vector for user k.
x	Transmit signal at BS.
y_k	Received signal at user k.
$\mathcal{H}_k$	Effective channel for user k.
n_k	Noise at user k.
$\mathcal{R}_{\text{R-}k}$	IRS spatial correlation matrix for user k.
$\boldsymbol{\theta}$	IRS phase-shift vector.
$\boldsymbol{H}_{k,n}$	Channel contribution from IRS element n.
$\tilde{h}_{\text{BR-}k}$	Composite BS–IRS–user k channel.
$\mathbf{w}$	Beamforming vectors for all users.
$g_k(\mathbf{w}, \boldsymbol{\theta})$	SINR at user k.
$\alpha_k(\mathbf{w}, \boldsymbol{\theta})$	Interference-plus-noise power at user k.
$r_k(\mathbf{w}, \boldsymbol{\theta})$	Achievable rate at user k (LBL regime).

Symbol	Definition
$\mathcal{B}$	Communication bandwidth.
$\hat{r}_k(\mathbf{w}, \boldsymbol{\theta})$	URLLC achievable rate for user k.
a	Finite blocklength penalty coefficient.
$\upsilon_k(\mathbf{w}, \boldsymbol{\theta})$	Channel dispersion for user k.
$\beta_k(\mathbf{w}, \boldsymbol{\theta})$	Total received power plus noise at user k.
t_t	Transmission duration.
ϵ^c	Decoding error probability for URLLC.
$\hat{f}(\mathbf{w}, \boldsymbol{\theta})$	Geometric-mean URLLC rate objective.
$f(\mathbf{w}, \boldsymbol{\theta})$	Geometric-mean LBL rate objective.
P	Transmit power budget.
$\bar{r}$	Minimum target rate.
σ^2	Noise power.

Chapter 3: Secure Communications For All Users in Low-Resolution IRS-Aided Systems Under Imperfect and Unknown CSI

Symbol	Definition
M	Number of transmit antennas at Alice.
K	Number of legitimate users.
k	Legitimate user index.
e	Eavesdropper index.
N	Number of IRS reflecting elements.
s_k	Confidential message for user k.
$\mathbf{w}_k$	Beamforming vector for user k.
$\boldsymbol{\theta}$	IRS phase-shift vector.
y_i	Received signal at node i.
$\boldsymbol{h}_i(\boldsymbol{\theta})$	Cascaded channel from Alice to i.
n_i	Noise at node i.
σ_i^2	Noise power at node i.

Symbol	**Definition**
$\boldsymbol{h}_{A_i}$	Direct Alice-to-i channel.
$\tilde{\boldsymbol{h}}_{A_i}$	Small-scale fading of Alice-to-i channel.
β_{A_i}	Large-scale fading of Alice-to-i link.
$\boldsymbol{H}_{\mathrm{AR}}$	Alice-to-IRS channel matrix.
$\tilde{\boldsymbol{H}}_{\mathrm{AR}}$	Small-scale fading of Alice-to-IRS channel.
β_{AR}	Large-scale fading of Alice-to-IRS link.
$\boldsymbol{g}_i$	IRS-to-i channel.
$\tilde{\boldsymbol{g}}_i$	Small-scale fading of IRS-to-i channel.
$\beta_{\mathrm{R}i}$	Large-scale fading of IRS-to-i link.
$\mathcal{R}_{\mathrm{R}i}$	IRS spatial correlation matrix for link to i.
$\boldsymbol{\Phi}$	IRS phase-shift diagonal matrix.
$\widehat{\boldsymbol{g}}_i$	Estimated IRS-to-i channel.
$\Delta\boldsymbol{g}_i$	Channel estimation error.
ξ_i	Radius of channel uncertainty region.
$\widehat{\boldsymbol{h}}_i(\boldsymbol{\theta})$	Cascaded channel under imperfect CSI.
$\gamma_i(\mathbf{w},\boldsymbol{\theta})$	SINR at node i.
$\widehat{\gamma}_i(\mathbf{w},\boldsymbol{\theta})$	SINR at node i under imperfect CSI.
$\rho_i(\mathbf{w},\boldsymbol{\theta})$	Interference-plus-noise power at node i.
$\widehat{\rho}_i(\mathbf{w},\boldsymbol{\theta})$	Interference-plus-noise power under imperfect CSI.
b	Number of IRS quantisation bits.
ϵ_R	IRS phase-shift error.
$\mathrm{SR}_k(\mathbf{w},\boldsymbol{\theta})$	Secrecy rate of user k.
$\widehat{\mathrm{SR}}_k(\mathbf{w},\boldsymbol{\theta})$	Secrecy rate of user k under imperfect CSI.
$C_i(\mathbf{w},\boldsymbol{\theta})$	Achievable rate at node i.
$\widehat{C}_i(\mathbf{w},\boldsymbol{\theta})$	Achievable rate at node i under imperfect CSI.
P_T	Transmit power budget.
σ_k^2	Noise power at user k.
$\gamma_e(\mathbf{w},\boldsymbol{\theta})$	SINR at Eve.
σ_e^2	Noise power at Eve.

Symbol	**Definition**
$C_e(\mathbf{w}, \boldsymbol{\theta})$	Eavesdropping rate at Eve.
$\mathrm{SR}_k(\mathbf{w}, \boldsymbol{\theta})$	Secrecy rate of user k.
$\widehat{\mathrm{SR}}_k(\mathbf{w}, \boldsymbol{\theta})$	Secrecy rate of user k under imperfect CSI.
ξ_i	Radius of channel uncertainty region.
φ_k	Minimum data rate of user k.
μ_{k_e}	Maximum eavesdropping rate of Eve.
z	Lower bound of secrecy rate.
β_k	Interference-plus-noise power at user k.
$\mathbf{W}_{-k}$	Beamforming vectors excluding user k.
$\boldsymbol{u}_k$	Channel vector for user k.
$\mathbf{X}_k$	Linearised matrix for cascaded channel.
P_{tot}	Total transmit power.
P_T	Transmit power allocated to information signals.
P_J	Transmit power allocated to artificial noise.
$\widehat{\boldsymbol{h}}_e(\boldsymbol{\theta})$	Cascaded channel to Eve under imperfect CSI.
$\widehat{\rho}_e$	Interference-plus-noise power at Eve under imperfect CSI.
$\gamma_e(\mathbf{w}, \boldsymbol{\theta})$	SINR at Eve.
$\gamma_k(\mathbf{w}, \boldsymbol{\theta})$	SINR at user k.
γ	QoS threshold for user k.

Chapter 4: "Security for Everyone" in Finite Blocklength IRS-aided Systems With Perfect and Imperfect CSI

Symbol	**Definition**
N	Number of BS transmit antennas (Alice).
K	Number of legitimate users.
k	Legitimate user index.
e	Eavesdropper index.

Symbol	**Definition**
M	Number of IRS reflecting elements.
s_k	Confidential message for user k.
g_i	Received signal at node i.
$\boldsymbol{h}_i(\boldsymbol{\theta})$	Cascaded Alice–IRS–i channel.
$\mathbf{w}_k$	Beamforming vector for user k.
$\boldsymbol{\theta}$	IRS phase-shift vector.
$\bar{n}_i$	Noise at node i.
σ_i	Noise power at node i.
$\boldsymbol{L}_{\mathrm{AR}}$	Alice-to-IRS channel matrix.
$\tilde{\boldsymbol{L}}_{\mathrm{AR}}$	Small-scale fading of Alice-to-IRS channel.
$\aleph_{\mathrm{AR}}$	Large-scale fading of Alice-to-IRS link.
$\boldsymbol{l}_i$	IRS-to-i channel.
$\tilde{\boldsymbol{l}}_i$	Small-scale fading of IRS-to-i channel.
$\aleph_{\mathrm{R}i}$	Large-scale fading of IRS-to-i link.
$\mathcal{R}_{\mathrm{R}i}$	IRS spatial correlation matrix for link to i.
$\boldsymbol{\Phi}$	IRS phase-shift diagonal matrix.
$\widehat{\boldsymbol{l}}_i$	Estimated IRS-to-i channel.
$\Delta\boldsymbol{l}_i$	IRS-to-i channel estimation error.
Ω_i	Radius of channel uncertainty region.
$\widehat{\boldsymbol{h}}_i(\boldsymbol{\theta})$	Cascaded channel under imperfect CSI.
$\gamma_i(\mathbf{w},\boldsymbol{\theta})$	SINR at node i.
$\widehat{\gamma}_i(\mathbf{w},\boldsymbol{\theta})$	SINR at node i under imperfect CSI.
ρ_i	Interference-plus-noise power at node i.
$\widehat{\rho}_i$	Interference-plus-noise power under imperfect CSI.
$\mathcal{S}_k^{\mathcal{F}}(\mathbf{w},\boldsymbol{\theta})$	Secrecy rate of user k in FBR regime.
$\widehat{\mathcal{S}}_k^{\mathcal{F}}(\mathbf{w},\boldsymbol{\theta})$	Secrecy rate of user k in FBR under imperfect CSI.
$C_i(\mathbf{w},\boldsymbol{\theta})$	Achievable rate at node i.
$\widehat{C}_i(\mathbf{w},\boldsymbol{\theta})$	Achievable rate at node i under imperfect CSI.
ξ_i	Rate penalty factor due to finite blocklength.

Symbol	**Definition**
N_t	Packet length.
$\mathcal{B}$	Communication bandwidth.
t_t	Transmission duration.
τ_k	Decoding error probability at user k.
τ_e	Information leakage probability at Eve.
$V_i(\mathbf{w}, \boldsymbol{\theta})$	Dispersion factor at node i.
$\widehat{V}_i(\mathbf{w}, \boldsymbol{\theta})$	Dispersion factor at node i under imperfect CSI.
υ_i	Total received power plus noise at node i.
$\widehat{\upsilon}_i$	Total received power plus noise under imperfect CSI.
$\mathcal{S}_k^{\mathcal{L}}(\mathbf{w}, \boldsymbol{\theta})$	Secrecy rate of user k in LBR regime.
$\widehat{\mathcal{S}}_k^{\mathcal{L}}(\mathbf{w}, \boldsymbol{\theta})$	Secrecy rate of user k in LBR under imperfect CSI.
P	Transmit power budget.
$\tau_{\max}$	Maximum decoding error probability in FBR.
$\tau_{e_{\max}}$	Maximum information leakage in FBR.
$t_{\max}$	Maximum transmission duration in FBR.
$\widetilde{\mathcal{S}}_k^{\mathcal{F}}(\mathbf{w}, \boldsymbol{\theta})$	Surrogate FBR secrecy rate for user k.
$\mathcal{Z}$	Lower bound of the FBR secrecy rate under imperfect CSI.
β_k	Minimum achievable rate for user k under imperfect CSI.
Υ_{k_e}	Maximum eavesdropping rate of Eve under imperfect CSI.
$\tilde{\beta}_i$	Maximum dispersion penalty for node i.
α_k	Interference-plus-noise power at user k under imperfect CSI.
α_{ke}	Interference-plus-noise power at Eve.
$\mathbf{A}_k$	Linearised matrix for the cascaded channel at user k.
d_k	Quadratic term evaluated at the estimated channel for user k.
$\mathfrak{Y}$	Scaling factor for dispersion term.

Symbol	Definition
ζ_k	Interference-plus-noise power for dispersion at user k.
$\tilde{\beta}_i$	Maximum dispersion penalty for node i.

Chapter 5: Secrecy Sum-Rate Maximisation in Finite Blocklength IRS-Aided Systems With Perfect and Imperfect CSI

Symbol	Definition
M	Number of antennas at Alice.
N	Number of IRS reflecting elements.
K	Number of legitimate URLLC users.
e	Eavesdropper index.
$\boldsymbol{G}_{\text{AR}}$	Alice-to-IRS channel matrix.
β_{AR}	Large-scale fading of Alice-to-IRS link.
$\tilde{\boldsymbol{G}}_{\text{AR}}$	Small-scale fading of Alice-to-IRS link.
$\boldsymbol{u}_i$	IRS-to-i channel vector.
$\beta_{\text{R}i}$	Large-scale fading of IRS-to-i link.
$\tilde{\boldsymbol{u}}_i$	Small-scale fading of IRS-to-i link.
$\mathcal{R}_{\text{R}i}$	IRS spatial correlation matrix for link to i.
s_k	Confidential symbol for user k.
y_i	Received signal at node i.
$\boldsymbol{h}_i(\boldsymbol{\theta})$	Cascaded channel from Alice to i.
$\mathbf{w}_k$	Beamforming vector for user k.
$\boldsymbol{\theta}$	IRS phase-shift vector.
n_i	Noise at node i.
σ_i^2	Noise power at node i.
$\boldsymbol{\Phi}$	IRS diagonal phase-shift matrix.
$\widehat{\boldsymbol{u}}_i$	Estimated IRS-to-i channel.
$\Delta\boldsymbol{u}_i$	IRS-to-i channel estimation error.
Ω_i	Radius of channel uncertainty region.

Symbol	**Definition**
$\widehat{\boldsymbol{h}}_i(\boldsymbol{\theta})$	Estimated cascaded channel under imperfect CSI.
$\gamma_i(\mathbf{w}, \boldsymbol{\theta})$	SINR at node i.
$\widehat{\gamma}_i(\mathbf{w}, \boldsymbol{\theta})$	SINR at node i under imperfect CSI.
ρ_i	Interference-plus-noise power at node i.
$\widehat{\rho}_i$	Interference-plus-noise power under imperfect CSI.
$\mathcal{S}_k^{\mathcal{F}}(\mathbf{w}, \boldsymbol{\theta})$	FBR secrecy rate of user k.
$\widehat{\mathcal{S}}_k^{\mathcal{F}}(\mathbf{w}, \boldsymbol{\theta})$	FBR secrecy rate under imperfect CSI.
$C_i(\mathbf{w}, \boldsymbol{\theta})$	Achievable rate at node i.
$\widehat{C}_i(\mathbf{w}, \boldsymbol{\theta})$	Achievable rate at node i under imperfect CSI.
ξ_i	Reliability parameter for node i.
N_t	URLLC packet length.
$\mathcal{B}$	Communication bandwidth.
t_t	Transmission duration.
$V_i(\mathbf{w}, \boldsymbol{\theta})$	Dispersion factor at node i.
$\widehat{V}_i(\mathbf{w}, \boldsymbol{\theta})$	Dispersion factor under imperfect CSI.
υ_i	Total received power at node i.
$\widehat{\upsilon}_i$	Total received power under imperfect CSI.
ς_k	Decoding error probability at user k.
ς_e	Information leakage probability at Eve.
$\varsigma_{\max}$	Maximum allowable decoding error probability.
$\varsigma_{e_{\max}}$	Maximum tolerated leakage probability.
t_t	Transmission duration.
$t_{\max}$	Maximum permitted transmission duration.
$R_s(\mathbf{w}, \boldsymbol{\theta})$	Secrecy sum-rate under FBR.
P	Total power budget at Alice.
$\mathcal{S}_k^{\mathcal{L}}(\mathbf{w}, \boldsymbol{\theta})$	Secrecy rate of user k in LBR regime.
$\widehat{\mathcal{S}}_k^{\mathcal{L}}(\mathbf{w}, \boldsymbol{\theta})$	Secrecy rate of user k in LBR under imperfect CSI.
$\widetilde{\mathcal{S}}_k^{\mathcal{F}}(\mathbf{w}, \boldsymbol{\theta})$	Lower bound approximation of FBR secrecy rate for user k.

Symbol	**Definition**
θ_n	Phase shift of IRS element n.
$\widehat{R}_s(\mathbf{w}, \boldsymbol{\theta})$	Secrecy sum-rate under imperfect CSI.
z	Lower bound on FBR secrecy sum-rate.
φ_k	Minimum achievable rate for user k.
μ_{k_e}	Maximum eavesdropping rate of Eve.
$\tilde{\varphi}_i$	Maximum dispersion factor for node i.
ξ_i	Radius of CSI uncertainty region for node i.
β_k	Interference-plus-noise power at user k.
β_{ke}	Interference-plus-noise power at Eve.
$\mathfrak{L}$	Constant term for dispersion factor linearisation.
$\mathfrak{Y}$	Scaling term for dispersion factor linearisation.
ζ_k	Interference-plus-noise term for dispersion at user k.

Chapter 1

Introduction and Literature Review

This chapter* provides a comprehensive overview of the future 6G network applications, with a particular emphasis on the applications of Intelligent Reflecting Surfaces (IRSs) and their role in enhancing users data rate and Physical Layer Security (PLS). It then discusses the latest development of this paradigm. The research objectives and major contributions are presented in the following section. Finally, the chapter concludes with an overview of the thesis structure.

1.1 Background

1.1.1 Enabling the Future: Applications and Advancements of 6G Networks

The 6G of wireless communication is anticipated to redefine the landscape of digital connectivity by offering enhanced capabilities far beyond those of 5G. With expected features such as high data rates, massive device connectivity, and integrated intelligence, 6G is poised to support a wide range of emerging applications, including extended reality, holographic telepresence, autonomous systems, and large-scale Internet of Things (IoT) deployments. To realise these ambitions, 6G networks will integrate a host of enabling technologies, such as terahertz (THz) communication, intelligent reflecting surfaces (IRS), reconfigurable holographic surfaces, and AI-native network design [1, 2]. In this context, the design of efficient, reliable,

*This chapter partially corresponds to the journal papers J-1 to J-5 and the conference papers C-1 to C-1 in the list of Publications.

and secure communication strategies becomes critical, particularly in scenarios demanding ultra-reliable low-latency communication (URLLC) and massive machine-type communication (mMTC). The foundational standardisation of 6G networks began in early 2025, with commercial deployment projected by 2030 [3]. In [3], the authors presented a comprehensive overview of 6G networks and their developmental roadmap. 6G is expected to incorporate a range of cutting-edge technologies to accommodate the rapidly growing number of IoT devices, as stated before. These advancements position 6G as a highly intelligent and adaptive communication paradigm designed to enable seamless connectivity across diverse applications and environments. In [4], the authors highlighted the key technologies expected to evolve as part of 6G networks, which are anticipated to move beyond personalised communication and enable the comprehensive realisation of the IoT paradigm by interconnecting, not only individuals, but also computing infrastructures, vehicles, devices, sensors, and robotic agents. 6G networks are anticipated to significantly advance key communication paradigms, including enhanced mobile broadband (eMBB), mMTC, and URLLC. These technologies demand extremely high data rates, large bandwidth, and end-to-end latency, below 1 ms, to meet the requirements of future applications [5]. Such enhancements are expected to enable dense, low-latency, and highly reliable communication, thereby supporting large-scale deployments of both massive eMBB and massive URLLC services [6].

6G networks are expected to enhance communication in the finite blocklength regime (FBR), which is an enabler of URLLC and mMTC technologies. FBR has attracted paramount attention in recent years thanks to its potential applications in the IoT, with particular attention to holographic communications, the tactile Internet, autonomous driving, etc. Unlike long blocklength regime (LBR) systems, maintaining high reliability in FBR is more challenging due to reduced channel coding gains and stringent latency requirements [7]. Moreover, in applications such as

intelligent transportation, leakage of information may compromise user privacy by revealing sensitive data such as location or identity [8, 9]. In [9], the authors shed light on technologies and methods to support URLLC systems and their application. In [10], Wang *et. al.* studied the URLLC system's performance limits from the asymptotic cross-layer analysis point in a high signal-to-noise ratio (SNR) environment. They studied the system from the perspective of the service capability, latency, and error probability. They derived an equation to trade off between the latency and the error probability. However, the study did not cover the power allocation problem, and it only considered the high SNR situation, which is rare in wireless environments. Furthermore, other works have been focusing on reducing latency in URLLC systems [11–14]. In [14], Sach *et al.* addressed the functionality of two radio technology components, the Long-Term Evolution (LTE) and the new radio interface technology, to support URLLC services. The authors evaluated the spectral efficiency and showed that both systems can perform similarly in FBR. In [12], the authors studied a URLLC system when a shared channel is assigned to multiple users in Grant Free (GF) transmission. In this case, the packet collision could highly harm the GF transmission potential, and the authors analysed the system of an extensive urban macro network in uplink GF transmission. The study focused on K-Repetition and the proactive scheme in Hybrid Automatic Repeat Request, which is done by investigating the K-Repetition and the proactive scheme within the URLLC environment. They evaluated the system performance against the baseline GF transmission. The results show that the algorithm has better reliability than the GF systems. The authors in [15] studied the mmWave in the URLLC environment. They considered the spectrum to be shared between regular users and enhanced mobile broadband users (eMBB). They studied the problem of maximising the throughput of the eMBB users under the constraint of time transmission. The optimised problem was subdivided into three subproblems: power

allocation, resource matching, and user paring. The proposed solution has improved the system's performance. However, the solution complexity was high, and the mathematical tractability was difficult. A trade-off between latency and system reliability has been investigated thoroughly [9, 16–18]. In [19], the authors studied the bandwidth minimisation problem in a single-input-single-output (SISO) system under the URLLC's quality of service (QoS) constraint. To tackle the minimisation problem, they proposed a joint bandwidth allocation and packet-dropping policy. They also introduced a packet delivery technique to save bandwidth and gain the same QoS. The authors in [20] studied an algorithm to maximise energy efficiency under the constraint of latency reliability. The algorithm was based on configuring the bandwidth, the antenna constellation and power allocation.

While 6G promises significant advancements in communication capabilities, it also introduces new and complex security challenges across mMTC, and URLLC services. Security attacks, such as jamming, eavesdropping, and pilot contamination, can degrade the URLLC's signal quality, posing a high risk to 6G networks. For example, a malicious user/eavesdropper poses a high risk to URLLC and mMTC due to their ability to intercept the legitimate user's signal [6]. To tackle such challenges, physical layer security (PLS) has emerged as a promising solution to enhance users' security in mMTc/URLLC 6G networks. Unlike traditional encryption-based methods, PLS exploits the inherent characteristics of the wireless channel to ensure confidentiality, thereby aligning well with the latency and complexity constraints of mMTC and URLLC [6]. Furthermore, to improve reliability and secrecy in 6G networks, intelligent reflecting surfaces (IRSs) have gained paramount attention due to their ability to strategically control the direction of the signal towards the intended users. This IRS's capability can improve the users' signal while thwarting the eavesdropper's signal, hence improving the PLS of the mMTC/URLLC systems [21].

In summary, future 6G networks are envisioned to enable intelligent, adapt-

ive, and ultra-reliable wireless environments, where technologies such as IRS and communication under the FBR will play a crucial role. IRS offers programmable control over the wireless channel, improving coverage, energy efficiency, and signal quality, while FBR provides a practical framework for analysing performance under stringent latency and reliability constraints. However, these advancements also introduce new security challenges, particularly at the physical layer. Ensuring secure communication in dynamic and densely connected environments requires robust PLS mechanisms that can withstand eavesdropping and adversarial interference. The integration of IRS and FBR designs with PLS techniques will be essential to meet the confidentiality and resilience demands of future 6G applications.

1.1.2 Intelligent Reflecting Surfaces in 6G: Fundamentals and Emerging Applications

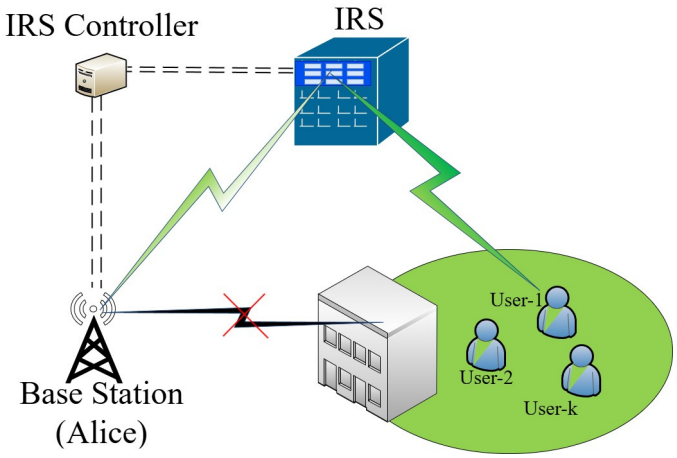

Figure 1.1 : 6G IRS-aided wireless communication system, in which a multi-antenna transmitter (Alice) communicates with a set of single-antenna users (Bob) via an IRS. The IRS is strategically deployed on the facade of a nearby building to enable indirect line-of-sight (LoS) communication between Alice and the users.

In recent years, IRS-aided wireless communication systems have attracted para-

mount attention due to their potential to support high data rate transmissions [22–26]. An IRS is typically composed of low-cost, programmable reflective elements (PREs) [26]. The effectiveness of these PREs has been substantially improved through recent advancements in real-time metasurface tuning, enabling the maximisation of spectral efficiency via optimal configuration [25, 27–29]. IRS technology enables dynamic reconfiguration of the wireless propagation environment by manipulating incident signals. Among its key applications are enhancements in user data rates, communication security, and privacy. These benefits are realised by intelligently steering reflected signals toward intended receivers while suppressing signal quality at unintended or malicious ones, thereby mitigating multi-user interference and safeguarding information confidentiality.

In general, an IRS mounted on the facade of a high-rise building can assist a base station in communicating with users, as illustrated in Fig. 1.1. Numerous studies have focused on enhancing wireless system performance by optimising the IRS PREs. In [30], the authors investigated a joint passive beamforming and the IRS's PRE optimisation problem to improve user rates in a multi-input single-output (MISO) IRS-aided downlink system. To address this problem, a semi-definite relaxation (SDR) technique was employed to obtain an upper-bound approximation of the objective function. Their findings highlight the benefits of incorporating IRS as a passive assistant in wireless networks. In [31], the authors analysed the impact of the number of IRS elements (N) on the received SNR, revealing that the SNR increases on the order of N^2, consistent with the results of [30]. Simulation results demonstrate that when hundreds or thousands of PREs are deployed, the resulting SNR approaches that of massive multi-input multi-output (MIMO) systems. The study in [32] also considered a MISO system, with the goal of maximising the achievable spectral efficiency through joint optimisation of the beamforming vector and IRS PREs. The authors addressed the resulting nonconvex problem using

manifold optimisation techniques and fixed-point iteration, effectively handling the IRS PREs' unit modulus constraint (UMC). In [33], the authors examined the use of multiple IRSs to enhance system performance. Similar to previous works, they jointly optimised the beamforming vector and IRS PREs to maximise both the coverage area and the system's SNR, leveraging the characteristics of millimetre wave (mmWave) propagation. The simulation results reaffirm that increasing the number of IRS elements leads to significant SNR improvements, aligning with earlier conclusions.

Research on MISO systems has been further extended to encompass MIMO configurations. In [34], the authors investigated an IRS-aided orthogonal frequency division multiplexing (OFDM)-MIMO system, aiming to maximise the system's capacity under the PREs' UMC, and the MIMO transmit covariance matrix. The results demonstrated that incorporating an IRS can significantly enhance system capacity. In the same study, the authors derived an upper bound for the ergodic capacity by optimising the IRS PRE matrix using Gaussian randomisation techniques. Ying et al. [35] examined a MIMO IRS-aided system in which the beamforming matrix and IRS phase shift matrix were optimised separately to achieve a lower bit error rate. In [36], the authors focused on maximising the data rate in a similar MIMO IRS-aided setup. They employed an alternating direction method to determine the phase shifts of individual reflecting elements, while the beamforming vector was obtained using a water-filling solution.

Most existing works on IRS systems assume a constant reflection amplitude and continuous phase shift (CPS). However, experimental results in [37] challenge these assumptions. The authors proposed a more realistic phase shift model that captures the inherent relationship between the phase shift and the amplitude of the IRS elements. Using this model, they studied the problem of maximising the data rate in a MISO system through joint optimisation of the beamforming vectors and IRS

PREs. Inspired by [37], the authors in [38] investigated the capacity degradation in MISO systems when employing discrete phase shift IRSs. Their results indicate that a 2-bit phase resolution is sufficient to achieve performance close to that of the CPS model. Similarly, [39] analysed the performance of an IRS-aided MISO downlink system. The authors derived a lower bound on the users' asymptotic rate under the assumptions of unknown CSI and quantised phase shifts. Their findings demonstrate that discrete phase shift configurations can achieve near-optimal performance compared to CPS models.

IRSs are generally classified into three categories: passive, active, and hybrid architectures, each presenting unique trade-offs between system performance and implementation complexity [40]. A passive IRS consists of passive PREs that adjust the phase of incident signals without performing amplification. This architecture is inherently energy-efficient, cost-effective, and highly scalable, enabling the deployment of large PRE arrays to achieve precise and adaptive beamforming. Such scalability enhances the received signal power at the intended user while suppressing the signal at unintended or malicious receivers, thereby improving physical-layer security [41]. Furthermore, the absence of active components ensures that passive IRSs do not introduce additional circuit or thermal noise into the reflected signal.

In contrast, an active IRS incorporates amplification modules within its PREs to partially offset the double-fading effect caused by the reflected IRS-receiver [42]. While this amplification enhances the received signal power at the intended user, it also introduces amplified noise and increases power consumption and hardware complexity. Furthermore, the amplified noise is reflected in all directions, which may inadvertently improve the eavesdropper's signal quality and reduce secrecy gains. A hybrid IRS aims to strike a balance by activating only a subset of PREs while keeping the remaining elements passive [42]. Although this approach mitigates overall noise and power overhead, it still demands more sophisticated coordination and con-

trol strategies. Overall, due to its low-noise operation, high scalability, and strong secrecy enhancement capability, the passive IRS architecture remains a compelling choice for secure wireless communication systems, particularly in scenarios where eavesdropper channel state information (CSI) is imperfect or unavailable.

To this end, the passive IRS architecture aligns most naturally with the objectives of secrecy maximisation. Because passive IRSs neither amplify the incident signal nor inject additional noise, they preserve the legitimate receiver's SNR advantage while enabling directional and interference-aware reflection control. This property is particularly advantageous in PLS, where secrecy depends not only on improving the intended link quality but also on deliberately degrading the eavesdropper's channel. In contrast, active and hybrid IRS architectures inevitably introduce amplified noise and leakage toward unintended directions, which can inadvertently strengthen the eavesdropper's reception and undermine secrecy guarantees in IRS-aided systems.

As previously discussed, IRSs can enhance the desired signal reception or suppress unwanted signals, making it highly effective for PLS applications in 6G networks. In [43], the authors addressed the problem of maximising the secrecy rate (SR) in an IRS-aided MISO system by jointly optimising the transmit beamforming vectors and the IRS phase shifts. Simulation results demonstrated a significant improvement in SR when an IRS is employed. In [44], the authors investigated a more challenging scenario where the legitimate user experiences a worse fading channel than the eavesdropper, and the two channels are correlated, severely limiting SR. To address this, they jointly optimised the IRS reflection coefficients and the beamforming vectors of the legitimate user, ensuring that signals destructively interfere at the eavesdropper. This approach is particularly practical in real-world environments where the exact location of the eavesdropper is often unknown. Furthermore, the authors in [45] introduced the concept of signal jamming, whereby the legitimate user injects artificial noise into the channel. This noise is incorporated into the transmit-

ted beamforming vectors, effectively degrading the eavesdropper's reception. The results showed an improvement in SR compared to conventional systems. Building on this work, Xu *et al.* in [46], further enhanced the SR by jointly optimising artificial noise, IRS phase shifts, and beamforming vectors. Numerical simulations indicated an improvement of nearly 20%. In [47], a cell-free IRS-assisted network was examined with the objective of improving users' SR by maximising the weighted sum of users' secrecy rates (WSSR). The optimisation problem was tackled by jointly optimising the transmit beamforming vector and the IRS's PREs. To handle the resulting nonconvex problem, the authors employed an AO framework to decouple the variables using SDR and continuous convex approximation techniques. Building on this line of work, Shi *et al.* in [48], investigated the SR maximisation in a MIMO IRS-assisted system with a single eavesdropper. The IRS was utilised to support both uplink communication and downlink energy transfer. The WSSR problem was handled by jointly optimising the transmit beamformer, the time allocation between uplink and downlink phases, and the energy transmit covariance matrix to enhance SR performance.

When CSI between the IRS and the users is partially known or unavailable, alternative formulations are necessary. For instance, the authors in [49], addressed a multi-user IRS-aided scenario where the eavesdropper's channel is only partially known at the receiver. A secrecy sum rate (SSR) maximisation problem was formulated under these constraints. Likewise, a cognitive radio system with unknown eavesdropper's CSI was investigated in [50]. The authors proposed a power minimisation strategy to ensure secrecy by optimising the beamforming vector and assuming continuous-phase IRS phase shifts. Notably, much of the literature on IRS-based secrecy enhancement and signal-to-interference-plus-noise ratio (SINR) optimisation relies on idealised assumptions, such as perfect CSI or continuous phase shifts (CPS) [47, 51, 52]. However, such assumptions are often inaccurate due to hardware

limitations [53], as discussed before. To address this, the authors in [54] proposed a system with quantised phase shifts (QPS), formulating a transmit power minimisation problem to meet SNR requirements. The authors tackled the problem by jointly optimising the beamforming vector and quantised PREs. Furthermore, [55] demonstrated that a 2-bit quantisation resolution can nearly match the performance of CPS-based designs. In scenarios involving partial or imperfect CSI at the transmitter, the IRS phase design becomes susceptible to phase shift errors (PSE). This issue was specifically examined in [56], which analysed the impact of PSE in large-scale IRS deployments and its implications for system performance.

The transition to 6G introduces stringent requirements for reliability, latency, and security, particularly in scenarios such as URLLC and IoT. These applications rely on short-packet transmissions, where the FBR becomes critical for accurate performance characterisation. Conventional asymptotic assumptions fail to capture the trade-offs between reliability, latency, and secrecy in these contexts. Integrating PLS with IRS control provides a dynamic mechanism to enhance channel conditions and mitigate eavesdropping risks without excessive signalling overhead. IRS-aided systems enables adaptive propagation shaping, improving reliability and secrecy while supporting low-latency constraints. When combined with finite blocklength analysis, this approach offers precise optimisation of key performance metrics, addressing fundamental challenges in 6G design. The proposed framework therefore aligns with mission-critical and resource-constrained applications, delivering a scalable and secure solution for next-generation wireless networks.

While significant progress has been made in enhancing users' data rate and secrecy in IRS-aided systems in 6G networks, the area still demands substantial further research. In particular, PLS in FBR-IRS-aided 6G networks introduces complex challenges related to decoding errors, transmission latency, and SR optimisation. Additionally, practical limitations such as low-resolution IRS and imperfect

or unknown CSI in IRS systems remain significant obstacles. Addressing these issues is essential to unlock the full potential of the IRS in meeting the stringent reliability, latency, and security requirements of future 6G applications.

1.2 Literature Review and Contributions

In this thesis, we focus on enhancing the users' data rate and security in the upcoming 6G network by exploiting the IRS capability of strategically directing the signal towards the desired users. We first address the problem of maximising users' data rate in an LBR/FBR-IRS-aided system by optimising the beamforming vector and the IRS PREs. In the second stage, we extend the study to address the problem of ensuring the system's secrecy. To this end, we aim to enhance the users' secrecy in IRS-aided systems under multiple system configurations, such as perfect/imperfect/unknown IRS-to-users/eavesdropper CSI, and low-resolution IRS.

1.2.1 Maximising Users' Data Rate in FBR-IRS-Aided Network

IRSs constitute planar arrays of PREs, which can potentially augment the coverage of wireless networks [57–59]. In particular, the spectral efficiency of networks can be maximised by the joint design of the transmit beamformer at base station (BS/Alice) and the IRS PREs [60–63].

In parallel, URLLC has also attracted recent research attention thanks to its potential applications in the IoT, with special attention to holographic communications, the tactile Internet, autonomous driving, etc. [1,2]. Under the URLLC framework, low-latency requires short (finite) block length (FBL) while ultra-reliability imposes extra low error probability constraints [64]. As a consequence, the rate function of URLLC is dependent not only on the SNR but also on the block length and the decoding error probability. Hence, its definition is much more computationally challenging than that of Shannon's rate function in the long block regime.

Resource allocation and transmit beamforming used for optimising the users' rates under the FBR have been recently considered e.g. in [65, 66]. The authors in [67, 68] analysed IRS-aided URLLC systems of a single antenna BS and an IRS serving a single user. The more advanced joint design of the transmit beamformer at multiple BSs and IRS PREs maximising the sum-rate subject to specific QoS constraints in terms of the users' rates was considered in [69]. However, the computational complexity of the algorithm proposed in [69] is extremely high, as it iterates by observing convex problems of escalating dimension. Hence Ghanem *et al.* [69] considered only up to 20 PREs for the IRS, even though IRSs should employ very large numbers of PREs [70]. Regarding this problem, one can combine the techniques proposed in [62] and [65] to develop an algorithm that iterates by evaluating convex problems of the same size as the original nonconvex problem. However, this size is already large for practical IRS-aided networks due to the large numbers of PREs and beamforming decision variables, which makes the computation of these convex problems impractical.

Against the above background, in chapter 2 we derive a computationally tractable solution for the joint design of transmitter beamforming vectors and IRS PREs to optimise all the users' rates in the FBL regime. Following the earlier results in [63] for optimising all the users' rates in the LBR (Shannon rate), we now aim to maximise the geometric mean of the users' rates (GM-rate) and we explicitly demonstrate that it is capable of providing a fair users' rate distribution without enforcing computationally intractable rate constraints. As a further novelty, we avoid the computationally intractable UMC on the PREs by directly optimising their arguments. As such, the design of PREs is based on trigonometric function optimisation.

1.2.2 Robust Secrecy Enhancement for All Users in low-resolution IRS-Aided System Under Perfect/Imperfect/Unknown CSI

By optimising signal reflections, IRSs improve reception by creating favourably reflected multi-path signals at the receivers. Thanks to their cost-effective design and convenient deployment typically on the facades of high-rise buildings, IRSs hold immense potential for various applications, particularly in urban areas where line-of-sight channels between transmitters (Tx) and receivers (Rx) frequently face obstructions [71]. Particularly, for the IoT devices that have limited computing capability and battery/energy, the IRS has gained paramount attention aiming to enhance both spectral and energy efficiency [72]. Another potential application of IRSs is to enhance the security/privacy of users by purposely manipulating reflected signals from the Tx so as to facilitate the signal reception at legitimate users while maximising the multi-user interference/degrading the signals at potential eavesdroppers. In [51], the authors studied the design of an IRS to maximise the legitimate user's SR, which is defined as the difference between the rate of the legitimate channel and that of the channel from the transmitter to a potential eavesdropper. The authors studied SR maximisation by jointly optimising the beamforming vector at the transmitter and the IRS's PREs. A MISO IRS-aided system with the presence of multiple eavesdroppers was considered in [73]. The transmitter introduced AN as a countermeasure to enhance user security. In [47], the authors studied a cell-free IRS-aided network, where they aimed to enhance the users' secrecy by maximising the users' WSSR by jointly optimising the beamforming vector and the IRS's PREs. The AO algorithm was used to decouple the beamforming factor and the IRS's PREs, and the resulting problem was tackled using the SDR and continuous convex approximation. Shi *et al.* in [48] investigated the SR in a MIMO IRS-aided system with the presence of a single eavesdropper. The IRS was deployed to enhance the uplink transmission and the downlink energy transfer. The authors investigated the

problem of SR maximisation by jointly optimising the transmit beamform vector, the downlink/uplink time allocation, and the energy transmit covariance matrix.

When the CSI from the IRS to the users/receivers is unknown or imperfect, the authors in [49] studied an IRS-aided multi-user system, where they formulated an SSR maximisation problem with the eavesdropper's channel partially known to the receiver. In [50], the authors investigated an IRS-aided cognitive radio system when the eavesdropper's CSI is not available at Alice. The authors also proposed a power minimisation problem to guarantee users' secrecy by optimising the beamforming vector and the IRS PREs, which were modelled by continuous phase shift (PS). It is worth mentioning that most of the research on IRS's secrecy and SINR maximisation assumes perfect phase estimation and/or full resolution/continuous phase shift [47, 51, 52]. However, assuming CPS of the IRS's PREs is not practical in real-life scenarios due to hardware limitations [53]. In [54], the authors studied an IRS-aided system with a discrete/quantised phase shift. The authors proposed a transmission power minimisation problem to achieve a certain user's SNR by jointly optimising the beamforming vector and the discrete PREs. In [55], it was shown that using a 2-bit QPS can nearly achieve the same performance as a CPS. When the transmitter can obtain partial/imperfect CSI, the IRS's PREs are affected by phase shift error (PSE). The PSE was investigated in [56], where the IRS PREs PSE was presented in a large IRS system.

In Chapter 3, we aim to achieve secrecy for *all the users* under low-resolution IRS-aided systems with both perfect and imperfect CSI. To that end, we consider a popular use case where a low-resolution IRS is used to enhance/aid the signal reception at legitimate users (from a transmitter) in the presence of a potential eavesdropper. We then maximise the minimum SR by optimising the transmit beamforming vector and the IRS's PREs.

When Alice can only obtain partial or erroneous knowledge of the IRS-to-Users/Eve's CSI, the problem becomes more challenging. Mathematically, imperfect CSI introduces non-convex constraints into the problem. To tackle it, we use slack variables to manage the coupling between the transmitter's beamforming vectors and the PREs PS within the objective function. We then apply the successive convex approximation (SCA) technique [74], and the $\mathcal{S}$-procedure [75] to reformulate the semi-infinite constraints into linear matrix inequalities (LMI). While the SCA framework combined with the $\mathcal{S}$-procedure transforms the semi-infinite constraints into an LMI, the resulting LMIs remain nonconvex. To address this, we employ a first-order Taylor approximation to linearise these non-convex components, enabling an efficient convex reformulation that can be solved at each iteration. Finally, to handle the UMC of the IRSs, we employ the penalty convex-concave procedure (PCCP) [76]. Unlike other research that doesn't account for PSE [52], in this work, we leverage the PCCP algorithm to account for PSE in the IRS optimisation. For comparison purposes, we also consider the SSR maximisation problem. When the eavesdropper's CSI is unknown to the transmitter, the IRS PREs modelled by QPS suffer from PSE. To provide secrecy for *all users*, we develop a power minimisation problem while introducing a residual power that acts as an AN to lower the eavesdropper's SINR. Extensive simulations with practical settings show that by maximising the minimum SR among all the users or minimising transmit power and using AN, we can achieve a better chance of ensuring secure communications for *all users* (subject to the location of the eavesdropper) even under imperfect CSI and low-resolution IRS. Where feasible, as expected, we observe that maximising the minimum SR can achieve greater fairness among the users compared to the SSR maximisation problem. The main contributions are summarised as follows:

- We study the SR guarantee for *all users* and the impact of the low-resolution IRS in a multi-user downlink IRS-aided network. We formulate three optim-

isation problems: maximising the minimum SR, maximising the SSR, and minimising the transmission power, by jointly optimising the transmitter's beamforming vector and the IRS's PREs. We then study the problems under both perfect and imperfect CSI cases.

- In the first case, we tackle the non-convex problem under perfect CSI. We linearise its objective function using mathematical approximations that yield a mathematically tractable approximate surrogate function. To handle the UMC, and in contrast to conventional approaches such as semi-definite relaxation (SDR), we circumvent the computationally intractable UMC by directly optimising the quantised PREs argument. Consequently, the PRE design reduces to an optimisation over trigonometric functions, yielding a low-complexity, scalable solution for large-scale IRS deployments. The proposed algorithm is analytically shown to converge to a locally optimal solution of the original non-convex problem.

- When only partial CSI is known to Alice, we leverage the SCA to tackle the imperfect CSI-related semi-infinite constraints to transform them into LMIs. We then linearise the non-convex terms within these LMIs using a first-order Taylor approximation. Next, we tackle the UMC using the PCCP algorithm, explicitly accounting for PSE arising from channel uncertainty.. We show that the proposed algorithm converges to, at least, a locally optimal solution of the non-convex problem.

- In the final scenario, where the eavesdropper's CSI is unknown, we formulate a power minimisation problem that ensures the users' data rates remain above a predefined quality-of-service (QoS) threshold. The residual transmit power is then allocated as AN to degrade the eavesdropper's SINR. The UMC is handled via PCCP while ensuring QoS constraints are met, and accounts for

the PSE. The proposed algorithm is proven to converge to a locally optimal solution, effectively enhancing secrecy for all users.

- Eventually, we conduct extensive simulations to assess the impact of optimising the IRS's PREs on users' SR. The results demonstrate that the proposed algorithms ensure secure communication for *all users*. In contrast, approaches that focus on maximising the SSR, i.e. [77], fail to guarantee secrecy for *all users*.

1.2.3 Secrecy Assurance for All Users in FBR-IRS-Aided System Under Perfect/Imperfect CSI

URLLC and mMTC, both relying on the finite blocklength (short packet) regime, have been envisioned as key technologies to serve critical missions of IoT. Since FBR often requires a stricter design approach than the long blocklength regime/communication (LBR) systems [7], maintaining high-reliability communication is more challenging due to the lower channel coding gain. Moreover, in URLLC applications such as intelligent transportation, leakage information could expose the user's location or identity. As a potential solution to secure URLLC, the use of IRS has recently attracted paramount interest. IRS links exhibit low latency that is beneficial for the FBR strict requirements [78]. Zhao et al. studied the information freshness in a single-user FBR-IRS-aided system with the presence of an eavesdropper in [78]. The authors derived a closed-form expression for the upper bound secrecy outage probability under statistical CSI. The single user's secrecy outage is minimised by jointly optimising the blocklength and the IRS PREs. The authors in [79] studied the secrecy performance of an IRS-assisted URLLC system, where an FBR coding scheme was proposed to secure the link, showing that secrecy is achievable beyond a certain blocklength threshold. However, it does not consider the joint optimisation of secrecy rate and transmission parameters, which is crucial

for practical deployment. Nevertheless, the assumption that Alice/Tx can obtain Eve's CSI, as stated before, is not always feasible. Note that most earlier work focused only on single-user systems. The SSR maximisation approach in LBR-IRS systems is neither applicable to nor can it guarantee the secrecy for all users in FBR-IRS systems due to the additional latency requirements of the FBR.

Guaranteeing secrecy in FBR is significantly more challenging than in conventional LBR applications. Unlike LBR, where sufficiently long codewords can asymptotically drive both error probability and leakage to zero, these factors remain strictly non-zero in FBR due to the coding limits imposed by short blocklengths [80]. In particular, the square-root of the channel dispersion in the FBR-SR expression directly captures the effect of finite blocklength on the decoding error probability, making the SR a non-linear function. Consequently, the optimisation problem is significantly more complex, as these non-zero error and leakage terms introduce additional nonconvex penalties that must be jointly considered with power and beamforming constraints. Unlike other research, which only considers secrecy enhancement in LBR-IRS-aided systems, or FBR secrecy improvement with full CSI [81], we tackle the problem of secrecy guarantee in FBR-IRS-aided systems under perfect/imperfect IRS to users' CSI.

In Chapter 4, we consider a widely studied scenario in which IRSs are employed to enhance signal reception at legitimate users, in the presence of a potential eavesdropper. It is assumed that no direct or line-of-sight channel exists between the transmitter and any user or the eavesdropper, for example, due to environmental blockages.[†] Under this setting, we aim to maximise the minimum SR across all users while satisfying FBR constraints, by jointly optimising the transmit beamforming

[†]In practical deployments, it is unrealistic to assume that the eavesdropper has a line-of-sight channel while the legitimate users do not. In such scenarios, the deployment of a friendly jammer is necessary to preserve user confidentiality [50].

vector and the IRS's PREs. Both perfect and imperfect CSI scenarios are considered for the channels from the IRS to the users and the eavesdropper. In the perfect CSI case, it is assumed that the transmitter has access to accurate CSI of all users and the eavesdropper. This can occur when one of the legitimate users is compromised and acts as an eavesdropper, thereby making its CSI known to Alice.

When only partial or erroneous CSI (from the IRS to the users and Eve) is available, the problem becomes even more challenging. In particular, the semi-infinite constraints introduced by imperfect CSI are embedded within the dispersion term of the FBR-SR expression, which involves both the inverse Q-function and the square-root of the channel dispersion. This embedding makes the decoding error probability highly sensitive to channel estimation errors [82], while the square-root further increases the nonlinearity. To tackle the problem, we first introduce slack variables to deal with the transmit beamforming vectors and the IRS's PREs coupling within the objective function. Secondly, we leverage the SCA technique [74], and the $\mathcal{S}$-procedure [75] to convert the semi-infinite constraints into LMI. Although the SCA framework with the $\mathcal{S}$-procedure converts the semi-infinite constraints into LMIs, they remain nonconvex. We address this by applying a first-order Taylor approximation to linearise the nonconvex components, yielding a convex reformulation solvable at each iteration. Then, we propose a PCCP [76] to tackle the UMC of the IRS. Extensive simulations with practical settings show that maximising the minimum SR among all the users can achieve a better chance of ensuring secure communications for all users (subject to the location of the eavesdropper) under the FBR constraints even under imperfect CSI conditions. The main contributions are summarised as follows:

- We take the first step toward ensuring secure communications for all URLLC users operating in the finite blocklength regime (FBR), where IRSs are employed to enhance the reception of legitimate users while preventing a potential

eavesdropper from intercepting the transmitted signal. To this end, we aim to maximise the minimum SR among all users by jointly optimising the transmitter's beamforming and the IRS's PREs, subject to the latency constraints imposed by FBR. The resulting optimisation problem is inherently nonconvex and becomes more intricate under imperfect CSI.

- In the case of perfect CSI, we address the nonconvexity of the problem by linearizing the objective function using tractable approximation functions, which results in a computationally efficient solution algorithm. To handle the UMC, we deviate from conventional approaches such as standard SDR and instead directly optimise the phase arguments of the PREs, enabling a low-complexity and scalable solution for large-scale IRSs. The proposed algorithm is shown to converge to a locally optimal solution of the original problem.

- Under imperfect CSI conditions, we adopt the SCA framework to reformulate the semi-infinite constraints induced by CSI uncertainty into finite LMI. Owing to the closed-form linearization embedded in our approach, the resulting algorithm maintains low computational complexity and remains scalable for large IRS deployments, while still ensuring convergence to a locally optimal solution.

- Finally, we conduct extensive simulations under realistic system configurations. The results demonstrate that the proposed framework can guarantee secure communication for all users while satisfying FBR constraints, even in the presence of imperfect CSI. Furthermore, the impact of CSI imperfections in the reflected channels on overall system performance is thoroughly evaluated.

Lastly, in Chapter 5, we provide a system secrecy guarantee for FBR-IRS-aided systems with multiple URLLC users. Specifically, we consider a similar case to the above, where the IRS is used to enhance the legitimate users' signal in the presence of

a potential eavesdropper. However, in this scenario, we enhance the system's secrecy by maximising the SSR of all the users while maintaining the FBR constraints. We tackle the problem by optimising the transmit beamforming vector and the IRS's PREs. We consider both cases with perfect and imperfect CSI from the IRS to the users and the eavesdropper. The main contributions are summarised as follows:

- We tackle the secrecy maximisation problem of the URLLC users in the FBR-IRS-aided system, in which the IRS enhances the users' SINR and thwarts Eve's SINR to ensure the system's SR. To this end, we maximise the SSR by jointly optimising the beamforming vectors and the IRS's PREs, while maintaining the FBR latency and transmission durations conditions.

- When CSI is available, we solve the above nonconvex problem by linearizing its objective function with tractable approximation functions, leading to a computationally efficient algorithm. To tackle the UMC, unlike traditional methods, i.e., conventional SDR, we directly optimise the PREs arguments to provide a low-complexity solution that can scale with large IRSs. The resulting solution is proved to converge to a locally optimal solution of the original nonconvex problem.

- In the case of imperfect CSI, we transform the semi-infinite constraints imposed by the imperfect CSI constraint into finite LMIs by leveraging the SCA approach for the transformation. We then prove that our proposed algorithm converges to a locally optimal solution with low computational complexity thanks to our closed-form linearization approach. This makes the solution scalable for large IRS deployments.

- Finally, we perform extensive simulations with practical settings. The simulation results show that our approach can ensure secure communication for all

the users while satisfying FBR constraints even under imperfect CSI. Additionally, the impact of the reflected channel's imperfect CSI on the system is also evaluated.

1.3 Thesis Organisation

The rest of the thesis is organised as follows:

- Chapter 2: This chapter presents our proposed GM maximisation and the Max-Min algorithms to maximise the users' rate in the FBR-IRS-aided system. Section 2.1 is devoted to the problem statement and solution, which is supported by our simulation results provided in Section 2.2. Finally, Section 2.3 concludes the chapter.

- Chapter 3: This chapter presents the enhancement of the user's SR in a a low-resolution IRS-aided downlink under perfect/imperfect/unknown CSI. The system model is discussed in Sections 3.1. Then, Sections 3.2, 3.3, and 3.4 present the problem and corresponding solutions under prefect/imperfect/unknown CSI, respectively. The extensive simulations and discussion are in Section 3.5. Finally, Section 3.6 concludes the paper and discusses potential future directions.

- Chapter 4: This chapter presents the secrecy fairness an FBR-IRS-aided downlink system under perfect/imperfect CSI. We aim to enhance multiple users' SR with the presence of an eavesdropper. The system model is discussed in Sections 4.1. Then, Sections 4.2 and 4.3 present the problem and corresponding solutions under perfect and imperfect CSI, respectively. The extensive simulations and discussion are in Section 4.4. Finally, Section 4.5 concludes the paper.

- Chapter 5: This chapter presents the system secrecy enhancement in an FBR-IRS-aided downlink system under perfect/imperfect CSI. The system model is discussed in Sections 5.1. Then, Sections 5.2 and 5.3 present the problem and corresponding solutions under perfect and imperfect CSI, respectively. The extensive simulations and discussion are provided in Section 5.4. Finally, Section 5.5 concludes the paper.

- Chapter 6: The final chapter provides a concise summary of the thesis and its key contributions, and concludes by outlining potential future research directions in FBR-IRS-assisted networks.

Fig. 1.2 illustrates the structural flow of the thesis, highlighting the interrelation between chapters and the specific research problems addressed in each.

1.4 Notation

This thesis uses the following notation: bold letters denote vectors and matrices. $\boldsymbol{I}_M$ denotes an M dimensional identity matrix. $\text{Diag}(n_1, \ldots, n_n)$ denotes the diagonal matrix with diagonal entries of $\{n_1, \ldots, n_n\}$. The symbols $\Re$ and $\mathbb{C}$ represent the real and the complex field, respectively. $\mathcal{C}(0, \bar{z})$ denotes the circular Gaussian random variable with zero mean and variance $\bar{z}$. For matrices $\mathbf{C}$ and $\mathbf{D}$, $\langle \mathbf{C}, \mathbf{D} \rangle \triangleq \text{trace}\left(\mathbf{C}^H \mathbf{D}\right)$. For matrix $\mathbf{A}$, $\Re\{\mathbf{A}\}$ denotes the real part, $\langle \mathbf{A} \rangle \triangleq \text{trace}(\mathbf{A})$, the symbol $\|\mathbf{A}\|_1$ denotes the 1-norm, $\|\mathbf{A}\|$ denotes the Frobenius norm, $\mathbf{A}^*$ denotes the conjugate, $\mathbf{A}^H$ denotes the Hermitian (conjugate transpose), $\lambda_{\max}(\mathbf{A})$ denotes the maximal eigenvalue, $\angle(\mathbf{A})$ denotes its argument, and $\mathbf{A} \succeq 0$ means positive semi-definite.

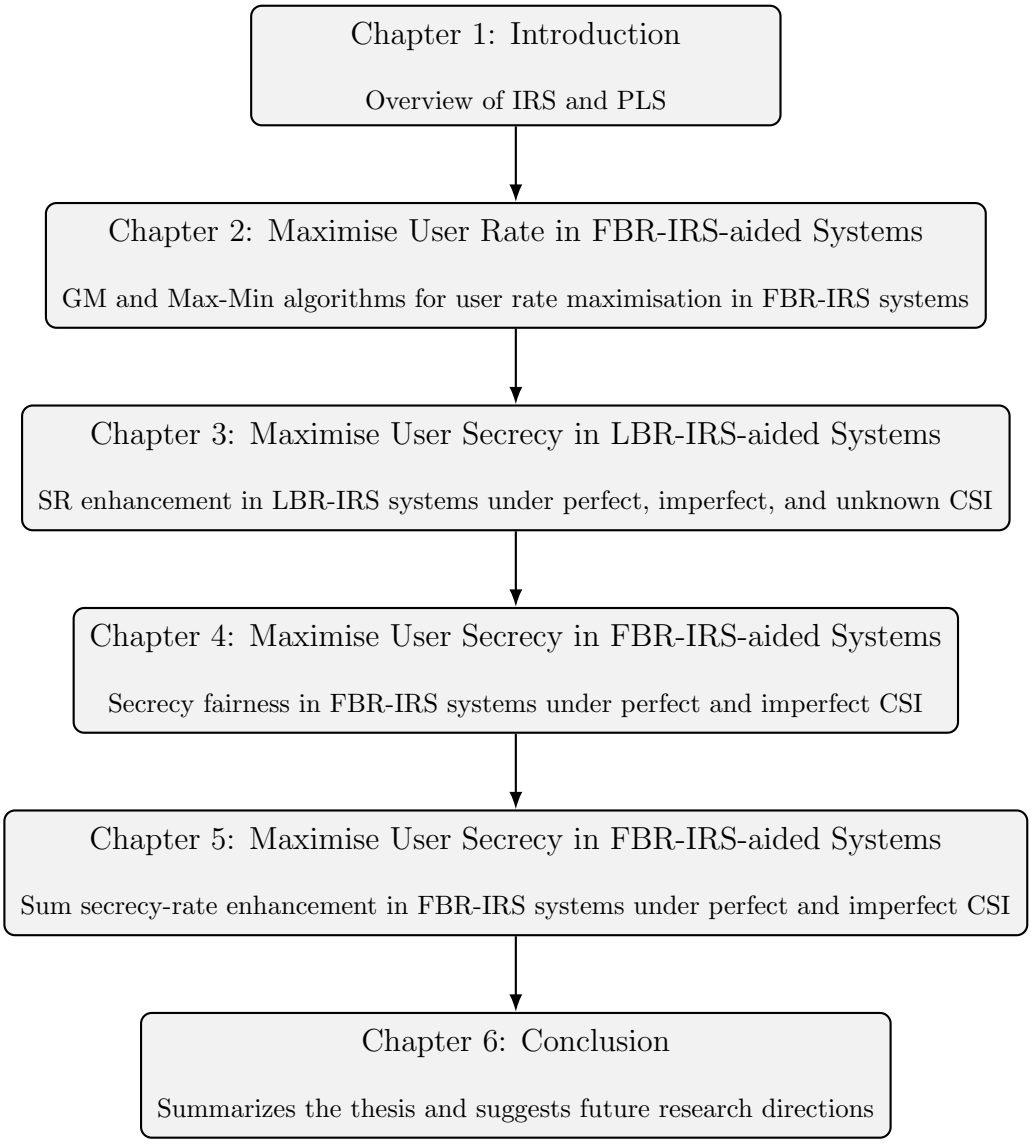

Figure 1.2 : Flowchart showing the thesis's chapters connection.

Chapter 2

Finite-Blocklength IRS-Aided Transmit Beamforming

This chapter*, considers the downlink of an ultra-reliable low-latency communication (URLLC) system in which a base station (BS) serves multiple single-antenna users in the short (finite) blocklength (FBL) regime with the assistance of a intelligent reflective surface (IRS). In the FBL regime, the users' achievable rates are complex functions of the beamforming vectors and of the IRS's programmable reflecting elements (PREs). We propose the joint design of the transmit beamformers and PREs to maximise the geometric mean (GM) of these rates (GM-rate) and show that this approach provides fair rate distribution and thus reliable links to all the users. A novel computational algorithm is developed, which is based on closed forms to generate improved feasible points. Simulations show the merit of our solution.

The rest of the chapter is organised as follows. Section 2.1 is devoted to the problem statement and solution, which is supported by our simulation results provided in Section 2.2. Finally, Section 2.3 concludes the paper.

2.1 Problem Statement

As illustrated by Fig. 2.1, we consider the downlink of a system, in which an M-antenna BS serves K single-antenna users (UEs) $k \in \mathcal{K} \triangleq \{1, \ldots, K\}$ with the aid of an IRS having N PREs as the BS cannot see the UEs. As the IRS is seen by the BS and the UEs are seen by the IRS line-of-sight (LoS), the channels

*This chapter corresponds to the journal paper J-1 in the list of Publications.

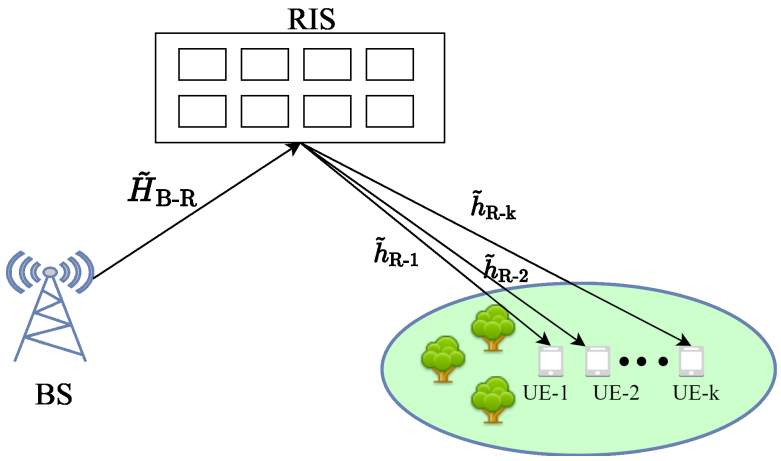

Figure 2.1 : IRS-aided system model, where the direct link between the BS and the users is blocked.

spanning from the BS to the IRS (from the IRS to UE k, resp.) are modeled by $\tilde{H}_{\text{B-R}} = \sqrt{\beta_{\text{B-R}}} H_{\text{B-R}} \in \mathbb{C}^{N \times M}$ ($\tilde{h}_{\text{R-k}} = \sqrt{\beta_{\text{R-k}}} h_{\text{R-k}} \in \mathbb{C}^{1 \times N}$, resp.), where $\sqrt{\beta_{\text{R-k}}}$ and $\sqrt{\beta_{\text{B-R}}}$ respectively represents the path-loss and large-scale fading of the IRS-to-UE k link and the BS-to-IRS link, while $h_{\text{R-k}}$ and $H_{\text{B-R}}$ are modelled by Rician fading [83].

Let $s_k \in \mathcal{C}(0,1)$ be the information symbol intended for UE k, which is beamformed by the array of weights $\mathbf{w}_k \triangleq (\mathbf{w}_k(1), \ldots, \mathbf{w}_k(M))^T \in \mathbb{C}^M$ to create the transmit signal $x = \sum_{k \in \mathcal{K}} \mathbf{w}_k s_k$. The signal received at UE k is given by

$$y_k = \boldsymbol{H}_k(\boldsymbol{\theta}) \sum_{k \in \mathcal{K}} \mathbf{w}_k s_k + n_k, \tag{2.1}$$

for

$$\tilde{h}_{\text{BR-k}} \triangleq \sqrt{\beta_{\text{B-R}}} \sqrt{\beta_{\text{R-k}}}\, h_{\text{R-k}}\, \mathcal{R}_{\text{R-k}}^{1/2}, \in \mathbb{C}^{1 \times N}$$

$$\boldsymbol{H}_k(\boldsymbol{\theta}) \triangleq \tilde{h}_{\text{BR-k}}\, \text{diag}\left(e^{\jmath \boldsymbol{\theta}}\right) H_{\text{B-R}} = \sum_{n=1}^{N} \boldsymbol{H}_{k,n} e^{\jmath \boldsymbol{\theta}_n}, \in \mathbb{C}^{1 \times M}$$

where $\mathcal{R}_{\text{R-k}} \in \mathbb{C}^{N \times N}$ encompasses the spatial correlation of the PREs with respect to user k [83], $n_k \in \mathcal{C}(0, \sigma^2)$ is the background noise, $\boldsymbol{\theta} = (\boldsymbol{\theta}_1, \ldots, \boldsymbol{\theta}_N)^T \in [0, 2\pi)^N$ is the vector of the PREs' angles, and $\boldsymbol{H}_{k,n} \triangleq \tilde{h}_{\text{BR-k}} \Upsilon_n H_{\text{B-R}}$, where Υ_n is the matrix of size $N \times N$ with all-zero entries apart from $\Upsilon_n(n,n) = 1$.

For $\mathbf{w} \triangleq \{\mathbf{w}_k, k \in \mathcal{K}\}$, the effective signal-to-interference-plus-noise (SINR) at UE k is defined by

$$g_k(\mathbf{w}, \boldsymbol{\theta}) = \frac{|\boldsymbol{H}_k(\boldsymbol{\theta})\mathbf{w}_k|^2}{\alpha_k(\mathbf{w}, \boldsymbol{\theta})}, \tag{2.2}$$

for $\alpha_k(\mathbf{w}, \boldsymbol{\theta}) \triangleq \sum_{j \in \mathcal{K} \setminus \{k\}} |\boldsymbol{H}_k(\boldsymbol{\theta})\mathbf{w}_j|^2 + \sigma^2$. In the LBL regime, the rate in nats/sec/Hz at UE k is $r_k(\mathbf{w}, \boldsymbol{\theta}) = \ln[1 + g_k(\mathbf{w}, \boldsymbol{\theta})]$.

Let $\mathcal{B}$ be the communication bandwidth. According to [84], by treating other terms there as Gaussian noise the achievable URLLC rate in nats/sec/Hz for the signal s_k in (2.1) is approximated by

$$\hat{r}_k(\mathbf{w}, \boldsymbol{\theta}) \triangleq r_k(\mathbf{w}, \boldsymbol{\theta}) - a v_k^{1/2}(\mathbf{w}, \boldsymbol{\theta}), \tag{2.3}$$

where the channel dispersion $v_k(\mathbf{w}, \boldsymbol{\theta})$ under the SINR $g_k(\mathbf{w}, \boldsymbol{\theta})$ is defined by [84, eq. (27)]

$$v_k(\mathbf{w}, \boldsymbol{\theta}) \triangleq 2\frac{g_k(\mathbf{w}, \boldsymbol{\theta})}{1 + g_k(\mathbf{w}, \boldsymbol{\theta})} = 2\left(1 - \frac{\alpha_k(\mathbf{w}, \boldsymbol{\theta})}{\beta_k(\mathbf{w}, \boldsymbol{\theta})}\right), \tag{2.4}$$

in conjunction with

$$\beta_k(\mathbf{w}, \boldsymbol{\theta}) \triangleq \alpha_k(\mathbf{w}, \boldsymbol{\theta}) + |\boldsymbol{H}_k(\boldsymbol{\theta})\mathbf{w}_k|^2 = \sum_{j \in \mathcal{K}} |\boldsymbol{H}_k(\boldsymbol{\theta})\mathbf{w}_j|^2 + \sigma^2. \tag{2.5}$$

Also, $a \triangleq \frac{1}{\sqrt{\mathcal{B}t_t}} Q_G^{-1}(\epsilon^c)$, where t_t is the URLLC transmission duration, $Q_G^{-1}(\cdot)$ is the inverse of the Gaussian Q-function $Q(x) = \int_x^\infty \frac{1}{\sqrt{2\pi}} \exp(-t^2/2)dt$, and ϵ^c is defined as an acceptable decoding error probability, which implies that under the block fading channel model considered, one out of $1/\epsilon_c$ short packets (URLLC transmissions) may experience outage.

We consider the following problem of jointly designing the beamformer $\mathbf{w}$ and the PREs $\boldsymbol{\theta}$ for maximising the GM-rate:

$$\max_{\mathbf{w}, \boldsymbol{\theta}} \hat{f}(\mathbf{w}, \boldsymbol{\theta}) \triangleq \left(\prod_{k=1}^{K} \hat{r}_k(\mathbf{w}, \boldsymbol{\theta})\right)^{1/K} \tag{2.6a}$$

$$\text{s.t.} \quad \sum_{k=1}^{K} ||\mathbf{w}_k||^2 \leq P, \tag{2.6b}$$

where (2.6b) sets the transmit sum power constraint within a given power budget P. Our previous paper [63], which considered the problem

$$\max_{\mathbf{w},\boldsymbol{\theta}} f(\mathbf{w},\boldsymbol{\theta}) \triangleq \left(\prod_{k=1}^{K} r_k(\mathbf{w},\boldsymbol{\theta})\right)^{1/K} \quad \text{s.t.} \quad (2.6b) \tag{2.7}$$

in the LBL regime showed that GM-rate maximisation naturally leads to fair user rate distributions without imposing the rate constraints of $r_k(\mathbf{w},\boldsymbol{\theta}) \geq \bar{r}$, which are nonconvex and thus computationally intractable. As a compelling benefit, by directly optimising the angles $\boldsymbol{\theta} \in [0, 2\pi)^N$ of PREs, both (2.6) and (2.7) circumvent the unit modulus constraints on the latter.

Compared to the rate function r_k in the LBL regime, we have the rate-reduction term $\upsilon_k^{1/2}(\mathbf{w},\boldsymbol{\theta})$ arising in the rate function $\hat{r}_k$ in the FBL regime. Therefore, the main challenge in considering (2.6) is to handle this term.

Initialised by $(w^{(0)}, \theta^{(0)})$ as the optimal solution of (2.7) computed by [63], let $(\mathbf{w}^{(\kappa)},\boldsymbol{\theta}^{(\kappa)})$ be a feasible point for (2.6) that is found from the $(\kappa-1)$-st round, and

$$\gamma_k^{(\kappa)} \triangleq \frac{\max_{k'\in\mathcal{K}} \hat{r}_{k'}(\mathbf{w}^{(\kappa)},\boldsymbol{\theta}^{(\kappa)})}{\hat{r}_k(\mathbf{w}^{(\kappa)},\boldsymbol{\theta}^{(\kappa)})}, k \in \mathcal{K}. \tag{2.8}$$

As discussed in [63], the descent iterations are based on the following problem:

$$\max_{\mathbf{w},\boldsymbol{\theta}} \hat{f}^{(\kappa)}(\mathbf{w},\boldsymbol{\theta}) \triangleq \sum_{k=1}^{K} \gamma_k^{(\kappa)} \hat{r}_k(\mathbf{w},\boldsymbol{\theta}) \quad \text{s.t.} \quad (2.6b). \tag{2.9}$$

2.1.1 Beamforming Descent Iteration

We seek $w^{(\kappa+1)}$ satisfying

$$\hat{f}^{(\kappa)}(\mathbf{w}^{(\kappa+1)},\boldsymbol{\theta}^{(\kappa)}) > \hat{f}^{(\kappa)}(\mathbf{w}^{(\kappa)},\boldsymbol{\theta}^{(\kappa)}). \tag{2.10}$$

Define $r_{b,k}^{(\kappa)}(\mathbf{w}) \triangleq r_k(\mathbf{w},\boldsymbol{\theta}^{(\kappa)})$, $\upsilon_{b,k}^{(\kappa)}(\mathbf{w}) \triangleq \upsilon_k(\mathbf{w},\boldsymbol{\theta}^{(\kappa)})$, $\hat{r}_{b,k}^{(\kappa)}(\mathbf{w}) \triangleq \hat{r}_k(\mathbf{w},\boldsymbol{\theta}^{(\kappa)})$, $\alpha_{b,k}^{(\kappa)}(\mathbf{w}) \triangleq \alpha_k(\mathbf{w},\boldsymbol{\theta}^{(\kappa)})$, $\beta_{b,k}^{(\kappa)}(\mathbf{w}) \triangleq \beta_k(\mathbf{w},\boldsymbol{\theta}^{(\kappa)})$, $\upsilon_{b,k}^{(\kappa)}(\mathbf{w}) \triangleq \upsilon_k(\mathbf{w},\boldsymbol{\theta}^{(\kappa)})$, and $\boldsymbol{H}_k^{(\kappa)} \triangleq \boldsymbol{H}_k(\boldsymbol{\theta}^{(\kappa)})$. As such,

$$\hat{f}^{(\kappa)}(\mathbf{w},\boldsymbol{\theta}^{(\kappa)}) = \sum_{k=1}^{K} \gamma_k^{(\kappa)} \hat{r}_{b,k}^{(\kappa)}(\mathbf{w}), \tag{2.11}$$

and

$$\hat{r}_{b,k}^{(\kappa)}(\mathbf{w}) = r_{b,k}^{(\kappa)}(\mathbf{w}) - a\sqrt{v_{b,k}^{(\kappa)}(\mathbf{w})}. \tag{2.12}$$

The following lower bounding concave approximation of $r_{b,k}^{(\kappa)}(\mathbf{w})$ was obtained in [62]:

$$r_{b,k}^{(\kappa)}(\mathbf{w}) \geq a_{k,1}^{(\kappa)} + 2\Re\{\langle \boldsymbol{b}_{k,k}^{(\kappa)}, \mathbf{w}_k \rangle\} - c_{k,1}^{(\kappa)} \sum_{j=1}^{K} |\boldsymbol{H}_k^{(\kappa)} \mathbf{w}_j|^2, \tag{2.13}$$

with $a_{k,1}^{(\kappa)} \triangleq r_{b,k}^{(\kappa)}(\mathbf{w}^{(\kappa)}) - g_k(\boldsymbol{\theta}^{(\kappa)}, \mathbf{w}^{(\kappa)}) - \sigma^2 c_{k,1}^{(\kappa)}$, $\boldsymbol{b}_{k,k}^{(\kappa)} \triangleq (\boldsymbol{H}_k^{(\kappa)})^H \boldsymbol{H}_k^{(\kappa)} \mathbf{w}_k^{(\kappa)} / \alpha_{b,k}^{(\kappa)}(\mathbf{w}^{(\kappa)})$, and $0 < c_{k,1}^{(\kappa)} \triangleq 1/\alpha_{b,k}^{(\kappa)}(\mathbf{w}^{(\kappa)}) - 1/\beta_{b,k}^{(\kappa)}(\mathbf{w}^{(\kappa)})$.

Our next step is now to develop an upper bounding convex approximation of $\sqrt{v_{b,k}^{(\kappa)}(\mathbf{w})}$, which together with (2.13) gives a lower bounding concave approximation of $\hat{r}_{b,k}^{(\kappa)}$ in (2.12).

Using inequality A.4 is Appendix A, we can reformulate $\sqrt{v_{b,k}^{(\kappa)}(\mathbf{w})}$ as:

$$\sqrt{v_{b,k}^{(\kappa)}(\mathbf{w})} \leq \frac{\sqrt{v_{b,k}^{(\kappa)}(\mathbf{w}^{(\kappa)})}}{2} \left(1 + \frac{2}{v_{b,k}^{(\kappa)}(\mathbf{w}^{(\kappa)})}\right) - \frac{1}{\sqrt{v_{b,k}^{(\kappa)}(\mathbf{w}^{(\kappa)})}} \frac{\alpha_{b,k}^{(\kappa)}(\mathbf{w})}{\beta_{b,k}^{(\kappa)}(\mathbf{w})}. \tag{2.14}$$

Next, applying inequality A.5 in Appendix A, yields:

$$\frac{\alpha_{b,k}^{(\kappa)}(\mathbf{w})}{\beta_{b,k}^{(\kappa)}(\mathbf{w})} \geq \frac{\alpha_{b,k}^{(\kappa)}(\mathbf{w}^{(\kappa)})}{\beta_{b,k}^{(\kappa)}(\mathbf{w}^{(\kappa)})} \left(2\frac{\sum_{j\in\mathcal{K}\setminus\{k\}} \Re\{(\mathbf{w}_j^{(\kappa)})^H [(\boldsymbol{H}_k^{(\kappa)})^H]^2 \mathbf{w}_j\} + \sigma^2}{\alpha_{b,k}^{(\kappa)}(\mathbf{w}^{(\kappa)})} - \frac{\beta_{b,k}^{(\kappa)}(\mathbf{w})}{\beta_{b,k}^{(\kappa)}(\mathbf{w}^{(\kappa)})}\right), \tag{2.15}$$

which together with (2.14) gives the following upper bounding convex approximation of $a\sqrt{v_{b,k}^{(\kappa)}(\mathbf{w})}$:

$$a\sqrt{v_{b,k}^{(\kappa)}(\mathbf{w})} \;\leq\; a_{k,2}^{(\kappa)} - 2\sum_{j\in\mathcal{K}\setminus\{k\}} \Re\{\langle \boldsymbol{b}_{k,j}^{(\kappa)}, \mathbf{w}_j \rangle\} + c_{k,2}^{(\kappa)} \sum_{j=1}^{K} |\boldsymbol{H}_k^{(\kappa)} \mathbf{w}_j|^2, \tag{2.16}$$

for

$$a_{k,2}^{(\kappa)} \triangleq a\frac{\sqrt{v_{b,k}^{(\kappa)}(\mathbf{w}^{(\kappa)})}}{2}\left(1 + \frac{2}{v_{b,k}^{(\kappa)}(\mathbf{w}^{(\kappa)})}\right) + \sigma^2 \frac{\alpha_{b,k}^{(\kappa)}(\mathbf{w}^{(\kappa)})}{\beta_{b,k}^{(\kappa)}(\mathbf{w}^{(\kappa)})\sqrt{v_{b,k}^{(\kappa)}(\mathbf{w}^{(\kappa)})}}\left(\frac{-2}{\alpha_{b,k}^{(\kappa)}(\mathbf{w}^{(\kappa)})} + \frac{1}{\beta_{b,k}^{(\kappa)}(\mathbf{w}^{(\kappa)})}\right),$$

$$\boldsymbol{b}_{k,j}^{(\kappa)} \triangleq \frac{a}{\beta_{b,k}^{(\kappa)}(\mathbf{w}^{(\kappa)})\sqrt{v_{b,k}^{(\kappa)}(\mathbf{w}^{(\kappa)})}} (\boldsymbol{H}_k^{(\kappa)})^H \boldsymbol{H}_k^{(\kappa)} \mathbf{w}_j^{(\kappa)}, \quad j \in \mathcal{K}\setminus\{k\},$$

$$c_{k,2}^{(\kappa)} \triangleq a\frac{\alpha_{b,k}^{(\kappa)}(\mathbf{w}^{(\kappa)})}{(\beta_{b,k}^{(\kappa)}(\mathbf{w}^{(\kappa)}))^2\sqrt{v_{b,k}^{(\kappa)}(\mathbf{w}^{(\kappa)})}}.$$

The bounds (2.13) and (2.16) yield the following lower bounding concave approximation for $\hat{r}_{b,k}^{(\kappa)}(\mathbf{w})$ in (2.12):

$$\hat{r}_{b,k}^{(\kappa)}(\mathbf{w}) \geq a_k^{(\kappa)} + 2\sum_{j=1}^{K} \Re\{\langle \boldsymbol{b}_{k,j}^{(\kappa)}, \mathbf{w}_j \rangle - c_k^{(\kappa)} \sum_{j \in \mathcal{K}} |\boldsymbol{H}_k^{(\kappa)} \mathbf{w}_j|^2, \tag{2.17}$$

for $a_k^{(\kappa)} \triangleq a_{k,1}^{(\kappa)} - a_{k,2}^{(\kappa)}$, and $c_k^{(\kappa)} \triangleq c_{k,1}^{(\kappa)} + c_{k,2}^{(\kappa)}$.

We now generate $\mathbf{w}^{(\kappa+1)}$ as the optimal solution of the following problem:

$$\max_{\mathbf{w}} \ \hat{f}_b^{(\kappa)}(\mathbf{w}), \quad \text{s.t. } (2.6b), \tag{2.18}$$

where $\hat{f}_b^{(\kappa)}(\mathbf{w}) \triangleq \sum_{k=1}^{K} \gamma_k^{(\kappa)} a_k^{(\kappa)} + 2\sum_{k=1}^{K} \Re\{\langle \boldsymbol{b}_k^{(\kappa)}, \mathbf{w}_k \rangle\} - \sum_{k=1}^{K} (\mathbf{w}_k)^H \boldsymbol{\Psi}_b^{(\kappa)} \mathbf{w}_k$ with $\boldsymbol{b}_k^{(\kappa)} \triangleq \sum_{j=1}^{K} \gamma_j^{(\kappa)} \boldsymbol{b}_{j,k}^{(\kappa)}$, and $0 \preceq \boldsymbol{\Psi}_b^{(\kappa)} \triangleq \sum_{j=1}^{K} \gamma_j^{(\kappa)} c_j^{(\kappa)} (\boldsymbol{H}_j^{(\kappa)})^H \boldsymbol{H}_j^{(\kappa)}$. It can be readily checked that

$$\hat{f}^{(\kappa)}(\mathbf{w}^{(\kappa)}, \boldsymbol{\theta}^{(\kappa)}) = \hat{f}_b^{(\kappa)}(\mathbf{w}^{(\kappa)}). \tag{2.19}$$

The problem (2.18) admits the following closed-form solution:

$$\mathbf{w}_k^{(\kappa+1)} = \begin{cases} (\boldsymbol{\Psi}_b^{(\kappa)})^{-1} \boldsymbol{b}_k^{(\kappa)} & \text{if} \quad \sum_{k=1}^{K} ||(\boldsymbol{\Psi}_b^{(\kappa)})^{-1} \boldsymbol{b}_k^{(\kappa)}||^2 \leq P, \\ \left(\boldsymbol{\Psi}_b^{(\kappa)} + \mu \boldsymbol{I}_M\right)^{-1} \boldsymbol{b}_k^{(\kappa)} & \text{otherwise,} \end{cases} \tag{2.20}$$

where $\mu > 0$ is chosen by bisection such that $\sum_{k=1}^{K} || \left(\boldsymbol{\Psi}_b^{(\kappa)} + \mu \boldsymbol{I}_M\right)^{-1} \boldsymbol{b}_k^{(\kappa)}||^2 = P$.

It follows from (2.11) and (2.17) that $\hat{f}^{(\kappa)}(\mathbf{w}^{(\kappa+1)}, \boldsymbol{\theta}^{(\kappa)}) \geq \hat{f}_b^{(\kappa)}(\mathbf{w}^{(\kappa+1)})$, while $\hat{f}_b^{(\kappa)}(\mathbf{w}^{(\kappa+1)}) > \hat{f}_b^{(\kappa)}(\mathbf{w}^{(\kappa)}) = \hat{f}^{(\kappa)}(\mathbf{w}^{(\kappa)}, \boldsymbol{\theta}^{(\kappa)})$, because $\mathbf{w}^{(\kappa+1)}$ and $\mathbf{w}^{(\kappa)}$ represent the optimal solution and a feasible point for (2.18). We thus have (2.10) as sought.

2.1.2 Programmable Reflecting Elements' Descent Iteration

We seek the next iterative point $\theta^{(\kappa+1)}$ such that

$$\hat{f}^{(\kappa)}(\mathbf{w}^{(\kappa+1)}, \boldsymbol{\theta}^{(\kappa+1)}) > \hat{f}^{(\kappa)}(\mathbf{w}^{(\kappa+1)}, \boldsymbol{\theta}^{(\kappa)}). \tag{2.21}$$

Define $r_{p,k}^{(\kappa)}(\boldsymbol{\theta}) \triangleq r_k(\mathbf{w}^{(\kappa+1)}, \boldsymbol{\theta})$, $\upsilon_{p,k}^{(\kappa)}(\boldsymbol{\theta}) \triangleq \upsilon_k(\mathbf{w}^{(\kappa+1)}, \boldsymbol{\theta})$, $\hat{r}_{p,k}^{(\kappa)}(\boldsymbol{\theta}) \triangleq \hat{r}_k(\mathbf{w}^{(\kappa+1)}, \boldsymbol{\theta})$, $\alpha_{p,k}^{(\kappa)}(\boldsymbol{\theta}) \triangleq \alpha_k(\mathbf{w}^{(\kappa+1)}, \boldsymbol{\theta})$, $\beta_{p,k}^{(\kappa)}(\boldsymbol{\theta}) \triangleq \beta_k(\mathbf{w}^{(\kappa+1)}, \boldsymbol{\theta})$, $\upsilon_{p,k}^{(\kappa)}(\boldsymbol{\theta}) \triangleq \upsilon_k(\mathbf{w}^{(\kappa+1)}, \boldsymbol{\theta})$, and $\ell_{k,j}^{(\kappa)} \triangleq \boldsymbol{H}_k(\boldsymbol{\theta}^{(\kappa)}) \mathbf{w}_j^{(\kappa+1)}$,

$(k,j) \in \mathcal{K} \times \mathcal{K}$. As such,

$$\hat{f}^{(\kappa)}(\mathbf{w}^{(\kappa+1)}, \boldsymbol{\theta}) = \sum_{k=1}^{K} \gamma_k^{(\kappa)} \hat{r}_{p,k}^{(\kappa)}(\boldsymbol{\theta}), \tag{2.22}$$

and

$$\hat{r}_{p,k}^{(\kappa)}(\boldsymbol{\theta}) = r_{p,k}^{(\kappa)}(\boldsymbol{\theta}) - a\sqrt{v_{p,k}^{(\kappa)}(\boldsymbol{\theta})}. \tag{2.23}$$

Recall that $\boldsymbol{H}_{k,n}$ are defined in (2.1). The following lower bounding approximation of $r_{p,k}^{(\kappa)}(\boldsymbol{\theta})$ was obtained in [62]:

$$r_{p,k}^{(\kappa)}(\boldsymbol{\theta}) \;\geq\; \tilde{a}_{k,1}^{(\kappa)} + 2\Re\{\sum_{n=1}^{N} \tilde{\boldsymbol{b}}_{k,1}^{(\kappa)}(n) e^{\jmath\boldsymbol{\theta}_n}\} - \tilde{c}_{k,1}^{(\kappa)} (e^{\jmath\boldsymbol{\theta}})^H \boldsymbol{\Psi}_p^{(\kappa)} e^{\jmath\boldsymbol{\theta}}, \tag{2.24}$$

with $\tilde{a}_{k,1}^{(\kappa)} \triangleq r_{p,k}^{(\kappa)}(\boldsymbol{\theta}^{(\kappa)}) - g_k(\boldsymbol{\theta}^{(\kappa)}, \mathbf{w}^{(\kappa+1)}) - \sigma^2 \tilde{c}_{k,1}^{(\kappa)}$, $0 < \tilde{c}_{k,1}^{(\kappa)} \triangleq 1/\alpha_{p,k}^{(\kappa)}(\boldsymbol{\theta}^{(\kappa)}) - 1/\beta_{p,k}^{(\kappa)}(\boldsymbol{\theta}^{(\kappa)})$, and $\tilde{\boldsymbol{b}}_{k,1}^{(\kappa)}(n) \triangleq \dfrac{1}{\alpha_{p,k}^{(\kappa)}(\boldsymbol{\theta}^{(\kappa)})} (\ell_{k,k}^{(\kappa)})^H \boldsymbol{H}_{k,n} \mathbf{w}_k^{(\kappa+1)}$, $n = 1, \ldots N$, $\mathcal{W}^{(\kappa+1)} \triangleq \sum_{j=1}^{K} [\mathbf{w}_j^{(\kappa+1)}]^2$, $\boldsymbol{\Psi}_p^{(\kappa)}(n', n) \triangleq \langle \boldsymbol{H}_{k,n} \mathcal{W}^{(\kappa+1)} \boldsymbol{H}_{k,n'}^H \rangle$, $n' = 1, \ldots, N$; $n = 1, \ldots, N$.

Similarly to (2.16), we have

$$a\sqrt{v_{p,k}^{(\kappa)}(\boldsymbol{\theta})} \;\leq\; \tilde{a}_{k,2}^{(\kappa)} - 2\Re\{\sum_{n=1}^{N} \tilde{\boldsymbol{b}}_{k,2}^{(\kappa)}(n) e^{\jmath\boldsymbol{\theta}_n}\} + \tilde{c}_{k,2}^{(\kappa)} \sum_{j=1}^{K} (e^{\jmath\boldsymbol{\theta}})^H \boldsymbol{\Psi}_p^{(\kappa)} e^{\jmath\boldsymbol{\theta}}, \tag{2.25}$$

for $\tilde{a}_{k,2}^{(\kappa)} \triangleq a\frac{\sqrt{v_{p,k}^{(\kappa)}(\boldsymbol{\theta}^{(\kappa)})}}{2}\left(1 + \frac{2}{v_{p,k}^{(\kappa)}(\boldsymbol{\theta}^{(\kappa)})}\right) + \sigma^2 \frac{\alpha_{p,k}^{(\kappa)}(\boldsymbol{\theta}^{(\kappa)})}{\beta_{p,k}^{(\kappa)}(\boldsymbol{\theta}^{(\kappa)})\sqrt{v_{p,k}^{(\kappa)}(\boldsymbol{\theta}^{(\kappa)})}}\left(\frac{-2}{\alpha_{p,k}^{(\kappa)}(\boldsymbol{\theta}^{(\kappa)})} + \frac{1}{\beta_{p,k}^{(\kappa)}(\boldsymbol{\theta}^{(\kappa)})}\right)$, and $\tilde{\boldsymbol{b}}_{k,2}^{(\kappa)}(n) \triangleq \frac{a}{\beta_{p,k}^{(\kappa)}(\boldsymbol{\theta}^{(\kappa)})\sqrt{v_{p,k}^{(\kappa)}(\boldsymbol{\theta}^{(\kappa)})}} \sum_{j \in \mathcal{K}\setminus\{k\}} (\ell_{k,j}^{(\kappa)})^H \boldsymbol{H}_{k,n} \mathbf{w}_j^{(\kappa+1)}$, $n = 1, \ldots, N$, and $\tilde{c}_{k,2}^{(\kappa)} \triangleq a\frac{\alpha_{p,k}^{(\kappa)}(\boldsymbol{\theta}^{(\kappa)})}{(\beta_{p,k}^{(\kappa)}(\boldsymbol{\theta}^{(\kappa)}))^2\sqrt{v_{p,k}^{(\kappa)}(\boldsymbol{\theta}^{(\kappa)})}}$. Based on (2.24) and (2.25) we obtain the following lower bound:

$$\hat{r}_{p,k}^{(\kappa)}(\boldsymbol{\theta}) \geq \tilde{a}_k^{(\kappa)} + 2\Re\{\sum_{n=1}^{N} \tilde{\boldsymbol{b}}_k^{(\kappa)}(n) e^{\jmath\boldsymbol{\theta}_n}\} - \tilde{c}_k^{(\kappa)} (e^{\jmath\boldsymbol{\theta}})^H \boldsymbol{\Psi}_p^{(\kappa)} e^{\jmath\boldsymbol{\theta}}, \tag{2.26}$$

where $\tilde{a}_k^{(\kappa)} \triangleq \tilde{a}_{k,1}^{(\kappa)} - \tilde{a}_{k,2}^{(\kappa)}$, $\tilde{c}_k^{(\kappa)} \triangleq \tilde{c}_{k,1}^{(\kappa)} + \tilde{c}_{k,2}^{(\kappa)}$), and $\tilde{\boldsymbol{b}}_k^{(\kappa)} \triangleq \tilde{\boldsymbol{b}}_{k,1}^{(\kappa)} + \tilde{\boldsymbol{b}}_{k,2}^{(\kappa)}$. Then,

$$\hat{f}^{(\kappa)}(\mathbf{w}^{(\kappa+1)}, \boldsymbol{\theta}) \;\geq\; \tilde{a}^{(\kappa)} + 2\Re\{\sum_{n=1}^{N} \tilde{\boldsymbol{b}}^{(\kappa)}(n) e^{\jmath\boldsymbol{\theta}_n}\} - (e^{\jmath\boldsymbol{\theta}})^H \hat{\boldsymbol{\Psi}}_p^{(\kappa)} e^{\jmath\boldsymbol{\theta}}, \tag{2.27}$$

for $\tilde{a}^{(\kappa)} \triangleq \sum_{k=1}^{K} \gamma_k^{(\kappa)} \tilde{a}_k^{(\kappa)}$, $\tilde{\boldsymbol{b}}^{(\kappa)}(n) \triangleq \sum_{k=1}^{K} \gamma_k^{(\kappa)} \tilde{\boldsymbol{b}}_k^{(\kappa)}(n), n = 1, \ldots, N$, and $0 \preceq \hat{\boldsymbol{\Psi}}_p^{(\kappa)} \triangleq \left(\sum_{k=1}^{K} \gamma_k^{(\kappa)} \tilde{c}_k^{(\kappa)}\right) \boldsymbol{\Psi}_p^{(\kappa)}$. Furthermore, we have

$$\tilde{a}^{(\kappa)} + 2\Re\{\sum_{n=1}^{N} \tilde{\boldsymbol{b}}^{(\kappa)}(n) e^{\jmath\boldsymbol{\theta}_n}\} - (e^{\jmath\boldsymbol{\theta}})^H \hat{\boldsymbol{\Psi}}_p^{(\kappa)} e^{\jmath\boldsymbol{\theta}} \geq \hat{f}_p^{(\kappa)}(\boldsymbol{\theta}), \tag{2.28}$$

for $\hat{f}_p^{(\kappa)}(\boldsymbol{\theta}) \triangleq \tilde{a}^{(\kappa)}+2\Re\{\sum_{n=1}^{N}(\tilde{\boldsymbol{b}}^{(\kappa)}(n)-\sum_{m=1}^{N} e^{-\jmath\boldsymbol{\theta}_m^{(\kappa)}}\hat{\boldsymbol{\Psi}}_p^{(\kappa)}(m,n)+\lambda_{\max}(\hat{\boldsymbol{\Psi}}_p^{(\kappa)})e^{-\jmath\boldsymbol{\theta}_n^{(\kappa)}})e^{\jmath\boldsymbol{\theta}_n}\}-(e^{\jmath\boldsymbol{\theta}^{(\kappa)}})^H\hat{\boldsymbol{\Psi}}_p^{(\kappa)}e^{\jmath\boldsymbol{\theta}^{(\kappa)}} - 2\lambda_{\max}(\hat{\boldsymbol{\Psi}}_p^{(\kappa)})N$. We thus generate $\boldsymbol{\theta}^{(\kappa+1)}$ as the optimal solution of the problem

$$\max_{\boldsymbol{\theta}} \ \tilde{\hat{f}}_p^{(\kappa)}(\boldsymbol{\theta}), \tag{2.29}$$

which admits the closed-form solution[†] of

$$\boldsymbol{\theta}_n^{(\kappa+1)} =2\pi - \angle\left(\tilde{\boldsymbol{b}}^{(\kappa)}(n) - \sum_{m=1}^{N} e^{-\jmath\boldsymbol{\theta}_m^{(\kappa)}}\hat{\boldsymbol{\Psi}}_p^{(\kappa)}(m,n) + \lambda_{\max}(\hat{\boldsymbol{\Psi}}_p^{(\kappa)})e^{-\jmath\boldsymbol{\theta}_n^{(\kappa)}}\right), n=1,\ldots,N. \tag{2.30}$$

It follows from (2.28) that $\hat{f}^{(\kappa)}(\mathbf{w}^{(\kappa+1)},\boldsymbol{\theta}^{(\kappa+1)}) \geq \hat{f}_p^{(\kappa)}(\boldsymbol{\theta}^{(\kappa+1)}) \geq \tilde{\hat{f}}_p^{(\kappa)}(\boldsymbol{\theta}^{(\kappa+1)}) > \tilde{\hat{f}}_p^{(\kappa)}(\boldsymbol{\theta}^{(\kappa)}) = \hat{f}_p^{(\kappa)}(\boldsymbol{\theta}^{(\kappa)}) = \hat{f}^{(\kappa)}(\mathbf{w}^{(\kappa+1)},\boldsymbol{\theta}^{(\kappa)})$, confirming (2.21). Hence $\boldsymbol{\theta}^{(\kappa+1)}$ is a better feasible point than $\boldsymbol{\theta}^{(\kappa)}$.

2.1.3 Algorithm

Algorithm 2.1 URLLC GM-rate Descent Algorithm

1: **Initialisation:** Use the algorithm of [63] to initialise a feasible $(w^{(0)},\theta^{(0)})$. Set $\kappa=0$.

2: **κ-th iteration:** Generate $\mathbf{w}^{(\kappa+1)}$ by (2.20) and $\boldsymbol{\theta}^{(\kappa+1)}$ by (2.30). Given the convergence tolerance ν_t, stop if $|\hat{f}(\mathbf{w}^{(\kappa+1)},\boldsymbol{\theta}^{(\kappa+1)})-\hat{f}(\mathbf{w}^{(\kappa)},\boldsymbol{\theta}^{(\kappa)})|/\hat{f}(\mathbf{w}^{(\kappa)},\boldsymbol{\theta}^{(\kappa)}) \leq \nu_t$. Reset $\kappa \leftarrow \kappa+1$.

3: **Output** $(\mathbf{w}^{(\kappa)},\boldsymbol{\theta}^{(\kappa)})$ and URLLC rates $\hat{r}_k(\mathbf{w}^{(\kappa)},\boldsymbol{\theta}^{(\kappa)})$, $k \in \mathcal{K}$ with their GM $\left(\prod_{k=1}^{K}\hat{r}_k(\mathbf{w}^{(\kappa)},\boldsymbol{\theta}^{(\kappa)})\right)^{1/K}$.

Algorithm 2.1 provides the pseudo-code for the proposed steepest descent computational procedure of (2.6) as the iterations (2.20) and (2.30) seek a descent direction by seeking a better feasible point for the nonconvex problem (2.6).

[†] $[(\hat{\boldsymbol{\Psi}}_p^{(\kappa)} - \mu\boldsymbol{I}_N)e^{\jmath\boldsymbol{\theta}^{(\kappa)}}](n)$ is the n-th entry of $(\hat{\boldsymbol{\Psi}}_p^{(\kappa)} - \mu\boldsymbol{I}_N)e^{\jmath\boldsymbol{\theta}^{(\kappa)}}$

Remark 1: One can see that the above algorithm invokes the nonconvex problem (2.9) at each iteration, which is a problem of weighted sum rate maximisation associated with the weights $\gamma_k^{(\kappa)}$ iteratively updated according to (2.8), to generate a better feasible point.

Remark 2: While increasing the number of IRS elements N enhances beamforming flexibility and channel shaping capabilities, it also introduces significant scalability challenges. For $N > 256N$, the computational complexity of joint optimisation grows rapidly. This is the computational time that has very marginal if none on the communications latency. Moreover, channel estimation overhead becomes prohibitive because the number of parameters to estimate scales with N, requiring extensive pilot signalling and feedback. This overhead not only increases training time but also consumes valuable system resources, making real-time adaptation impractical for very large IRSs.

2.2 Numerical examples

This section evaluates the performance of the proposed algorithm using numerical examples. The set up is the same as that in [63]: the large-scale fading and the IRS-to-UE k path-loss is $\beta_{\text{R-k}} = G_{\text{IRS}} - 33.05 - 30\log_{10}(d_{\text{R-k}})$ dB, where $d_{\text{R-k}}$ is the distance between the IRS and UE k in meters, while G_{IRS} is the antenna gain of the IRS elements [70,83]. The large-scale fading and the path-loss between the BS and IRS is $\beta_{\text{B-R}} = G_{\text{BS}} + G_{\text{IRS}} - 35.9 - 22\log_{10}(d_{\text{B-R}})$ dB, where $d_{\text{B-R}}$ is the distance between the BS and IRS in meters, while G_{BS} is the BS antenna gain [70, 83]. The coordinates of the BS and the IRS are $(20, 0, 25)$ and $(0, 30, 40)$, while the users are randomly located in a $(60m \times 60m)$ area to the right of the BS and IRS. The entries of the BS-to-IRS LoS channel matrix are $[H_{B-R}]_{n,m} = e^{j\pi\left((n-1)\sin\overline{\theta}_n \sin\overline{\phi}_n + (m-1)\sin\theta_n \sin\phi_n\right)}$, where θ_n and ϕ_n are uniformly distributed over $(0, \pi)$ and $(0, 2\pi)$, and $\overline{\theta}_n = \pi - \theta_n$, $\overline{\phi}_n = \pi + \phi_n$. The small-scale fading channel gain $h_{\text{R-k}}$ follows the Rician distribution

having K-factor of 3. The spatial correlation matrix is $[R_{R-k}]_{n,n'} = e^{j\pi(n-n')\sin\tilde{\phi}\sin\tilde{\theta}}$, where $\tilde{\phi}$ and $\tilde{\theta}$ are the azimuth and elevation angle for UE k, respectively. Unless stated otherwise, the following parameters have been used in our simulation, $G_{\text{BS}} = G_{\text{IRS}} = 5$ dBi, $\mathcal{B} = 1$ Mhz, $\sigma^2 = -174$ dBm/Hz, $M = 10$, $K = 10$, $P = 20$ dBm, $N = 100$, $\epsilon^c = 10^{-5}$, and $t_t = 0.1$ ms which is suitable for URLLC transmission [2], and the choice of 1 ms end-to-end delay ensures having a quasi-static channel during URLLC communication [85]. The results are multiplied by $\log_2(e)$ to convert the unit nats/sec into the unit bps/Hz. Lastly we set the convergence tolerance ν_t to 10^{-3}.

Furthermore, we use the following terms for interpreting the results:

- LBR refers to the performance in the LBL regime [63].
- URLLC refers to the performance resulting from applying Algorithm 2.1.

The problem of maximising the sum rate (SR) can also be solved by Algorithm 2.1 upon setting $\gamma_k^{(\kappa)} \equiv 1$ in (2.8). Note that the maximisation of the SR represents the maximisation of the arithmetic mean (AM) of the users' rates (AM-rate) because the latter is defined as the former divided by K. Fig. 2.2 plots the AM-rate achieved by maximising the GM-rate and SR. As expected, the SR maximisation achieves better AM-rate than GM-rate maximisation. However, SR maximisation is unable to provide fairness for all the users, as it assigns some users having low channel quality zero rate, which can be seen in Fig. 2.3 that plots the ratio between the minimum user rate and the maximum user rate. As it can be seen, the RR under SR maximisation is always zero because SR maximisation cannot avoid having zero rate in either LBR or in URLLC. This remains the case even when the number M of transmit antennas is higher than the number K of users. By contrast, GM maximisation manages to assign nonzero rates to all the users, even when M is lower than K. This demonstrates that using GM rate maximisation is capable of

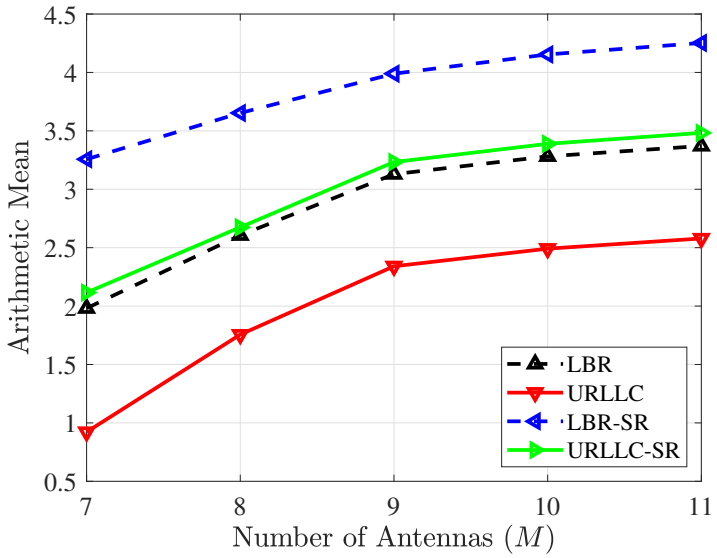

Figure 2.2 : AM-rate versus M.

improving all the users' rates. Furthermore, Fig. 4 portrays the users' rate variance (URV) versus M achieved by GM-rate maximisation and SR maximisation. As expected the URV attained by SR-maximisation is very high, as it tends to assign a high fraction of the total SR to a few users. By contrast, the URV of GM-rate maximisation is low and in fact it is not sensitive to the number M of transmit antennas.

Fig. 2.5 plots the GM rate versus M. As expected, the GM rate increases with M, since the system's ability to mitigate the multi user interference improves with M, especially when M is higher than or equal to K. The URLLC GM rate increases similarly to the LBR GM rate. However, the gap between the LBR-GM rate and the URLLC-GM rate does not decrease with increasing M.

Fig. 2.6 depicts the GM rate of LBR and URLLC versus P; observe that as anticipated the GM rate increases with P. Furthermore, the URLLC behaviour is similar to LBR with the gap between the rates being almost the same, which indicates that increasing P does not affect the overall URLLC rate.

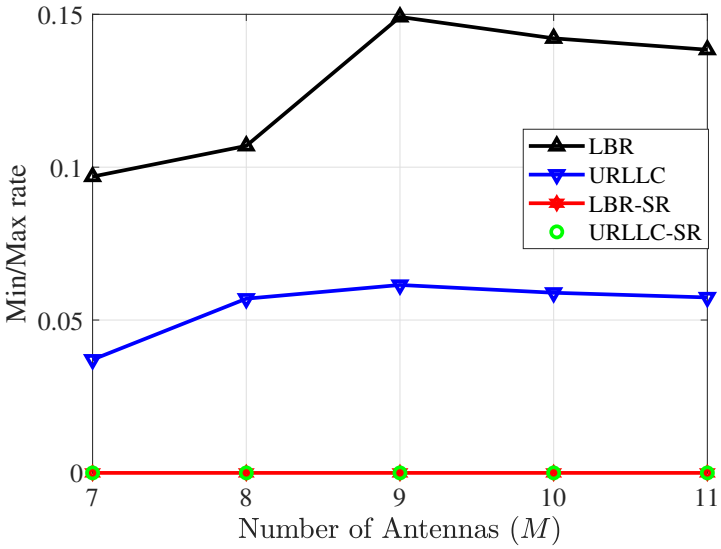

Figure 2.3 : The ratio of the highest and lowest users rates versus M.

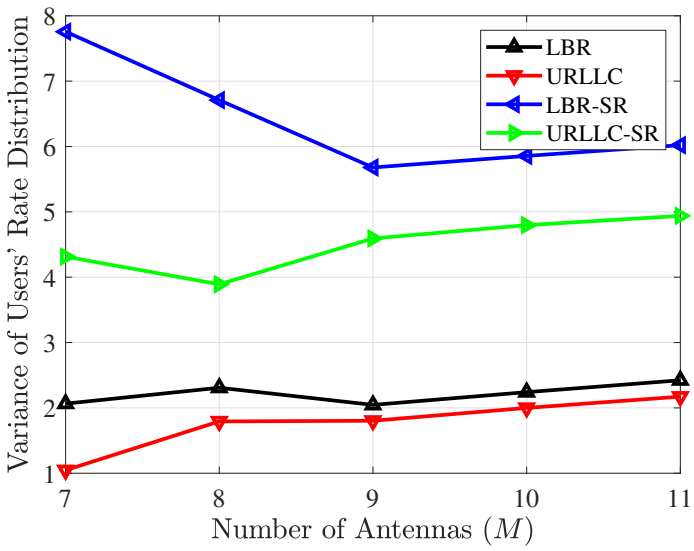

Figure 2.4 : Users' Rate variance versus M.

Fig. 2.7 portrays the URLLC-GM rate against t_t, which increases with t_t but the rate increase gradually slows down. Nevertheless, even for low t_t the system is still able to achieve a good rate, which represents the advantages of our algorithm. Note that the LBR assumes the transmission duration to be ∞, and therefore it serve

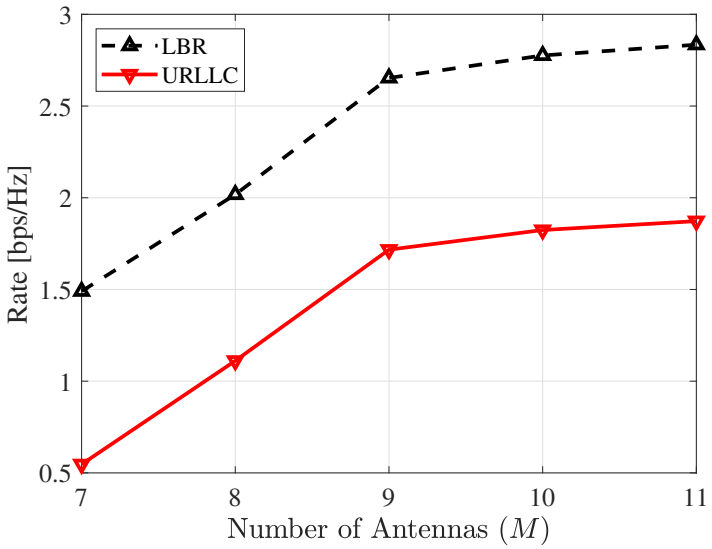

Figure 2.5 : GM Rate versus M.

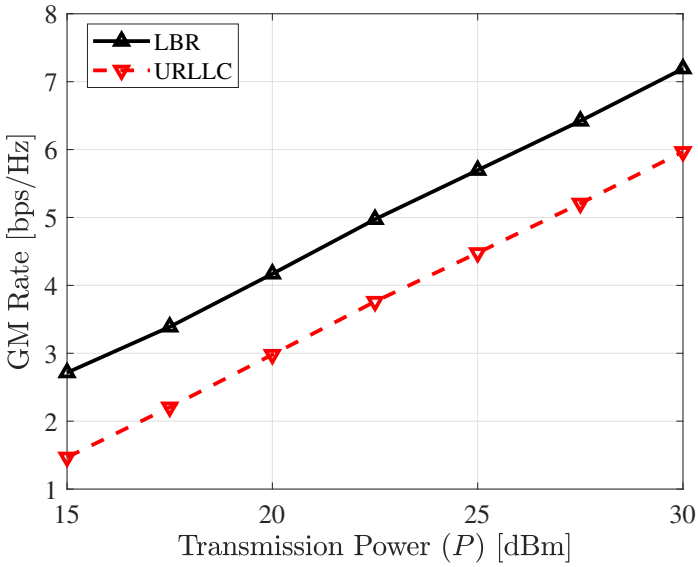

Figure 2.6 : GM rate versus P.

as an upper bound on the URLLC. Moreover Fig. 2.7 can be used for choosing t_t depending on the quality of service required.

Lastly, Fig. 2.8 plots the RR versus t_t. The SR maximisation in the FBL cannot avoid having zero rate even for long transmission duration of $t_t = 0.1$ ms, while GM

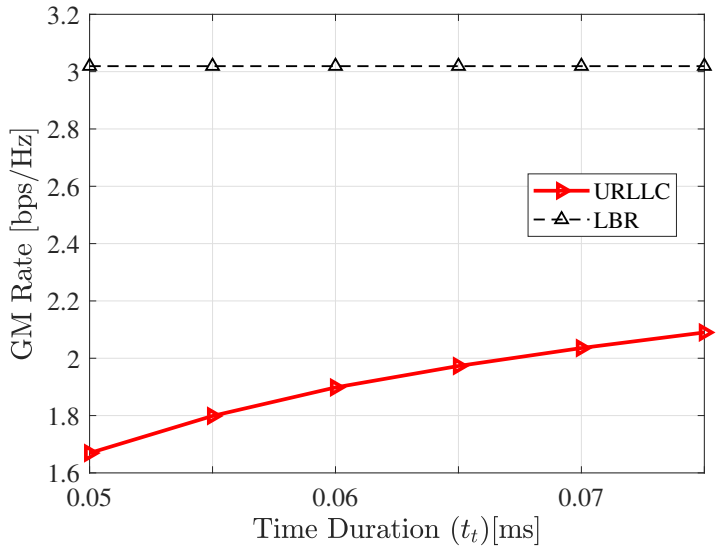

Figure 2.7 : GM rate versus t_t.

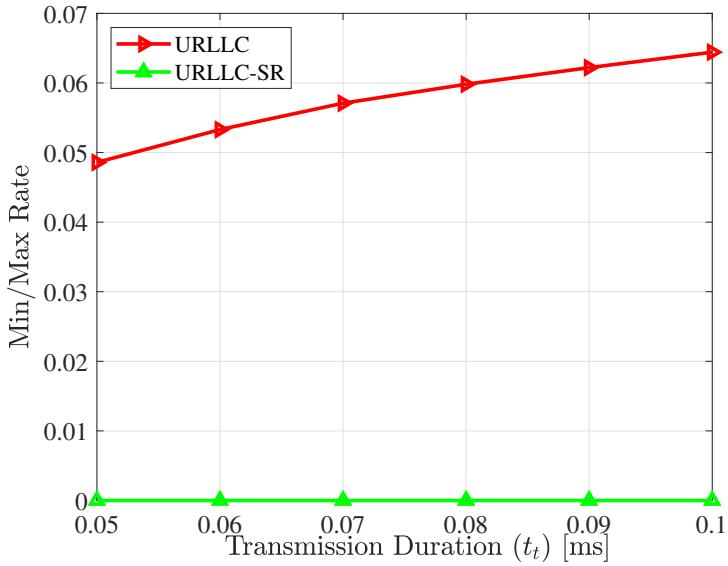

Figure 2.8 : The ratio of the highest and lowest users' rates versus t_t.

maximisation always assigns fair rates to all the users, regardless of the transmission duration t_t. Hence the advantage of using GM maximisation over SR maximisation becomes quite convincing.

2.3 Conclusions

This chapter has considered the joint design of transmit beamforming at the base station and IRS PREs for IRS-aid multi-user URLLC. To guarantee the required quality-of-service in terms of downlink throughput in FBL regime while maintaining computational tractability, we have developed an algorithm, which invokes closed-form expressions at each iteration for generating a better point for the maximising the geometric mean of the users' rates (GM-rate). The algorithm has been supported by simulations.

Chapter 3

Secure Communications For All Users in Low-Resolution IRS-aided Systems Under Imperfect and Unknown CSI

In this chapter*, we take the first step to guarantee secrecy for all the users where a low resolution intelligent reflecting surface (IRS) is used to enhance legitimate users' reception and thwart the potential eavesdropper (Eve) from intercepting. In real-life scenarios, due to hardware limitations of the IRS's passive reflective elements (PREs), the use of a full-resolution (continuous) phase shift (CPS) is impractical. In this paper, we thus consider a more practical case where the phase shift (PS) is modelled by a low-resolution (quantised) phase shift (QPS) while addressing the phase shift error (PSE) induced by the imperfect channel state information (CSI). To that end, we aim to maximise the minimum secrecy rate (SR) among *all the users* by jointly optimising the transmitter's beamforming vector and the IRS's passive reflective elements (PREs) under perfect/imperfect/unknown CSI. The resulting optimisation problem is nonconvex and even more complicated under imperfect/unknown CSI. To tackle it, we linearise the objective function and decompose the problem into sequential subproblems. When the perfect CSI is not available, we use the successive convex approximation (SCA) approach to transform imperfect CSI related semi-infinite constraints into finite linear matrix inequalities (LMI). We prove that our proposed algorithm converges to a locally optimal solution with low computational complexity thanks to our closed-form linearization approach. This

*This chapter corresponds to the journal paper J-2 and the conference paper C-1 in the list of Publications.

makes the solution scalable for large IRS deployments. Extensive simulations with practical settings show that our approach can ensure secure communication for all the users while the IRS's PREs are quantised and are affected by the PSE.

The remainder of this chapter is organised as follows. The system model is discussed in Sections 3.1. Then, Sections 3.2, 3.3, and 3.4 present the problem and corresponding solutions under prefect/imperfect/unknown CSI, respectively. The extensive simulations and discussion are in Section 3.5. Finally, Section 3.6 concludes the paper and discusses potential future directions.

3.1 System Model

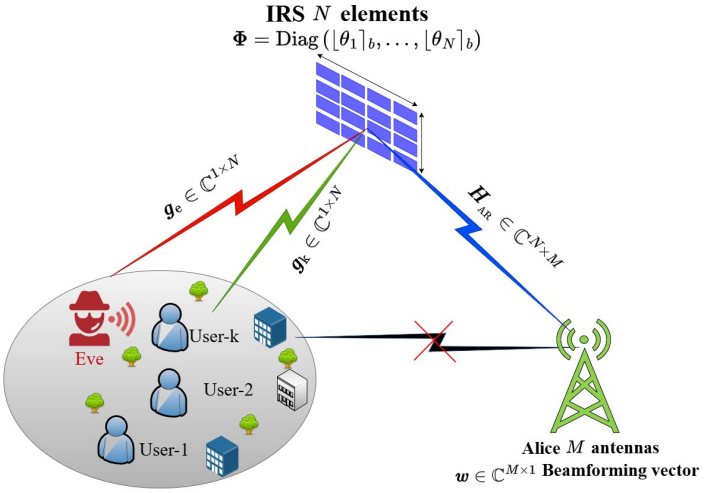

Figure 3.1 : Low-resolution IRS-aided system model.

We consider a downlink system aided by a low-resolution IRS as illustrated in Fig. 3.1. An M-antenna transmitter (Alice) transmits confidential messages to $\mathcal{K}$ single antenna legitimate users, while a single antenna eavesdropper (Eve) attempts to wiretap the transmission. To support the transmission between Alice and the users, an IRS with N PREs is deployed (e.g., at the facade of a building) to establish a link between Alice and the users. Let $k \triangleq \{1, 2, \ldots, K\}$ denote the set of legitimate users

and e denote Eve in the system. The direct channel from Alice to the users/Eve is denoted by $\boldsymbol{h}_{A_i} \triangleq \sqrt{\beta_{A_i}}\tilde{\boldsymbol{h}}_{A_i}$, where $\tilde{\boldsymbol{h}}_{A_i}$ is modelled by Rician fading, and $\sqrt{\beta_{A_i}}$ is the large scale fading from the Alice-to-users/Eve link, $\boldsymbol{H}_{\mathrm{AR}} \triangleq \sqrt{\beta_{\mathrm{AR}}}\tilde{\boldsymbol{H}}_{\mathrm{AR}} \in \mathbb{C}^{N\times M}$ denote the channel from Alice to the IRS, while $\tilde{\boldsymbol{H}}_{\mathrm{AR}}$ is modelled by Rician fading, and $\sqrt{\beta_{\mathrm{AR}}}$ is the large scale fading factor of the Alice-to-IRS link. The channel from the IRS to user k and to Eve is modelled by $\boldsymbol{g}_i \triangleq \sqrt{\beta_{\mathrm{R}i}}\tilde{\boldsymbol{g}}_i\mathcal{R}_{\mathrm{R}i}^{1/2} \in \mathbb{C}^{1\times N}$, where $i \in \{k, e\}$, $\beta_{\mathrm{R}i}$ is the large-scale fading factor of the IRS-to-i [86], $\tilde{\boldsymbol{g}}_i$ is modelled by Rician fading, and $\mathcal{R}_{\mathrm{R}i} \in \mathbb{C}^{N\times N}$ is the IRS elements' spatial correlation matrix [86]. For the confidential message intended for user k, s_k, the signal received by user k and Eve with corresponding to the intended user, respectively, can be expressed as:

$$y_i \triangleq \boldsymbol{h}_i(\boldsymbol{\theta})\sum\nolimits_{k=1}^{\mathcal{K}}\mathbf{w}_k s_k + n_i,\ i \in \{k, e\}, \tag{3.1}$$

where $\boldsymbol{h}_i(\boldsymbol{\theta}) \in \mathbb{C}^{1\times M}$ is the cascaded channel gain from Alice to $i \in \{k, e\}$, $\mathbf{w}_k \in \mathbb{C}^{M\times 1}$ represents the beamforming vector applied for user k, $\boldsymbol{\theta} \triangleq (\theta_1, \ldots, \theta_N)^T \in [0, 2\pi)^N$ denotes the IRS's PREs PS vector, n_i is the zero-mean Additive White Gaussian Noise (AWGN) with power σ_i for $i \in \{k, e\}$. The cascade channel gain $\boldsymbol{h}_i(\boldsymbol{\theta})$ from Alice to $i \in \{k, e\}$, can be expressed in terms of the direct channel gain from Alice to the IRS, and the channel gain from the IRS to the user or Eve as follows:

$$\boldsymbol{h}_i(\boldsymbol{\theta}) \triangleq \boldsymbol{g}_i\boldsymbol{\Phi}\boldsymbol{H}_{\mathrm{AR}} \triangleq \boldsymbol{g}_i\sum\nolimits_{n=1}^{N}\exp(j\theta_n)\Xi_n\boldsymbol{H}_{\mathrm{AR}}, \tag{3.2}$$

where $\boldsymbol{\Phi} \triangleq \mathrm{Diag}(e^{j\boldsymbol{\theta}})$, $\boldsymbol{\Xi}_n$ is an $N \times N$ matrix with all zeros except for its (n, n) entry which is 1.

Since the IRS is typically deployed at a known fixed location, such as the facade of a high-rise building, the CSI between Alice and the IRS can be accurately estimated by exploiting the angles of arrival and departure [77], or by employing advanced channel estimation techniques [87, 88]. However, obtaining the IRS-users' reflected channel's CSI is considerably more challenging due to the passive nature of the IRS and the mobility and dynamic environment of the users [89]. For Eve, pinpointing

its location or its accurate CSI is hardly possible. To address these uncertainties, we adopt a bounded CSI error model wherein the reflected channels from the IRS to the users and Eve are expressed as

$$\boldsymbol{g}_i \triangleq \widehat{\boldsymbol{g}}_i + \Delta\boldsymbol{g}_i, i \in \{k, e\}, \tag{3.3a}$$

$$\omega_i \triangleq \{\|\Delta\boldsymbol{g}_i\|_2 \leq \xi_i\}, i \in \{k, e\}, \tag{3.3b}$$

where $\hat{\boldsymbol{g}}_i$ denotes the (imperfect) estimated channel vector, $\Delta\boldsymbol{g}_i$ represents the channel estimation error of the corresponding estimation, ω_i is a set for all possible channel estimation errors, and ξ_i is the radii of the uncertainty regions as known to Alice. Hence, (5.4) can be reformulated as:

$$\widehat{\boldsymbol{h}}_i(\boldsymbol{\theta}) \triangleq (\widehat{\boldsymbol{g}}_i + \Delta\boldsymbol{g}_i)\,\boldsymbol{\Phi}\boldsymbol{H}_{\mathrm{AR}}. \tag{3.4}$$

Hence, the signal-to-interference-plus-noise ratio (SINR) of the received signal at the user-k and Eve, under perfect/imperfect CSI, can be expressed as:

$$\gamma_i(\mathbf{w}, \boldsymbol{\theta}) \triangleq \frac{|\boldsymbol{h}_i(\boldsymbol{\theta})\mathbf{w}_k|^2}{\rho_i(\mathbf{w}, \boldsymbol{\theta})},\ i \in \{k, e\}, \tag{3.5}$$

$$\widehat{\gamma}_i(\mathbf{w}, \boldsymbol{\theta}) \triangleq \frac{|\widehat{\boldsymbol{h}}_i(\boldsymbol{\theta})\mathbf{w}_k|^2}{\widehat{\rho}_i(\mathbf{w}, \boldsymbol{\theta})},\ i \in \{k, e\}, \tag{3.6}$$

where $\rho_i(\mathbf{w}, \boldsymbol{\theta}) \triangleq \sum_{j=1, j\neq k}^{\mathcal{K}} |\boldsymbol{h}_i(\boldsymbol{\theta})\mathbf{w}_j|^2 + \sigma_i^2$, and $\widehat{\rho}_i(\mathbf{w}, \boldsymbol{\theta}) \triangleq \sum_{j=1, j\neq k}^{\mathcal{K}} |\widehat{\boldsymbol{h}}_i(\boldsymbol{\theta})\mathbf{w}_j|^2 + \sigma_i^2$. However, in a low-resolution IRS-aided system with imperfect CSI from the IRS to the users/Eve, the IRS PREs are affected by PSE [56]. Thus, in the following, we consider three cases to model the IRS's PREs as:

- The CPS adjustment at the IRS; this is the ideal case when the IRS PREs can be modelled by a continuous PS.
- The low resolution/QPS at the IRS; where the PS can be modelled by a uniform distribution in $\lfloor\boldsymbol{\theta}\rceil_b \in [\frac{-\pi}{2^b}, \frac{\pi}{2^b})$, where b is the number of bits in the QPS modulation.

- with imperfect/unknown CSI, and when only a discrete set of 2^b phases can be configured; this leads to a PSE ϵ_R which can be approximated by a uniform distribution in $[-2^{-b}\pi, 2^{-b}\pi)$, hence, (3.1) can be reformulated as:

$$\boldsymbol{h}_i(\lfloor\boldsymbol{\theta}\rceil_b) \triangleq \boldsymbol{g}_i \text{Diag}(e^{j(\lfloor\boldsymbol{\theta}\rceil_b+\epsilon_R)})\boldsymbol{H}_{\text{AR}}. \tag{3.7}$$

In the sequel, we consider both perfect and imperfect CSI scenarios for the IRS to the users and Eve. In the latter, only partial or estimated CSI $\widehat{\boldsymbol{g}}_i$ is available. To capture different levels of CSI imperfection, one can vary the magnitude of $\Delta\boldsymbol{g}_i$, i.e., the radii ξ_i of the uncertainty region. In a more extreme scenario, we assume that Alice has access only to imperfect IRS-to-users CSI, while the CSI of Eve remains completely unknown to Alice.

Under the presence of Eve, the closed-form expression for the SR of the user-k under perfect/imperfect/unknown IRS to users/Eve CSI is defined as [90]:

$$\text{SR}_k(\mathbf{w}, \lfloor\boldsymbol{\theta}\rceil_b) \triangleq [C_k(\mathbf{w}, \boldsymbol{\theta}) - C_e(\mathbf{w}, \boldsymbol{\theta})]^+, \tag{3.8}$$

$$\widehat{\text{SR}}_k(\mathbf{w}, \lfloor\boldsymbol{\theta}\rceil_b) \triangleq [\widehat{C}_k(\mathbf{w}, \boldsymbol{\theta}) - \widehat{C}_e(\mathbf{w}, \boldsymbol{\theta})]^+, \tag{3.9}$$

where $[x]^+ \triangleq \max[0, x]$, the user-$k$ data rate, and the eavesdropping rate under perfect/imperfect CSI are defined as [90]:

$$C_i(\mathbf{w}, \lfloor\boldsymbol{\theta}\rceil_b) \triangleq \ln\left(1 + \gamma_i(\mathbf{w}, \boldsymbol{\theta})\right), i \in \{k, e\}, \tag{3.10}$$

$$\widehat{C}_i(\mathbf{w}, \lfloor\boldsymbol{\theta}\rceil_b) \triangleq \ln\left(1 + \widehat{\gamma}_i(\mathbf{w}, \boldsymbol{\theta})\right), i \in \{k, e\}. \tag{3.11}$$

3.2 Minimum user's SR Maximisation Under Perfect CSI

3.2.1 MAXMIN SR Under Perfect CSI

In this section, we first address the problem of maximising the minimum SR among all the users, under the perfect CSI assumption, to guarantee secure communications for all the users. The optimisation problem can be formally stated as

$$(\mathcal{P}1): \max_{\mathbf{w},\lfloor\boldsymbol{\theta}\rceil_b} \min_{k\in\mathcal{K}} \mathrm{SR}_k(\mathbf{w}, \lfloor\boldsymbol{\theta}\rceil_b), \tag{3.12a}$$

$$\text{s.t.} \quad \sum\nolimits_{k=1}^{\mathcal{K}} \|\mathbf{w}_k\|^2 \leq P_T, \tag{3.12b}$$

$$|e^{(j\lfloor\boldsymbol{\theta}\rceil_b)}| = 1, \tag{3.12c}$$

where P_T is the transmit power, (3.12b) captures the sum of the transmitted power constraint, and (3.12c), captures the UMC of the PREs' PS.

The optimisation problem $(\mathcal{P}1)$ is nonconvex since the objective function (3.12a) is nonlinear and not concave, and the UMC (3.12c) is nonconvex. Moreover, the coupling between $\mathbf{w}$ and $\lfloor\boldsymbol{\theta}\rceil_b$ within the objective function (3.12a) further complicates solving problem $(\mathcal{P}1)$. To address this coupling, one can employ the AO technique [91]. Specifically, at iteration (ι), the feasible point $(\mathbf{w}^{(\iota)}, \lfloor\boldsymbol{\theta}^{(\iota)}\rceil_b)$ is generated from $(\mathcal{P}1)$ by solving two sub-problems. Firs, we tackle the subproblem by optimising $\mathbf{w}$ with a fixed $\lfloor\boldsymbol{\theta}\rceil_b$,

$$(\mathcal{P}1.1): \max_{\mathbf{w}} \min_{k} \mathrm{SR}_k(\mathbf{w}, \lfloor\boldsymbol{\theta}^{(\iota)}\rceil_b), \text{ s.t. } (3.12b),$$

then, we optimise $\lfloor\boldsymbol{\theta}\rceil_b$ with a fixed $\mathbf{w}$ by solving the following AO problem,

$$(\mathcal{P}1.2): \max_{\lfloor\boldsymbol{\theta}\rceil_b} \min_{k} \mathrm{SR}_k(\mathbf{w}^{(\iota+1)}, \lfloor\boldsymbol{\theta}\rceil_b), \text{ s.t. } (3.12c).$$

However, the AO approach requires solving two subproblems $(\mathcal{P}1.1)$ and $(\mathcal{P}1.2)$, which are computationally demanding, particularly due to the large number of PREs of the IRS. To address this, we propose a linearization method employing mathematically tractable approximation functions, leading to a computationally efficient algorithm that is able to handle a large number of IRSs' PREs.

Sub-Problem for Optimising the Beamforming Vectors

We fix the quantised $\lfloor\boldsymbol{\theta}\rceil_b$ given $\mathbf{w}^{(\iota)}$ and solve the problem ($\mathcal{P}1.1$) to obtain $\mathbf{w}^{(\iota+1)}$ satisfying $\mathrm{SR}_k(\mathbf{w}^{(\iota+1)}, \lfloor\boldsymbol{\theta}^{(\iota)}\rceil_b) > \mathrm{SR}_k(\mathbf{w}^{(\iota)}, \lfloor\boldsymbol{\theta}^{(\iota)}\rceil_b)$. We begin by linearizing the objective function in (5.17a), which comprises two parts: the data rate of user-k and Eve's negative eavesdropping rate. First, we transform the user-k's data rate into a linear form. Specifically, applying the inequality (A.1) in Appendix A, we define $\boldsymbol{\Lambda} \triangleq \boldsymbol{h}_k(\lfloor\boldsymbol{\theta}\rceil_b^{(\iota)})\mathbf{w}_k$, $\boldsymbol{\digamma} \triangleq \rho_k(\mathbf{w}, \lfloor\boldsymbol{\theta}^{(\iota)}\rceil_b)$, $\hat{\Lambda} \triangleq \boldsymbol{h}_k(\lfloor\boldsymbol{\theta}\rceil_b^{(\iota)})\mathbf{w}_k^{(\iota)}$ and $\hat{\boldsymbol{\digamma}} \triangleq \rho_k(\mathbf{w}^{(\iota)}, \lfloor\boldsymbol{\theta}\rceil_b^{(\iota)})$, hence, the users' data rate (3.10) can be written as:

$$C_k(\mathbf{w}, \lfloor\boldsymbol{\theta}^{(\iota)}\rceil_b) \geq q_{1,k}^{(\iota)} + 2\Re\left\{\left\langle \boldsymbol{m}_{k,k}^{(\iota)}, \mathbf{w}_k \right\rangle\right\} - n_{1,k}^{(\iota)} \upsilon_k^{(\iota)}, \tag{3.13}$$

where,

$$\begin{aligned}
\upsilon_k^{(\iota)} &\triangleq \sum\nolimits_{j=1}^{\mathcal{K}} |\boldsymbol{h}_k(\lfloor\boldsymbol{\theta}^{(\iota)}\rceil_b)\mathbf{w}_j|^2 + \sigma_k^2, \\
q_{1,k}^{(\iota)} &\triangleq C_k(\mathbf{w}, \lfloor\boldsymbol{\theta}^{(\iota)}\rceil_b) - \gamma_k(\mathbf{w}, \lfloor\boldsymbol{\theta}^{(\iota)}\rceil_b) - \sigma_k^2 n_{1,k}, \\
\boldsymbol{m}_{k,k}^{(\iota)} &\triangleq (\boldsymbol{h}_k^H(\lfloor\boldsymbol{\theta}^{(\iota)}\rceil_b)\boldsymbol{h}_k(\lfloor\boldsymbol{\theta}^{(\iota)}\rceil_b)\mathbf{w}_k)/(\rho_k^{(\iota)}), \\
n_{1,k}^{(\iota)} &\triangleq 1/\rho_k^{(\iota)} - 1/\upsilon_k^{(\iota)}.
\end{aligned}$$

Second, we tackle the nonlinear Eve's negative eavesdropping rate, which can be expressed as:

$$-\ln(1+\gamma_e(\mathbf{w}, \lfloor\boldsymbol{\theta}^{(\iota)}\rceil_b)) \triangleq \overbrace{\ln(1+\rho_e^{(\iota)})}^{a_1} - \overbrace{\ln(1+\upsilon_e^{(\iota)})}^{a_2}, \tag{3.14}$$

where $\upsilon_e^{(\iota)} \triangleq \sum_{j=1}^{\mathcal{K}} |\boldsymbol{h}_e(\lfloor\boldsymbol{\theta}^{(\iota)}\rceil_b)\mathbf{w}_j|^2 + \sigma_e^2$. To linearise the term (a_1) in (5.21), we adopt the idea in [92]. The term (a_1) in (3.14) can be linearised by introducing the auxiliary function $\boldsymbol{z} \triangleq \rho_e^{(\iota)}$, which is then incorporated into inequality (A.2) in Appendix A. The term (a_2) in (3.14) can be linearised by defining $\boldsymbol{\Upsilon} \triangleq \upsilon_e^{(\iota)}$ and substituting it in the inequality (A.3) in Appendix A.

Hence, Eve's eavesdropping rate can be expressed as:

$$C_e(\mathbf{w}, \lfloor \boldsymbol{\theta}^{(\iota)} \rceil_b) \geq q_{1,k_e}^{(\iota)} + 2\Re \sum_{j=1, j\neq k}^{K} \left\{ \left\langle \boldsymbol{m}_{j,k_e}^{(\iota)}, \mathbf{w}_j \right\rangle \right\} - \frac{\rho_e^{(\iota)}}{1+\rho_e^{(\iota)}} \left(\sum_{j=1, j\neq k}^{K} |\boldsymbol{h}_e(\lfloor \boldsymbol{\theta}^{(\iota)} \rceil_b)\mathbf{w}_j|^2 \right) - \frac{1}{\upsilon_e^{(\iota)}} \sum_{j=1}^{K} |\boldsymbol{h}_e(\lfloor \boldsymbol{\theta}^{(\iota)} \rceil_b)\mathbf{w}_j|^2, \tag{3.15}$$

where,

$$\begin{aligned} q_{1,k_e}^{(\iota)} &\triangleq \ln\left(\rho_e^{(\iota)}\right) - \rho_e^{(\iota)} - \ln\left(\upsilon_e^{(\iota)}\right) + n_{1,k_e}^{(\iota)} + 1, \\ n_{1,k_e}^{(\iota)} &\triangleq \left(-\frac{\rho_e^{(\iota)}}{1+\rho_e^{(\iota)}} - \frac{1}{\upsilon_e^{(\iota)}} \right) \sigma_e^2, \\ \boldsymbol{m}_{j,k_e}^{(\iota)} &\triangleq \boldsymbol{h}_e^H(\boldsymbol{\theta}^{(\iota)}) \boldsymbol{h}_e(\boldsymbol{\theta}^{(\iota)}) \mathbf{w}_j^{(\iota)}. \end{aligned}$$

By substituting (3.13) and (3.15) into (3.8), we can express the approximate surrogate SR as

$$\mathrm{SR}_k(\mathbf{w}, \lfloor \boldsymbol{\theta}^{(\iota)} \rceil_b) \geq q_k^{(\iota)} + 2\Re \left\{ \left\langle \boldsymbol{m}_k^{(\iota)}, \mathbf{w}_k \right\rangle \right\} - (\mathbf{w}_k)^H \boldsymbol{\psi}_k^{(\iota)} \mathbf{w}_k, \tag{3.16}$$

where,

$$\begin{aligned} \boldsymbol{\psi}_k^{(\iota)} &\triangleq \sum_{j=1}^{\mathcal{K}} n_{1,k}^{(\iota+1)} \boldsymbol{h}_k^H(\lfloor \boldsymbol{\theta}^{(\iota)} \rceil_b) \boldsymbol{h}_k(\lfloor \boldsymbol{\theta}^{(\iota)} \rceil_b) + \frac{\rho_e^{(\iota)}}{1+\rho_e^{(\iota)}} \sum_{j=1, j\neq k}^{\mathcal{K}} \boldsymbol{h}_e^H(\lfloor \boldsymbol{\theta}^{(\iota)} \rceil_b) \boldsymbol{h}_e(\lfloor \boldsymbol{\theta}^{(\iota)} \rceil_b) \\ &\quad + \frac{1}{\upsilon_e^{(\iota)}} \sum_{j=1}^{\mathcal{K}} \boldsymbol{h}_e^H(\lfloor \boldsymbol{\theta}^{(\iota)} \rceil_b) \boldsymbol{h}_e(\lfloor \boldsymbol{\theta}^{(\iota)} \rceil_b), \\ q_k^{(\iota)} &\triangleq q_{1,k}^{(\iota)} + q_{1,ke}^{(\iota)} + n_{1,ke}^{(\iota)}, \\ \boldsymbol{m}_k^{(\iota)} &\triangleq \boldsymbol{m}_{k,k}^{(\iota)} + \sum\nolimits_{j=1, j\neq k}^{\mathcal{K}} \tilde{\boldsymbol{m}}_{j,k}^{(\iota)}, \\ \tilde{\boldsymbol{m}}_{j,k}^{(\iota)} &\triangleq \boldsymbol{h}_e^H(\lfloor \boldsymbol{\theta}^{(\iota)} \rceil_b) \boldsymbol{h}_e(\lfloor \boldsymbol{\theta}^{(\iota)} \rceil_b) \mathbf{w}_j. \end{aligned}$$

Finally, with (3.16), problem ($\mathcal{P}1.1$) can be reformulated as the following problem:

$$(\mathcal{P}1.3) : \max_{\mathbf{w}} \Gamma, \tag{3.17a}$$

$$\text{s.t.} \qquad \Gamma \leq \mathrm{SR}_k(\mathbf{w}, \lfloor \boldsymbol{\theta}^{(\iota)} \rceil_b), \ \forall k, \tag{3.17b}$$

$$(3.12\text{b}), \tag{3.17c}$$

where Γ is an auxiliary variable as the lower bound of the SR. Problem ($\mathcal{P}1.3$) is an SDP problem characterised by the linearised objective function (3.16). This problem can be efficiently solved using standard convex optimisation solvers, such as the interior-point method or the CVX toolbox [93].

Sub-Problem for Optimising the PREs

Similarly, by fixing $\mathbf{w}$, we seek $\lfloor\boldsymbol{\theta}\rceil_b^{(\iota+1)}$ such that,

$$\mathrm{SR}_k(\mathbf{w}_k^{(\iota+1)}, \lfloor\boldsymbol{\theta}^{(\iota+1)}\rceil_b) > \mathrm{SR}_k(\mathbf{w}_k^{(\iota+1)}, \lfloor\boldsymbol{\theta}^{(\iota)}\rceil_b).$$

Following the same method in the previous section, and using the inequality (A.1) in Appendix A the user's data rate lower bound approximation can be expressed as:

$$C_k(\mathbf{w}^{(\iota+1)}, \lfloor\boldsymbol{\theta}\rceil_b) \geq q_{1,k}^{(\iota+1)} + 2\Re\left\{\sum\nolimits_{n=1}^{N} \boldsymbol{m}_{k,k}^{(\iota+1)}(n) e^{j\lfloor\theta_n\rceil_b}\right\} + \left(e^{j\lfloor\boldsymbol{\theta}\rceil_b}\right)^H \boldsymbol{\varphi}_{1,k}^{(\iota+1)} e^{j\lfloor\boldsymbol{\theta}\rceil_b}, \tag{3.18}$$

where,

$$\begin{aligned}
q_{1,k}^{(\iota+1)} &\triangleq C_k(\mathbf{w}^{(\iota+1)}, \lfloor\boldsymbol{\theta}^{(\iota)}\rceil_b) - \gamma_k(\mathbf{w}^{(\iota+1)}, \lfloor\boldsymbol{\theta}^{(\iota)}\rceil_b) - \sigma_k^2 n_{1,k}^{(\iota+1)},\\
n_{1,k}^{(\iota+1)} &\triangleq 1/\rho_k^{(\iota+1)} - 1/\upsilon_k^{(\iota+1)},\\
\boldsymbol{m}_{k,k}^{(\iota+1)}(n) &\triangleq \hat{\boldsymbol{m}}_{k,k}^{(\iota+1)}(n)/\rho_k^{(\iota+1)},\\
\hat{\boldsymbol{m}}_{k,k}^{(\iota+1)}(n) &\triangleq \left(\mathbf{w}_k^{(\iota+1)}\right)^H \boldsymbol{h}_k^H(\lfloor\boldsymbol{\theta}^{(\iota)}\rceil_b)\boldsymbol{g}_k \boldsymbol{\Xi}_n \boldsymbol{H}_{\mathrm{AR}} \mathbf{w}_k^{(\iota+1)},\\
\boldsymbol{\varphi}_{1,k}^{(\iota+1)} &\triangleq -n_{1,k}^{(\iota+1)} \sum\nolimits_{j=1}^{\mathcal{K}} \boldsymbol{\varphi}_{k,j}^{(\iota+1)},\\
\boldsymbol{\varphi}_{k,j}^{(\iota+1)} &\triangleq \left(\boldsymbol{\aleph}_{k,j}^{(\iota+1)}(n)\right)^* \boldsymbol{\aleph}_{k,j}^{(\iota+1)}(m),\ n \in N, m \in N,\\
\boldsymbol{\aleph}_{k,j}^{(\iota+1)}(n) &\triangleq \boldsymbol{g}_k \boldsymbol{\Xi}_n \boldsymbol{H}_{\mathrm{AR}} \mathbf{w}_j^{(\iota+1)}.
\end{aligned}$$

Similarly, we can express Eve's eavesdropping rate as:

$$\begin{aligned}
C_e(\mathbf{w}^{(\iota+1)}, \lfloor\boldsymbol{\theta}\rceil_b) \geq\ & q_{1,k_e}^{(\iota+1)} + 2\Re\left\{\sum\nolimits_{n=1}^{N} \boldsymbol{m}_{k_e}^{(\iota+1)}(n) e^{(j\lfloor\theta_n\rceil_b)}\right\} + \left(e^{j\boldsymbol{\theta}}\right)^H \boldsymbol{\varphi}_{1,k_e}^{(\iota+1)} e^{j\lfloor\boldsymbol{\theta}\rceil_b}\\
&+ \left(e^{j\lfloor\boldsymbol{\theta}\rceil_b}\right)^H \boldsymbol{\varphi}_{1,k_e}^{(\iota+1)} e^{j\lfloor\boldsymbol{\theta}\rceil_b},
\end{aligned} \tag{3.19}$$

where,

$$
\begin{aligned}
q_{1,k_e}^{(\iota+1)} &\triangleq \ln\left(\rho_e^{(\iota+1)}\right) - \rho_e^{(\iota+1)} - \ln\left(\upsilon_e^{(\iota+1)}\right) + n_{1,k_e}^{(\iota+1)} + 1,\\
n_{1,k_e}^{(\iota+1)} &\triangleq \left(-\frac{\rho_e^{(\iota+1)}}{1+\rho_e^{(\iota+1)}} - \frac{1}{\upsilon_e^{(\iota+1)}}\right)\sigma_e^2,\\
\boldsymbol{m}_{k_e}^{(\iota+1)}(n) &\triangleq \sum\nolimits_{j=1,j\neq k}^{\mathcal{K}} \boldsymbol{m}_{j,k_e}^{(\iota+1)}(n),\\
\boldsymbol{m}_{j,k_e}^{(\iota+1)}(n) &\triangleq \left(\mathbf{w}_k^{(\iota+1)}\right)^H \boldsymbol{h}_e^H(\lfloor\boldsymbol{\theta}^{(\iota)}\rceil_b)\boldsymbol{g}_e\boldsymbol{\Xi}_n\boldsymbol{H}_{\text{AR}}\mathbf{w}_k^{(\iota+1)},\\
\boldsymbol{\varphi}_{1,k_e}^{(\iota+1)} &\triangleq \left(\frac{-\rho_e^{(\iota+1)}}{(1+\rho_e^{(\iota+1)})} - \frac{1}{(\sigma_e^2+\upsilon_e^{(\iota+1)})}\right)\left(\sum_{j=1}^{\mathcal{K}}\boldsymbol{\varphi}_{k_e,j}^{(\iota+1)}\right),\\
\boldsymbol{\varphi}_{k_e,j}^{(\iota+1)} &\triangleq \left(\boldsymbol{\aleph}_{k_e,j}^{(\iota+1)}(n)\right)^* \boldsymbol{\aleph}_{k_e,j}^{(\iota+1)}(m),\\
\boldsymbol{\aleph}_{k_e,j}^{(\iota+1)}(n) &\triangleq \boldsymbol{g}_e\boldsymbol{\Xi}_n\boldsymbol{H}_{\text{AR}}\mathbf{w}_j^{(\iota+1)}.
\end{aligned}
$$

By combining (3.18) and (3.19) into (3.8), we can express the closed-form SR as:

$$
\text{SR}_k(\mathbf{w}^{(\iota+1)}, \lfloor\boldsymbol{\theta}\rceil_b) \geq q_k^{(\iota+1)} + 2\sum\nolimits_{n=1}^{N}\Re\left\{\boldsymbol{m}_k^{(\iota+1)}(n)e^{j\lfloor\theta_n\rceil_b}\right\}, \tag{3.20}
$$

where,

$$
\begin{aligned}
q_k^{(\iota+1)} &\triangleq q_{1,k}^{(\iota+1)} + q_{1,ke}^{(\iota+1)} - \left(e^{j\lfloor\boldsymbol{\theta}^{(\iota)}\rceil_b}\right)^H \tilde{\boldsymbol{\varphi}}_k^{(\iota+1)} e^{j\lfloor\boldsymbol{\theta}^{(\iota)}\rceil_b} - 2\lambda_{\max}\left(\tilde{\boldsymbol{\varphi}}_k^{(\iota+1)}\right)N,\\
\boldsymbol{m}_k^{(\iota+1)}(n) &\triangleq \hat{\boldsymbol{m}}_{k,k}^{(\iota+1)}(n) + \tilde{\boldsymbol{m}}_k^{(\iota+1)}(n) + \sum\nolimits_{m=1}^{N} e^{-j\lfloor\theta_m^{(\iota)}\rceil_b}\tilde{\boldsymbol{\varphi}}_k^{(\iota+1)}(m,n) + \lambda_{\max}\left(\tilde{\boldsymbol{\varphi}}_k^{(\iota+1)}\right),\\
\boldsymbol{\varphi}_k^{(\iota+1)} &\triangleq \boldsymbol{\varphi}_{1,k}^{(\iota+1)} + \boldsymbol{\varphi}_{1,k_e}^{(\iota+1)} + \boldsymbol{\varphi}_{k_e,j}^{(\iota+1)}.
\end{aligned}
$$

With (3.20), we formulate the following optimisation problem to obtain $\lfloor\boldsymbol{\theta}^{(\iota+1)}\rceil_b$:

$$
(\mathcal{P}1.4): \max_{\lfloor\boldsymbol{\theta}\rceil_b} \min_{k\in\mathcal{K}} \text{SR}_k\left(\mathbf{w}^{(\iota+1)}, \lfloor\boldsymbol{\theta}^{(\iota)}\rceil_b\right), \tag{3.21a}
$$

$$
\text{s.t.} \quad (3.12\text{c}). \tag{3.21b}
$$

To tackle problem $(\mathcal{P}1.4)$ we define

$$
\lfloor\theta_n\rceil_b^{(\iota+1),k} = 2\pi - \angle\boldsymbol{m}_k^{(\iota+1)}(n), n = 1,\ldots,N, \tag{3.22}
$$

then we find $\lfloor\boldsymbol{\theta}^{(\iota+1)}\rceil_b$ that maximise the $\text{SR}(\mathbf{w}^{(\iota+1)}, \lfloor\boldsymbol{\theta}\rceil_b)$ as:

$$
\lfloor\boldsymbol{\theta}^{(\iota+1)}\rceil_b \triangleq \arg \max_{\lfloor\boldsymbol{\theta}^{(\iota+1)}\rceil_b \in \left\{\lfloor\boldsymbol{\theta}\rceil_b^{(\iota+1),k}, k=1,\ldots,K\right\}} \text{SR}_k(\mathbf{w}^{(\iota+1)}, \lfloor\boldsymbol{\theta}\rceil_b). \tag{3.23}
$$

Algorithm 3.1 Proposed Iterative Algorithm for Solving Problem ($\mathcal{P}1$)

1: **Initialise:** $(\mathbf{w}^{(1)}, \lfloor\boldsymbol{\theta}\rceil_b^{(1)})$, convergence tolerance $\epsilon_t > 0$, and Set $\iota = 1$.

2: **Repeat**

3: Update $\mathbf{w}^{(\iota+1)}$ by (3.17), and $\boldsymbol{\theta}^{(\iota+1)}$ by (3.23);

4: **if** $\frac{|\min\limits_k \mathrm{SR}_k(\mathbf{w}^{(\iota+1)}, \lfloor\boldsymbol{\theta}^{(\iota+1)}\rceil_b) - \min\limits_k \mathrm{SR}_k(\mathbf{w}^{(\iota)}, \lfloor\boldsymbol{\theta}^{(\iota)}\rceil_b)|}{\min\limits_k \mathrm{SR}_k(\mathbf{w}^{(\iota)}, \lfloor\boldsymbol{\theta}^{(\iota)}\rceil_b)} \leq \epsilon_t$.

5: **Then** $\lfloor\boldsymbol{\theta}^{(\iota)}\rceil_b \leftarrow \boldsymbol{\theta}^{(\iota+1)}$, $\mathbf{w}^{(\iota)} \leftarrow \mathbf{w}^{(\iota+1)}$ and terminate.

6: **Otherwise** $\iota \leftarrow \iota + 1$ and continue.

7: **Output** $(\mathbf{w}_k^{(\iota)}, \boldsymbol{\theta}^{(\iota)})$.

The procedure to solve problem ($\mathcal{P}1$) is described in Algorithm 3.1, which converges to a locally optimal solution of ($\mathcal{P}1$) as formally stated in the following theorem.

Theorem 3.1. *The obtained solution by Algorithm 3.1 is a locally optimal solution for problem* ($\mathcal{P}1$).

Proof: See Appendix B.1.

Complexity Analysis

Algorithm 3.1 addresses problem ($\mathcal{P}1$) by decoupling the beamforming vector and the IRS PREs in the objective function. The recast problem ($\mathcal{P}1$) is an SDP, which can be efficiently solved using the interior-point method [93]. The algorithm's computational complexity can be characterised in terms of its worst-case runtime and the number of decision variables [94]. Specifically, in Algorithm 3.1, the complexity of computing $\mathbf{w}$ given $\lfloor\boldsymbol{\theta}\rceil_b$ is $\mathcal{O}(M^3)$, while that of computing $\lfloor\boldsymbol{\theta}\rceil_b$ given $\mathbf{w}$ is $\mathcal{O}(N^3(N+1))$. One can notice that the overall complexity grows with the number of IRS PREs, N.

3.2.2 SSR Maximisation Under Perfect CSI

In this section, we address the problem of maximising the SSR under the perfect CSI assumption to achieve users' secrecy. The SSR maximisation problem can be stated as:

$$(\mathcal{P}2): \max_{\mathbf{w},\lfloor\boldsymbol{\theta}\rceil_b} \sum\nolimits_{k=1}^{\mathcal{K}} \mathrm{SR}_k(\mathbf{w}, \lfloor\boldsymbol{\theta}\rceil_b) \text{ s.t.}(3.12b)\&(3.12c). \tag{3.24}$$

Similar to the previous section, we seek $\mathbf{w}$ and $\lfloor\boldsymbol{\theta}\rceil_b$ that maximise the SSR.

Sub-Problem for Optimising the Beamforming Vectors

Using (3.16), the SSR can be expressed as:

$$\sum\nolimits_{k=1}^{\mathcal{K}} \mathrm{SR}_k(\mathbf{w}, \lfloor\boldsymbol{\theta}^{(\iota)}\rceil_b) \geq \sum\nolimits_{k=1}^{\mathcal{K}} q_k^{(\iota)} + 2\sum\nolimits_{k=1}^{\mathcal{K}} \Re\left\{\left\langle \boldsymbol{m}_k^{(\iota)}, \mathbf{w}_k \right\rangle\right\} - \sum\nolimits_{k=1}^{\mathcal{K}} \mathbf{w}_k^H \boldsymbol{\psi}_k^{(\iota)} \mathbf{w}_k. \tag{3.25}$$

Therefore, we can rewrite problem $(\mathcal{P}2)$ as:

$$(\mathcal{P}2.1): \max_{\mathbf{w}} \sum\nolimits_{k=1}^{\mathcal{K}} \mathrm{SR}_k(\mathbf{w}, \lfloor\boldsymbol{\theta}^{(\iota)}\rceil_b), \text{ s.t. } (3.12b). \tag{3.26}$$

Problem $(\mathcal{P}2.1)$ is a convex problem that can be solved using the Lagrangian multiplier method to generate $\mathbf{w}^{(\iota+1)}$ as follows [95]:

$$\mathbf{w}_k^{(\iota+1)} \triangleq \begin{cases} (\boldsymbol{\psi}_k^{(\iota)})^{-1}\boldsymbol{m}_k^{(\iota)} \text{ if } \sum\nolimits_{k=1}^{\mathcal{K}} ||(\boldsymbol{\psi}_k^{(\iota)})^{-1}\boldsymbol{m}_k^{(\iota)}||^2 \leq P_T, \\ \left(\boldsymbol{\psi}_k^{(\iota)} + \varpi \boldsymbol{I}_M\right)^{-1} \boldsymbol{m}_k^{(\iota)} \text{ otherwise,} \end{cases} \tag{3.27}$$

where bisection method is used to find ϖ such that $\left\| \frac{\boldsymbol{m}_k^{(\iota)}}{\left(\boldsymbol{\psi}_k^{(\iota)} + \varpi \boldsymbol{I}_M\right)} \right\|^2 = P_T$.

Sub-Problem for Optimising the PREs

In this part, we aim to find $\lfloor\boldsymbol{\theta}^{(\iota+1)}\rceil_b$ such that it maximises the SSR. Using (3.20), we can express the SSR as:

$$\sum\nolimits_{k=1}^{\mathcal{K}} \mathrm{SR}_k(\mathbf{w}^{(\iota+1)}, \lfloor\boldsymbol{\theta}\rceil_b) \geq q^{(\iota+1)} + 2\sum\nolimits_{n=1}^{N} \Re\left\{\boldsymbol{m}^{(\iota+1)}(n) e^{\jmath\boldsymbol{\theta}_n}\right\}, \tag{3.28}$$

where,

$$\begin{aligned} q^{(\iota+1)} &\triangleq \sum\nolimits_{k=1}^{\mathcal{K}} q_k^{(\iota+1)}, \\ \boldsymbol{m}^{(\iota+1)}(n) &\triangleq \sum\nolimits_{k=1}^{\mathcal{K}} \boldsymbol{m}_k^{(\iota+1)}(n). \end{aligned}$$

We can recast problem $(\mathcal{P}2)$ to generate $(\lfloor\boldsymbol{\theta}^{(\iota+1)}\rceil_b)$ as:

Algorithm 3.2 Proposed AO Algorithm for Solving Problem $(\mathcal{P}2)$

1: **Initialise:** $(\mathbf{w}^{(1)}, \lfloor\boldsymbol{\theta}^{(1)}\rceil_b)$, convergence tolerance $\epsilon_t > 0$, and Set $\iota = 1$.

2: **Repeat**

3: Update $\mathbf{w}^{(\iota+1)}$ by (3.27), and $\lfloor\boldsymbol{\theta}\rceil_b$ by (3.30);

4: **if** $\frac{|\sum_{k=1}^{\mathcal{K}}\mathrm{SR}_k(\mathbf{w}^{(\iota+1)},\lfloor\boldsymbol{\theta}^{(\iota+1)}\rceil_b)-\sum_{k=1}^{\mathcal{K}}\mathrm{SR}_k(\mathbf{w}^{(\iota)},\boldsymbol{\theta}^{(\iota)})|}{\sum_{k=1}^{\mathcal{K}}\mathrm{SR}_k(\mathbf{w}^{(\iota)},\lfloor\boldsymbol{\theta}^{(\iota)}\rceil_b)} \leq \epsilon_t$

5: **Then** $\lfloor\boldsymbol{\theta}^{(\iota)}\rceil_b \leftarrow \lfloor\boldsymbol{\theta}\rceil_b$, $\mathbf{w}^{(\iota)} \leftarrow \mathbf{w}^{(\iota+1)}$ and terminate.

6: **Otherwise** $\iota \leftarrow \iota + 1$ and continue.

7: **Output** $(\mathbf{w}_k^{(\iota)}, \lfloor\boldsymbol{\theta}^{(\iota)}\rceil_b)$.

$$(\mathcal{P}2.2) : \max_{\boldsymbol{\theta}} \sum\nolimits_{k=1}^{\mathcal{K}} \mathrm{SR}_k(\mathbf{w}^{(\iota+1)}, \lfloor\boldsymbol{\theta}\rceil_b), \text{ s.t. (3.12c)}, \tag{3.29a}$$

and the closed-form solution is obtained by,

$$\lfloor\boldsymbol{\theta}^{(\iota+1)}\rceil_b = 2\pi - \angle\boldsymbol{m}^{(\iota+1)}(n), n = 1, \ldots, N. \tag{3.30}$$

Algorithm 3.2 demonstrates the steps to solve problem $(\mathcal{P}2)$. Algorithm 3.2 converges to at least a locally optimal solution of $(\mathcal{P}2)$ as formally stated in the following theorem.

Theorem 3.2. *The obtained solution by the AO Algorithm 3.2 is a locally optimal solution for problem $\mathcal{P}2$.*

Proof: See Appendix B.3.

Complexity Analysis

The complexity analysis of Algorithm 3.2 is similar to that of Algorithm 3.1. Hence, the complexity of problem $\mathcal{P}2.1$ and problem $\mathcal{P}2.2$ is about $\mathcal{O}(M^3)$ and $\mathcal{O}(N^3(N+1))$, respectively.

3.3 Dealing With Imperfect CSI

3.3.1 MAXMIN SR Under Imperfect CSI

In this case, we deal with the IRS-to-users/Eve imperfect CSI. To this end, when only imperfect channel $\widehat{\boldsymbol{g}}_i$ CSI is available, we adopt the channel modelling in (3.3). Nevertheless, in the following analysis, we opt for the case of QPS with PSE, which is the most practical case. One can notice that by setting $b = \infty$ and $\epsilon_R = 0$, the PS is reduced to the CPS case. Hence, we can write the minimum SR maximisation problem as follows:

$$(\mathcal{P}3): \max_{\mathbf{w}, \lfloor \boldsymbol{\theta} \rceil_b + \epsilon_R} \min_k \widehat{\mathrm{SR}}_k(\mathbf{w}, \boldsymbol{\theta}), \tag{3.31a}$$

$$\text{s.t.} \quad \sum\nolimits_{k=1}^{\mathcal{K}} \|\mathbf{w}_k\|^2 \leq P_T, \tag{3.31b}$$

$$|e^{(j(\lfloor \boldsymbol{\theta} \rceil_b + \epsilon_R))}| = 1, \tag{3.31c}$$

$$\|\Delta \boldsymbol{g}_i\|_2 \leq \xi_i, i \in \{k, e\}, \forall k. \tag{3.31d}$$

Problem $(\mathcal{P}3)$ is a nonconvex problem due to the coupling between the beamforming vector and the IRS's PREs in the objective function, and the UMC (3.31c). However, problem $(\mathcal{P}3)$ is even more challenging due to the semi-infinite nonconvex constraint (3.31d) that captures the imperfection of the CSI from the IRS to the users/Eve. In addition, the imperfect CSI introduces PE into the IRS's PREs, which makes the problem more challenging.

To tackle problem $(\mathcal{P}3)$, we first introduce slack variables to decompose the coupling of the beamforming vector and the IRS's PREs in the objective function.

To this end, we first substitute (3.9) into (3.31a). Then we introduce a slack variable z as the SR's lower bound, φ_k represents the minimum data rate, and μ_{k_e} represents the maximum eavesdropping rate of Eve. Thus, problem $(\mathcal{P}3)$ can be recast as:

$$(\mathcal{P}3.1): \max_{\mathbf{w}, \lfloor \boldsymbol{\theta} \rceil_b + \epsilon_R} \quad z, \tag{3.32a}$$

$$\text{s.t.} \quad z \leq \varphi_k - \mu_{k_e}, \forall k, \tag{3.32b}$$

$$\varphi_k \leq \widehat{C}_k(\mathbf{w}, \lfloor \boldsymbol{\theta} \rceil_b + \epsilon_R), \forall \|\Delta \boldsymbol{g}_k\|_2 \leq \xi_k, \forall k, \tag{3.32c}$$

$$\mu_{k_e} \geq \widehat{C}_e(\mathbf{w}, \lfloor \boldsymbol{\theta} \rceil_b + \epsilon_R), \forall \|\Delta \boldsymbol{g}_e\|_2 \leq \xi_e, \forall k, \tag{3.32d}$$

$$(3.31\text{b}), (3.31\text{c}). \tag{3.32e}$$

One can notice that the constraint (3.31d) in problem $(\mathcal{P}3)$ has been embedded within the constraints (3.32c), and (3.32d) in problem $(\mathcal{P}3.1)$, since the channel estimation error $\Delta \boldsymbol{g}_i$ is embedded within the channel definition (3.4). To this end, we transform the semi-infinite nonconvex constraints (3.32c) and (3.32d) into finite LMIs using the SCA technique and the $\mathcal{S}$-procedure. Then, we tackle the UMC (3.31c) using the PCCP algorithm.

Sub-Problem for Optimizing the Beamforming Vectors

We start by linearizing the semi-infinite inequalities in (3.32c). By substituting (3.11) into (3.32c), we can express (3.32c) as:

$$2^{\varphi_k} - 1 \leq \frac{|(\boldsymbol{g}_k \boldsymbol{\Phi} \boldsymbol{H}_{\text{AR}}) \mathbf{w}_k|^2}{\|(\boldsymbol{g}_k \boldsymbol{\Phi} \boldsymbol{H}_{\text{AR}}) \mathbf{W}_{-k}\|^2 + \sigma_k^2}, \forall k. \tag{3.33}$$

Next, we introduce an auxiliary function $\boldsymbol{\beta} \triangleq [\beta_1, \ldots, \beta_K]$ to deal with the interference plus noise signal, hence, (3.33) can be expressed as:

$$|(\boldsymbol{g}_k \boldsymbol{\Phi} \boldsymbol{H}_{\text{AR}}) \mathbf{w}_k|^2 \geq (2^{\varphi_k} - 1) \beta_k, \forall k, \tag{3.34a}$$

$$\|(\boldsymbol{u}_k \boldsymbol{\Phi} \boldsymbol{H}_{\text{AR}}) \mathbf{W}_{-k}\|^2 + \sigma_k^2 \leq \beta_k, \forall k. \tag{3.34b}$$

To address the nonconvex semi-infinite inequalities in (3.34a), we substitute their left-hand side with their corresponding lower bounds derived from the following lemma.

Lemma 1. *At iteration* (ι)*, let* $\mathbf{w}^{(\iota)}$ *and* $\lfloor \boldsymbol{\theta}^{(\iota)} \rceil_b$ *be the optimal solution, then at the point* $(\mathbf{w}^{(\iota)}, \lfloor \boldsymbol{\theta}^{(\iota)} \rceil_b)$ *we can express the linear lower bound of* (3.34a) *as:*

$$|(\boldsymbol{g}_k \boldsymbol{\Phi} \boldsymbol{H}_{AR}) \boldsymbol{w}_k|^2 \triangleq \boldsymbol{g}_k \mathbf{X}_k \boldsymbol{g}_k^H, \tag{3.35}$$

where,

$$\begin{aligned} \mathbf{X}_k \triangleq\ & \boldsymbol{\Phi} \boldsymbol{H}_{AR} \boldsymbol{w}_k (\boldsymbol{w}_k^{(\iota)})^H \boldsymbol{H}_{AR}^H (\boldsymbol{\Phi}^{(\iota)})^H + \boldsymbol{\Phi}^{(\iota)} \boldsymbol{H}_{AR} \boldsymbol{w}_k^{(\iota)} \boldsymbol{w}_k^H \boldsymbol{H}_{AR}^H (\boldsymbol{\Phi}^{(\iota)})^H \\ & - \boldsymbol{\Phi}^{(\iota)} \boldsymbol{H}_{AR} \boldsymbol{w}_k^{(\iota)} (\boldsymbol{w}_k^{(\iota)})^H \boldsymbol{H}_{AR}^H (\boldsymbol{\Phi}^{(\iota)})^H. \end{aligned}$$

Proof: Please refer to Appendix B.2.

By substituting (3.35) into (3.34a), and applying (3.3a) along with Lemma 1, the inequality in (3.34a) can be recast as:

$$\Delta \boldsymbol{g}_k \mathbf{X}_k \Delta \boldsymbol{g}_k^H + 2\Re\{(\mathbf{x}_k^H + \widehat{h}_{r,k}^H \mathbf{X}_k) \Delta \boldsymbol{g}_k\} + d_k \geq (2^{\varphi_k} - 1)\beta_k, \forall \|\Delta \boldsymbol{g}\|_2 \leq \xi_k, \forall k, \tag{3.36}$$

where $d_k \triangleq \widehat{\boldsymbol{g}}_k \mathbf{X}_k \widehat{\boldsymbol{g}}_k^H$.

Next, we handle the uncertainty of $\{\Delta \boldsymbol{g}_k\}$ in (3.36) by employing the $\mathcal{S}$-procedure [75].

Lemma 2. *($\mathcal{S}$-procedure) Let* $\mathbf{O}_r \in \mathbb{C}^{\mathcal{L} \times \mathcal{L}}$ *be a Hermitian matrix,* $\mathbf{o}_r \in \mathbb{C}^{\mathcal{L} \times 1}$ *be a complex vector, and* o_r*, for* $r = 0, \ldots, R$ *be scalar. A quadratic function of a variable* v *is defined as:*

$$f_r(v) \triangleq v^H \mathbf{O}_r x + 2\Re\{\mathbf{o}_r^H v\} + o_r. \tag{3.37}$$

The condition $f_0(v) \geq 0$ *such that* $f_r(v) \geq 0,\ r = 1, \ldots, R$*, holds, if and only if*

there exists $\mathfrak{m}_i \geq 0, r = 0, \ldots, R$, *such that,*

$$\begin{bmatrix} \mathbf{O}_0 & \mathbf{o}_0 \\ \mathbf{o}_0^H & o_0 \end{bmatrix} - \sum\nolimits_{r=0}^{R} \mathfrak{m}_r \begin{bmatrix} \mathbf{O}_r & \mathbf{o}_r \\ \mathbf{o}_r^H & o_r \end{bmatrix} \succeq 0. \tag{3.38}$$

Using Lemma 2, we can transform (3.36) into its equivalent LMI as:

$$\begin{bmatrix} \varpi_k \mathbf{I}_M + \mathbf{X}_k & (\widehat{\boldsymbol{g}}_k \mathbf{X}_k)^H \\ (\widehat{\boldsymbol{g}}_k \mathbf{X}_k) & d_k - (2^{\varphi_k} - 1)\beta_k - \eta_k \xi_k^2 \end{bmatrix} \succeq 0, \forall k, \tag{3.39}$$

where $\boldsymbol{\eta} \triangleq [\eta_1, \ldots, \eta_K]^T \geq 0$ are slack variables.

The uncertainty in $\{\Delta \boldsymbol{g}_k\}$ leads to a quadratic constraint that must remain valid for all channel error realisations $\{\Delta \boldsymbol{g}_k\}$ within the uncertainty set ω_i. Directly enforcing this condition is intractable because it involves an infinite number of possibilities. The $\mathcal{S}$-procedure provides a systematic way to reformulate this requirement into an LMI by introducing non-negative multipliers. Intuitively, this approach replaces the original implication with a sufficient condition that guarantees robustness under uncertainty. Specifically, by applying Lemma 2, the quadratic constraint is transformed into an LMI with slack variables $\boldsymbol{\eta}$, enabling efficient optimisation through semidefinite programming.

Although (3.34a) has been converted into an LMI form, it remains nonconvex due to the nonconvexity nature of the term $2^{\varphi_k}\beta_k$. To address this, we employ the SCA technique to approximate the nonconvex constraint (3.39) with a convex expression. In particular, by applying a first-order Taylor expansion, the term $2^{\varphi_k}\beta_k$ can be upper bounded as follows:

$$(\beta_k(2^{\varphi_k}))^{ub} \triangleq ((\varphi_k - \varphi_k^{(\iota)})(\beta_k^{(\iota)}) \ln 2 + \beta_k) 2^{\varphi_k^{(\iota)}}, \tag{3.40}$$

where $\varphi_k^{(\iota)}, \beta_k^{(\iota)}$ are the value of the variables φ_k, β_k at iteration (ι) in the SCA-based algorithm, respectively. Lastly, substituting (3.40) in (3.39), the LMIs in (3.39) can

be expressed as:

$$\begin{bmatrix} \varpi_k \mathbf{I}_M + \mathbf{X}_k & (\widehat{\boldsymbol{g}}_k \mathbf{X}_k)^H \\ (\widehat{\boldsymbol{g}}_k \mathbf{X}_k) & d_k - (\beta_k (2^{\varphi_k}))^{ub} + \beta_k - \varpi_k \xi_k^2 \end{bmatrix} \succeq 0, \forall k. \tag{3.41}$$

Next, to tackle the uncertainties in (3.34b), we leverage the Schur's complement [96].

Lemma 3. *(Schur's complement) For a Hermitian positive definite matrix* $\mathbf{F} \succeq 0$*,* $\mathbf{D}$*, and* $\mathbf{S}$*, define a Hermitian matrix* $\mathbf{A}$ *as:*

$$\mathbf{A} \triangleq \begin{bmatrix} \mathbf{S} & \mathbf{D}^H \\ \mathbf{D} & \mathbf{F} \end{bmatrix}. \tag{3.42}$$

Then, $\mathbf{A}$ *is positive semidefinite* ($\mathbf{A} \succeq 0$) *if and only if* $\Delta\mathbf{F} \succeq 0$*, and* $\mathbf{S} - \mathbf{D}^H \mathbf{F}^{-1} \mathbf{D} \succeq 0$.

Using Lemma (3), we can equivalently reformulate (3.34b) as:

$$\begin{bmatrix} \beta_k & \mathbf{t}_k^H \\ \mathbf{t}_k^H & \mathbf{I}_{K-1} \end{bmatrix} \succeq 0, \forall \|\Delta \boldsymbol{g}_k\|_2 \leq \xi_k, \forall k, \tag{3.43}$$

where,

$$\mathbf{t}_k \triangleq \left((\widehat{\boldsymbol{g}}_k^H \boldsymbol{\Phi} \boldsymbol{H}_{\text{AR}}) \mathbf{W}_{-k} \right)^H,$$

$$\mathbf{W}_{-k} \triangleq [\mathbf{w}_1, \ldots, \mathbf{w}_{k-1}, \mathbf{w}_{k+1}, \ldots, \mathbf{w}_{\mathcal{K}}].$$

Next, to handle (3.43), we employ the Nemirovski's Lemma [97].

Lemma 4. *(Nemirovski's Lemma) Let* $\mathbf{R}$ *be a Hermitian matrix, and* $\mathbf{E}$*,* $\mathbf{F}$*,* $\mathbf{Z}$ *be matrices with compatible dimensions. For a scalar* $t > 0$*, the following linear matrix inequality holds:*

$$\mathbf{R} \succeq \mathbf{E}^H \mathbf{Z} \mathbf{F} + \mathbf{F}^H \mathbf{Z}^H \mathbf{E}, \quad \textit{for} \quad \|\mathbf{Z}\| \leq t,$$

if and only if there exists a scalar $\alpha \geq 0$ *such that:*

$$\begin{bmatrix} \mathbf{R} - \alpha \mathbf{F}^H \mathbf{F} & -t\mathbf{E}^H \\ -t\mathbf{E} & \alpha \mathbf{I} \end{bmatrix} \succeq 0.$$

Using Lemma (4) and introducing the slack variable $\boldsymbol{\varkappa} \triangleq [\varkappa_1, \ldots, \varkappa_k] \geq 0$, (3.43) is recast as:

$$\begin{bmatrix} B_{11,k} & \widehat{t}_k^H & \mathbf{0}_{1\times M} \\ \widehat{t}_k & \mathbf{I}_{K-1} & \xi_{\mathbf{H}_k}(\boldsymbol{\Phi}\boldsymbol{H}_{\text{AR}}\mathbf{W}_{-k})^H \\ \mathbf{0}_{M\times 1} & \xi_{\mathbf{H}_k}(\boldsymbol{\Phi}\boldsymbol{H}_{\text{AR}}\mathbf{W}_{-k}) & \varkappa_k \mathbf{I}_M \end{bmatrix} \succeq 0, \tag{3.44}$$

where

$$B_{11,k} \triangleq \beta_k - \sigma_k^2 - \varkappa_k,$$
$$\widehat{t}_k \triangleq ((\widehat{\boldsymbol{g}}_k \boldsymbol{\Phi}\boldsymbol{H}_{\text{AR}})\mathbf{W}_{-k})^H.$$

Next, we tackle (3.32d) by firstly substituting (3.11) in (3.32d), and then treating the interference plus noise signal in (3.32d) as an auxiliary function $\boldsymbol{\beta}_{e_k} \triangleq [\beta_{e_1}, \ldots, \beta_{e_k}]$. We hence can recast (3.32d) as:

$$|(\boldsymbol{g}_e \boldsymbol{\Phi}\boldsymbol{H}_{\text{AR}})\mathbf{w}_k|^2 \leq (2^{\mu_{k_e}} - 1)\beta_{ke}, \forall k, \tag{3.45a}$$

$$\|(\boldsymbol{g}_e \boldsymbol{\Phi}\boldsymbol{H}_{\text{AR}})\mathbf{W}_{-k}\|^2 + \sigma_e^2 \geq \beta_{ke}, \ \ \forall k. \tag{3.45b}$$

The uncertainties of $\{\Delta\boldsymbol{g}_e\}$ in constraints (3.45a) and (3.45b) can be tackled by a similar approach as in (3.34b). Hence, the equivalent LMIs of (3.45a) and (3.45b) are, respectively,

$$\begin{bmatrix} C_{e,k} & \widehat{c}_{ke}^H & \mathbf{0}_{1\times M} \\ \widehat{c}_{ke} & 1 & \xi_e(\boldsymbol{\Phi}\boldsymbol{H}_{\text{AR}}\mathbf{w}_k)^H \\ \mathbf{0}_{M\times 1} & \xi_e(\boldsymbol{\Phi}\boldsymbol{H}_{\text{AR}}\mathbf{w}_k) & y_k \mathbf{I}_M \end{bmatrix} \succeq 0, \tag{3.46}$$

$$\begin{bmatrix} C_{11,k} & -\widehat{c}_{ke}^H & \mathbf{0}_{1\times M} \\ -\widehat{c}_{ke} & \mathbf{I}_{K-1} & -\xi_e(\boldsymbol{\Phi}\boldsymbol{H}_{\text{AR}}\mathbf{W}_{-k})^H \\ \mathbf{0}_{M\times 1} & -\xi_e(\boldsymbol{\Phi}\boldsymbol{H}_{\text{AR}}\mathbf{W}_{-k}) & s_k \mathbf{I}_M \end{bmatrix} \succeq 0, \tag{3.47}$$

where $\boldsymbol{y} \triangleq [y_1, \ldots, y_K] \geq 0$ and $\boldsymbol{s} \triangleq [s_1, \ldots, s_K] \geq 0$ are a slack variables, and,

$$C_{e,k} \triangleq (\beta_{ke}(2^{\mu_{k_e}}))^{ub} - \beta_{ke} - \vartheta_k,$$

$$(\beta_{ke}(2^{\mu_{k_e}}))^{ub} \triangleq ((\mu_{k_e} - \mu_{k_e}^{(\iota)})(\beta_{ke}^{(\iota)}) \ln 2 + \beta_{ke}) 2^{\mu_{ke}^{(\iota)}},$$

$$\widehat{c}_{ke} \triangleq ((\widehat{\boldsymbol{g}}_e^H \boldsymbol{\Phi} \boldsymbol{H}_{\text{AR}}) \mathbf{W}_{-k})^H,$$

$$C_{11,k} \triangleq \beta_{ke} - \sigma_e^2 - \varrho_k.$$

Eventually, reformulating problem ($\mathcal{P}$3.2) with (3.41), (3.44), (3.46), and (3.47) yields the following optimisation problem:

$$(\mathcal{P}3.2) : \max_{\mathbf{w}} \; z, \tag{3.48a}$$

$$\text{s.t.} \quad z \leq \varphi_k - \mu_{k_e}, \; \forall k, \tag{3.48b}$$

$$(3.41), (3.44), (3.46), (3.47), \tag{3.48c}$$

$$\boldsymbol{\eta} \geq 0, \; \boldsymbol{\varkappa} \geq 0, \; \boldsymbol{y} \geq 0, \; \boldsymbol{s} \geq 0, \tag{3.48d}$$

$$(3.31b). \tag{3.48e}$$

To this end, we have linearise all the nonlinear constraints (3.32c) and (3.32d) into their equivalent LMIs (3.41), (3.44), (3.46), and (3.47); hence, problem ($\mathcal{P}$3.2) is an SDP problem and solved efficiently using standard solvers such as the interior point method or the CVX toolbox [93].

Sub-Problem for Optimising the PREs

With the beamforming vector $\mathbf{w}$ kept fixed, we aim to find the next feasible point $\lfloor \boldsymbol{\theta}^{(\iota+1)} \rceil_b$, such that,

$$\text{SR}_k(\mathbf{w}_k^{(\iota+1)}, \lfloor \boldsymbol{\theta}^{(\iota+1)} \rceil_b) > \text{SR}_k(\mathbf{w}_k^{(\iota+1)}, \lfloor \boldsymbol{\theta}^{(\iota)} \rceil_b).$$

Similar to the previous section, constraints (3.32c) and (3.32d) can be recast as their equivalent LMIs (3.41), (3.44), (3.46), and (3.47), respectively.

However, Problem ($\mathcal{P}$3) still nonconvex due to the nonconvexity nature of the UMC (3.31c). To this end, we leverage the PCCP method to tackle the UMC

(3.31c). The PCCP idea is to introduce slack variables that relax the problem, allowing violations of the UMC to be penalised through the sum of these violations. The solution obtained upon convergence of the PCCP method is an approximate first-order optimal solution to the original problem [76].

To implement the PCCP method, we introduce an auxiliary variable set $\mathcal{Q} \triangleq \{\mathcal{Q}_n | n \in N\}$, where each $\mathcal{Q}_n$ satisfies $\mathcal{Q}_n \triangleq |e^{(j\lfloor \boldsymbol{\theta}_n \rceil_b)}|^* |e^{(j\lfloor \boldsymbol{\theta}_n \rceil_b)}|$. Thus, the UMC (3.31c) can be written as $\mathcal{Q}_n \leq |e^{(j\lfloor \boldsymbol{\theta}_n \rceil_b)}|^* |e^{(j\lfloor \boldsymbol{\theta}_n \rceil_b)}| \leq \mathcal{Q}_n$. The nonconvex inequality $\mathcal{Q}_n \leq |e^{(j\lfloor \boldsymbol{\theta}_n \rceil_b)}|^* |e^{(j\lfloor \boldsymbol{\theta}_n \rceil_b)}|$ is then approximated using its first order Taylor expansion as $\mathcal{Q}_n \leq 2\Re\{|e^{(j\lfloor \boldsymbol{\theta}_n \rceil_b)}|^* |e^{(j\lfloor \boldsymbol{\theta}_b^{(\iota)} \rceil_b)}| - |e^{(j\lfloor \boldsymbol{\theta}_b^{(\iota)} \rceil_b)}|^* |e^{(j\lfloor \boldsymbol{\theta}_b^{(\iota)} \rceil_b)}|\}$.

The PCCP framework tackles nonconvex optimisation problems by successively solving convex approximations. It introduces slack variables to temporarily relax nonconvex constraints, with a penalty term incorporated into the objective function to discourage constraint violations. At each iteration, the concave parts of the constraints are linearised via a first-order Taylor expansion around the current solution, yielding a locally tight convex surrogate. By iteratively refining these approximations and increasing the penalty on infeasibility, PCCP converges to a first-order stationary solution of the original nonconvex problem, thereby balancing computational tractability and solution accuracy [76].

By applying the PCCP framework, we penalise the objective function (3.32a),

and thus reformulate problem ($\mathcal{P}3.1$) as:

$$(\mathcal{P}3.3): \max_{\boldsymbol{\theta}} \; z - o\mathcal{T}, \tag{3.49a}$$

$$\text{s.t.} \quad (3.41), (3.44), (3.46), (3.47), \tag{3.49b}$$

$$|e^{(j\lfloor \boldsymbol{\theta}_n^{(\iota)} \rceil_b)}|^* |e^{(j\lfloor \boldsymbol{\theta}_n^{(\iota)} \rceil_b)}| \leq \mathcal{Q}_n + d_n, \tag{3.49c}$$

$$\mathcal{Q}_n - \hat{d}_n \leq 2\Re\left\{|e^{(j\lfloor \boldsymbol{\theta}_n^{(\iota)} \rceil_b)}|^* |e^{(j\lfloor \boldsymbol{\theta}_n^{(\iota)} \rceil_b}|\right\} - |e^{(j\lfloor \boldsymbol{\theta}_n^{(\iota)} \rceil_b)}|^* |e^{(j\lfloor \boldsymbol{\theta}_n^{(\iota)} \rceil)}|, \tag{3.49d}$$

$$\mathcal{Q}_n \geq 0, \; \forall n \in N, \tag{3.49e}$$

where $\mathcal{T} \triangleq \sum_{n=1}^{N} d_n + \hat{d}_n$ is the penalty term, $\mathbf{d} \triangleq \{d_n, \hat{d}_n\}$ denotes the slack

Algorithm 3.3 PCCP Algorithm to Solve Problem ($\mathcal{P}3.3$)

Initialise: $(\mathbf{w}^{(1)}, \lfloor \boldsymbol{\theta}^{(1)} \rceil_b + \epsilon_R)$, maximum penalty factor $o_{\max}$, scaling factor $\nu \geq 1$, convergence tolerances ϵ_{t_1}, ϵ_{t_2}, maximum iterations $\iota_{\max}$, and set $\iota = 1$.
repeat
  Solve problem ($\mathcal{P}3.3$) to obtain $\lfloor \boldsymbol{\theta}_n^{(\iota)} \rceil_b$;
  if $\left\| e^{j\lfloor \boldsymbol{\theta}_n^{(\iota)} \rceil_b} - e^{j\lfloor \boldsymbol{\theta}_n^{(\iota-1)} \rceil_b} \right\|_1 \leq \epsilon_{t_1}$ and $Q \leq \epsilon_{t_2}$ **then**
    break
  else
    Update penalty factor: $o^{(\iota+1)} = \min\{\nu o^{(\iota)}, o_{\max}\}$;
    Update iteration count: $\iota \leftarrow \iota + 1$;
  end if
  if $\iota > \iota_{\max}$ **then**
    Re-initialise $\lfloor \boldsymbol{\theta}^{(1)} \rceil_b + \epsilon_R$, set $\nu > 1$, and $\iota = 0$;
  end if
until convergence
Output: feasible solution $\boldsymbol{\theta}^* = \lfloor \boldsymbol{\theta}^{(\iota)} \rceil_b + \epsilon_R$.

variable introduced to relax the UMC (5.33c), and o is the regularisation factor.

The regularisation factor o is imposed to scale the penalty term $\mathcal{T}$ to control the UMC (5.33c).

Problem ($\mathcal{P}$3.3) is an SDP problem that can be solved by the CVX toolbox. Unlike the semi-definite relaxation (SDR) method, which is the conventional method to tackle UMC, the PCCP method is guaranteed to find a feasible point for problem ($\mathcal{P}$3.3) [98]. The PCCP algorithm to solve problem ($\mathcal{P}$3.3) is described in Algorithm 3.3. The following points are emphasised from Algorithm 3.3:

Algorithm 3.4 Proposed AO Algorithm for Solving Problem ($\mathcal{P}$3)

1: **Initialise:** $(\mathbf{w}^{(1)}, \lfloor \boldsymbol{\theta}^{(1)} \rceil_b + \epsilon_R$, $\iota = 1$, and convergence tolerance $\epsilon_t > 0$.

2: **Repeat**

3: Update $\mathbf{w}^{(\iota+1)}$ by solving ($\mathcal{P}$3.2), and $\lfloor \boldsymbol{\theta}_n^{(\iota+1)} \rceil_b$ by solving problem ($\mathcal{P}$3.2);

4: **if** $\frac{\left| \min\limits_k \mathrm{SR}_k(\mathbf{w}^{(\iota+1)}, \lfloor \boldsymbol{\theta}_n^{(\iota+1)} \rceil_b + \epsilon_R) - \min\limits_k \mathrm{SR}_k(\mathbf{w}^{(\iota)}, \lfloor \boldsymbol{\theta}^{(\iota)} \rceil_b + \epsilon_R) \right|}{\min\limits_k \mathrm{SR}_k(\mathbf{w}^{(\iota)}, \lfloor \boldsymbol{\theta}^{(\iota)} \rceil_b + \epsilon_R)} \leq \epsilon_t$.

5: **Then** $\lfloor \boldsymbol{\theta}^{(\iota)} \rceil_b \leftarrow \lfloor \boldsymbol{\theta}_n^{(\iota+1)} \rceil_b$, $\mathbf{w}^{(\iota)} \leftarrow \mathbf{w}^{(\iota+1)}$ and terminate.

6: **Otherwise** $\iota \leftarrow \iota + 1$ and continue.

7: **Output** $(\mathbf{w}_k^{(\iota)}, \lfloor \boldsymbol{\theta}^{(\iota)} \rceil_b + \epsilon_R)$.

(a) We invoke $o_{\max}$ to prevent numerical instability in the algorithm when the penalty parameter o grows too large [99];

(b) The stopping criteria $Q \leq \epsilon_{t_2}$ ensures satisfaction of the UMC (5.33c), provided that the tolerance ϵ_{t_2} is small [52];

(c) The convergence of Algorithm 5.2 is controlled by $\left\| e^{(j \lfloor \boldsymbol{\theta}^{(\iota+1)} \rceil_b)} - e^{(j \lfloor \boldsymbol{\theta}^{(\iota)} \rceil_b)} \right\|_1 \leq \epsilon_{t_1}$, which controls the incremental change in the PREs PS updates.

Algorithm 3.4 demonstrates the AO algorithm to solve problem ($\mathcal{P}$3), which converges to at least a locally optimal solution of ($\mathcal{P}$3), and can be proved in the following theorem.

Theorem 3.3. *The AO Algorithm 3.4 generates a locally optimal solution for problem* ($\mathcal{P}3$).

Proof: See Appendix B.3.

Complexity Analysis

Problems ($\mathcal{P}3.2$) and ($\mathcal{P}3.3$) are convex problems, and involve linear constraints and LMIs (3.41), (3.44), (3.46), (3.47), hence, they can be solved efficiently using the interior point method [93]. The complexity of Algorithm 3.4 is determined by its worst-case runtime and the number of operations performed [52]. For problem ($\mathcal{P}3.3$), the number of variables is $c \triangleq 2M$, the size of LMI (3.41) is $a_1 \triangleq MN+M+1$, the size of LMIs (3.44), and (3.47) is $a_2 \triangleq 2M+1$, and the size of the LMI (3.46) is $a_3 \triangleq 2M+1$. Thus, the complexity of solving problems ($\mathcal{P}3.2$) and ($\mathcal{P}3.3$), respectively,

$$\mathcal{O}_{\mathbf{w}} \triangleq \mathcal{O}\left\{\sqrt{b_1+2}(c)(c^2+cb_2+b_3+(c+1)^2)\right\}, \tag{3.50}$$

$$\mathcal{O}_{\mathbf{\Phi}} \triangleq \mathcal{O}\left\{\sqrt{b_1+4N}(2N)(4N^2+2Nb_2+b_3+4NM)\right\}, \tag{3.51}$$

where,

$$\begin{aligned}
b_1 &\triangleq \sum\nolimits_k^{\mathcal{K}}(a_1+a_2)+2k(a_2+a_3)+(k-2)(a_1+a_3),\\
b_2 &\triangleq \sum\nolimits_k^{\mathcal{K}}({a_1}^2+{a_2}^2)+2k({a_2}^2+{a_3}^2)+(k-2)({a_1}^2+{a_3}^2),\\
b_3 &\triangleq \sum\nolimits_k^{\mathcal{K}}({a_1}^3+{a_2}^3)+2k({a_2}^3+{a_3}^3)+(k-2)({a_1}^3+{a_3}^3).
\end{aligned}$$

3.3.2 SSR maximisation Under Imperfect CSI

Previous research, such as [49], has considered a similar problem with the presence of a direct link between Alice and the users and Eve. The SSR maximisation problem under imperfect CSI from the IRS to users/Eve can be formally formulated

as:

$$(\mathcal{P}4) : \max_{\mathbf{w},\boldsymbol{\theta}} \sum\nolimits_{k=1}^{\mathcal{K}} \widehat{\mathrm{SR}}_k(\mathbf{w},\boldsymbol{\theta}), \tag{3.52a}$$

$$\text{s.t.} \quad (3.31\text{b}), (3.31\text{c}), (3.31\text{d}). \tag{3.52b}$$

Similar to ($\mathcal{P}3$), problem ($\mathcal{P}4$) is a nonconvex problem due to the coupling between the beamforming vector and the IRS's PREs within the objective function, and the UMC (3.31c).

To tackle problem ($\mathcal{P}4$), we first substitute (3.9) in (3.52a), and introduce the slack variables $\tilde{z}$ as lower bound of the SSR, $\tilde{\varphi}_k$ and $\tilde{\mu}_{k_e}$ as the minimum data rate, and the maximum eavesdropping rate of Eve, respectively, hence, problem ($\mathcal{P}4$) can be recast as:

$$(\mathcal{P}4.1) : \max_{\mathbf{w},\lfloor\boldsymbol{\theta}\rceil_b} \ \tilde{z}, \tag{3.53a}$$

$$\text{s.t.} \quad \tilde{z} \leq \sum\nolimits_{k=1}^{\mathcal{K}} \left(\tilde{\varphi}_k - \tilde{\mu}_{e_k}\right), \forall k, \tag{3.53b}$$

$$\tilde{\varphi}_k \leq \widehat{C}_k(\mathbf{w}, \lfloor\boldsymbol{\theta}\rceil_b + \epsilon_R), \forall \|\Delta \boldsymbol{g}_k\|_2 \leq \xi_k, \tag{3.53c}$$

$$\tilde{\mu}_{k_e} \geq \widehat{C}_e(\mathbf{w}, \lfloor\boldsymbol{\theta}\rceil_b + \epsilon_R), \forall \|\Delta \boldsymbol{g}_e\|_2 \leq \xi_e, \tag{3.53d}$$

$$(3.31\text{b}), (3.31\text{c}). \tag{3.53e}$$

To tackle problem ($\mathcal{P}4.1$), we use a similar approach that dealt with problem ($\mathcal{P}3.1$).

Sub-Problem for Optimising the Beamforming Vectors

Similar to the analysis to linearise (3.34a) and (3.34b) in Section 3.3.1. First, we introduce an auxiliary variable $\tilde{z}$ as the lower bound of the SSR. Then, we express (3.53c) and (3.53d) with their equivalent LMIs (3.41), (3.44), (3.46) and (3.47),

respectively. Thus, problem ($\mathcal{P}4.1$) can be recast as:

$$(\mathcal{P}4.2) : \max_{\mathbf{w},\boldsymbol{\theta}} \ \tilde{z}, \tag{3.54a}$$

$$\text{s.t.} \quad \tilde{z} \leq \sum\nolimits_{k=1}^{\mathcal{K}} \left(\tilde{\varphi}_k - \tilde{\mu}_{e_k}\right), \forall k, \tag{3.54b}$$

$$(3.31\text{b}), (3.41), (3.44), (3.46), (3.47), (3.48\text{d}). \tag{3.54c}$$

Problem ($\mathcal{P}4.2$) is a convex problem that can be solved using the CVX toolbox.

Sub-Problem for Optimising the PREs

Similarly, we can express (3.53c) and (3.53d) with their equivalent LMIs (3.41), (3.44), (3.46) and (3.47), respectively. To tackle the UMC (3.31c), we use the PCCP method as described in Algorithm 3.3. Finally, the steps to solve problem ($\mathcal{P}4$) are described in Algorithm 3.5.

Theorem 3.4. *The obtained solution by Algorithm 3.5 is a locally optimal solution for problem $\mathcal{P}4$.*

Proof: See Appendix B.3.

Algorithm 3.5 Proposed AO Algorithm for Solving Problem ($\mathcal{P}4$)

1: **Initialise:** $(\mathbf{w}^{(1)}, \lfloor\boldsymbol{\theta}^{(1)}\rceil_b + \epsilon_R)$, convergence tolerance $\epsilon_t > 0$, and Set $\iota = 1$.

2: **Repeat**

3: Update $\mathbf{w}^{(\iota+1)}$ by solving problem $\mathcal{P}4.2$, and $\lfloor\boldsymbol{\theta}_n^{(\iota+1)}\rceil_b + \epsilon_R$ by solving problem $\mathcal{P}4.3$;

4: **if** $\dfrac{\left|\sum\limits_{k=1}^{\mathcal{K}} \mathrm{SR}_k(\mathbf{w}^{(\iota+1)}, \lfloor\boldsymbol{\theta}_n^{(\iota+1)}\rceil_b + \epsilon_R) - \sum\limits_{k=1}^{\mathcal{K}} \mathrm{SR}_k(\mathbf{w}^{(\iota)}, \lfloor\boldsymbol{\theta}^{(\iota)}\rceil_b + \epsilon_R)\right|}{\sum\limits_{k=1}^{\mathcal{K}} \mathrm{SR}_k(\mathbf{w}^{(\iota)}, \lfloor\boldsymbol{\theta}^{(\iota)}\rceil_b + \epsilon_R)} \leq \epsilon_t.$

5: **Then** $\lfloor\boldsymbol{\theta}^{(\iota)}\rceil_b \leftarrow \lfloor\boldsymbol{\theta}_n^{(\iota+1)}\rceil_b$, $\mathbf{w}^{(\iota)} \leftarrow \mathbf{w}^{(\iota+1)}$ and terminate.

6: **Otherwise** $\iota \leftarrow \iota + 1$ and continue.

7: **Output** $(\mathbf{w}_k^{(\iota)}, \lfloor\boldsymbol{\theta}^{(\iota)}\rceil_b + \epsilon_R)$.

Complexity Analysis

The complexity analysis of Algorithm 3.5 is similar to Algorithm 3.4. Hence, the complexity of problem $\mathcal{P}4$ is expressed in (3.50) and (3.51).

3.4 Dealing with Eve's Unknown CSI

In this case, we assume that Alice can not obtain Eve's CSI (even just the imperfect CSI). To provide secure communications for *all the users*, we propose to optimise a minimum transmit power P_T subject to a quality of service (QoS) constraint (i.e. $\gamma_k \geq \gamma_e$) to allow us to use the residual power available at Alice as AN so as to decrease the SINR at Eve γ_e. Unlike other research [100, 101], that only deals with a single user and assumes perfect CSI under IRS' PREs CPS, we address the power minimisation problem under the multi-users settings, where only partial users' CSI is available, and the IRS's PREs are modelled by the QPS and suffer PSE due to the imperfect CSI. To this end, we can express the total transmit power P_{tot} as follows:

$$P_{tot} \triangleq P_T + P_J, \tag{3.55}$$

where the residual power $P_J \triangleq \sum_{k=1}^{\mathcal{K}} \mathbf{E}\{\|\mathbf{Vr}\|^2\}$ is used as AN, and $\mathbf{Vr}$ is the AN vector, while $\mathbf{V} \in \mathbb{C}^{M \times M-1}$ is the null space of the user's channel with $\boldsymbol{h}_k(\lfloor \boldsymbol{\theta} \rceil_b + \epsilon_R)\mathbf{V} = 0$, and $\mathbf{r} \in \mathbb{C}^{M-1}$ is a random vector whose elements are independent Gaussian random variables with mean 0 and variance $\sigma_r^2 \triangleq \frac{P_J}{M-1}$. Hence, we can express the SINR at user-k as in (3.6), and Eve's eavesdropping rate as:

$$\gamma_e(\mathbf{w}, \lfloor \boldsymbol{\theta} \rceil_b + \epsilon_R) \triangleq \frac{|\widehat{\boldsymbol{h}}_e(\lfloor \boldsymbol{\theta} \rceil_b + \epsilon_R)\mathbf{w}_k|^2}{\widehat{\rho}_e + |\widehat{\boldsymbol{h}}_e(\lfloor \boldsymbol{\theta} \rceil_b + \epsilon_R)\mathbf{Vr}|^2}. \tag{3.56}$$

To that end, we can formulate the problem as:

$$(\mathcal{P}5) : \min_{\mathbf{w},\boldsymbol{\theta}} \; P_T, \tag{3.57a}$$

$$\text{s.t.} \quad \gamma_k(\mathbf{w}, \lfloor \boldsymbol{\theta} \rceil_b + \epsilon_R) \geq \gamma \sigma_k^2, \tag{3.57b}$$

$$(3.31\text{b}), (3.31\text{c}), (3.31\text{d}), \tag{3.57c}$$

where γ represents the QoS constraint at user-k. Due to the coupling of $\mathbf{w}$ and $\boldsymbol{\theta}$ in (3.57b), problem $(\mathcal{P}3)$ is a nonconvex problem.

Sub-Problem for Optimising the Beamforming Vectors

similar to the previous sections, we propose an AO method to tackle problem $(\mathcal{P}5)$, by designing the beamform vector $\mathbf{w}$ with fixed $\boldsymbol{\theta}$. Hence, problem $(\mathcal{P}5)$ can be recast as:

$$(\mathcal{P}5.1) : \min_{\mathbf{w}} \; P_T, \tag{3.58a}$$

$$\text{s.t.} \quad |(\boldsymbol{g}_k \boldsymbol{\Phi} \boldsymbol{H}_{\text{AR}}) \mathbf{w}_k|^2 \geq (2^{\gamma_k} - 1) \hat{\beta}_k, \forall k, \tag{3.58b}$$

$$\|(\boldsymbol{g}_k \boldsymbol{\Phi} \boldsymbol{H}_{\text{AR}}) \mathbf{W}_{-k}\|^2 + \sigma_k^2 \leq \hat{\beta}_k, \forall k, \tag{3.58c}$$

$$(3.31\text{b}), \tag{3.58d}$$

where $\hat{\boldsymbol{\beta}} \triangleq [\hat{\beta}_1, \ldots, \hat{\beta}_K]$ is an auxiliary function. Similar to the analysis to linearise (5.36a) and (3.34b) in section 3.3.1, we can express (3.58b) and (3.58c) with their equivalent LMIs (3.41), (3.44), (3.46) and (3.47), respectively. Thus, problem $(\mathcal{P}5.1)$ can be recast as:

$$(\mathcal{P}5.2) : \min_{\mathbf{w}} \; P_T, \tag{3.59a}$$

$$\text{s.t.} \quad (3.31\text{b}), (3.41), (3.44), (3.46), (3.47), (3.48\text{d}). \tag{3.59b}$$

Problem $(\mathcal{P}5.2)$ is a convex problem that can be solved using the CVX toolbox.

Sub-Problem for Optimising the PREs

Similarly, we aim to find $\lfloor \boldsymbol{\theta}^{(\iota+1)} \rceil_b$ that minimises P_T while meeting the QoS constraint (3.57b). This problem is a search problem to find any feasible $\lfloor \boldsymbol{\theta} \rceil_b$ satisfying the QoS (3.57b) and the UMC constraint (3.31c), where the obtained result can be the optimal solution. Hence, one can use the residual power (3.55) and the PCCP algorithm as described in Algorithm 3.3 to find the optimal $\lfloor \boldsymbol{\theta} \rceil_b$.

Finally, the algorithm to solve problem ($\mathcal{P}5.3$) is described in Algorithm 3.6.

Theorem 3.5. *The obtained solution by the AO Algorithm 3.6 is a locally optimal solution for problem* ($\mathcal{P}5$).

Proof: See Appendix B.3.

Complexity Analysis

Algorithm 3.6 involves linear constraints and LMIs (3.41), (3.44), (3.46), (3.47), hence, its complexity is similar to Algorithm 3.4, which can be expressed as in (3.50) and (3.51).

Algorithm 3.6 Proposed AO Algorithm for Solving Problem ($\mathcal{P}5$)

1: **Initialise:** $(\mathbf{w}^{(1)}, \lfloor \boldsymbol{\theta}^{(1)} \rceil_b + \epsilon_R)$, convergence tolerance $\epsilon_t > 0$, and Set $\iota = 1$.

2: **Repeat**

3: Update $\mathbf{w}^{(\iota+1)}$ by solving problem ($\mathcal{P}5.2$), and $\lfloor \boldsymbol{\theta}_n^{(\iota+1)} \rceil_b$ by solving problem ($\mathcal{P}5.3$);

4: **if** $\frac{\left|\sum_{k=1}^{\mathcal{K}} \|\mathbf{w}^{(\iota+1)}\|^2 - \sum_{k=1}^{\mathcal{K}} \|\mathbf{w}^{(\iota)}\|^2\right|}{\sum_{k}^{\mathcal{K}} \|\mathbf{w}^{(\iota)}\|^2} \leq \epsilon_t$.

5: **Then** $\lfloor \boldsymbol{\theta}^{(\iota)} \rceil_b \leftarrow \lfloor \boldsymbol{\theta}_n^{(\iota+1)} \rceil_b$, $\mathbf{w}^{(\iota)} \leftarrow \mathbf{w}^{(\iota+1)}$ and terminate.

6: **Otherwise** $\iota \leftarrow \iota + 1$ and continue.

7: **Output** $(\mathbf{w}_k^{(\iota)}, \lfloor \boldsymbol{\theta}^{(\iota)} \rceil_b + \epsilon_R)$.

3.5 Simulations Results

To evaluate the performance of our proposed algorithms, we conduct extensive simulations using MATLAB and CVX toolboxes. In this setup, we consider the downlink transmission, where Alice is positioned at $(15, 0, 15)$, and the IRS is placed at $(0, 25, 40)$. Legitimate users are randomly distributed within a $(60m \times 60m)$ area located to the left of Alice. The Eve is randomly located in $(60m \times 60m)$ outside the user's area. Notably, when Eve is positioned in close proximity to a legitimate user, ensuring a positive secrecy is unattainable [102]. In such cases, alternative techniques, such as cryptographic encryption or friendly jamming, can be employed to enhance secrecy.

The direct path loss factor of Alice-to-IRS is modelled as $\beta_{\text{AR}} \triangleq G_{\text{A}} + G_{\text{IRS}} - 35.9 - 22\log_{10}(d_{\text{AR}})$ in dB, where d_{AR} is the distance between Alice and the IRS in meters, and G_{IRS} is the IRS elements' antenna gain [70]. The IRS-users/Eve is $\beta_{\text{R}i} \triangleq G_{\text{IRS}} - 33.05 - 30\log_{10}(d_{\text{R}i})$ dB, for $i \in \{k, e\}$, $d_{\text{R}i}$ is the distance between the IRS and the users and Eve in meters. The small-scale fading channel gain $\widehat{\boldsymbol{g}}_i$ for $i \in \{k, e\}$ is modelled as a Rician fading channel with K-factor= 3. The spatial correlation matrix is $[R_{Ri}]_{q,\bar{q}} \triangleq \exp\left(j\pi(q-\bar{q})\sin\hat{\vartheta}\sin\hat{\aleph}\right)$ for $i \in \{k, e\}$, where $\hat{\aleph}$ is the elevation angle and $\hat{\vartheta}$ is the azimuth angle. The elements of the Alice-to-IRS channel are generated by $[G_{\text{AR}}]_{a,b} \triangleq \exp(j\pi\left((b-1)\sin\overline{\Theta}_b\sin\overline{\vartheta}_b + (a-1)\sin(\Theta_n)\sin(\vartheta_b)\right))$, where $\Theta_n \in (0, 2\pi)$, $\vartheta_n \in (0, 2\pi)$, and $\overline{\Theta}_n \triangleq \pi - \Theta_n$, and $\overline{\vartheta}_n \triangleq \pi + \vartheta_n$ [86].

In the imperfect CSI case, the channel estimation error bounds are defined as $\xi_i \triangleq \delta_i\|\widehat{\boldsymbol{g}}_i\|_2, \forall k$, where $\delta_i \in [0, 1), i \in \{k, e\}$ is the relative amount of CSI uncertainty. The special case $\delta = 0$, corresponds to perfect CSI at Alice for the IRS-to-user/Eve reflected channels. Unless stated otherwise, the simulation parameters are defined in Table 3.1. Lastly, the computed rates are multiplied by $\log_2(e)$ to convert them to bps/Hz.

Table 3.1 : Low Resolution IRS System Simulation Parameters

Parameter	**Numerical Value**
Noise power density, σ_i^2	-174 dBm/Hz
Alice transmission power, P	20 dBm
Antenna gains, G_{A} and G_{IRS}	5 dBi
Convergence tolerances, ϵ_t, ϵ_{t_1}, ϵ_{t_2}	10^{-3}
Simulation initial settings	$\beta_k^{(\iota)} = 1$, $\beta_{ke}^{(\iota)} = 1$, $o^{(1)} = 10$, $o_{\max} = 30$

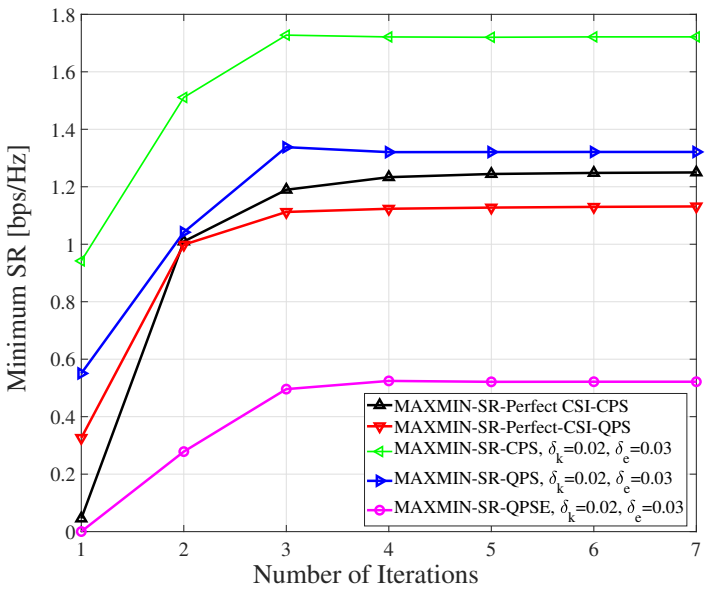

Figure 3.2 : Convergence rate of the Max-Min algorithm with $M = 10$, $\mathcal{K} = 6$, $N = 16$.

Fig. 3.2 illustrates the convergence rate of the Max-Min algorithms under the perfect and imperfect CSI for the CPS, the QPS, and the QPSE cases with $M = 10$, $\mathcal{K} = 6$, and $N = 16$. All algorithms achieve convergence within a few iterations. The obtained results show the robustness of the proposed algorithm, even when the IRS's PREs PS are subject to phase error and CSI uncertainty, the system still can

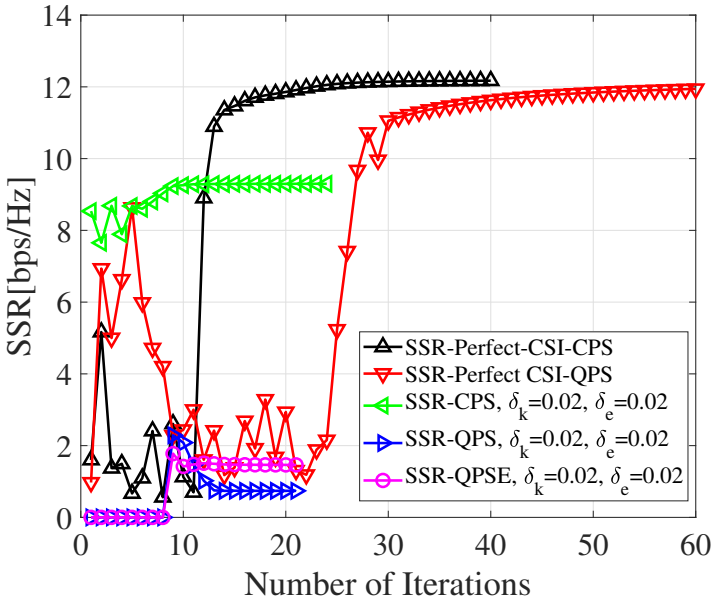

Figure 3.3 : Convergence rate of SSR maximisation with $M = 10$, $\mathcal{K} = 6$, $N = 16$.

achieve secrecy for *all the users*. The SSR counterpart convergence rate is shown in Fig. 3.3. One can notice the oscillation at the beginning of the convergence curve at the first iterations before the convergence, which occurs when the SSR algorithm is trying to provide secrecy to *all the users*. It can be noticed that the convergence is unreachable until the algorithm drops the users with zero secrecy, which is visible in all cases. The results show that the SSR algorithm suffers from the PS error more than the Max-Min algorithm.

Fig. 3.4 shows the users' SR distribution with $M = 10$, $\mathcal{K} = 6$, and $N = 16$, under the Max-Min algorithms for perfect and imperfect CSI cases with CPS, QPS, and QPSE. The CPS achieves the highest fairness between the three cases, which is expected. However, both the QPS and QPSE cases achieved secrecy for *all the users* with less fairness compared to the CPS case, and the QPSE case, which has the least fairness in SR among the three cases. However, when the IRS's PREs are not practically optimised, the algorithms fail to achieve secrecy fairness among the users.

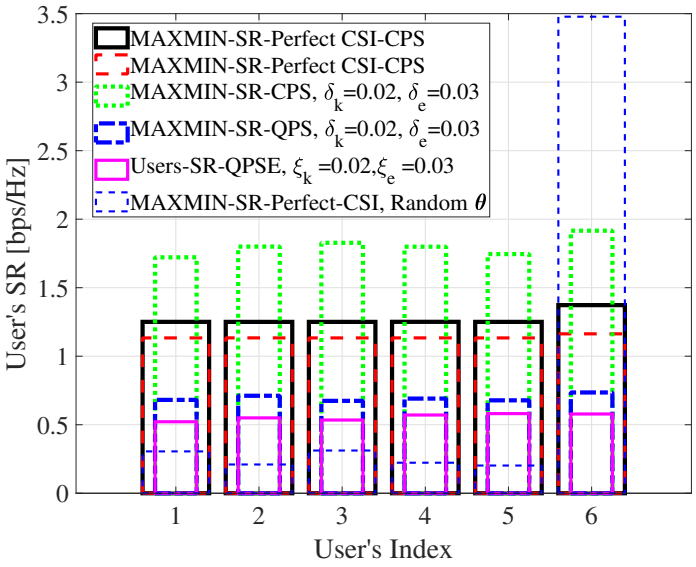

Figure 3.4 : Users' SR with $M = 10$, $\mathcal{K} = 6$, $N = 16$.

The results demonstrate the importance of properly optimising the IRS's PREs to achieve secrecy fairness. The users' SR under the SSR maximisation counterparts is shown in Fig. 3.5. The SSR maximisation algorithms fail to provide secrecy to *all the users* and focus most of the transmission power toward the users with better channels.

Fig. 3.6 depicts the users' SR under different values of the IRS to the users/Eve's imperfect CSI. The Max-Min algorithm achieves secrecy fairness in all cases, even when Eve's reflected channel has higher uncertainty than the users' reflected channel.

To evaluate the degree of fairness in the proposed algorithms under imperfect CSI using the Jain's index. Jain's index is defined as, Jain's Index $= \frac{\left(\sum_{k=1}^{\mathcal{K}} \mathrm{SR}_k(\mathbf{w},\boldsymbol{\theta})\right)^2}{\mathcal{K}\sum_{k=1}^{\mathcal{K}}(\mathrm{SR}_k(\mathbf{w},\boldsymbol{\theta})}$)^2, and it is bounded in $[1/\mathcal{K}, 1]$, where the higher value indicates a better fairness [103]. Fig. 3.7 depicts Jain's index while varying the number of Alice's antennas M, with $\mathcal{K} = 6$, and $N = 16$. The proposed Max-Min algorithm achieves almost one for the Jain's index in the CPS/QPS/QPSE cases. As expected, the SSR counterpart

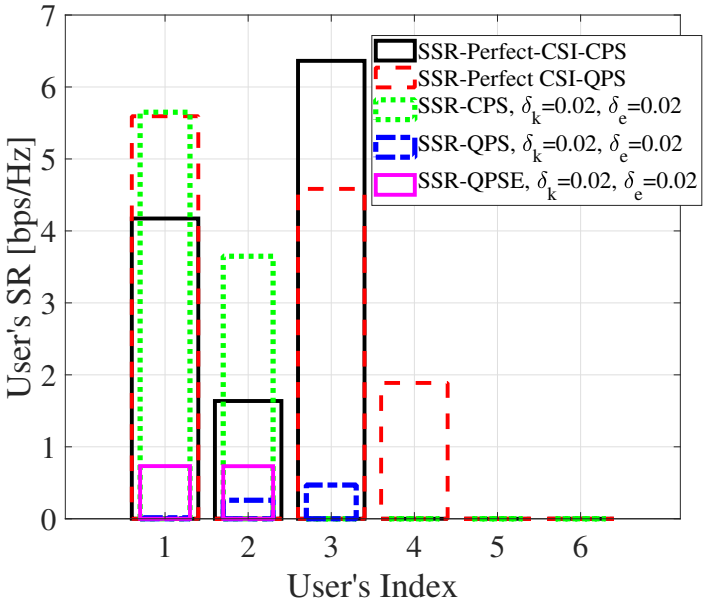

Figure 3.5 : Users' SR with $M = 10$, $\mathcal{K} = 7$, $N = 16$.

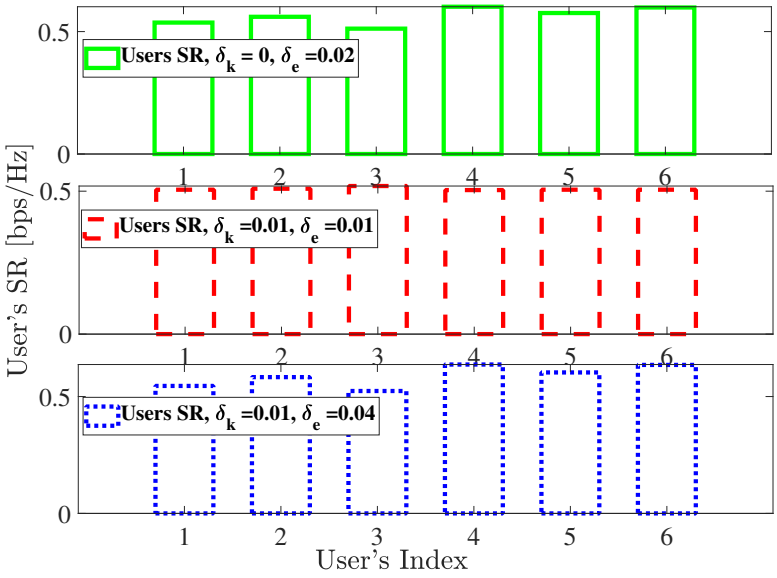

Figure 3.6 : Users' SR with with $M = 10, \mathcal{K} = 6, N = 16$.

achieves low fairness between the users since it favours most of the transmission power P_T towards the users with a better channel while discarding other users, which matches the previous results.

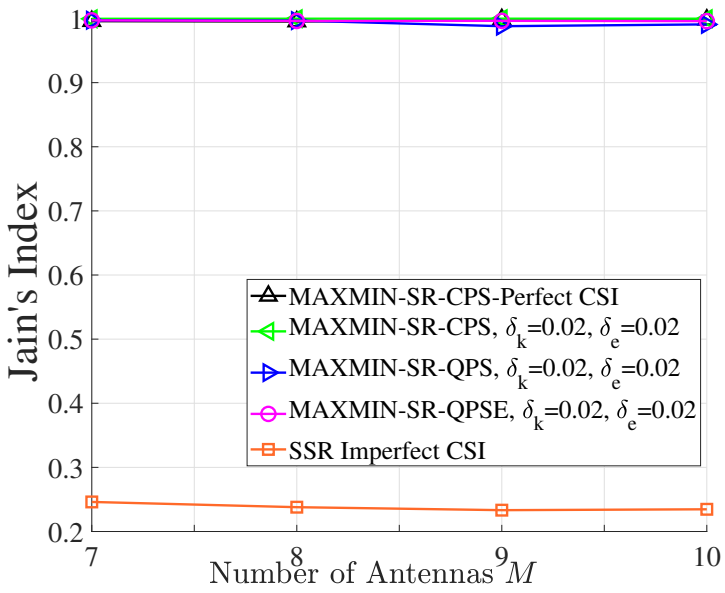

Figure 3.7 : Jain's Index versus the number of Alice's antennas M, with $\mathcal{K} = 4, N = 16$. The proposed Max–Min algorithm attains near-unity fairness across CPS/QPS/QPSE cases, while the SSR scheme shows lower fairness due to power concentration on stronger users.

Fig. 3.8 shows the Jain's index against the relative amount of CSI uncertainty δ. The Max-Min algorithm achieves almost one in all cases, CPS/QPS/QPSE, while the SSR counterpart has nearly zero. The results demonstrate the Max-Min algorithm's robustness even when the phase error is introduced at high uncertainty CSI for the users and Eve counterpart.

Fig. 3.9 illustrates the convergence rate of Algorithm 3.6 with the QPS and the QPSE cases. The algorithm converges within a few iterations. Fig. 3.10 shows the users' SR distribution with $M = 10$, $\mathcal{K} = 5$, and $N = 16$, under the power minimisation algorithm for the imperfect CSI case with QPS, and QPSE. *all the users* have achieved secrecy while maintaining the minimum QoS constraint $\gamma_k = 0.5$[dB], which demonstrates the robustness of the proposed algorithm even with

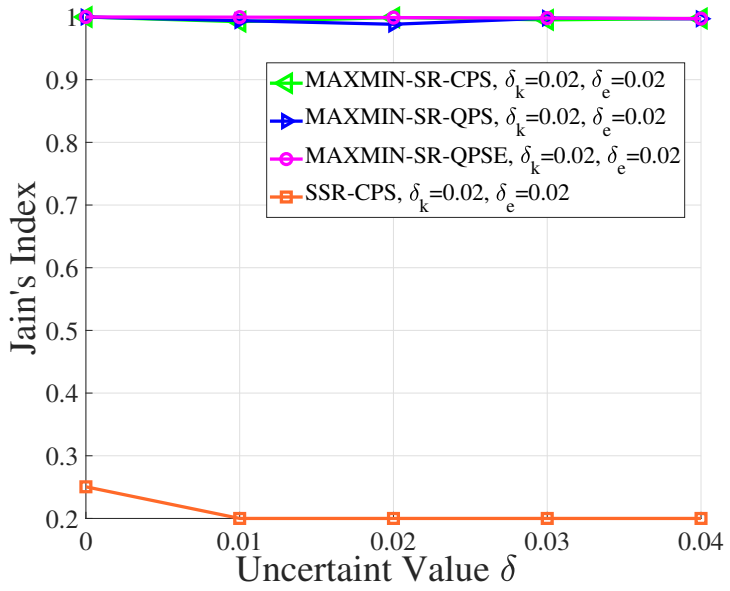

Figure 3.8 : Jain's Index versus the uncertainty level $\delta_k = \delta_e$ with $M = 10, \mathcal{K} = 5, N = 16$. The proposed Max–Min algorithm maintains near-unity fairness across CPS/QPS/QPSE cases, while the SSR scheme exhibits nearly zero fairness.

QPSE and the users' imperfect CSI introduced, while Eve's CSI is unknown to Alice.

Lastly, Fig. 3.11 depicts the minimum transmit power P_T against the minimum user's SINR γ_k. The minimum power increases with γ_k as expected, since the system requires more transmit power to achieve higher users' SINR. The results show that the system will require higher transmit power to achieve secrecy for *all the users* with increasing $\mathcal{K}$, and it can achieve secrecy even when the PREs are subject to the QPSE.

3.6 Conclusions

In this paper, we proposed a framework to achieve secure communications for all the users in a low resolution IRS-aided system with the presence of an eavesdropper under both perfect and imperfect CSI. Specifically, through linearization and

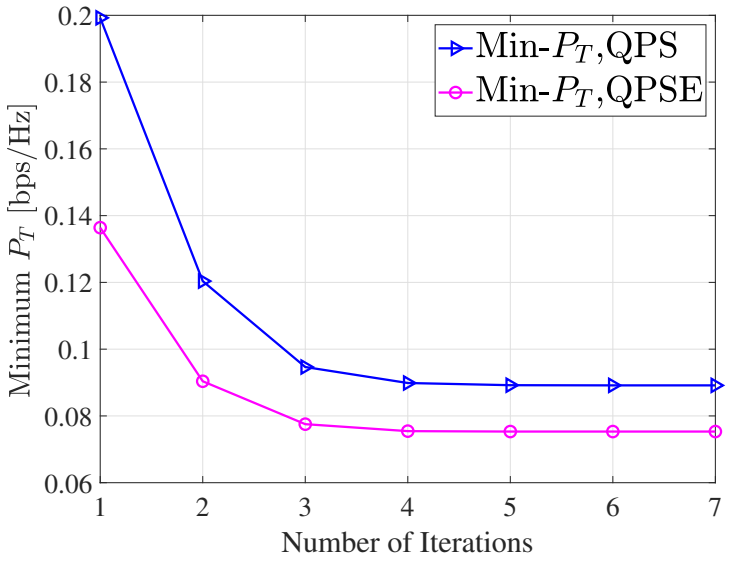

Figure 3.9 : Convergence rate of the Min P_T algorithm with $M = 10$, $\mathcal{K} = 5$, $N = 16$, $b = 3$, $\delta_k = 0.01$,$\gamma_k = 0.5$[dB], showing that the algorithm converges within a few iterations in both scenarios.

different nonconvex optimisation techniques, we designed computationally efficient algorithms to maximise the minimum SR among all the users under both perfect and imperfect CSI from IRS to the users and the eavesdropper, and minimise the transmit power subject to minimum SR constraints, where the IRS's PREs are modeled by quantised phase shift (QPS) and affected by phase shift error (PSE). Extensive simulation results showed that the Max-Min algorithm can provide secure communications for all the users even with only imperfect CSI. In the future, one can consider a multi-hop scenario with the joint coding over multiple IRSs or distributed beamforming, similar to the cooperative MIMO setting [104].

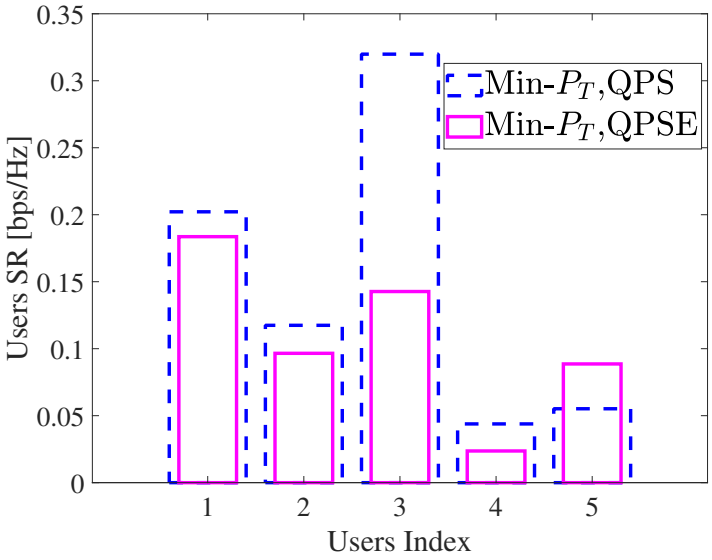

Figure 3.10 : Users' SR with with $M = 10$, $\mathcal{K} = 5$, $N = 16$, $b = 3$, $\delta_k = 0.01$, $\gamma_k = 0.5$ [dB]. All users achieve the minimum QoS $\gamma_k = 0.5$ [dB], demonstrating the algorithm's robustness despite imperfect user CSI and unknown Eve's CSI.

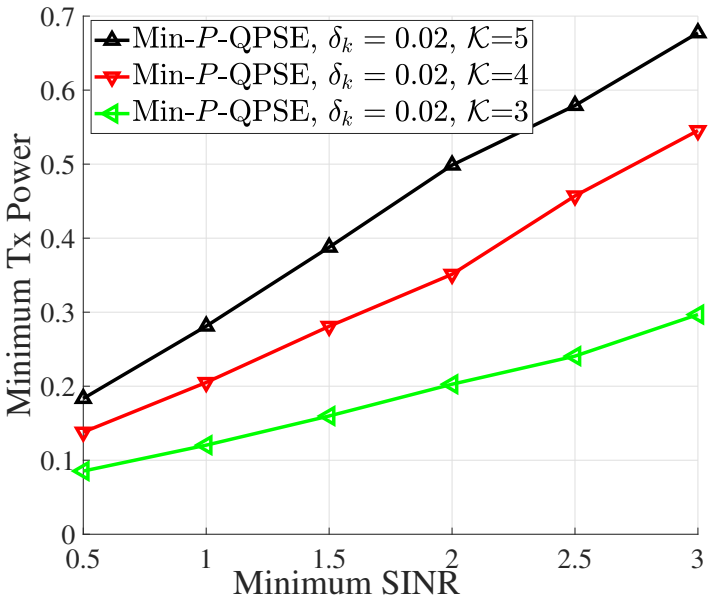

Figure 3.11 : Minimum transmit power P_T versus the users' minimum SINR γ_k. The required power increases with γ_k and $\mathcal{K}$, while the system maintains secrecy for all users even under QPSE conditions.

Chapter 4

"Security for Everyone" in Finite Blocklength IRS-aided Systems With Perfect and Imperfect CSI

In this chapter*, we take the first step to guarantee secrecy for all URLLC users in the finite blocklength regime (FBR) where intelligent reflecting surfaces (IRS) are used to enhance legitimate users' reception and thwart the potential eavesdropper (Eve) from intercepting. To this end, we aim to maximise the minimum secrecy rate (SR) across all users by jointly optimising the transmitter's beamforming vectors and the IRS's passive reflective elements (PREs) under FBR latency constraints. In the FBR-SR expression, the square-root dispersion factor under the FBR, couples with the latency and reliability constraints, making the problem significantly more challenging than the same problem in the long blocklength regime (LBR). Under imperfect CSI, the problem becomes even more challenging due to nonconvex, semi-infinite constraints arising from channel estimation errors. To address this, we approximately linearise the objective function, constraints, and decompose the problem into sequential subproblems. We then apply the successive convex approximation (SCA), and the $\mathcal{S}$-procedure approach to transform imperfect CSI-related semi-infinite constraints into finite linear matrix inequalities (LMIs) that can be efficiently solved. We prove that our proposed algorithms converge to a locally optimal solution with low computational complexity thanks to our closed-form linearization approach. This makes the solution scalable for large IRS deployments.

*This chapter corresponds to the journal paper J-3 as well as the conference paper C-2 in the list of Publications.

Extensive simulations with practical settings show that our approach can ensure secure communication for all users while satisfying FBR constraints even with only imperfect CSI.

The remainder of this section is organised as follows. The system model is discussed in Sections 4.1. Then, Sections 4.2 and 4.3 present the problem and corresponding solutions under perfect and imperfect CSI, respectively. The extensive simulations and discussion are in Section 4.4. Finally, Section 4.5 concludes the paper.

4.1 System Model

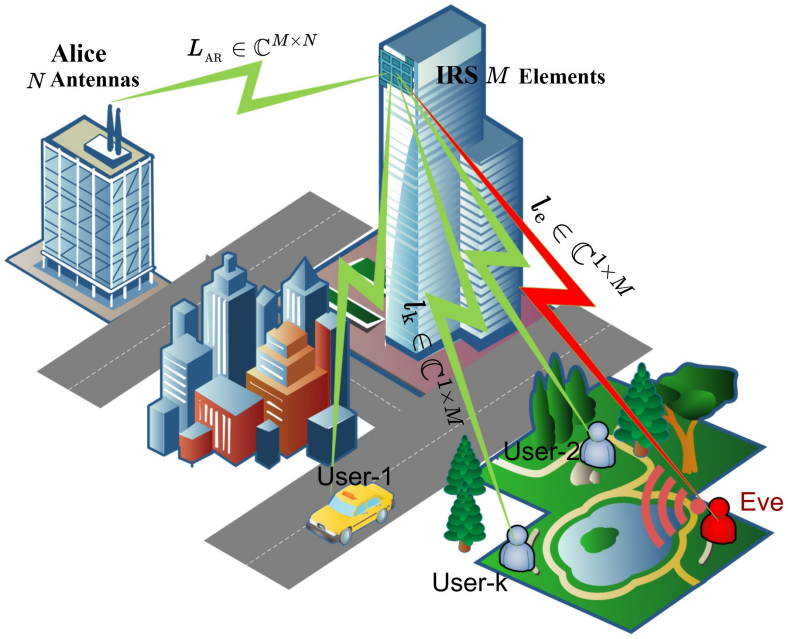

Figure 4.1 : FBR IRS-aided system model.

We consider an FBR-IRS-aided downlink system as depicted in Fig. 4.1, in which an N-antenna BS (Alice) transmits confidential information to $\mathcal{K}$ single antenna users under the presence of a single antenna eavesdropper (Eve). Here, we assume

the direct radio links between Alice and the users are severely blocked[†]. This scenario is usually the case in highly populated areas with high-rise buildings. An IRS with M PREs is thus deployed (e.g., at the facade of a building) to support the transmission between Alice and the users. Let $k \triangleq \{1, 2, \ldots, \mathcal{K}\}$ denote the set of the legitimate users, and e denote the Eve in the system. Let $\boldsymbol{L}_{\mathrm{AR}} = \sqrt{\aleph_{\mathrm{AR}}}\tilde{\boldsymbol{L}}_{\mathrm{AR}} \in \mathbb{C}^{M\times N}$ denote the channel from Alice to the IRS, while $\tilde{\boldsymbol{L}}_{\mathrm{AR}}$ is modelled by Rician fading, and $\sqrt{\aleph_{\mathrm{AR}}}$ is the large scale fading factor of the Alice-to-IRS link. The channel from the IRS to user-k and to Eve is modelled by $\boldsymbol{l}_i = \sqrt{\aleph_{\mathrm{R}i}}\tilde{\boldsymbol{l}}_i\mathcal{R}_{\mathrm{R}i}^{1/2} \in \mathbb{C}^{1\times M}$, where $i \in \{k, e\}$, $\aleph_{\mathrm{R}i}$ is the large-scale fading factor of the IRS-to-i [86], $\tilde{\boldsymbol{l}}_i$ is modelled by Rician fading, and $\mathcal{R}_{\mathrm{R}i} \in \mathbb{C}^{M\times M}$ is the IRS elements' spatial correlation matrix [86]. For the confidential message intended for user-k, i.e., s_k, the signal received by user-k and Eve, corresponding to the intended user, can be respectively expressed by:

$$g_i \triangleq \boldsymbol{h}_i(\boldsymbol{\theta})\sum\nolimits_{k=1}^{\mathcal{K}} \mathbf{w}_k s_k + \bar{n}_i, i \in \{k, e\}, \tag{4.1}$$

where $\boldsymbol{h}_i(\boldsymbol{\theta}) \in \mathbb{C}^{1\times N}$ is the cascaded channel gain from Alice to $i \in \{k, e\}$, $\mathbf{w}_k \in \mathbb{C}^{N\times 1}$ is the beamforming vector applied for user-k, $\boldsymbol{\theta} = (\theta_1, \ldots, \theta_m)^T \in [0, 2\pi)^M$ denotes the phase shift vector the IRS's PREs, $\bar{n}_i$ is the zero-mean Additive White Gaussian Noise (AWGN) with power density σ_i^2 for $i \in \{k, e\}$. The cascade channel gain $\boldsymbol{h}_i(\boldsymbol{\theta})$ from Alice to $i \in \{k, e\}$, can be written in terms of the channel gain from Alice to the IRS and the channel gain from the IRS to the user or Eve as follows:

$$\boldsymbol{h}_i(\boldsymbol{\theta}) \triangleq \boldsymbol{l}_i\boldsymbol{\Phi}\boldsymbol{L}_{\mathrm{AR}} \triangleq \boldsymbol{l}_i \sum_{m=1}^{M} \exp(j\theta_m)\boldsymbol{\Gamma}_m\boldsymbol{L}_{\mathrm{AR}}, \tag{4.2}$$

where $\boldsymbol{\Gamma}_m$ is an $M \times M$ matrix with all zeros except for its (n, n) entry which is 1, and $\boldsymbol{\Phi} = \mathrm{Diag}(e^{j\boldsymbol{\theta}})$.

Given that the IRS is deployed at a known location, such as the facade of a high-rise building, the CSI between Alice and the IRS can be accurately estimated

[†]The effectiveness of the IRS in enhancing users' rate/confidentiality is limited when a strong direct link between the transmitter and the receiver exists [105].

by exploiting the angles of arrival and departure [77], or through advanced channel estimation techniques [87,88]. However, the reflected channel's CSI from the IRS to the IoT users is much more challenging to obtain due to the passive nature of the IRS and the mobility/varying nature of the users' environment and location [89]. For Eve, it is also hardly possible to pinpoint its location or its accurate CSI from the IRS. To account for the CSI imperfection, we adopt the bounded CSI model in which the reflected channel from the IRS to the users and Eve can be expressed as [106]:

$$\boldsymbol{l}_i \triangleq \widehat{\boldsymbol{l}}_i + \Delta\boldsymbol{l}_i, \forall i \in \{k, e\}, \tag{4.3a}$$

$$\omega_i \triangleq \{\|\Delta\boldsymbol{l}_i\|_2 \leq \Omega_i\}, \forall i \in \{k, e\}, \tag{4.3b}$$

where $\widehat{\boldsymbol{l}}_i$ denotes the (imperfect) estimated channel vector, $\Delta\boldsymbol{l}_i$ represents the channel estimation error of the corresponding estimation, ω_i is a set for all possible channel estimation errors, and Ω_i is the radii of the uncertainty regions as known to Alice. Hence, (4.2) can be reformulated as:

$$\widehat{\boldsymbol{h}}_i(\boldsymbol{\theta}) \triangleq (\widehat{\boldsymbol{u}}_i + \Delta\boldsymbol{u}_i)\,\boldsymbol{\Phi}\boldsymbol{G}_{\text{AR}}. \tag{4.4}$$

In the sequel, we deal with perfect and imperfect CSI from the IRS to the users and Eve. For the former, we assume that the CSI of all the users and Eve can be accurately obtained by Alice [107, 108]. As aforementioned, in this case we assume that Eve acts as a legitimate user in one period/slot but then tries to eavesdrop on other users. Using different well-established channel estimation methods, such as the anchor-assisted channel estimation approach [109], Alice can practically obtain the CSI of all the users. In this case, the reflected channel from the IRS to the users and Eve can be captured by setting $\Delta\boldsymbol{l}_i$ to zero in (4.3a), i.e., $\boldsymbol{l}_i = \widehat{\boldsymbol{l}}_i, i \in \{k, e\}$. In the second case, only partial/imperfect CSI $\widehat{\boldsymbol{l}}_i$ is available. In this case, one can vary the magnitude of $\Delta\boldsymbol{l}_i$, i.e., the radii Ω_i of the uncertainty region to capture different levels of CSI imperfection.

The corresponding signal-to-interference-plus-noise ratio (SINR) of the received signal at the user-k and Eve under perfect and imperfect IRS to users/Eve CSI can be written as, respectively,

$$\gamma_i(\mathbf{w},\boldsymbol{\theta}) \triangleq |\boldsymbol{h}_i(\boldsymbol{\theta})\mathbf{w}_k|^2/\rho_i,\ i \in \{k,e\}, \tag{4.5}$$

$$\widehat{\gamma}_i(\mathbf{w},\boldsymbol{\theta}) \triangleq |\widehat{\boldsymbol{h}}_i(\boldsymbol{\theta})\mathbf{w}_k|^2/\widehat{\rho}_i,\ i \in \{k,e\}, \tag{4.6}$$

where $\rho_i \triangleq \sum_{j=1,j\neq k}^{\mathcal{K}} |\boldsymbol{h}_i(\boldsymbol{\theta})\mathbf{w}_j|^2 + \sigma_i^2$, and $\widehat{\rho}_i \triangleq \sum_{j=1,j\neq k}^{\mathcal{K}} |\widehat{\boldsymbol{h}}_i(\boldsymbol{\theta})\mathbf{w}_j|^2 + \sigma_i^2$. Under the presence of Eve, the closed-form expressions for the FBR-SR of the user-k under perfect and imperfect IRS to users/Eve CSI are defined as, respectively, [110, Eq.115]:

$$\mathcal{S}_k^{\mathcal{F}}(\mathbf{w},\boldsymbol{\theta}) \triangleq \left[C_k - C_e - \xi_k\sqrt{V_k} - \xi_e\sqrt{V_e}\right]^+, \tag{4.7}$$

$$\widehat{\mathcal{S}}_k^{\mathcal{F}}(\mathbf{w},\boldsymbol{\theta}) \triangleq \left[\widehat{C}_k - \widehat{C}_e - \xi_k\sqrt{\widehat{V}_k} - \xi_e\sqrt{\widehat{V}_e}\right]^+, \tag{4.8}$$

where $[x]^+ \triangleq \max[0,x]$, while the user's data rate, and the eavesdropping rate of Eve decoding s_k, are respectively given by,

$$C_i(\mathbf{w},\boldsymbol{\theta}) \triangleq \ln\left(1+\gamma_i(\mathbf{w},\boldsymbol{\theta})\right), i \in \{k,e\}. \tag{4.9}$$

$$\widehat{C}_i(\mathbf{w},\boldsymbol{\theta}) \triangleq \ln\left(1+\widehat{\gamma}_i(\mathbf{w},\boldsymbol{\theta})\right), i \in \{k,e\}, \tag{4.10}$$

$\xi_i \triangleq Q^{-1}(\tau_i)/\ln(2)\sqrt{N_t}$, $Q^{-1}(\cdot)$ is the inverse of the Gaussian Q-function, $N_t \triangleq \mathcal{B}t_t$ is the packet length, $\mathcal{B}$ is the bandwidth, t_t is the transmission duration, τ_k is the decoding error probability, τ_e is the information leakage [111], and V_k and V_e are the dispersion factors defined as [111],

$$V_i(\mathbf{w},\boldsymbol{\theta}) \triangleq \frac{2\gamma_i(\mathbf{w},\boldsymbol{\theta})}{(1+\gamma_i(\mathbf{w},\boldsymbol{\theta}))} \triangleq 2\left(1-(\rho_i/\upsilon_i)\right), \tag{4.11}$$

$$\widehat{V}_i(\mathbf{w},\boldsymbol{\theta}) \triangleq \frac{2\widehat{\gamma}_i(\mathbf{w},\boldsymbol{\theta})}{(1+\widehat{\gamma}_i(\mathbf{w},\boldsymbol{\theta}))} \triangleq 2\left(1-(\widehat{\rho}_i/\widehat{\upsilon}_i)\right), \tag{4.12}$$

where $\upsilon_i \triangleq \sum_{j=1}^{\mathcal{K}} |\boldsymbol{h}_i(\boldsymbol{\theta})\mathbf{w}_j|^2 + \sigma_i^2$, and $\widehat{\upsilon}_i \triangleq \sum_{j=1}^{\mathcal{K}} |\widehat{\boldsymbol{h}}_i(\boldsymbol{\theta})\mathbf{w}_j|^2 + \sigma_i^2,\ i \in \{k,e\}$.

Unlike the asymptotic Shannon capacity, which assumes infinite blocklength and negligible variance, the dispersion term captures the penalty on the achievable SR

due to finite coding lengths. A larger dispersion reduces the effective secrecy rate, as it increases the uncertainty in reliable decoding and secure transmission. Hence, optimising secrecy under FBR inherently involves balancing both the coding rate and the dispersion effect to ensure reliability and confidentiality within the given latency constraints.

Unlike the traditional SR definition in the LBR, the FBR imposes more constraints on the SR. Specifically, the reliable transmission in FBR requires that the decoding error probability τ_k at user-k is not larger than the maximum decoding error probability in FBR $\tau_{\max}$, the information leakage constraint imposes that the information leakage τ_e does not exceed $\tau_{e_{\max}}$, the maximum information leakage in FBR [111]. Additionally, the transmission duration t_t doesn't exceed the maximum transmission duration $t_{\max}$. Moreover, ensuring secure communication in the FBR regime with packet length N_t, is more challenging than in its LBR counterpart. This increased difficulty arises from the inherent limitations on the achievable SR in the FBR setting, which are due to the combined effects of non-negligible decoding error probabilities and information leakage. These two conditions distinguish the FBR case from its LBR counterpart. One may notice that when the transmission duration t_t approaches infinity, the dispersion factor V_i reaches zero, and the FBR definitions (4.7) and (4.8) reduce to the traditional LBR-SR case, which can be expressed as [90]:

$$\mathcal{S}_k^{\mathcal{L}}(\mathbf{w},\boldsymbol{\theta}) \triangleq [C_k(\mathbf{w},\boldsymbol{\theta}) - C_e(\mathbf{w},\boldsymbol{\theta})]^+, \tag{4.13}$$

$$\widehat{\mathcal{S}}_k^{\mathcal{L}}(\mathbf{w},\boldsymbol{\theta}) \triangleq [\widehat{C}_k(\mathbf{w},\boldsymbol{\theta}) - \widehat{C}_e(\mathbf{w},\boldsymbol{\theta})]^+. \tag{4.14}$$

4.2 MAXMIN SR Under Perfect CSI in FBR Systems

In this section, we first address the problem of maximising the minimum SR among all the users under the perfect CSI assumption to provide secure communications for all the users. The optimisation problem can be formally stated as:

$$(\mathcal{P}1): \max_{\mathbf{w},\boldsymbol{\theta}} \min_{k\in\mathcal{K}} \mathcal{S}_k^{\mathcal{F}}(\mathbf{w},\boldsymbol{\theta}), \tag{4.15a}$$

$$\text{s.t.} \quad \sum\nolimits_{k=1}^{\mathcal{K}} \|\mathbf{w}_k\|^2 \leq P, \tag{4.15b}$$

$$|e^{(j\boldsymbol{\theta})}| = 1, \tag{4.15c}$$

$$\tau_k \leq \tau_{\max},\ \tau_e \leq \tau_{e_{\max}},\ t_t \leq t_{\max}, \tag{4.15d}$$

where P is Alice's power budget, (4.15b) captures the sum of the transmitted power constraint, (4.15c) captures the UMC of the PREs' phase shift, and (4.15d) captures the maximum decoding error probability, the maximum information leakage, and the maximum transmission duration, respectively. It is worth noting that the FBR constraints shown in (4.15d), are inherently embedded within the objective function, since the SR expression $\mathcal{S}_k^{\mathcal{F}}(\mathbf{w},\boldsymbol{\theta})$ incorporates the square root of the dispersion factors, as shown in (4.7). As a result, the optimisation problem falls outside the scope of standard convex formulations and is more challenging to solve than its LBR counterpart.

The optimisation problem $(\mathcal{P}1)$ is nonconvex since the objective function (4.15a) is not concave the UMC (4.15c) is nonconvex. To tackle this nonconvex problem, one can employ the AO technique [91]. Specifically, at iteration (n), the feasible point $(\mathbf{w}^{(n)},\boldsymbol{\theta}^{(n)})$ is generated from $(\mathcal{P}1)$ by solving two sub-problems, the first one is to optimise $\mathbf{w}$ with a fixed $\boldsymbol{\theta}$:

$$(\mathcal{P}1.1): \max_{\mathbf{w}} \min_{k\in\mathcal{K}} \mathcal{S}_k^{\mathcal{F}}(\mathbf{w}^{(n)},\boldsymbol{\theta}),\ \text{s.t. (4.15b)}, \tag{4.16}$$

then, we optimise $\boldsymbol{\theta}$ with a fixed $\mathbf{w}$ by solving the following problem

$$(\mathcal{P}1.2): \max_{\boldsymbol{\theta}} \min_{k\in\mathcal{K}} \mathcal{S}_k^{\mathcal{F}}(\mathbf{w},\boldsymbol{\theta}^{(n)}),\ \text{s.t. (4.15c)}. \tag{4.17}$$

However, with AO, solving two subproblems $(\mathcal{P}1.1)$ and $(\mathcal{P}1.2)$ is computationally demanding, especially given the large number of PREs of the IRS. Our proposed

linearization method in the sequel uses mathematically tractable approximation functions leading to a computationally efficient algorithm that can be used for a large number of IRS's PREs.

4.2.1 Sub-Problem for Optimising the Beamforming Vectors

We fix $\boldsymbol{\theta}$ given $\mathbf{w}^{(n)}$ and solve the problem $(\mathcal{P}1)$ to obtain $\mathbf{w}^{(n+1)}$ satisfying $\mathcal{S}_k^{\mathcal{F}}(\mathbf{w}^{(n+1)},\boldsymbol{\theta}^{(n)}) \geq \mathcal{S}_k^{\mathcal{F}}(\mathbf{w}^{(n)},\boldsymbol{\theta}^{(n)})$. We start by linearizing the objective function in (4.15a), which consists of four parts: the user-k's SR $C_k(\mathbf{w},\boldsymbol{\theta})$, Eve's negative eavesdropping rate $C_e(\mathbf{w},\boldsymbol{\theta})$, the user-$k$ dispersion factor $V_k(\mathbf{w},\boldsymbol{\theta})$, and Eve's dispersion factor $V_e(\mathbf{w},\boldsymbol{\theta})$ as shown in (4.7).

First, we adopt the idea in [95] to convert user-k's SR into a linear form. Specifically, using the inequality (A.1) in Appendix A, let's define $\boldsymbol{\Lambda} \triangleq \boldsymbol{h}_k(\boldsymbol{\theta}^{(n)})\mathbf{w}_k$, $\boldsymbol{\digamma} \triangleq \rho_k$, $\hat{\Lambda} \triangleq \boldsymbol{h}_k(\boldsymbol{\theta}^{(n)})\mathbf{w}_k^{(n)}$ and $\hat{\boldsymbol{\digamma}} \triangleq \rho_k$, hence, the users' data rate can be written as:

$$C_k(\mathbf{w},\boldsymbol{\theta}^{(n)}) \geq x_{1,k}^{(n)} + 2\Re\left\{\left\langle \boldsymbol{y}_{k,k}^{(n)}, \mathbf{w}_k \right\rangle\right\} - z_{1,k}^{(n)}\upsilon_k^{(n)}, \tag{4.18}$$

where

$$\begin{aligned}
x_{1,k}^{(n)} &\triangleq C_k(\mathbf{w}^{(n)},\boldsymbol{\theta}^{(n)}) - \gamma_k(\mathbf{w}^{(n)},\boldsymbol{\theta}^{(n)}) - \sigma_k^2 z_{1,k}^{(n)},\\
\boldsymbol{y}_{k,k}^{(n)} &\triangleq \boldsymbol{h}_k^H(\boldsymbol{\theta}^{(n)})\boldsymbol{h}_k(\boldsymbol{\theta}^{(n)})\mathbf{w}_k^{(n)}/\rho_k^{(n)},\\
z_{1,k}^{(n)} &\triangleq 1/\rho_k^{(n)} - 1/\upsilon_k^{(n)}.
\end{aligned}$$

Second, we linearise Eve's eavesdropping rate, which can be written as:

$$-\ln(1+\gamma_e(\mathbf{w},\boldsymbol{\theta}^{(n)})) \triangleq \overbrace{\ln(1+\rho_e^{(n)})}^{a_1} - \overbrace{\ln(1+\upsilon_e^{(n)})}^{a_2}. \tag{4.19}$$

Here, we adopt the idea in [92], where the term (a_1) in (4.19) can be linearised by defining $\boldsymbol{z} \triangleq \rho_e$ and substituting it in the inequality (A.2) in Appendix A. The term (a_2) in (4.19) can be linearised by defining $\boldsymbol{\Upsilon} \triangleq \upsilon_e$ and substituting it in the inequality (A.3) in Appendix A. Hence, Eve's eavesdropping rate can be expressed

as:

$$C_e(\mathbf{w},\boldsymbol{\theta}^{(n)}) \geq x_{1,k_e}^{(n)} + z_{1,k_e}^{(n)} + 2\Re \sum_{j=1,j\neq k}^{\mathcal{K}} \left\{ \left\langle \boldsymbol{y}_{j,k_e}^{(n)}, \mathbf{w}_j \right\rangle \right\} - \frac{\rho_e^{(n)}}{1+\rho_e^{(n)}} \left(\sum_{j=1,j\neq k}^{\mathcal{K}} |\boldsymbol{h}_e(\boldsymbol{\theta}^{(n)})\mathbf{w}_j|^2 \right) - \frac{1}{\upsilon_e^{(n)}} \sum_{j=1}^{\mathcal{K}} |\boldsymbol{h}_e(\boldsymbol{\theta}^{(n)})\mathbf{w}_j|^2, \tag{4.20}$$

where,

$$\begin{aligned} x_{1,k_e}^{(n)} &\triangleq \ln\left(\rho_e^{(n)}\right) - \rho_e^{(n)} - \ln\left(\upsilon_e^{(n)}\right) + 1, \\ z_{1,k_e}^{(n)} &\triangleq \left(-\frac{\rho_e^{(n)}}{1+\rho_e^{(n)}} - \frac{1}{\upsilon_e^{(n)}} \right) \sigma_e^2, \\ \boldsymbol{y}_{k_e,j}^{(n)} &\triangleq \boldsymbol{h}_e^H(\boldsymbol{\theta}^{(n)}) \boldsymbol{h}_e(\boldsymbol{\theta}^{(n)}) \mathbf{w}_j^{(n)}. \end{aligned}$$

Next, we linearise the FBR dispersion factors $V_i(\mathbf{w},\boldsymbol{\theta}), i \in \{k,e\}$. Using (4.11), the inequalities (A.4) and (A.5) in Appendix A, and by defining $x \triangleq V_i(\mathbf{w}^{(n)},\boldsymbol{\theta})$, $\mathbf{A} \triangleq \rho_i$, and $B \triangleq \varsigma_i$, the dispersion factors can be expressed as:

$$\xi_i \sqrt{V_i(\mathbf{w},\boldsymbol{\theta}^{(n)})} \leq q_{2,i}^{(\iota)} - 2 \sum_{j=1,j\neq k}^{\mathcal{K}} \Re\left\{ \left\langle \boldsymbol{d}_{j,i}^{(\iota)}, \mathbf{w}_j \right\rangle \right\} - n_{2,i}^{(\iota)} \upsilon^{(\kappa)}, \tag{4.21}$$

where

$$\begin{aligned} x_{2,i}^{(n)} &\triangleq \xi_i \left(\frac{\sqrt{V_i(\mathbf{w}^{(n)},\boldsymbol{\theta}^{(n)})}}{2} + \frac{\left(\upsilon_i^{(n)}\right)^2 + \rho_i^{(n)}\sigma_i^2 - 2\upsilon_i^{(n)}\sigma_i^2}{\left(\upsilon_i^{(n)}\right)^2 \sqrt{V_i(\mathbf{w}^{(n)},\boldsymbol{\theta}^{(n)})}} \right), \\ \boldsymbol{f}_{j,i}^{(n)} &\triangleq \xi_i [\boldsymbol{h}_i(\boldsymbol{\theta}^{(n)})]^2 \mathbf{w}_j^{(n)} / \upsilon_i^{(n)} \sqrt{V_i(\mathbf{w}^{(n)},\boldsymbol{\theta}^{(n)})}, \\ z_{2,i}^{(n)} &\triangleq \frac{\xi_i \rho_i^{(n)}}{\left(\upsilon_i^{(n)}\right)^2 \sqrt{V_i(\mathbf{w}^{(n)},\boldsymbol{\theta}^{(n)})}}. \end{aligned}$$

By substitution (4.18), (4.20), and (4.21) into (4.7), the approximated surrogate FBR-SR function can be written as:

$$\widetilde{\mathcal{S}}_k^{\mathcal{F}}(\mathbf{w},\boldsymbol{\theta}^{(n)}) \geq x_k^{(n)} + 2\Re\left\{ \left\langle \boldsymbol{y}_k^{(n)}, \mathbf{w}_k \right\rangle \right\} - (\mathbf{w}_k)^H \boldsymbol{\psi}_k^{(n)} \mathbf{w}_k, \tag{4.22}$$

where

$$
\begin{aligned}
x_k^{(n)} &\triangleq x_{1,k}^{(n)} + x_{1,k_e}^{(n)} + z_{1,k_e}^{(n)} + x_{2,k}^{(n)} + x_{2,k_e}^{(n)},\\
\boldsymbol{y}_k^{(n)} &\triangleq \sum\nolimits_{j=1}^{\mathcal{K}} \boldsymbol{y}_{j,k}^{(n)} + \sum\nolimits_{j=1, j\neq k}^{\mathcal{K}} \left(\boldsymbol{y}_{k_e,j}^{(n)} - \boldsymbol{f}_{j,k}^{(n)} - \boldsymbol{f}_{j,k_e}^{(n)}\right),\\
\boldsymbol{\psi}_k^{(n)} &\triangleq \sum\nolimits_{j=1}^{\mathcal{K}} z_j^{(n)} \boldsymbol{h}_j^H(\boldsymbol{\theta}^{(n)}) \boldsymbol{h}_j(\boldsymbol{\theta}^{(n)}) + z_{k_e}^{(n)} \boldsymbol{h}_e^H(\boldsymbol{\theta}^{(n)}) \boldsymbol{h}_e(\boldsymbol{\theta}^{(n)}),\\
z_k^{(n)} &\triangleq z_{1,k}^{(n)} + z_{2,k}^{(n)},\\
z_{k_e}^{(n)} &\triangleq \rho_e^{(n)} / \left(1 + \rho_e^{(n)}\right) + 1/\upsilon_e^{(n)} + z_{2,k_e}.
\end{aligned}
$$

Finally, by substitution (4.22) in (4.16), and introducing an auxiliary variable $\mathcal{D}$ as the lower bound of the FBR-SR, we can recast problem ($\mathcal{P}$1.1) as:

$$
(\mathcal{P}1.3): \max_{\mathbf{w}} \mathcal{D}, \tag{4.23a}
$$

$$
\text{s.t.} \quad \mathcal{D} \leq \widetilde{\mathcal{S}}_k^{\mathcal{F}}(\mathbf{w}, \boldsymbol{\theta}^{(n)}),\ \forall k, \tag{4.23b}
$$

$$
(4.15\text{b}),\ (4.15\text{d}). \tag{4.23c}
$$

problem ($\mathcal{P}$1.3) is a Semidefinite Programming problem (SDP), with its linearised objective function in (4.22). This problem can be solved using standard solvers, e.g., the interior point method or the CVX toolbox [93].

4.2.2 Sub-Problem for Optimising the PREs

Likewise, given $\mathbf{w}$, we aim to find $\boldsymbol{\theta}^{(\iota+1)}$ such that, $\mathcal{S}_k(\mathbf{w}_k^{(n+1)}, \boldsymbol{\theta}^{(n+1)}) \geq \mathcal{S}_k(\mathbf{w}_k^{(n+1)}, \boldsymbol{\theta}^{(n)})$. Similar to the previous section, the lower bound approximation of the user's SR can be obtained using the inequality (A.1) in Appendix A. The user's data rate can be expressed as:

$$
C_k(\mathbf{w}^{(n+1)}, \boldsymbol{\theta}) \geq x_{1,k}^{(n+1)} + 2\Re\left\{\sum\nolimits_{m=1}^{M} \boldsymbol{y}_{k,k}^{(n+1)}(m) e^{j\theta_m}\right\} + \left(e^{j\boldsymbol{\theta}}\right)^H \boldsymbol{\varphi}_{1,k}^{(n+1)} e^{j\boldsymbol{\theta}}, \tag{4.24}
$$

where,

$$\begin{aligned}
x_{1,k}^{(n+1)} &\triangleq C_k(\mathbf{w}^{(n+1)}, \boldsymbol{\theta}^{(n)}) - \gamma_k(\mathbf{w}^{(n+1)}, \boldsymbol{\theta}^{(n)}) - \sigma_k^2 z_{1,k}^{(n+1)}, \\
z_{1,k}^{(n+1)} &\triangleq 1/\rho_k^{(n+1)} - 1/\upsilon_k^{(n+1)}, \\
\boldsymbol{y}_{k,k}^{(n+1)}(m) &\triangleq \tilde{\boldsymbol{y}}_{k,k}^{(n+1)}(m)/\rho_k^{(n+1)}, \\
\tilde{\boldsymbol{y}}_{k,k}^{(n+1)}(m) &\triangleq \left(\mathbf{w}_k^{(n+1)}\right)^H \boldsymbol{h}_k^H(\boldsymbol{\theta}^{(n)}) \boldsymbol{l}_k \boldsymbol{\Gamma}_m \boldsymbol{L}_{\mathrm{AR}} \mathbf{w}_k^{(n+1)}, \\
\boldsymbol{\varphi}_{1,k}^{(n+1)} &\triangleq -z_{1,k}^{(n+1)} \sum\nolimits_{j=1}^{\mathcal{K}} \boldsymbol{\varphi}_{k,j}^{(n+1)}, \\
\boldsymbol{\varphi}_{k,j}^{(n+1)} &\triangleq \left(\boldsymbol{\Lambda}_{k,j}^{(n+1)}(m)\right)^* \boldsymbol{\Lambda}_{k,j}^{(n+1)}(\dot{m}), m \in M, \dot{m} \in M, \\
\boldsymbol{\Lambda}_{k,j}^{(n+1)}(m) &\triangleq \boldsymbol{l}_k \boldsymbol{\Gamma}_m \boldsymbol{L}_{\mathrm{AR}} \mathbf{w}_j^{(n+1)}.
\end{aligned}$$

Similarly, we can express Eve's eavesdropping rate as:

$$\begin{aligned}
C_e(\mathbf{w}^{(n+1)}, \boldsymbol{\theta}) \geq x_{1,k_e}^{(n+1)} + z_{1,k_e}^{(n+1)} + 2\Re\left\{\sum\nolimits_{m=1}^{M} \boldsymbol{y}_{k_e}^{(n+1)}(m) e^{(j\theta_m)}\right\} + \left(e^{j\boldsymbol{\theta}}\right)^H \boldsymbol{\varphi}_{1,k_e}^{(n+1)} e^{j\boldsymbol{\theta}} + \\
\left(e^{j\boldsymbol{\theta}}\right)^H \boldsymbol{\varphi}_{k_e,j}^{(n+1)} e^{j\boldsymbol{\theta}},
\end{aligned} \tag{4.25}$$

where,

$$\begin{aligned}
x_{1,k_e}^{(n+1)} &\triangleq \ln\left(\rho_e^{(n+1)}\right) - \rho_e^{(n+1)} - \ln\left(\upsilon_e^{(n+1)}\right) + 1, \\
z_{1,k_e}^{(n+1)} &\triangleq \left(-\rho_e^{(n+1)}/1 + \rho_e^{(n+1)} - 1/\upsilon_e^{(n+1)}\right) \sigma_e^2, \\
\boldsymbol{y}_{k_e}^{(n+1)}(m) &\triangleq \sum\nolimits_{j=1, j\neq k}^{\mathcal{K}} \boldsymbol{y}_{j,k_e}^{(n+1)}(m), \\
\boldsymbol{y}_{j,k_e}^{(n+1)}(m) &\triangleq \left(\mathbf{w}_k^{(n+1)}\right)^H \boldsymbol{h}_e^H(\boldsymbol{\theta}^{(n)}) \boldsymbol{l}_e \boldsymbol{\Gamma}_m \boldsymbol{L}_{\mathrm{AR}} \mathbf{w}_k^{(n+1)}, \\
\boldsymbol{\varphi}_{1,k_e}^{(n+1)} &\triangleq -\frac{\rho_e^{(n+1)} \sum_{j=1}^{\mathcal{K}} \boldsymbol{\varphi}_{k_e,j}^{(n+1)}}{(1+\rho_e^{(n+1)})} - \frac{\sum_{j=1}^{\mathcal{K}} \boldsymbol{\varphi}_{k_e,j}^{(n+1)}}{(\sigma_e^2 + \upsilon_e^{(n+1)})}, \\
\boldsymbol{\varphi}_{k_e,j}^{(n+1)} &\triangleq \left(\boldsymbol{\Lambda}_{k_e,j}^{(n+1)}(m)\right)^* \boldsymbol{\Lambda}_{k_e,j}^{(n+1)}(\dot{m}), \\
\boldsymbol{\Lambda}_{k_e,j}^{(n+1)}(m) &\triangleq \boldsymbol{l}_e \boldsymbol{\Gamma}_m \boldsymbol{L}_{\mathrm{AR}} \mathbf{w}_j^{(n+1)}.
\end{aligned}$$

Next, we express the user-k's and Eve dispersion factor. For $i \in \{k, e\}$, we can express the dispersion factors as:

$$\xi_i \sqrt{V_i(\mathbf{w}^{(n+1)}, \boldsymbol{\theta})} \leq x_{2,i}^{(n+1)} - 2\Re\left\{\sum\nolimits_{m=1}^{M} \boldsymbol{f}_i^{(n+1)} e^{(j\theta_m)}\right\} + \left(e^{(j\boldsymbol{\theta})}\right)^H \boldsymbol{\varphi}_{2,i}^{(n+1)} e^{(j\boldsymbol{\theta})}, i \in \{k, e\}, \tag{4.26}$$

where,

$$x_{2,i}^{(n+1)} \triangleq \frac{\xi_i\left(\left(\upsilon_i^{(n+1)}\right)^2\sqrt{V_i(\mathbf{w}^{(n+1)},\boldsymbol{\theta}^{(n)})}+2\left(\upsilon_i^{(n+1)}\right)^2+2\sigma_i^2\rho_i^{(n+1)}-4\sigma_i^2\left(\upsilon_i^{(n+1)}\right)\right)}{\left(2\left(\upsilon_i^{(n+1)}\right)^2\sqrt{V_i(\mathbf{w}^{(n+1)},\boldsymbol{\theta}^{(n)})}\right)},$$

$$\boldsymbol{f}_{i,j}^{(n+1)}(m) \triangleq \frac{\xi_i\left(\mathbf{w}_j^{(n+1)}\right)^H\boldsymbol{h}_i^H(\boldsymbol{\theta}^{(n)})\boldsymbol{l}_i\Lambda_m\boldsymbol{L}_{\text{AR}}\mathbf{w}_j^{(n+1)}}{\left(\upsilon_i^{(n+1)}\sqrt{V_i(\mathbf{w}^{(n+1)},\boldsymbol{\theta}^{(n)})}\right)}, m\in M, j\in K, j\neq k,$$

$$\boldsymbol{f}_i^{(n+1)} \triangleq \sum\nolimits_{j=1,j\neq k}^{\mathcal{K}}\boldsymbol{f}_{i,j}^{(n+1)},$$

$$\boldsymbol{\varphi}_{2,i}^{(n+1)} \triangleq z_{2,i}^{(n+1)}\sum\nolimits_{j=1}^{\mathcal{K}}\boldsymbol{\varphi}_{i,j}^{(n+1)},$$

$$z_{2,i}^{(n+1)} \triangleq \frac{\left(\xi_i\rho_i^{(n+1)}\right)}{\left(\upsilon_i^{(n+1)}\right)^2\sqrt{V_i(\mathbf{w}^{(n+1)},\boldsymbol{\theta}^{(n)})}}.$$

By substituting (4.24), (4.25), and (4.26) in (4.7), the lower bounding concave approximation of the FBR-SR can be expressed as:

$$\widetilde{\mathcal{S}}_k^{\mathcal{F}}\left(\mathbf{w}^{(n+1)},\boldsymbol{\theta}\right) \geq x_k^{(n+1)}+2\sum\nolimits_{m=1}^{M}\Re\left\{\boldsymbol{y}_k^{(n+1)}(m)e^{j\theta_m}\right\}, \tag{4.27}$$

where,

$$x_k^{(n+1)} \triangleq x_{1,k}^{(n+1)}+x_{1,k_e}^{(n+1)}+x_{2,k}^{(n+1)}+x_{2,k_e}^{(n+1)}+z_{1,ke}^{(n+1)}-\left(e^{j\boldsymbol{\theta}^{(n)}}\right)^H\boldsymbol{\varphi}_k^{(n+1)}e^{j\boldsymbol{\theta}}-$$
$$2\lambda_{\max}\left(\boldsymbol{\varphi}_k^{(n+1)}\right)M,$$

$$\boldsymbol{y}_k^{(n+1)}(m)\boldsymbol{y}_k^{(n+1)}(m) \triangleq \boldsymbol{y}_{k,k}^{(n+1)}(m)+\boldsymbol{y}_{k_e}^{(n+1)}(m)+\boldsymbol{f}_k^{(n+1)}(m)+\boldsymbol{f}_{k_e}^{(n+1)}(m)+$$
$$\sum\nolimits_{m=1}^{N}e^{-j\theta_m^{(n)}}\boldsymbol{\varphi}_k^{(n+1)}(m,n)+\lambda_{\max}\left(\boldsymbol{\varphi}_k^{(n+1)}\right),$$

$$\boldsymbol{\varphi}_k^{(n+1)} \triangleq \boldsymbol{\varphi}_{1,k}^{(n+1)}+\boldsymbol{\varphi}_{1,k_e}^{(n+1)}+\boldsymbol{\varphi}_{k_e,j}^{(n+1)}+\boldsymbol{\varphi}_{2,k}^{(n+1)}+\boldsymbol{\varphi}_{2,k_e}^{(n+1)}.$$

With (4.27), we formulate the following optimisation problem to obtain $\boldsymbol{\theta}^{(n+1)}$,

$$(\mathcal{P}1.4): \max_{\boldsymbol{\theta}}\min_{k\in\mathcal{K}}\mathcal{S}_k^{\mathcal{F}}\left(\mathbf{w}^{(n+1)},\boldsymbol{\theta}^{(n)}\right), \tag{4.28a}$$

$$\text{s.t.} \quad (4.15\text{c}). \tag{4.28b}$$

To tackle problem ($\mathcal{P}1.4$) we define,

$$\theta_m^{(n+1),k} \triangleq 2\pi-\angle\boldsymbol{y}_k^{(n+1)}(m), m=1,\ldots,M, \tag{4.29}$$

Algorithm 4.1 Proposed Iterative Algorithm for Solving ($\mathcal{P}1$)

1: **Initialise:** ($\boldsymbol{w}^{(1)} = \mathbf{w}^*$, $\boldsymbol{\theta}^{(1)} = \boldsymbol{\theta}^*$, $\tau_{\max}$, $\tau_{e_{\max}}$, $t_{\max}$), convergence tolerance $\epsilon_t > 0$, and Set $n = 1$.

2: **Repeat**

3: Update $\mathbf{w}^{(n+1)}$ by (4.23), and $\boldsymbol{\theta}^{(n+1)}$ by (4.30);

4: **if** $\frac{|\min\limits_{k\in\mathcal{K}} \mathcal{S}_k^{\mathcal{F}}(\mathbf{w}^{(n+1)},\boldsymbol{\theta}^{(n+1)}) - \min\limits_{k\in\mathcal{K}} \mathcal{S}_k^{\mathcal{F}}(\mathbf{w}^{(n)},\boldsymbol{\theta}^{(n)})|}{\min\limits_{k\in\mathcal{K}} \mathcal{S}_k^{\mathcal{F}}(\mathbf{w}^{(n)},\boldsymbol{\theta}^{(n)})} \leq \epsilon_t$.

5: **Then** $\boldsymbol{\theta}^{(n)} \leftarrow \boldsymbol{\theta}^{(n+1)}$, $\mathbf{w}^{(n)} \leftarrow \mathbf{w}^{(n+1)}$ and terminate.

6: **Otherwise** $n \leftarrow n + 1$ and continue.

7: **Output** ($\mathbf{w}^* = \mathbf{w}_k^{(n)}, \boldsymbol{\theta}^* = \boldsymbol{\theta}^{(n)}$).

then we find $\boldsymbol{\theta}^{(\iota+1)}$ that maximise the SR($\mathbf{w}^{(n+1)}, \boldsymbol{\theta}$) and satisfies the UMC constraint (4.15c),

$$\boldsymbol{\theta}^{(n+1)} \triangleq \arg \max_{\boldsymbol{\theta}\in\left\{\boldsymbol{\theta}^{(n+1),k}, k=1,\ldots,\mathcal{K}\right\}} \widetilde{\mathcal{S}}_k^{\mathcal{F}}(\mathbf{w}^{(n+1)}, \boldsymbol{\theta}). \tag{4.30}$$

One can notice that by setting $V_i = 0$, the above FBR optimisation problem ($\mathcal{P}1$) is reduced to the LBR optimisation problem, which can be solved similarly.

The procedure to solve problem ($\mathcal{P}1$) is described in Algorithm 4.1, which converges to a locally optimal solution of ($\mathcal{P}1$) as formally stated in the following theorem.

Theorem 4.1. *The obtained solution by Algorithm 4.1 is a locally optimal solution for problem* ($\mathcal{P}1$).

Proof: See Appendix C.1.

Complexity Analysis

The developed Algorithm 4.1 is designed to tackle problem ($\mathcal{P}1$) by decoupling the beamforming vector and the IRS's PREs within the objective function. The

resulting problem ($\mathcal{P}1$) is an SDP that can be solved by the interior point method [93]. The algorithm's complexity can be estimated by its worst-case runtime and the number of decision variables [94]. Thus, in Algorithm 4.1, the computational complexity of obtaining $\mathbf{w}$ given $\boldsymbol{\theta}$ is $\mathcal{O}(N^3)$, and the computational complexity of obtaining $\boldsymbol{\theta}$ given $\mathbf{w}$ is $\mathcal{O}(M^3(M+1))$. One can notice that the algorithm complexity increases with M.

4.3 MAXMIN SR Under Imperfect CSI With FBR Systems

To deal with the imperfect CSI from the IRS to the users and Eve, we adopt the channel modelling in equation (4.3) where only partial/imperfect CSI $\widehat{\boldsymbol{u}}_i$ is available. First, we can cast the minimum SR maximisation problem as follows:

$$(\mathcal{P}2) : \max_{\mathbf{w},\boldsymbol{\theta}} \min_{k\in\mathcal{K}} \widehat{\mathcal{S}}_k^{\mathcal{F}}(\mathbf{w},\boldsymbol{\theta}), \tag{4.31a}$$

$$\text{s.t.} \quad \sum\nolimits_{k=1}^{\mathcal{K}} \|\mathbf{w}_k\|^2 \leq P, \tag{4.31b}$$

$$|e^{(j\boldsymbol{\theta})}| = 1, \tag{4.31c}$$

$$\|\Delta\boldsymbol{l}_i\|_2 \leq \Omega_i, i \in \{k, e\}. \tag{4.31d}$$

$$\tau_k \leq \tau_{\max},\ \tau_e \leq \tau_{e_{\max}},\ t_t \leq t_{\max}, \tag{4.31e}$$

where (4.31d) captures the channel estimation error. Unlike the traditional LBR case under imperfect CSI, problem ($\mathcal{P}2$) is more challenging. First, this is because the additional FBR constraints, which are captured by the nonconvex dispersion factor expression (4.12), are embedded within the objective function. In addition, the imperfect CSI condition (4.31d), introduces uncertainty in the IRS-users/Eve's channel, making the decoding error and consequently the inverse Q-function evaluation unreliable. This sensitivity significantly complicates the objective function, besides its nonlinearity and nonconvexity.

To solve problem ($\mathcal{P}2$), we first introduce slack variables to decompose the coupling of the beamforming vector and the IRS's PREs in the objective function to

facilitate the AO method. Specifically, we first substitute (4.13) into (4.31a), and then we introduce slack variables $\mathcal{Z}$ as the FBR-SR's lower bound, β_k represents the minimum users' rate, Υ_{k_e} represents the maximum eavesdropping rate of Eve, and $\tilde{\beta}_i, i \in \{k, e\}$ represents the maximum dispersion factor for the user-k and Eve, respectively. The problem $(\mathcal{P}2)$ can be recast as:

$$(\mathcal{P}2.1): \max_{\mathbf{w},\boldsymbol{\theta}} \ \mathcal{Z}, \tag{4.32a}$$

$$\text{s.t.} \quad \mathcal{Z} \leq \beta_k - \Upsilon_{k_e} - \tilde{\beta}_k - \tilde{\beta}_{k_e}, \forall k, \tag{4.32b}$$

$$\beta_k \leq \widehat{C}_k, \forall \|\Delta \boldsymbol{l}_k\|_2 \leq \xi_k, \forall k, \tag{4.32c}$$

$$\Upsilon_{k_e} \geq \widehat{C}_e, \forall \|\Delta \boldsymbol{l}_e\|_2 \leq \xi_e, \forall k, \tag{4.32d}$$

$$\tilde{\beta}_k \geq \xi_k \sqrt{\widehat{V}_k}, \forall \|\Delta \boldsymbol{l}_k\|_2 \leq \xi_k, \forall k, \tag{4.32e}$$

$$\tilde{\beta}_{k_e} \geq \xi_e \sqrt{\widehat{V}_e}, \forall \|\Delta \boldsymbol{l}_e\|_2 \leq \xi_e, \forall k, \tag{4.32f}$$

$$(4.31b),\ (4.31c),\ (4.31e). \tag{4.32g}$$

Problem $\mathcal{P}2.1$ is still nonconvex due to the coupling between $\mathbf{w}$ and $\boldsymbol{\theta}$ within the constraints (4.32b), (4.32c), (4.32d), (4.32e), and (4.32f). In addition, the presence of the nonlinear square-root terms of the dispersion factors in (4.32e) and (4.32f) further increases the complexity of the problem. One can notice that the constraint (4.31d) in problem $(\mathcal{P}2)$ has been captured by the constraints (4.32c), (4.32d), (4.32e), and (4.32f) in problem $(\mathcal{P}2.1)$ (referring to the CSI factor in the channel definition (4.4)). Next, we linearise the square-root of the dispersion factors, and then we employ the SCA technique, the $\mathcal{S}$-procedure, and the first order Taylor approximation to transform the semi-infinite nonconvex constraints (4.32c), (4.32d), (4.32e), and (4.32f) to finite LMIs. Then, we leverage a PCCP algorithm to tackle the UMC (4.31c) [112].

4.3.1 Sub-Problem for Optimising the Beamforming Vectors

To linearise the semi-infinite inequalities in (4.32c), we first substitute (4.10) into (4.32c), hence, (4.32c) can be expressed as:

$$2^{\beta_k} - 1 \leq \frac{|(\boldsymbol{l}_k \boldsymbol{\Phi} \boldsymbol{L}_{\mathrm{AR}}) \mathbf{w}_k|^2}{\|(\boldsymbol{l}_k \boldsymbol{\Phi} \boldsymbol{L}_{\mathrm{AR}}) \mathbf{W}_{-k}\|^2 + \sigma_k^2}, \forall k, \tag{4.33}$$

where $\mathbf{W}_{-k} = [\mathbf{w}_1, \ldots, \mathbf{w}_{k-1}, \mathbf{w}_{k+1}, \ldots, \mathbf{w}_{\mathcal{K}}] \in \mathbb{C}^{M \times \mathcal{K}-1}$. By treating the interference plus noise signal as an auxiliary function $\boldsymbol{\alpha} = [\alpha_1, \ldots, \alpha_K]$, (4.33) can be expressed as:

$$|(\boldsymbol{l}_k \boldsymbol{\Phi} \boldsymbol{L}_{\mathrm{AR}}) \mathbf{w}_k|^2 \geq (2^{\beta_k} - 1)\alpha_k, \forall k, \tag{4.34a}$$

$$\|(\boldsymbol{u}_k \boldsymbol{\Phi} \boldsymbol{L}_{\mathrm{AR}}) \mathbf{W}_{-k}\|^2 + \sigma_k^2 \leq \alpha_k, \forall k. \tag{4.34b}$$

To circumvent the nonconvex semi-infinite inequalities in (4.34a), we replace the left-hand side of (4.34a) with their lower bounds using the following Lemma.

Lemma 5. *At iteration* (n)*, let* $\mathbf{w}^{(n)}$ *and* $\boldsymbol{\theta}^{(n)}$ *be the optimal solution, then at the point* $(\mathbf{w}^{(n)}, \boldsymbol{\theta}^{(n)})$ *we can express the linear lower bound of* (4.34a) *as:*

$$|(\boldsymbol{l}_k \boldsymbol{\Phi} \boldsymbol{L}_{AR}) \boldsymbol{w}_k|^2 \triangleq \boldsymbol{l}_k \mathbf{A}_k \boldsymbol{l}_k^H, \tag{4.35}$$

where

$$\begin{aligned} \mathbf{A}_k \triangleq & \boldsymbol{\Phi} \boldsymbol{L}_{AR} \boldsymbol{w}_k \boldsymbol{w}_k^{(n),H} \boldsymbol{L}_{AR}^H \boldsymbol{\Phi}^{(n),H} + \boldsymbol{\Phi}^{(n)} \boldsymbol{L}_{AR} \boldsymbol{w}_k^{(n)} \boldsymbol{w}_k^H \boldsymbol{L}_{AR}^H \boldsymbol{\Phi}^{(n),H} \\ & - \boldsymbol{\Phi}^{(n)} \boldsymbol{L}_{AR} \boldsymbol{w}_k^{(n)} \boldsymbol{w}_k^{(n),H} \boldsymbol{L}_{AR}^H \boldsymbol{\Phi}^{(n),H}. \end{aligned}$$

Proof: Refer to Appendix C.1.

Next, by substituting (4.35) in (4.34a), and using (4.3a) and Lemma 5, the inequality in (4.34a) is reformulated as:

$$\Delta \boldsymbol{l}_k \mathbf{A}_k \Delta \boldsymbol{l}_k^H + 2\Re\{(\widehat{\boldsymbol{l}}_k^H \mathbf{A}_k) \Delta \boldsymbol{l}_k\} + d_k \geq (2^{\beta_k} - 1)\alpha_k, \forall \|\Delta \boldsymbol{l}_k\|_2 \leq \Omega_k, \forall k. \tag{4.36}$$

where $d_k \triangleq \widehat{\boldsymbol{l}}_k \mathbf{X}_k \widehat{\boldsymbol{l}}_k^H$.

To address the uncertainty of $\{\Delta \boldsymbol{l}_k\}$ in (4.36), we leverage the $\mathcal{S}$-procedure [75].

Lemma 6. *($\mathcal{S}$-procedure) For any Hermitian matrix $\mathbf{U}_i \in \mathbb{C}^{L\times L}$, vector $\mathbf{u}_i \in \mathbb{C}^{L\times 1}$, and scalar u_i, for $i = 0, \ldots, Q$. A quadratic function of a variable x is defined as:*

$$f_i(x) \triangleq x^H \mathbf{U}_i x + 2\Re\{\mathbf{u}_i^H x\} + u_i. \tag{4.42}$$

The condition $f_0(x) \geq 0$ such that $f_i(x) \geq 0,\ i = 1, \ldots, Q$, holds, if an only if there exists $\mathfrak{n}_i \geq 0, i = 0, \ldots, Q$, such that,

$$\begin{bmatrix} \mathbf{U}_0 & \mathbf{u}_0 \\ \mathbf{u}_0^H & u_0 \end{bmatrix} - \sum\nolimits_{i=0}^{Q} \mathfrak{n}_i \begin{bmatrix} \mathbf{U}_i & \mathbf{u}_i \\ \mathbf{u}_i^H & u_i \end{bmatrix} \succeq 0. \tag{4.43}$$

Using Lemma 10, we can transform (4.36) into its equivalent LMIs as:

$$\begin{bmatrix} \eta_k \mathbf{I}_M + \mathbf{A}_k & (\widehat{\boldsymbol{l}}_k \mathbf{A}_k)^H \\ (\widehat{\boldsymbol{l}}_k \mathbf{A}_k) & d_k - (2^{\beta_k} - 1)\alpha_k - \eta_k \Omega_k^2 \end{bmatrix} \succeq 0, \forall k, \tag{4.44}$$

where $\boldsymbol{\eta} \triangleq [\eta_1, \ldots, \eta_{\mathcal{K}}]^T \geq 0$ are slack variables. Even though (4.34a) has been transformed into an LMI form, it is still nonconvex due to the nonconvexity nature of the term $2^{\beta_k}\alpha_k$. For that, we adopt the SCA technique [74] to convert the nonconvex constraint (4.34a) to a convex approximation expression. Specifically, performing the first order Taylor approximation, the term $2^{\beta_k}\alpha_k$ can be upper bounded by:

$$(\alpha_k(2^{\beta_k}))^{ub} \triangleq \left((\beta_k - \beta_k^{(n)})(\alpha_k^{(n)}) \ln 2 + \alpha_k\right) 2^{\beta_k^{(n)}}, \tag{4.45}$$

where $\beta_k^{(n)}, \alpha_k^{(n)}$ are the value of the variables β_k, α_k at iteration (n) in the SCA-based algorithm, respectively. Lastly, substituting (4.45) in (4.44), the LMIs in (4.44) can be expressed as:

$$\begin{bmatrix} \eta_k \mathbf{I}_M + \mathbf{A}_k & (\widehat{\boldsymbol{l}}_k \mathbf{A}_k)^H \\ (\widehat{\boldsymbol{l}}_k \mathbf{A}_k) & d_k - (\alpha_k(2^{\beta_k}))^{ub} + \alpha_k - \eta_k \Omega_k^2 \end{bmatrix} \succeq 0, \forall k. \tag{4.46}$$

Next, we tackle (4.34b) using Schur's complement [96].

Lemma 7. *(Schur's complement) For given matrices* $\mathbf{U} \succeq 0$, $\mathbf{Y}$, *and* $\mathbf{Z}$, *let a Hermitian matrix* $\mathbf{X}$ *be defined as:*

$$\mathbf{X} \triangleq \begin{bmatrix} \mathbf{Z} & \mathbf{Y}^H \\ \mathbf{Y} & \mathbf{U} \end{bmatrix}. \tag{4.47}$$

Then, $\mathbf{X} \succeq 0$ if and only if $\Delta\mathbf{U} \succeq 0$, where $\Delta\mathbf{U}$ is the Schur's complement define as $\Delta\mathbf{U} \triangleq \mathbf{Z} - \mathbf{Y}^H\mathbf{U}^{-1}\mathbf{Y}$.

Using Lemma (7), we can equivalently recast (4.34b) as:

$$\begin{bmatrix} \alpha_k & \mathbf{t}_k^H \\ \mathbf{t}_k^H & \mathbf{I}_{K-1} \end{bmatrix} \succeq 0, \forall \|\Delta\boldsymbol{l}_k\|_2 \leq \Omega_k, \forall k, \tag{4.48}$$

where $\mathbf{t}_k \triangleq \left((\widehat{\boldsymbol{l}}_k^H \boldsymbol{\Phi}\boldsymbol{L}_{\mathrm{AR}})\mathbf{W}_{-k}\right)^H$.

Next, we use the Nemirovski's Lemma [97] to further handle (4.48).

Lemma 8. *(Nemirovski's Lemma) For any Hermitian matrix* $\mathbf{A}$, *matrices* $\mathbf{B}$, $\mathbf{C}$, *and* $\mathbf{X}$, *and scalar* t, *the following LMI holds,*

$$\mathbf{A} \succeq \mathbf{B}^H\mathbf{X}\mathbf{C} + \mathbf{C}^{\mathbf{H}}\mathbf{X}^{\mathbf{H}}\mathbf{B}, \ \textit{for} \|\mathbf{X}\| \leq t, \tag{4.49}$$

if and only if

$$\begin{bmatrix} \mathbf{A} - a\mathbf{C}^H\mathbf{C} & -t\mathbf{B}^H \\ -t\mathbf{B} & a\mathbf{I} \end{bmatrix} \succeq 0, \tag{4.50}$$

where a is a non-negative real number.

Using Lemma (8) and introducing the slack variable $\boldsymbol{\varkappa} \triangleq [\varkappa_1, \ldots, \varkappa_k] \geq 0$, (4.48) is recast as:

$$\begin{bmatrix} Q_{11,k} & \widehat{t}_k^H & \mathbf{0}_{1\times M} \\ \widehat{t}_k & \mathbf{I}_{K-1} & \Omega_k(\boldsymbol{\Phi}\boldsymbol{L}_{\mathrm{AR}}\mathbf{W}_{-k})^H \\ \mathbf{0}_{M\times 1} & \Omega_k(\boldsymbol{\Phi}\boldsymbol{L}_{\mathrm{AR}}\mathbf{W}_{-k}) & \varkappa_k\mathbf{I}_M \end{bmatrix} \succeq 0, \forall k, \tag{4.51}$$

where $Q_{11,k} \triangleq \alpha_k - \sigma_k^2 - \varkappa_k$, and $\widehat{t}_k \triangleq \left((\widehat{\boldsymbol{l}}_k \boldsymbol{\Phi} \boldsymbol{L}_{\mathrm{AR}}) \mathbf{W}_{-k}\right)^H$. Next, we tackle (4.32d) by firstly substituting (4.10) in (4.32d), and then treat the interference plus noise signal in (4.32d) as an auxiliary function $\boldsymbol{\alpha}_{e_k} \triangleq [\alpha_{e_1}, \ldots, \alpha_{e_k}]$. We hence can recast (4.32d) as

$$|(\boldsymbol{l}_e \boldsymbol{\Phi} \boldsymbol{L}_{\mathrm{AR}}) \mathbf{w}_k|^2 \leq (2^{\Upsilon_{k_e}} - 1)\alpha_{ke}, \forall k, \tag{4.52a}$$

$$\|(\boldsymbol{l}_e \boldsymbol{\Phi} \boldsymbol{L}_{\mathrm{AR}}) \mathbf{W}_{-k}\|^2 + \sigma_e^2 \geq \alpha_{ke}, \forall k. \tag{4.52b}$$

To tackle the uncertainties of $\{\Delta \boldsymbol{l}_e\}$ in the constraints (4.52a) and (4.52b), we use a similar approach as in (4.34b). Hence, the equivalent LMIs of (4.52a) and (4.52b) are, respectively, given by,

$$\begin{bmatrix} C_{e,k} & \widehat{b}_{ke}^H & \mathbf{0}_{1\times M} \\ \widehat{b}_{ke} & 1 & \Omega_e(\boldsymbol{\Phi} \boldsymbol{L}_{\mathrm{AR}} \mathbf{w}_k)^H \\ \mathbf{0}_{M\times 1} & \Omega_e(\boldsymbol{\Phi} \boldsymbol{L}_{\mathrm{AR}} \mathbf{w}_k) & \vartheta_k \mathbf{I}_M \end{bmatrix} \succeq 0, \forall k, \tag{4.53}$$

$$\begin{bmatrix} B_{11,k} & -\widehat{b}_{ke}^H & \mathbf{0}_{1\times M} \\ -\widehat{b}_{ke} & \mathbf{I}_{K-1} & -\Omega_e(\boldsymbol{\Phi} \boldsymbol{L}_{\mathrm{AR}} \mathbf{W}_{-k})^H \\ \mathbf{0}_{M\times 1} & -\Omega_e(\boldsymbol{\Phi} \boldsymbol{L}_{\mathrm{AR}} \mathbf{W}_{-k}) & \varrho_k \mathbf{I}_M \end{bmatrix} \succeq 0, \forall k, \tag{4.54}$$

where $\boldsymbol{\vartheta} \triangleq [\vartheta_1, \ldots, \vartheta_K] \geq 0$ and $\boldsymbol{\varrho} \triangleq [\varrho_1, \ldots, \varrho_K] \geq 0$ are a slack variables, and,

$$C_{e,k} \triangleq (\alpha_{ke}(2^{\Upsilon_{k_e}}))^{ub} - \alpha_{ke} - \vartheta_k,$$

$$(\alpha_{ke}(2^{\Upsilon_{k_e}}))^{ub} \triangleq ((\Upsilon_{k_e} - \Upsilon_{k_e}^{(n)})(\alpha_{ke}^{(n)}) \ln 2 + \alpha_{ke}) 2^{\Upsilon_{k_e}^{(n)}},$$

$$\widehat{b}_{ke} \triangleq ((\widehat{\boldsymbol{l}}_e^H \boldsymbol{\Phi} \boldsymbol{L}_{\mathrm{AR}}) \mathbf{W}_{-k})^H,$$

$$B_{11,k} \triangleq \alpha_{ke} - \sigma_e^2 - \varrho_k.$$

Next, we show the steps to derive the LMI of equations (4.32e) and (4.32f). Using (4.12), the inequalities (A.4) and (A.5) in Appendix A, and by defining $x \triangleq V_i$, $\mathbf{A} \triangleq \rho_i$, and $B \triangleq \tau_i$, the dispersion factors for $i \in \{k, e\}$ can be expressed as:

$$\xi_i \sqrt{V_i} \leq \frac{\xi_i \sqrt{V_i^{(n)}}}{2} + \frac{\xi_i |(\boldsymbol{l}_i \boldsymbol{\Phi} \boldsymbol{L}_{\mathrm{AR}}) \mathbf{w}_k|^2}{\sqrt{V_i^{(n)}} \left(\|(\boldsymbol{l}_i \boldsymbol{\Phi} \boldsymbol{L}_{\mathrm{AR}}) \mathbf{W}_k\|_2^2 + \sigma_i^2\right)},$$

where $\mathbf{W}_k \triangleq [\mathbf{w}_1, \ldots, \mathbf{w}_{\mathcal{K}}] \in \mathbb{C}^{M \times \mathcal{K}}$. Hence, we can express (4.32e) and (4.32f) as,

$$\frac{(\tilde{\beta}_i - \mathfrak{L})}{\mathfrak{Y}} \geq \frac{|(\boldsymbol{l}_i \boldsymbol{\Phi} \boldsymbol{L}_{\mathrm{AR}}) \mathbf{w}_k|^2}{\|(\boldsymbol{l}_i \boldsymbol{\Phi} \boldsymbol{L}_{\mathrm{AR}}) \mathbf{W}_k\|_2^2 + \sigma_i^2}, \tag{4.55}$$

where $\mathfrak{L} \triangleq \xi_i \sqrt{V_i^{(n)}}/2$ and $\mathfrak{Y} \triangleq \xi_i / \sqrt{V_i^{(n)}}$.

Similar to (4.33), by treating the interference plus noise signal as an auxiliary function $\boldsymbol{\zeta} \triangleq [\zeta_1, \ldots, \zeta_K]$, (4.55) can be expressed as:

$$|(\boldsymbol{l}_i \boldsymbol{\Phi} \boldsymbol{L}_{\mathrm{AR}}) \mathbf{w}_k|^2 \leq \zeta_i (\tilde{\beta}_i - \mathfrak{L})/\mathfrak{Y}, \forall k, i \in \{k, e\}, \tag{4.56a}$$

$$\|(\boldsymbol{u}_i \boldsymbol{\Phi} \boldsymbol{L}_{\mathrm{AR}}) \mathbf{W}_k\|^2 + \sigma_i^2 \geq \zeta_k, \forall k, i \in \{k, e\}. \tag{4.56b}$$

Similar to (4.54), we can express (4.56b) by its equivalent LMI as:

$$\begin{bmatrix} \widetilde{C}_{11,i} & -\tilde{c}_i^H & \mathbf{0}_{1\times M} \\ -\tilde{c}_i & \mathbf{I}_K & -\Omega_i(\boldsymbol{\Phi} \boldsymbol{L}_{\mathrm{AR}}) \mathbf{W}_k)^H \\ \mathbf{0}_{M\times 1} & -\Omega_i(\boldsymbol{\Phi} \boldsymbol{L}_{\mathrm{AR}}) \mathbf{W}_k) & \mathfrak{l}_i \mathbf{I}_M \end{bmatrix} \succeq 0, \tag{4.57}$$

where $\widetilde{C}_{11,i} \triangleq \zeta_k - \sigma_k^2 - \mathfrak{u}_i$, $\boldsymbol{\mathfrak{l}} \triangleq [\mathfrak{l}_1, \mathfrak{u}_2, \ldots, \mathfrak{l}_{\mathcal{K}}] \geq 0$ is a slack variable, and $\tilde{c}_i \triangleq (\widehat{\boldsymbol{l}}_i^H \boldsymbol{\Phi} \boldsymbol{L}_{\mathrm{AR}})) \mathbf{W}_k)^H$.

Next, we can express (4.56a) as the following LMI:

$$\begin{bmatrix} D_{11,i} & \tilde{d}_i^H & \mathbf{0}_{1\times M} \\ \tilde{d}_i & 1 & \Omega_e(\boldsymbol{\Phi} \boldsymbol{L}_{\mathrm{AR}}) \mathbf{w}_k)^H \\ \mathbf{0}_{M\times 1} & \Omega_e(\boldsymbol{\Phi} \boldsymbol{L}_{\mathrm{AR}}) \mathbf{w}_k) & \tilde{\mathfrak{l}}_i \mathbf{I}_M \end{bmatrix} \succeq 0, \tag{4.58}$$

where $D_{11,i} \triangleq \frac{\tilde{\beta}_i \zeta_i}{\mathfrak{Y}} - \frac{\mathfrak{L} \zeta_i}{\mathfrak{Y}} - \tilde{\mathfrak{l}}_i$, $\tilde{\mathfrak{l}} \triangleq [\tilde{\mathfrak{l}}_1, \ldots, \tilde{\mathfrak{l}}_{\mathcal{K}}] \geq 0$ is a slack variable, and $\tilde{d}_i \triangleq (\widehat{\boldsymbol{l}}_e \boldsymbol{\Phi} \boldsymbol{L}_{\mathrm{AR}}) \mathbf{w}_k)^H$.

However, (4.58) is still nonconvex due to the nonconvex nature of the term $\tilde{\beta} \zeta_k$. Similar to (4.44), we employ the SCA technique to tackle the nonconvex expression as:

$$\left(\tilde{\beta} \zeta_i\right)^{ub} \triangleq \tilde{\beta}^{(n)} \zeta_i + (\tilde{\beta} - \tilde{\beta}^{(n)}) \zeta_i^{(n)} \tag{4.59}$$

Algorithm 4.2 PCCP Algorithm for solving ($\mathcal{P}2.3$)

Initialise: $(\boldsymbol{w}^{(1)}, \boldsymbol{\theta}^{(1)})$, penalty factor $a_{\max}$, scaling $\nu \geq 1$, tolerances $(\epsilon_{t_1}, \epsilon_{t_2})$, $n_{\max}$, set $n = 1$.
repeat
  Solve ($\mathcal{P}2.3$) to obtain $\boldsymbol{\theta}^{(n+1)}$.
  if $\|e^{j\boldsymbol{\theta}^{(n)}} - e^{j\boldsymbol{\theta}^{(n-1)}}\|_1 \leq \epsilon_{t_2}$ and $C \leq \epsilon_{t_1}$ **then**
    break
  else
    Update $a^{(n+1)} = \min\{\nu a^{(n)}, a_{\max}\}$, set $n = n + 1$.
  end if
until $n > n_{\max}$
Output: feasible solution $\boldsymbol{\theta}^* = \boldsymbol{\theta}^{(n)}$.

where $\tilde{\beta}^{(n)}$, $\zeta_i^{(n)}$ are the value of the variables $\tilde{\beta}_i$, ζ_i at iteration (n) in the SCA-based algorithm, respectively. Be substituting (4.59) in (4.58), we can express (4.58) as:

$$\begin{bmatrix} \widetilde{D}_i & \tilde{b}_{ke}^H & \mathbf{0}_{1\times M} \\ \tilde{d}_i & 1 & \Omega_e(\boldsymbol{\Phi}\boldsymbol{L}_{\mathrm{AR}})\mathbf{w}_k)^H \\ \mathbf{0}_{M\times 1} & \Omega_e(\boldsymbol{\Phi}\boldsymbol{L}_{\mathrm{AR}})\mathbf{w}_k) & \tilde{\mathfrak{l}}_i\mathbf{I}_M \end{bmatrix} \succeq 0, j \neq k, \tag{4.60}$$

where $\widetilde{D}_i \triangleq \frac{\left(\tilde{\beta}\zeta_i\right)^{ub}}{\mathfrak{Y}} - \frac{\mathfrak{L}\zeta_i}{\mathfrak{Y}} - \tilde{\mathfrak{l}}_i$.

Eventually, reformulating problem ($\mathcal{P}2.1$) with (4.46), (4.51), (4.53), (4.54),

(4.57), and (4.60) yields the following optimisation problem:

$$(\mathcal{P}2.2): \max_{\mathbf{w},\boldsymbol{\theta}} \ \mathcal{Z} \tag{4.61a}$$

$$\text{s.t.} \quad \mathcal{Z} \leq \beta_k - \Upsilon_{k_e} - \tilde{\beta}_k - \tilde{\beta}_{k_e}, \forall k, \tag{4.61b}$$

$$(4.46), (4.51), (4.53), (4.54), (4.57), (4.60), i \in \{k, e\}, \tag{4.61c}$$

$$\boldsymbol{\eta} \geq 0, \boldsymbol{\varkappa} \geq 0, \boldsymbol{\vartheta} \geq 0, \boldsymbol{\varrho} \geq 0, \mathfrak{l} \geq 0, \tilde{\mathfrak{l}} \geq 0, \tag{4.61d}$$

$$(4.31b), \ (4.31e). \tag{4.61e}$$

At this point, all nonlinear constraints (4.32c), (4.32d), (4.32e), and (4.32f) have been linearised as LMIs (4.46), (4.51), (4.53), (4.54), (4.57), and (4.60); thus, problem ($\mathcal{P}2.2$) is an SDP that can be efficiently solved using standard solvers, e.g., the interior point method or the CVX toolbox [93].

Sub-Problem for Optimising the PREs

For a given $\mathbf{w}$, we aim to find $\boldsymbol{\theta}^{(n+1)}$ such that, $\widehat{\mathcal{S}}_k^{\mathcal{F}}(\mathbf{w}_k^{(n+1)}, \boldsymbol{\theta}^{(n+1)}) > \widehat{\mathcal{S}}_k^{\mathcal{F}}(\mathbf{w}_k^{(n+1)}, \boldsymbol{\theta}^{(n)})$. Similar to the analysis in the previous section, we can express (4.32c) and (4.32d) with their equivalent LMIs (4.46), (4.51), (4.53) and (4.54), respectively. To tackle the UMC (4.31c), we leverage the PCCP method [76]. The PCCP's main idea is to add slack variables to relax the problem so that if the UMC is violated, we then can penalise the sum of violations. The converged PCCP solution is an approximate first-order optimal solution of the original problem [76].

To apply the PCCP method, we introduce an auxiliary variable set $\mathbf{q} \triangleq \{q_m | m \in M\}$ satisfying $q_m \triangleq |e^{(j\theta_m)}|^* |e^{(j\theta_m)}|$. Then, (4.31c) can be expressed as $q_m \leq |e^{(j\theta_m)}|^* |e^{(j\theta_m)}| \leq q_m$. The nonconvex part $q_m \leq |e^{(j\theta_m)}|^* |e^{(j\theta_m)}|$ can be approximated by $q_m \leq 2\Re\{|e^{(j\theta_m)}|^* |e^{(j\theta_n^{(n)})}| - |e^{(j\theta_n^{(n)})}|^* |e^{(j\theta_n^{(n)})}|\}$. Following the PCCP framework,

Algorithm 4.3 Proposed AO Algorithm for Solving Problem ($\mathcal{P}2$)

1: **Initialise:** ($\boldsymbol{w}^{(1)} = \mathbf{w}^*,\ \boldsymbol{\theta}^{(1)} = \boldsymbol{\theta}^*$), set $n = 1$, and tolerance $\epsilon_t > 0$.

2: **repeat**

3: Update $\mathbf{w}^{(n+1)}$ by solving ($\mathcal{P}2.2$) and $\boldsymbol{\theta}^{(n+1)}$ by solving ($\mathcal{P}2.3$).

4: $\Delta = \frac{|\min_{k\in\mathcal{K}} \mathcal{S}_k^{\mathcal{F}}(\mathbf{w}^{(n+1)},\boldsymbol{\theta}^{(n+1)}) - \min_{k\in\mathcal{K}} \mathcal{S}_k^{\mathcal{F}}(\mathbf{w}^{(n)},\boldsymbol{\theta}^{(n)})|}{\min_{k\in\mathcal{K}} \mathcal{S}_k^{\mathcal{F}}(\mathbf{w}^{(n)},\boldsymbol{\theta}^{(n)})}$.

5: Update $\mathbf{w}^{(n)} \leftarrow \mathbf{w}^{(n+1)},\ \boldsymbol{\theta}^{(n)} \leftarrow \boldsymbol{\theta}^{(n+1)}$, and set $n \leftarrow n+1$.

6: **until** $\Delta \leq \epsilon_t$

7: **Output:** ($\mathbf{w}^* = \mathbf{w}^{(n)},\ \boldsymbol{\theta}^* = \boldsymbol{\theta}^{(n)}$).

we penalise the objective function (4.32a), hence, problem ($\mathcal{P}2.1$) can be recast as:

$$(\mathcal{P}2.3): \max_{\boldsymbol{\theta}}\ \mathcal{Z} - a\mathcal{T}, \tag{4.62a}$$

$$\text{s.t.} \quad (4.46), (4.51), (4.53), (4.54), (4.57), (4.60), \tag{4.62b}$$

$$|e^{(j\theta_m)}|^*|e^{(j\theta_m)}| \leq q_m + t_m, \tag{4.62c}$$

$$q_m - \hat{t}_m \leq 2\Re\left\{|e^{(j\theta_m)}|^*|e^{(j\theta_n^{(n)})}|\right\} - |e^{(j\theta_n^{(n)})}|^*|e^{(j\theta_n^{(n)})}|, \tag{4.62d}$$

$$q_m \geq 0, \forall m \in M, \tag{4.62e}$$

where $\mathcal{T} \triangleq \sum_{m=1}^{N} t_m + \hat{t}_m$ is the penalty term, $\mathbf{c} \triangleq \{c_n, \hat{c}_n\}$ is the slack variable imposed over the modulus constraint (4.31c), and a is the regularisation factor. The regularisation factor is imposed to control the UMC constraint (4.31c) by scaling the penalty term Q.

Problem ($\mathcal{P}2.3$) is an SDP that can be solved by the CVX toolbox. Unlike the conventional SDR method to tackle UMC, the PCCP method, summarised in Algorithm 4.2, is guaranteed to find a feasible point for problem ($\mathcal{P}2.3$) [98]. The following points are helpful for the numerical implementation of the Algorithm 4.2:

(a) We invoke $a_{\max}$ to avoid numerical complications if a grows too large [99];

(b) The stopping criteria $\mathcal{T} \leq \epsilon_{t_1}$ guarantees the UMC (4.31c) when ϵ_{t_1} is small

[52];

(c) The convergence of Algorithm 4.2 is controlled by $\left\| e^{(j\boldsymbol{\theta}^{(n+1)})} - e^{(j\boldsymbol{\theta}^{(n)})} \right\|_1 \leq \epsilon_{t_2}$.

Finally, the pseudo code of the AO algorithm to solve problem $(\mathcal{P}2)$ is shown in Algorithm 4.3. This algorithm converges to a locally optimal solution of $(\mathcal{P}2)$, which can be proved in the following theorem.

Theorem 4.2. *Algorithm 4.3 generates a locally optimal solution for problem* $(\mathcal{P}2)$.

Proof: See Appendix C.3.

Complexity Analysis

Since convex problems $(\mathcal{P}2.2)$ and $(\mathcal{P}2.3)$ involve linear constraints and LMIs (4.46), (4.51), (4.53), (4.54), (4.57) and (4.60), they can be solved by the interior point method [93]. The algorithm's complexity is defined by its worst-case runtime and the number of operations [52]. For problem $(\mathcal{P}2.2)$, the number of variables is $a \triangleq 2M$, the size of (4.46) is $b_1 \triangleq NM + N + 1$, the size of (4.51), and (4.54) is $b_2 \triangleq 2N + 1$, and the size of (4.53) is $b_3 \triangleq 2N + 1$. Thus, the complexity of solving problems $(\mathcal{P}2.2)$ and $(\mathcal{P}2.3)$, respectively,

$$\mathcal{O}_{\mathbf{w}} \triangleq \mathcal{O}\left\{\sqrt{c_1 + 2}(a)(a^2 + ac_2 + c_3 + (a+1)^2)\right\},$$
$$\mathcal{O}_{\mathbf{\Phi}} \triangleq \mathcal{O}\left\{\sqrt{c_1 + 4M}(2M)(4M^2 + 2Mc_2 + c_3 + 4MN)\right\},$$

where

$$c_1 \triangleq \sum\nolimits_k^{\mathcal{K}} b_1(k-1) + b_2(2k+1) + b_3(3k-2),$$
$$c_2 \triangleq \sum\nolimits_k^{\mathcal{K}} b_1^2(k-1) + b_2^2(2k+1) + b_3^2(3k-2),$$
$$c_3 \triangleq \sum\nolimits_k^{\mathcal{K}} b_1^3(k-1) + b_2^3(2k+1) + b_3^3(3k-2),$$

Table 4.1 : IRS-FBR Max-Min Maximisation Simulation Parameters

Parameter	**Value**
Number of IRS elements (M)	16
Noise power density (σ_i^2)	-174 dBm/Hz
Alice's transmission power (P)	20 dBm
Antenna gains ($G_{\mathrm{A}}, G_{\mathrm{IRS}}$)	5 dBi
The convergence tolerances $\epsilon_t, \epsilon_{t_1}, \epsilon_{t_1}$	10^{-3}
Simulation initial settings	$\alpha_k^{(n)} = 1$, $\alpha_{ke}^{(n)} = 1$, $a^{(1)} = 10$, $a_{\max} = 30$, $\delta_k = \delta_e = 0.02$.

4.4 Numerical Results

In this section, we perform an extensive simulation to evaluate the performance of the proposed approach. The results are obtained using MATLAB and CVX toolboxes. In this setup, Alice is located at $(15, 0, 15)$, the IRS is located at $(0, 25, 40)$, and the users are randomly distributed to the right of Alice over a $(60m \times 60m)$ area. The Eve (e.g., a compromised legitimate user) is randomly located in $(100m \times 100m)$ outside the users' area. Note that if Eve is too close to one of the users, it is mainly impossible to guarantee the positive SR for all the users [102]. In this case, other methods, e.g., encryption or friendly jamming, can provide users' secrecy [50].

The Alice-to-IRS direct path loss factor is $\aleph_{\mathrm{AR}} \triangleq \boldsymbol{G}_{\mathrm{A}} + \boldsymbol{G}_{\mathrm{IRS}} - 35.9 - 22\log_{10}(d_{\mathrm{AR}})$ in dB, where d_{AR} is the distance between Alice and the IRS in meters, while $\boldsymbol{G}_{\mathrm{A}}$ is Alice antenna gain, and $\boldsymbol{G}_{\mathrm{IRS}}$ is the IRS elements' antenna gain [70]. The path loss factor from the IRS to the users and the Eve is $\aleph_{\mathrm{R}i} \triangleq \boldsymbol{G}_{\mathrm{IRS}} - 33.05 - 30\log_{10}(d_{\mathrm{R}i})$ dB, for $i \in \{k, e\}$, $d_{\mathrm{R}i}$ is the distance between the IRS and the users and Eve in meters. The spatial correlation matrix is $[\boldsymbol{R}_{Ri}]_{l,\bar{l}} \triangleq \exp\left(j\pi(l-\bar{l})\sin\hat{\vartheta}\sin\hat{\aleph}\right)$ for $i \in \{k, e\}$,

where $\hat{\aleph}$ is the elevation angle and $\hat{\vartheta}$ is the azimuth angle [86]. The elements of the Alice-to-IRS channel are generated by
$[\boldsymbol{G}_{\text{AR}}]_{a,b} \triangleq \exp(j\pi\left((b-1)\sin\overline{\Theta}_b \sin\overline{\vartheta}_b + (a-1)\sin(\theta_m)\sin(\vartheta_b)\right))$, where $\Theta_n \in (0, 2\pi)$, $\vartheta_n \in (0, 2\pi)$, and $\overline{\Theta}_n \triangleq \pi - \theta_m$, and $\overline{\vartheta}_n \triangleq \pi + \vartheta_n$ [86]. The small-scale fading channel gain $\widehat{\boldsymbol{l}}_i$ for $i \in \{k, e\}$ is modelled as a Rician fading channel with K-factor= 3.

We define the CSI error bounds as $\Omega_i \triangleq \delta_i \|\widehat{\boldsymbol{l}}_i\|_2, \forall k$, where $\delta_i \in [0, 1), i \in \{k, e\}$ is the relative amount of CSI uncertainty. When $\delta = 0$, Alice can obtain the perfect CSI of the IRS to users/Eve reflected channel. In the FBR case, we set $\tau_{\max} = \tau_{e_{\max}} = 10^{-5}$. The packet length N_t is defined by the transmission duration t_t and the bandwidth $\mathcal{B}$, as previously defined $N_t \triangleq \mathcal{B}t_t$. Hence, we set the transmission duration as $t_t = 0.1$ ms, which is suitable for FBR transmission [2]. The choice of 0.1 ms end-to-end delay ensures having a quasi-static channel during FBR communication [85]. The bandwidth $\mathcal{B}$ is set at 1 MHz. Unless stated otherwise, the simulation parameters are defined in Table 4.1. We multiply the results by $\log_2(e)$ to convert them to bps/Hz. Lastly, for comparison purposes, we compare our Max-Min algorithm against the SSR maximisation algorithms. Lastly, for comparison purposes, we compare our Max-Min algorithm against the SSR maximisation algorithms. The SSR maximisation can be tackled by setting the objective function in problem $(\mathcal{P}1)$ and problem $(\mathcal{P}2)$ to $\max_{\mathbf{w},\boldsymbol{\theta}} \sum_k^{\mathcal{K}} \mathcal{S}_k^{\mathcal{F}}(\mathbf{w}, \boldsymbol{\theta})$. SSR maximisation problem is addressed in Chapter 5.

Fig. 4.2 illustrates the convergence rate of the Max-Min algorithms under perfect CSI and Imperfect CSI for the FBR and the LBR systems. All algorithms achieve convergence within a few numbers of iterations. It can be noticed that the FBR needs fewer iterations to converge since the local optimal solution obtained in the LBR case is used as the initial feasible point. Such a choice highlights the importance of choosing the best initial feasible points in the FBR case.

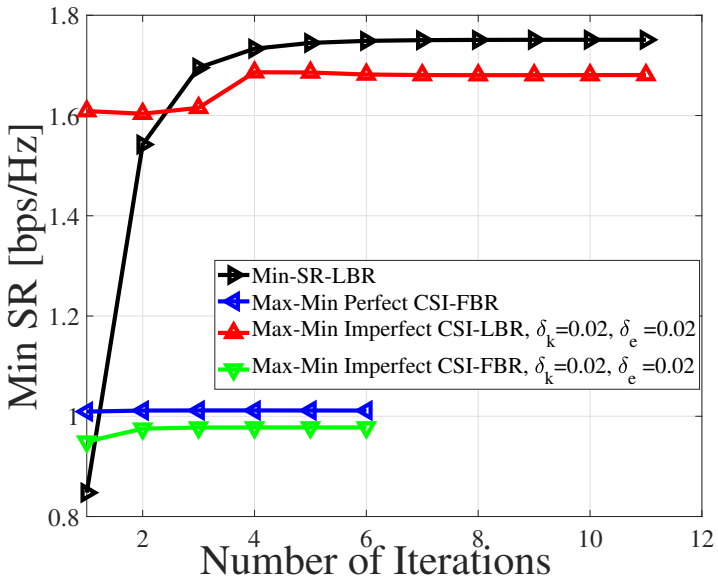

Figure 4.2 : Convergence rate of the Max-Min algorithm under prefect CSI with $M = 10$, $\mathcal{K} = 6$, $N = 16$.

Fig. 4.3 plots the users' SR distribution with $M = 10$, $\mathcal{K} = 6$, and $N = 16$ under the Max-Min algorithms. The Max-Min algorithms achieve almost the same SR for all the users when the IRS's PREs are optimised. However, when the IRS's PREs are not practically optimised, the algorithms fail to achieve secrecy fairness among the users. The results demonstrate the importance of properly optimising the IRS's PREs. The proposed algorithm for the FBR case achieves secrecy and SR fairness among the users. The results demonstrate the robustness of the proposed algorithms to achieve secrecy for all the users, even under the FBR constraints, namely, the transmission duration and the latency.

Fig. 4.4 portrays the users' SR under different values of the IRS to the users/Eve imperfect CSI. The Max-Min algorithm achieves secrecy fairness in the LBR/FBR cases, even when Eve's reflected channel has higher uncertainty than the users' reflected channel. The results show that the proposed algorithm is able to achieve secrecy guarantee even under a high level of uncertainty, which demonstrates the

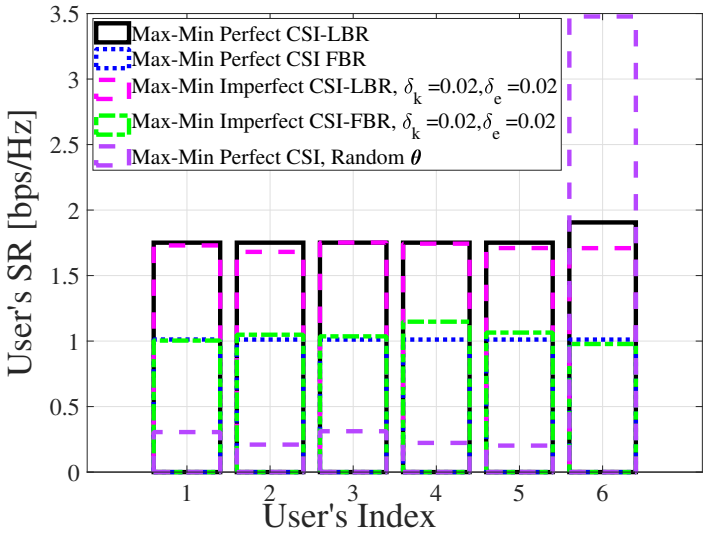

Figure 4.3 : Users' SR with $M = 10$, $\mathcal{K} = 6$, $N = 16$.

Figure 4.4 : Users' SR with with $M = 10, \mathcal{K} = 6, N = 16$.

robustness of the proposed algorithm.

One way to evaluate the degree of fairness in the proposed algorithms is by using the Jain's index. Jain's index is defined as, Jain's Index $= \frac{\left(\sum_{k=1}^{\mathcal{K}} \mathcal{S}_{\mathcal{K}}(\mathbf{w},\boldsymbol{\theta})\right)^2}{\mathcal{K}\sum_{k=1}^{\mathcal{K}}(\mathcal{S}_k(\mathbf{w},\boldsymbol{\theta}))^2}$, and it is bounded in $[1/\mathcal{K}, 1]$, where the higher value indicates a better fairness [103]. Fig. 4.5 shows Jain's index against the relative amount of CSI uncertainty δ. The Max-Min

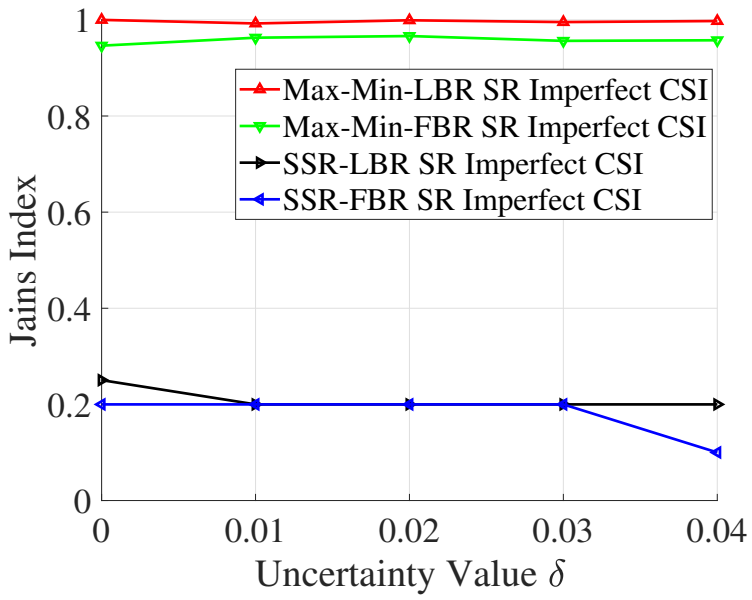

Figure 4.5 : Jain's Index Vs. the uncertainty level $\delta_k = \delta_e$ with $M = 10, \mathcal{K} = 5, N = 16$.

algorithm achieves almost one in the LBR/FBR cases, while the SSR counterpart has nearly zero. The results demonstrate the Max-Min algorithm's robustness in achieving secrecy fairness among all the users, even in the FBR environment.

Fig. 4.6 illustrates the minimum SR among all the users against the relative amount of CSI uncertainty δ. The Max-Min algorithm achieves secrecy for all the users. Even under high uncertainty, it achieves almost the same minimum SR as the full certainty case. The FBR case demonstrates results similar to those of the LBR case. As expected, the SSR-LBR/SSR-FBR algorithms achieve a higher minimum user SR since the SSR algorithm favours most of the transmission power towards the user with a better channel while discarding other users.

Fig. 4.7 depicts the minimum SR against the number of users $\mathcal{K}$. It can be seen that the minimum SR algorithm decreases with $\mathcal{K}$. This is expected as the multi-user interference increases with $\mathcal{K}$. The Max-Min FBR case provides secrecy

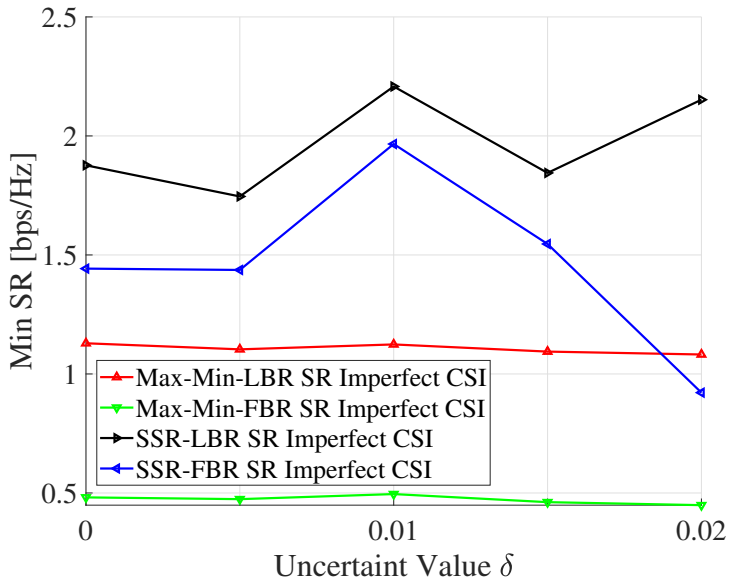

Figure 4.6 : Minimum SR Vs. the uncertainty level $\delta_k = \delta_e$ with $M = 10, \mathcal{K} = 5, N = 16$.

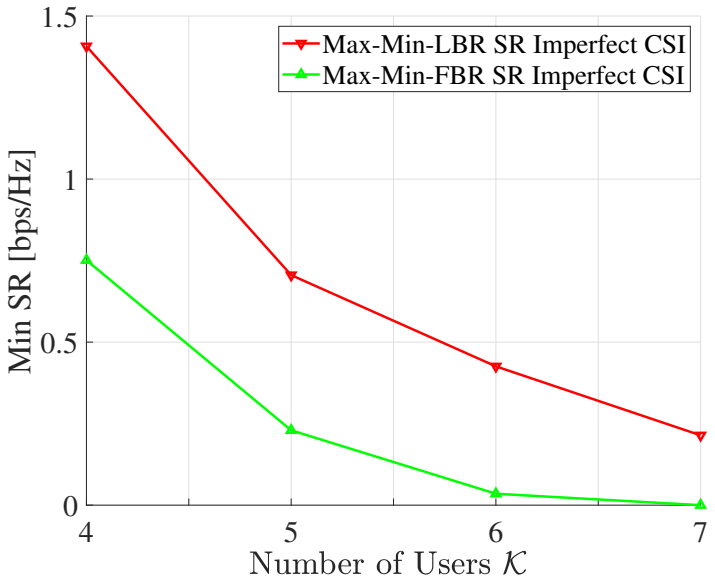

Figure 4.7 : Minimum SR Vs. the number of users $\mathcal{K}$ with $M = 10, N = 16$, $\delta_k = \delta_e = 0.02$.

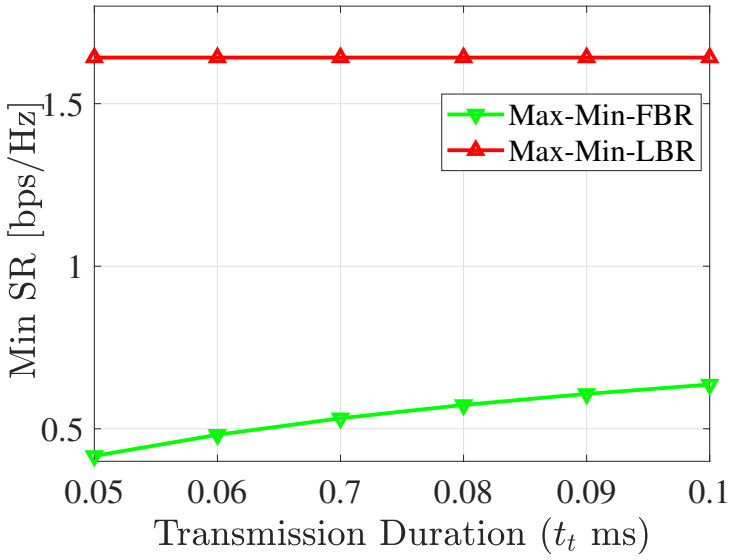

Figure 4.8 : user's min SR Vs. Transmission Duration t_t.

in all cases; however, as $\mathcal{K}$ increases, the minimum users' SR is approaching zero, which can be seen when $\mathcal{K} = 7$. The results show that obtaining secrecy for all the users in the FBR case is more challenging due to the FBR constraints.

Lastly, the minimum SR is illustrated against the transmission duration t_t in Fig. 4.8. The Max-Min algorithm guarantees secure communication for all the users even at low transmission duration (10^{-5}ms). It can be noticed that the achievable FBR's SR is capped by its LBR counterpart since the transmission duration is considered to be infinity in the latter.

4.5 Conclusions

In this paper, we proposed a framework to achieve secure communications for all the users under the FBR constraints for IoT setting in URLLC/mMTC applications aided by IRS. Specifically, through linearization and different nonconvex optimisation techniques, we designed computationally efficient algorithm to maximise the minimum SR among all the users under both perfect and imperfect CSI from

IRS to the users and the eavesdropper. Extensive simulations results showed that the Max-Min algorithm can provide secure communications for all the users under FBR constraints even with only imperfect CSI. Note that if Eve is too close to one user, it is infeasible to guarantee secrecy for all the users and other solutions like cryptography-based or friendly jamming-based methods should be in place. In the future, one can consider a multi-hop scenario with the joint coding over multiple IRSs, similar to the cooperative MIMO setting [104].

Chapter 5

Secrecy Sum-Rate Maximisation in Finite Blocklength IRS-aided Systems With Perfect and Imperfect CSI

In this chapter*, we investigates system secrecy for URLLC/mMTC IoT-users in the FBR-IRS-aided systems under both perfect and imperfect channel state information (CSI). In particular, we first formulate a nonconvex optimisation problem to maximise users' sum secrecy rate by jointly optimising the transmitter's beamforming and the IRS's passive reflective elements while considering FBR constraints, namely, latency and transmission durations. Nevertheless, the problem is even more challenging under imperfect CSI. To solve this, we linearise the objective and decompose it into sequential sub-problems. For imperfect CSI, we transform semi-infinite constraints into finite linear matrix inequalities to enable efficient optimisation. We then prove that the algorithms converge to a locally optimal solution and demonstrate their low computational complexity, making them scalable for large IRS deployments. Numerical results show that our approach ensures secure system communication even under imperfect CSI while satisfying FBR constraints.

Remark: In contrast to the fairness-driven design presented in Chapter 4, which employed a Max–Min optimisation problem to ensure balanced user performance by maximising the minimum secrecy rate, this chapter focuses on a throughput-driven optimisation based on the SR objective. The SSR formulation seeks to maximise the overall system throughput, typically favouring users with stronger channels, and

*This chapter corresponds to the journal paper J-4 in the list of Publications.

Table 5.1 : Key Parameters and Assumptions for Perfect and Imperfect CSI Cases

Parameter	**Perfect CSI**	**Imperfect CSI**
CSI Knowledge	Full and accurate CSI for users and eavesdropper	Estimated CSI with bounded uncertainty
Eavesdropper CSI	Known at Alice	Partially known to Alice
Algorithm Type	Step-decent algorithm	Robust SCA/PCCP under uncertainty algorithm

thereby prioritising spectral efficiency over fairness. This distinction underscores the inherent trade-off between equitable resource allocation and aggregate performance, particularly under varying CSI conditions. The key parameters and assumptions for each case (perfect and imperfect CSI) are presented in Table 5.1.

The remainder of this chapter is organised as follows. The system model is discussed in Sections 5.1. Then, Sections 5.2 and 5.3 present the problem and corresponding solutions under perfect and imperfect CSI, respectively. The extensive simulations and discussion are provided in Section 5.4. Finally, Section 5.5 concludes the paper.

5.1 System Model

We study an IRS-aided downlink system operating under the FBR, as depicted in Fig. 5.1. An M-antenna base station (Alice) transmits confidential data to $\mathcal{K}$ single-antenna URLLC users in the presence of a single-antenna eavesdropper (Eve). The direct links from Alice to the legitimate users are assumed to be heavily

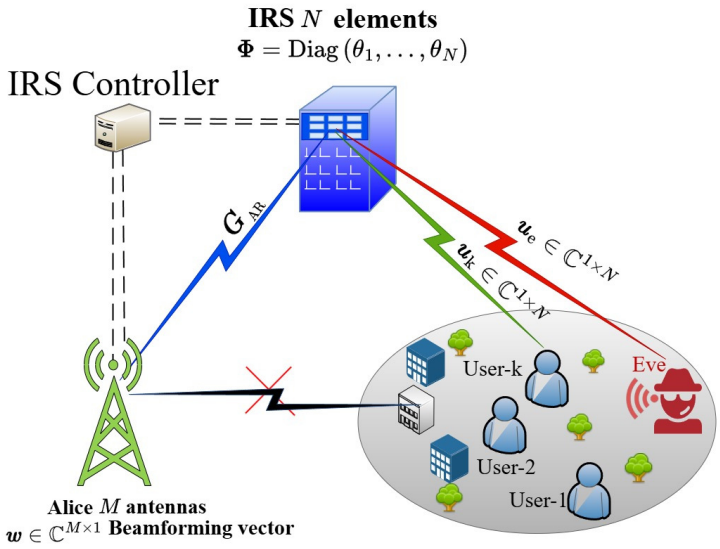

Figure 5.1 : FBR IRS-aided system model.

obstructed[†], a situation commonly encountered in dense urban environments with high-rise buildings.

An IRS with N passive reflecting elements (PREs) is deployed, e.g., on the facade of a high-rise building, to facilitate communication between Alice and the users. Let $\mathcal{K} = 1, 2, \ldots, \mathcal{K}$ denote the set of legitimate users, with $k \in \mathcal{K}$ and e representing Eve. The Alice-to-IRS channel is represented as:

$$\boldsymbol{G}_{\text{AR}} = \sqrt{\beta_{\text{AR}}}\tilde{\boldsymbol{G}}_{\text{AR}} \in \mathbb{C}^{N\times M}, \tag{5.1}$$

where β_{AR} denotes the large-scale fading coefficient and $\tilde{\boldsymbol{G}}_{\text{AR}}$ follows a Rician fading model. The IRS–i channel, for $i \in k, e$, is expressed as:

$$\boldsymbol{u}_i = \sqrt{\beta_{\text{R}i}}\tilde{\boldsymbol{u}}_i\mathcal{R}_{\text{R}i}^{1/2} \in \mathbb{C}^{1\times N}, \tag{5.2}$$

where $\beta_{\text{R}i}$ is the large-scale fading factor, $\tilde{\boldsymbol{u}}i$ models small-scale fading via the Rician distribution, and $\mathcal{R}\text{R}i \in \mathbb{C}^{N\times N}$ is the spatial correlation matrix of the IRS elements [86].

[†]The system secrecy and data rate enhancement from IRS deployment is limited in the presence of strong direct links [105].

Let s_k denote the confidential symbol for user k. The received signals at user k and Eve corresponding to s_k are then given by:

$$y_i \triangleq \boldsymbol{h}_i(\boldsymbol{\theta}) \sum_{k=1}^{\mathcal{K}} \mathbf{w}_k s_k + n_i, i \in \{k, e\}, \tag{5.3}$$

where $\boldsymbol{h}_i(\boldsymbol{\theta}) \in \mathbb{C}^{1\times M}$ denotes the cascaded channel gain from Alice to $i \in \{k, e\}$, $\mathbf{w}_k \in \mathbb{C}^{M\times 1}$ is the beamforming vector for user-k, $\boldsymbol{\theta} = (\theta_1, \ldots, \theta_N)^T \in [0, 2\pi)^N$ represents the IRS PRE phase-shift vector. The term n_i corresponds to zero-mean additive white Gaussian noise (AWGN) with power density σ_i^2 for $i \in \{k, e\}$. The cascade channel gain $\boldsymbol{h}_i(\boldsymbol{\theta})$ from Alice to $i \in \{k, e\}$, can be expressed using the Alice-IRS and the IRS-i channels as:

$$\boldsymbol{h}_i(\boldsymbol{\theta}) \triangleq \boldsymbol{u}_i \boldsymbol{\Phi} \boldsymbol{G}_{\text{AR}} \triangleq \boldsymbol{u}_i \sum_{n=1}^{N} \exp(j\theta_n) \Xi_n \boldsymbol{G}_{\text{AR}}, \tag{5.4}$$

where $\boldsymbol{\Xi}_n$ is an $N \times N$ matrix with all zeros except for a single 1 at the (n, n) position, and $\boldsymbol{\Phi} = \text{Diag}(e^{j\boldsymbol{\theta}})$ denotes the diagonal IRS phase-shift matrix.

The CSI for the channel from Alice to the IRS can be estimated through angle-of-arrival and angle-of-departure measurements [77]. However, obtaining accurate CSI for the reflected channels between the IRS and the URLLC users is more challenging due to the passive nature of the IRS and the dynamic nature of the users' environments and mobility [89]. Moreover, accurately determining the location or the CSI of Eve is generally infeasible. To address these uncertainties, we adopt a bounded CSI model that characterises the reflected channels from the IRS to both the legitimate users and Eve, which can be described as [106]:

$$\boldsymbol{u}_i \triangleq \widehat{\boldsymbol{u}}_i + \Delta \boldsymbol{u}_i, \forall i \in \{k, e\}, \tag{5.5a}$$

$$\omega_i \triangleq \{\|\Delta \boldsymbol{u}_i\|_2 \leq \Omega_i\}, \forall i \in \{k, e\}, \tag{5.5b}$$

where $\widehat{\boldsymbol{u}}_i$ denotes the (imperfect) estimated channel vector, $\Delta \boldsymbol{u}_i$ represents the channel estimation error of the corresponding estimation, ω_i is a set for all possible channel estimation errors, and Ω_i is the radii of the uncertainty regions as known to

Alice. Hence, (5.4) can be reformulated as:

$$\widehat{\boldsymbol{h}}_i(\boldsymbol{\theta}) \triangleq (\widehat{\boldsymbol{u}}_i + \Delta\boldsymbol{u}_i)\,\boldsymbol{\Phi}\boldsymbol{G}_{\text{AR}}. \tag{5.6}$$

In the following, we consider both perfect and imperfect CSI scenarios for the IRS-to-users and IRS-to-Eve channels. For the perfect CSI case, we assume that Alice has accurate channel knowledge of all users and Eve [107, 108]. As previously noted, Eve may act as a legitimate user during certain time slots but attempts to eavesdrop on other transmissions. Employing well-established channel estimation techniques, such as the anchor-assisted method [109], Alice can practically obtain the CSI of the users. Under this assumption, the reflected channels from the IRS to the users and Eve are modelled by setting the error term $\Delta\boldsymbol{u}_i$ in (5.5a) to zero, i.e., $\boldsymbol{u}_i = \widehat{\boldsymbol{u}}_i, i \in \{k, e\}$. In contrast, when only partial or imperfect CSI $\widehat{\boldsymbol{u}}_i$ is available, the uncertainty in the reflected channel can be captured by varying the magnitude of $\Delta\boldsymbol{u}_i$, which corresponds to the radius Ω_i of the uncertainty region. This approach allows modelling different degrees of CSI imperfection.

Accordingly, the signal-to-interference-plus-noise ratio (SINR) at user-k and Eve, under both perfect and imperfect IRS-to-users/Eve CSI, can be expressed as:

$$\gamma_i(\mathbf{w}, \boldsymbol{\theta}) \triangleq \frac{|\boldsymbol{h}_i(\boldsymbol{\theta})\mathbf{w}_k|^2}{\rho_i},\ i \in \{k, e\}, \tag{5.7}$$

$$\widehat{\gamma}_i(\mathbf{w}, \boldsymbol{\theta}) \triangleq \frac{|\widehat{\boldsymbol{h}}_i(\boldsymbol{\theta})\mathbf{w}_k|^2}{\widehat{\rho}_i},\ i \in \{k, e\}, \tag{5.8}$$

where $\rho_i \triangleq \sum_{j=1, j\neq k}^{\mathcal{K}} |\boldsymbol{h}_i(\boldsymbol{\theta})\mathbf{w}_j|^2 + \sigma_i^2$, and $\widehat{\rho}_i \triangleq \sum_{j=1, j\neq k}^{\mathcal{K}} |\widehat{\boldsymbol{h}}_i(\boldsymbol{\theta})\mathbf{w}_j|^2 + \sigma_i^2$.

In the presence of Eve, the closed-form expressions for the FBR-SR of user-k under perfect and imperfect IRS-to-users/Eve CSI are given, respectively, by [110, Eq. 115]:

$$\mathcal{S}_k^{\mathcal{F}}(\mathbf{w}, \boldsymbol{\theta}) \triangleq \left[C_k - C_e - \xi_k\sqrt{V_k} - \xi_e\sqrt{V_e}\right]^+, \tag{5.9}$$

$$\widehat{\mathcal{S}}_k^{\mathcal{F}}(\mathbf{w}, \boldsymbol{\theta}) \triangleq \left[\widehat{C}_k - \widehat{C}_e - \xi_k\sqrt{\widehat{V}_k} - \xi_e\sqrt{\widehat{V}_e}\right]^+, \tag{5.10}$$

where $[x]^+ \triangleq \max[0, x]$, and the user's data rate and Eve's eavesdropping rate are respectively expressed as:

$$C_i(\mathbf{w}, \boldsymbol{\theta}) \triangleq \ln\left(1 + \gamma_i(\mathbf{w}, \boldsymbol{\theta})\right), \quad i \in \{k, e\}, \tag{5.11}$$

$$\widehat{C}_i(\mathbf{w}, \boldsymbol{\theta}) \triangleq \ln\left(1 + \widehat{\gamma}_i(\mathbf{w}, \boldsymbol{\theta})\right), \quad i \in \{k, e\}. \tag{5.12}$$

The parameters ξ_i are defined as:

$$\xi_i \triangleq \frac{Q^{-1}(\varsigma_i)}{\ln(2)\sqrt{N_t}},$$

where $Q^{-1}(\cdot)$ is the inverse Gaussian Q-function, and $N_t \triangleq \mathcal{B}t_t$ is the URLLC packet length. The dispersion factors V_k and V_e are given by [111]:

$$V_i(\mathbf{w}, \boldsymbol{\theta}) \triangleq \frac{2\gamma_i(\mathbf{w}, \boldsymbol{\theta})}{(1 + \gamma_i(\mathbf{w}, \boldsymbol{\theta}))} \triangleq 2\left(1 - (\rho_i/\upsilon_i)\right), i \in \{k, e\}, \tag{5.13}$$

$$\widehat{V}_i(\mathbf{w}, \boldsymbol{\theta}) \triangleq \frac{2\widehat{\gamma}_i(\mathbf{w}, \boldsymbol{\theta})}{(1 + \widehat{\gamma}_i(\mathbf{w}, \boldsymbol{\theta}))} \triangleq 2\left(1 - (\widehat{\rho}_i/\widehat{\upsilon}_i)\right), i \in \{k, e\}, \tag{5.14}$$

where $\upsilon_i \triangleq \sum_{j=1}^{\mathcal{K}} |\boldsymbol{h}_i(\boldsymbol{\theta})\mathbf{w}_j|^2 + \sigma_i^2$, and $\widehat{\upsilon}_i \triangleq \sum_{j=1}^{\mathcal{K}} |\widehat{\boldsymbol{h}}_i(\boldsymbol{\theta})\mathbf{w}_j|^2 + \sigma_i^2,\ i \in \{k, e\}$.

Unlike the conventional SR definition in the LBR, the FBR introduces additional constraints on the SR. Specifically, reliable transmission in the FBR requires that the decoding error probability ς_k at user-k does not exceed the maximum allowable decoding error probability $\varsigma_{\max}$. Furthermore, the information leakage ς_e must remain below the maximum tolerated leakage $\varsigma_{\max}$ [111]. Additionally, the transmission duration t_t must not surpass the maximum permitted duration $t_{\max}$. These factors distinctly separate the FBR scenario from its LBR counterpart. Notably, as the transmission duration t_t approaches infinity, the dispersion factor V_i tends to zero, and the FBR expressions in (5.9) and (5.10) reduce to the conventional LBR SR formulation, which can be written as [90]:

$$\mathcal{S}_k^{\mathcal{L}}(\mathbf{w}, \boldsymbol{\theta}) \triangleq [C_k(\mathbf{w}, \boldsymbol{\theta}) - C_e(\mathbf{w}, \boldsymbol{\theta})]^+, \tag{5.15}$$

$$\widehat{\mathcal{S}}_k^{\mathcal{L}}(\mathbf{w}, \boldsymbol{\theta}) \triangleq [\widehat{C}_k(\mathbf{w}, \boldsymbol{\theta}) - \widehat{C}_e(\mathbf{w}, \boldsymbol{\theta})]^+. \tag{5.16}$$

5.2 SSR Maximisation Under Perfect CSI in FBR systems

In this section, we begin by formulating the secrecy sum-rate (SSR) maximisation problem under the assumption of perfect CSI. The optimisation problem is formally stated as:

$$(\mathcal{P}1): \max_{\mathbf{w},\boldsymbol{\theta}} R_s(\mathbf{w},\boldsymbol{\theta}), \tag{5.17a}$$

$$\text{s.t.} \quad \sum\nolimits_{k=1}^{\mathcal{K}} \|\mathbf{w}_k\|^2 \leq P, \tag{5.17b}$$

$$|e^{(j\boldsymbol{\theta})}| = 1, \tag{5.17c}$$

$$\varsigma_k \leq \varsigma_{\max},\ \varsigma_e \leq \varsigma_{e_{\max}},\ t_t \leq t_{\max}, \tag{5.17d}$$

where $R_s(\mathbf{w},\boldsymbol{\theta}) = \sum_{k=1}^{\mathcal{K}} \mathcal{S}_k^{\mathcal{F}}(\mathbf{w},\boldsymbol{\theta})$ denotes the SSR, and P represents Alice's total power budget. Constraint (5.17b) enforces the sum-power limitation on the transmitted signals, while (5.17c) ensures the unit modulus constraint (UMC) on the phase shifts of the PREs. It is important to highlight that the finite blocklength regime (FBR) constraints (5.17d), are implicitly incorporated into the objective function through the SSR expression $R_s(\mathbf{w},\boldsymbol{\theta})$, which includes the FBR dispersion factor as in (5.9).

The optimisation problem $(\mathcal{P}1)$ is inherently nonconvex because the objective function in (5.17a) is not concave, and the UMC (5.17c) is nonconvex. To address this challenge, the alternating optimisation (AO) technique can be applied [91]. Specifically, at the ι-th iteration, the feasible solution $(\mathbf{w}^{(\iota)},\boldsymbol{\theta}^{(\iota)})$ for $(\mathcal{P}1)$ is obtained by solving two subproblems sequentially. First, the beamforming vectors $\mathbf{w}$ are optimised while keeping $\boldsymbol{\theta}$ fixed:

$$(\mathcal{P}1.1): \max_{\mathbf{w}} R_s(\mathbf{w}^{(\iota)},\boldsymbol{\theta}),\ \text{s.t. } (5.17b), \tag{5.18}$$

followed by optimising the IRS phase shifts $\boldsymbol{\theta}$ with $\mathbf{w}$ held constant, by solving

$$(\mathcal{P}1.2): \max_{\boldsymbol{\theta}} R_s(\mathbf{w},\boldsymbol{\theta}^{(\iota)}),\ \text{s.t. } (5.17c). \tag{5.19}$$

Nonetheless, this AO approach involves solving the subproblems ($\mathcal{P}1.1$) and ($\mathcal{P}1.2$) iteratively, which can be computationally expensive, particularly when the IRS comprises a large number of PREs. To mitigate this, we propose a linearization strategy detailed in the sequel, which employs mathematically tractable approximation functions to develop a computationally efficient algorithm suitable for IRSs with many PREs.

5.2.1 Sub-Problem for Optimising the Beamforming Vectors

With $\boldsymbol{\theta}$ fixed at $\boldsymbol{\theta}^{(\iota)}$, we solve the problem ($\mathcal{P}1$) to find an updated beamforming vector $\mathbf{w}^{(\iota+1)}$ such that $R_s(\mathbf{w}^{(\iota+1)},\boldsymbol{\theta}^{(\iota)}) \geq R_s(\mathbf{w}^{(\iota)},\boldsymbol{\theta}^{(\iota)})$. The approach begins by linearizing the objective function in (5.17a), which is composed of four components: the data rate of user-k $C_k(\mathbf{w},\boldsymbol{\theta})$, the negative eavesdropping rate of Eve $C_e(\mathbf{w},\boldsymbol{\theta})$, and the dispersion factors of user-k and Eve, $V_k(\mathbf{w},\boldsymbol{\theta})$ and $V_e(\mathbf{w},\boldsymbol{\theta})$ respectively, as expressed in (5.9).

To this end, we first apply the methodology in [95] to linearise the user-k's secrecy rate. Specifically, by utilising inequality (A.1) from Appendix A, define $\boldsymbol{\Lambda} \triangleq \boldsymbol{h}_k(\boldsymbol{\theta}^{(\iota)})\mathbf{w}_k$, $\boldsymbol{\digamma} \triangleq \rho_k$, $\hat{\Lambda} \triangleq \boldsymbol{h}_k(\boldsymbol{\theta}^{(\iota)})\mathbf{w}_k^{(\iota)}$, and $\hat{\digamma} \triangleq \rho_k$. Accordingly, the user's data rate admits the following lower bound:

$$C_k(\mathbf{w},\boldsymbol{\theta}^{(\iota)}) \geq q_{1,k}^{(\iota)} + 2\Re\left\{\left\langle \boldsymbol{m}_{k,k}^{(\iota)}, \mathbf{w}_k \right\rangle\right\} - n_{1,k}^{(\iota)}\upsilon_k^{(\iota)}, \tag{5.20}$$

where

$$\begin{aligned} q_{1,k}^{(\iota)} &\triangleq C_k(\mathbf{w}^{(\iota)},\boldsymbol{\theta}^{(\iota)}) - \gamma_k(\mathbf{w}^{(\iota)},\boldsymbol{\theta}^{(\iota)}) - \sigma_k^2 n_{1,k}^{(\iota)}, \\ \boldsymbol{m}_{k,k}^{(\iota)} &\triangleq \frac{\boldsymbol{h}_k^H(\boldsymbol{\theta}^{(\iota)})\boldsymbol{h}_k(\boldsymbol{\theta}^{(\iota)})\mathbf{w}_k^{(\iota)}}{\rho_k^{(\iota)}}, \\ n_{1,k}^{(\iota)} &\triangleq \frac{1}{\rho_k^{(\iota)}} - \frac{1}{\upsilon_k^{(\iota)}}. \end{aligned}$$

Next, we proceed to linearise Eve's eavesdropping rate, which can be expressed

as:

$$-\ln(1+\gamma_e(\mathbf{w},\boldsymbol{\theta}^{(\iota)})) \triangleq \overbrace{\ln(1+\rho_e^{(\iota)})}^{a_1} - \overbrace{\ln(1+\upsilon_e^{(\iota)})}^{a_2}. \tag{5.21}$$

Following the approach in [92], the term a_1 in (5.21) is linearised by defining $\boldsymbol{z} \triangleq \rho_e$ and applying inequality (A.2) from Appendix A. Similarly, the term a_2 is linearised by setting $\boldsymbol{\Upsilon} \triangleq \upsilon_e$ and using inequality (A.3) from Appendix A. Consequently, Eve's eavesdropping rate is lower bounded as follows:

$$\begin{aligned} C_e(\mathbf{w},\boldsymbol{\theta}^{(\iota)}) \geq q_{1,k_e}^{(\iota)} + n_{1,k_e}^{(\iota)} + 2\Re\sum_{\substack{j=1\\ j\neq k}}^{\mathcal{K}} \left\{ \left\langle \boldsymbol{m}_{j,k_e}^{(\iota)}, \mathbf{w}_j \right\rangle \right\} - \frac{\rho_e^{(\iota)}}{1+\rho_e^{(\iota)}} \left(\sum_{\substack{j=1\\ j\neq k}}^{\mathcal{K}} |\boldsymbol{h}_e(\boldsymbol{\theta}^{(\iota)})\mathbf{w}_j|^2 \right) \\ - \frac{1}{\upsilon_e^{(\iota)}} \sum_{j=1}^{\mathcal{K}} |\boldsymbol{h}_e(\boldsymbol{\theta}^{(\iota)})\mathbf{w}_j|^2, \end{aligned} \tag{5.22}$$

where

$$\begin{aligned} q_{1,k_e}^{(\iota)} &\triangleq \ln\left(\rho_e^{(\iota)}\right) - \rho_e^{(\iota)} - \ln\left(\upsilon_e^{(\iota)}\right) + 1, \\ n_{1,k_e}^{(\iota)} &\triangleq \left(-\frac{\rho_e^{(\iota)}}{1+\rho_e^{(\iota)}} - \frac{1}{\upsilon_e^{(\iota)}} \right) \sigma_e^2, \\ \boldsymbol{m}_{k_e,j}^{(\iota)} &\triangleq \boldsymbol{h}_e^H(\boldsymbol{\theta}^{(\iota)}) \boldsymbol{h}_e(\boldsymbol{\theta}^{(\iota)}) \mathbf{w}_j^{(\iota)}. \end{aligned}$$

Lastly, we linearise the FBR dispersion factors $V_i(\mathbf{w},\boldsymbol{\theta}), i \in \{k,e\}$. By leveraging (5.13) alongside the inequalities (A.4) and (A.5) presented in Appendix A, and defining $x \triangleq V_i(\mathbf{w}^{(\iota)},\boldsymbol{\theta})$, $\mathbf{A} \triangleq \rho_i$, and $B \triangleq \varsigma_i$, the dispersion factors can be bounded as follows:

$$\xi_i \sqrt{V_i(\mathbf{w},\boldsymbol{\theta}^{(\iota)})} \leq q_{2,i}^{(\iota)} - 2\sum_{\substack{j=1\\ j\neq k}}^{\mathcal{K}} \Re\left\{ \left\langle \boldsymbol{d}_{j,i}^{(\iota)}, \mathbf{w}_j \right\rangle \right\} - n_{2,i}^{(\iota)} \upsilon^{(\kappa)}, \tag{5.23}$$

where,

$$q_{2,i}^{(\iota)} \triangleq \xi_i \left(\frac{\sqrt{V_i(\mathbf{w}^{(\iota)}, \boldsymbol{\theta}^{(\iota)})}}{2} + \frac{(\upsilon_i^{(\iota)})^2 + \rho_i^{(\iota)}\sigma_i^2 - 2\upsilon_i^{(\iota)}\sigma_i^2}{(\upsilon_i^{(\iota)})^2 \sqrt{V_i(\mathbf{w}^{(\iota)}, \boldsymbol{\theta}^{(\iota)})}} \right),$$

$$\boldsymbol{d}_{j,i}^{(\iota)} \triangleq \frac{\xi_i [\boldsymbol{h}_i(\boldsymbol{\theta}^{(\iota)})]^2 \mathbf{w}_j^{(\iota)}}{\upsilon_i^{(\iota)} \sqrt{V_i(\mathbf{w}^{(\iota)}, \boldsymbol{\theta}^{(\iota)})}}, \quad i \in \{k, e\},$$

$$n_{2,i}^{(\iota)} \triangleq \frac{\xi_i \rho_i^{(\iota)}}{(\upsilon_i^{(\iota)})^2 \sqrt{V_i(\mathbf{w}^{(\iota)}, \boldsymbol{\theta}^{(\iota)})}}, \quad i \in \{k, e\}.$$

By substituting (5.20), (5.22), and (5.23) into (5.9), the FBR-SR can be lower bounded as:

$$\mathcal{S}_k^{\mathcal{F}}(\mathbf{w}, \boldsymbol{\theta}^{(\iota)}) \geq q_k^{(\iota)} + 2\Re\left\{ \left\langle \boldsymbol{m}_k^{(\iota)}, \mathbf{w}_k \right\rangle \right\} - (\mathbf{w}_k)^H \boldsymbol{\psi}_k^{(\iota)} \mathbf{w}_k, \tag{5.24}$$

where,

$$q_k^{(\iota)} \triangleq q_{1,k}^{(\iota)} + q_{1,k_e}^{(\iota)} + n_{1,k_e}^{(\iota)} + q_{2,k}^{(\iota)} + q_{2,k_e}^{(\iota)},$$

$$\boldsymbol{m}_k^{(\iota)} \triangleq \sum_{j=1}^{\mathcal{K}} \boldsymbol{m}_{j,k}^{(\iota)} + \sum_{\substack{j=1 \\ j \neq k}}^{\mathcal{K}} \left(\boldsymbol{m}_{k_e,j}^{(\iota)} - \boldsymbol{d}_{j,k}^{(\iota)} - \boldsymbol{d}_{j,k_e}^{(\iota)} \right),$$

$$\boldsymbol{\psi}_k^{(\iota)} \triangleq \sum_{j=1}^{\mathcal{K}} n_j^{(\iota)} \boldsymbol{h}_j^H(\boldsymbol{\theta}^{(\iota)}) \boldsymbol{h}_j(\boldsymbol{\theta}^{(\iota)}) + n_{k_e}^{(\iota)} \boldsymbol{h}_e^H(\boldsymbol{\theta}^{(\iota)}) \boldsymbol{h}_e(\boldsymbol{\theta}^{(\iota)}),$$

$$n_k^{(\iota)} \triangleq n_{1,k}^{(\iota)} + n_{2,k}^{(\iota)},$$

$$n_{k_e}^{(\iota)} \triangleq \frac{\rho_e^{(\iota)}}{1 + \rho_e^{(\iota)}} + \frac{1}{\upsilon_e^{(\iota)}} + n_{2,k_e}.$$

Finally, by substituting (5.24) into (5.18), problem ($\mathcal{P}1.1$) can be recast as:

$$(\mathcal{P}1.3) : \min_{\mathbf{w}} \; -\sum\nolimits_{k=1}^{\mathcal{K}} \widetilde{\mathcal{S}}_k^{\mathcal{F}}(\mathbf{w}, \boldsymbol{\theta}^{(\iota)}), \tag{5.25a}$$

$$\text{s.t.} \quad (5.17\text{b}). \tag{5.25b}$$

The resulting problem ($\mathcal{P}1.3$) is convex and an SDP, which can be efficiently solved by standard optimisation tools, such as the interior point method or the CVX toolbox [93], to obtain the updated beamforming vector $\mathbf{w}^{(\iota+1)}$.

5.2.2 Sub-Problem for Optimising the PREs

Similarly, given a fixed $\mathbf{w}$, our objective is to determine $\boldsymbol{\theta}^{(\iota+1)}$ such that the FBR-SR satisfies $\mathcal{S}_k(\mathbf{w}_k^{(\iota+1)}, \boldsymbol{\theta}^{(\iota+1)}) \geq \mathcal{S}_k(\mathbf{w}_k^{(\iota+1)}, \boldsymbol{\theta}^{(\iota)})$.

Following the approach from the previous subsection, the lower bound approximation for the user's data rate can be derived by applying the inequality (A.1) from Appendix A. Consequently, the user's data rate is lower bounded by:

$$C_k(\mathbf{w}^{(\iota+1)}, \boldsymbol{\theta}) \geq q_{1,k}^{(\iota+1)} + 2\Re\left\{\sum_{n=1}^{N} \boldsymbol{m}_{k,k}^{(\iota+1)}(n) e^{j\theta_n}\right\} + \left(e^{j\boldsymbol{\theta}}\right)^H \boldsymbol{\varphi}_{1,k}^{(\iota+1)} e^{j\boldsymbol{\theta}}, \tag{5.26}$$

where,

$$\begin{aligned}
q_{1,k}^{(\iota+1)} &\triangleq C_k(\mathbf{w}^{(\iota+1)}, \boldsymbol{\theta}^{(\iota)}) - \gamma_k(\mathbf{w}^{(\iota+1)}, \boldsymbol{\theta}^{(\iota)}) - \sigma_k^2 n_{1,k}^{(\iota+1)}, \\
n_{1,k}^{(\iota+1)} &\triangleq \frac{1}{\rho_k^{(\iota+1)}} - \frac{1}{\upsilon_k^{(\iota+1)}}, \\
\boldsymbol{m}_{k,k}^{(\iota+1)}(n) &\triangleq \frac{\hat{\boldsymbol{m}}_{k,k}^{(\iota+1)}(n)}{\rho_k^{(\iota+1)}}, \\
\hat{\boldsymbol{m}}_{k,k}^{(\iota+1)}(n) &\triangleq (\mathbf{w}_k^{(\iota+1)})^H \boldsymbol{h}_k^H(\boldsymbol{\theta}^{(\iota)}) \boldsymbol{u}_k \boldsymbol{\Xi}_n \boldsymbol{G}_{\mathrm{AR}} \mathbf{w}_k^{(\iota+1)}, \\
\boldsymbol{\varphi}_{1,k}^{(\iota+1)} &\triangleq -n_{1,k}^{(\iota+1)} \sum_{j=1}^{\mathcal{K}} \boldsymbol{\varphi}_{k,j}^{(\iota+1)}, \\
\boldsymbol{\varphi}_{k,j}^{(\iota+1)} &\triangleq \left(\boldsymbol{\aleph}_{k,j}^{(\iota+1)}(n)\right)^* \boldsymbol{\aleph}_{k,j}^{(\iota+1)}(m), \quad n, m \in \{1, \ldots, N\}, \\
\boldsymbol{\aleph}_{k,j}^{(\iota+1)}(n) &\triangleq \boldsymbol{u}_k \boldsymbol{\Xi}_n \boldsymbol{G}_{\mathrm{AR}} \mathbf{w}_j^{(\iota+1)}.
\end{aligned}$$

Likewise, Eve's eavesdropping rate can be lower bounded as:

$$\begin{aligned}
C_e(\mathbf{w}^{(\iota+1)}, \boldsymbol{\theta}) \geq\ & q_{1,k_e}^{(\iota+1)} + n_{1,k_e}^{(\iota+1)} + 2\Re\left\{\sum_{n=1}^{N} \boldsymbol{m}_{k_e}^{(\iota+1)}(n) e^{j\theta_n}\right\} \\
& + \left(e^{j\boldsymbol{\theta}}\right)^H \boldsymbol{\varphi}_{1,k_e}^{(\iota+1)} e^{j\boldsymbol{\theta}} + \left(e^{j\boldsymbol{\theta}}\right)^H \boldsymbol{\varphi}_{k_e,j}^{(\iota+1)} e^{j\boldsymbol{\theta}}.
\end{aligned} \tag{5.27}$$

where,

$$
\begin{aligned}
q_{1,k_e}^{(\iota+1)} &\triangleq \ln\left(\rho_e^{(\iota+1)}\right) - \rho_e^{(\iota+1)} - \ln\left(\upsilon_e^{(\iota+1)}\right) + 1, \\
n_{1,k_e}^{(\iota+1)} &\triangleq \left(-\frac{\rho_e^{(\iota+1)}}{1+\rho_e^{(\iota+1)}} - \frac{1}{\upsilon_e^{(\iota+1)}}\right)\sigma_e^2, \\
\boldsymbol{m}_{k_e}^{(\iota+1)}(n) &\triangleq \sum\nolimits_{j=1,j\neq k}^{\mathcal{K}} \boldsymbol{m}_{j,k_e}^{(\iota+1)}(n), \\
\boldsymbol{m}_{j,k_e}^{(\iota+1)}(n) &\triangleq \left(\mathbf{w}_k^{(\iota+1)}\right)^H \boldsymbol{h}_e^H(\boldsymbol{\theta}^{(\iota)})\boldsymbol{u}_e\boldsymbol{\Xi}_n\boldsymbol{G}_{\text{AR}}\mathbf{w}_k^{(\iota+1)}, \\
\boldsymbol{\varphi}_{1,k_e}^{(\iota+1)} &\triangleq \left(\frac{-\rho_e^{(\iota+1)}}{(1+\rho_e^{(\iota+1)})} - \frac{1}{(\sigma_e^2+\upsilon_e^{(\iota+1)})}\right)\left(\sum_{j=1}^{\mathcal{K}}\boldsymbol{\varphi}_{k_e,j}^{(\iota+1)}\right), \\
\boldsymbol{\varphi}_{k_e,j}^{(\iota+1)} &\triangleq \left(\boldsymbol{\aleph}_{k_e,j}^{(\iota+1)}(n)\right)^* \boldsymbol{\aleph}_{k_e,j}^{(\iota+1)}(m), \\
\boldsymbol{\aleph}_{k_e,j}^{(\iota+1)}(n) &\triangleq \boldsymbol{u}_e\boldsymbol{\Xi}_n\boldsymbol{G}_{\text{AR}}\mathbf{w}_j^{(\iota+1)}.
\end{aligned}
$$

Next, we express the user-k's and Eve's dispersion factor, for $i \in \{k, e\}$, we can express the dispersion factors as:

$$
\xi_i\sqrt{V_i(\mathbf{w}^{(\iota+1)},\boldsymbol{\theta})} \leq q_{2,i}^{(\iota+1)} - 2\Re\left\{\sum\nolimits_{n=1}^{N}\boldsymbol{d}_i^{(\iota+1)}e^{(j\theta_n)}\right\} + \left(e^{(j\boldsymbol{\theta})}\right)^H\boldsymbol{\varphi}_{2,i}^{(\iota+1)}e^{(j\boldsymbol{\theta})}, i \in \{k, e\}, \tag{5.28}
$$

where,

$$
\begin{aligned}
q_{2,i}^{(\iota+1)} &\triangleq \frac{\xi_i\left(\left(\upsilon_i^{(\iota+1)}\right)^2\sqrt{V_i(\mathbf{w}^{(\iota+1)},\boldsymbol{\theta}^{(\iota)})} + 2\left(\upsilon_i^{(\iota+1)}\right)^2 + 2\sigma_i^2\rho_i^{(\iota+1)} - 4\sigma_i^2\left(\upsilon_i^{(\iota+1)}\right)\right)}{\left(2\left(\upsilon_i^{(\iota+1)}\right)^2\sqrt{V_i(\mathbf{w}^{(\iota+1)},\boldsymbol{\theta}^{(\iota)})}\right)}, \\
\boldsymbol{d}_{i,j}^{(\iota+1)}(n) &\triangleq \xi_i\Big/\left(\upsilon_i^{(\iota+1)}\sqrt{V_i(\mathbf{w}^{(\iota+1)},\boldsymbol{\theta}^{(\iota)})}\right)\left(\mathbf{w}_j^{(\iota+1)}\right)^H\boldsymbol{h}_i^H(\boldsymbol{\theta}^{(\iota)})\boldsymbol{u}_i\Xi_n\boldsymbol{G}_{\text{AR}}\mathbf{w}_j^{(\iota+1)}, \\
&\quad n \in N, j \in K, j \neq k, \\
\boldsymbol{d}_i^{(\iota+1)} &\triangleq \sum\nolimits_{j=1,j\neq k}^{\mathcal{K}}\boldsymbol{d}_{i,j}^{(\iota+1)}, \\
\boldsymbol{\varphi}_{2,i}^{(\iota+1)} &\triangleq n_{2,i}^{(\iota+1)}\sum\nolimits_{j=1}^{\mathcal{K}}\boldsymbol{\varphi}_{i,j}^{(\iota+1)}, \\
n_{2,i}^{(\iota+1)} &\triangleq (\xi_i\rho_i^{(\iota+1)})/\left(\left(\upsilon_i^{(\iota+1)}\right)^2\sqrt{V_i(\mathbf{w}^{(\iota+1)},\boldsymbol{\theta}^{(\iota)})}\right).
\end{aligned}
$$

By substituting (5.26), (5.27), and (5.28) into (5.9), the concave lower bound ap-

Algorithm 5.1 Proposed AO Algorithm for Solving ($\mathcal{P}1$)

Input: Initial values $\boldsymbol{w}^{(1)} = \boldsymbol{w}^*$, $\boldsymbol{\theta}^{(1)} = \boldsymbol{\theta}^*$, $\varsigma_{\max}$, $\varsigma_{e_{\max}}$, $t_{\max}$, convergence tolerance $\epsilon_t > 0$

Initialise: Set iteration index $\iota = 1$

repeat

  Update $\boldsymbol{w}^{(\iota+1)}$ using (5.25); update $\boldsymbol{\theta}^{(\iota+1)}$ using (5.32)

  if $\dfrac{\left|R_s(\boldsymbol{w}^{(\iota+1)}, \boldsymbol{\theta}^{(\iota+1)}) - R_s(\boldsymbol{w}^{(\iota)}, \boldsymbol{\theta}^{(\iota)})\right|}{R_s(\boldsymbol{w}^{(\iota)}, \boldsymbol{\theta}^{(\iota)})} \leq \epsilon_t$ **then**

    $\boldsymbol{w}^* \leftarrow \boldsymbol{w}^{(\iota+1)}$, $\boldsymbol{\theta}^* \leftarrow \boldsymbol{\theta}^{(\iota+1)}$

    Output: $(\boldsymbol{w}^*, \boldsymbol{\theta}^*)$; **terminate**

  else

    $\iota \leftarrow \iota + 1$

  end if

until convergence

proximation of the FBR-SR can be expressed as:

$$\widetilde{\mathcal{S}}_k^{\mathcal{F}}\left(\mathbf{w}^{(\iota+1)}, \boldsymbol{\theta}\right) \geq q_k^{(\iota+1)} + 2\sum_{n=1}^{N} \Re\left\{\boldsymbol{m}_k^{(\iota+1)}(n) e^{j\theta_n}\right\}, \tag{5.29}$$

where,

$$\begin{aligned}
q_k^{(\iota+1)} &\triangleq q_{1,k}^{(\iota+1)} + q_{1,k_e}^{(\iota+1)} + q_{2,k}^{(\iota+1)} + q_{2,k_e}^{(\iota+1)} + n_{1,ke}^{(\iota+1)} - \left(e^{j\boldsymbol{\theta}^{(\iota)}}\right)^H \boldsymbol{\varphi}_k^{(\iota+1)} e^{j\boldsymbol{\theta}} - 2\lambda_{\max}\left(\boldsymbol{\varphi}_k^{(\iota+1)}\right) N, \\
\boldsymbol{m}_k^{(\iota+1)}(n) &\triangleq \boldsymbol{m}_{k,k}^{(\iota+1)}(n) + \boldsymbol{m}_{k_e}^{(\iota+1)}(n) + \boldsymbol{d}_k^{(\iota+1)}(n) + \boldsymbol{d}_{k_e}^{(\iota+1)}(n) + \\
&\quad \sum\nolimits_{m=1}^{N} e^{-j\theta_m^{(\iota)}} \boldsymbol{\varphi}_k^{(\iota+1)}(m,n) + \lambda_{\max}\left(\boldsymbol{\varphi}_k^{(\iota+1)}\right), \\
\boldsymbol{\varphi}_k^{(\iota+1)} &\triangleq \boldsymbol{\varphi}_{1,k}^{(\iota+1)} + \boldsymbol{\varphi}_{1,k_e}^{(\iota+1)} + \boldsymbol{\varphi}_{k_e,j}^{(\iota+1)} + \boldsymbol{\varphi}_{2,k}^{(\iota+1)} + \boldsymbol{\varphi}_{2,k_e}^{(\iota+1)}.
\end{aligned}$$

Based on (5.29), we formulate the following optimisation problem to determine $\boldsymbol{\theta}^{(\iota+1)}$:

$$(\mathcal{P}1.4): \max_{\boldsymbol{\theta}} R_s\left(\mathbf{w}^{(\iota+1)}, \boldsymbol{\theta}\right), \tag{5.30a}$$

$$\text{s.t.} \quad (5.17\text{c}),\ (5.17\text{d}). \tag{5.30b}$$

To solve problem ($\mathcal{P}1.4$), we define

$$\theta_n^{(\iota+1),k} \triangleq 2\pi - \angle \boldsymbol{m}_k^{(\iota+1)}(n), \quad n = 1, \ldots, N, \tag{5.31}$$

and subsequently find $\boldsymbol{\theta}^{(\iota+1)}$ that maximises the secrecy rate $\mathrm{SR}(\mathbf{w}^{(\iota+1)}, \boldsymbol{\theta})$ while satisfying the unit modulus constraint (5.17c) as:

$$\boldsymbol{\theta}^{(\iota+1)} = 2\pi - \angle \boldsymbol{m}^{(\iota+1)}(n), \quad n = 1, \ldots, N. \tag{5.32}$$

It is worth noting that by setting the dispersion factor $V_i = 0$, the FBR optimisation problem ($\mathcal{P}1$) reduces to the conventional LBR optimisation problem, which can be addressed similarly.

The procedure to solve problem ($\mathcal{P}1$) is outlined in Algorithm 5.1, which is guaranteed to converge to a locally optimal solution of ($\mathcal{P}1$), as formally stated in the following theorem.

Theorem 5.1. *The solution obtained via Algorithm 5.1 constitutes a locally optimal solution to problem* ($\mathcal{P}1$).

Proof: Refer to Appendix D.1.

5.3 SSR Maximization Under Imperfect CSI With FBR Systems

To address the imperfect CSI from the IRS to the users and Eve, we utilize the channel model given in equation (5.5), where only partial/imperfect CSI $\widehat{\boldsymbol{u}}_i$ is accessible. Initially, the minimum SR maximization problem can be formulated as

follows:

$$(\mathcal{P}2) : \max_{\mathbf{w},\boldsymbol{\theta}} \widehat{R}_s(\mathbf{w},\boldsymbol{\theta}), \tag{5.33a}$$

$$\text{s.t.} \quad \sum\nolimits_{k=1}^{\mathcal{K}} \|\mathbf{w}_k\|^2 \leq P, \tag{5.33b}$$

$$|e^{(j\boldsymbol{\theta})}| = 1, \tag{5.33c}$$

$$\|\Delta \boldsymbol{u}_i\|_2 \leq \xi_i, i \in \{k, e\}, \tag{5.33d}$$

$$\varsigma_k \leq \varsigma_{\max}, \ \varsigma_e \leq \varsigma_{e_{\max}}, \ t_t \leq t_{\max}, \tag{5.33e}$$

where $\widehat{R}_s(\mathbf{w},\boldsymbol{\theta}) \triangleq \sum_{k=1}^{\mathcal{K}} \widehat{\mathcal{S}}_k^{\mathcal{F}}(\mathbf{w},\boldsymbol{\theta})$. Compared to the conventional LBR scenario under imperfect CSI, problem $(\mathcal{P}2)$ is more complex. This complexity arises primarily because the additional FBR constraints, captured by the nonconvex dispersion factor in (5.14), are embedded within the objective function (5.33a). Furthermore, the semi-infinite constraint in (5.33e), imposed by the imperfect CSI model (5.5), further intensifies the problem's difficulty.

To solve problem $(\mathcal{P}2)$, we begin by introducing slack variables to decouple the coupling between the beamforming vectors and the IRS's PREs in the objective function, which facilitates the application of the AO method. Specifically, we substitute (5.15) into (5.33a). Next, we define slack variables where z serves as a lower bound on the FBR-SSR, φ_k denotes the minimum user rates, μ_{k_e} represents the maximum eavesdropping rate of Eve, and $\tilde{\varphi}_i$, for $i \in \{k, e\}$, correspond to the maximum dispersion factors for user-k and Eve, respectively. With these definitions,

problem ($\mathcal{P}2$) can be equivalently reformulated as:

$$(\mathcal{P}2.1): \max_{\mathbf{w},\boldsymbol{\theta}} \ z, \tag{5.34a}$$

$$\text{s.t.} \quad z \leq \sum\nolimits_{k}^{\mathcal{K}} \varphi_k - \mu_{k_e} - \tilde{\varphi}_k - \tilde{\varphi}_{k_e}, \forall k, \tag{5.34b}$$

$$\varphi_k \leq \widehat{C}_k, \ \forall \|\Delta \boldsymbol{u}_k\|_2 \leq \xi_k, \ \forall k, \tag{5.34c}$$

$$\mu_{k_e} \geq \widehat{C}_e, \ \forall \|\Delta \boldsymbol{u}_e\|_2 \leq \xi_e, \ \forall k, \tag{5.34d}$$

$$\tilde{\varphi}_k \geq \xi_k \sqrt{\widehat{V}_k}, \ \forall \|\Delta \boldsymbol{u}_k\|_2 \leq \xi_k, \ \forall k, \tag{5.34e}$$

$$\tilde{\varphi}_{k_e} \geq \xi_e \sqrt{\widehat{V}_e}, \ \forall \|\Delta \boldsymbol{u}_e\|_2 \leq \xi_e, \ \forall k, \tag{5.34f}$$

$$(5.33\text{b}), \ (5.33\text{c}), \ (5.33\text{e}). \tag{5.34g}$$

It can be observed that the constraint (5.33e) in problem ($\mathcal{P}2$) is encompassed by the constraints (5.34c), (5.34d), (5.34e), and (5.34f) in problem ($\mathcal{P}2.1$) (which relate to the CSI uncertainty modeled in the channel definition (5.6)). Subsequently, we apply the SCA technique along with the $\mathcal{S}$-procedure to convert the semi-infinite and nonconvex constraints (5.34c), (5.34d), (5.34e), and (5.34f) into a finite set of LMIs. Finally, we utilise a PCCP algorithm to address the UMC (5.33c) [112].

5.3.1 Sub-Problem for Optimising the Beamforming Vectors

To linearise the semi-infinite inequalities in (5.34c), we first substitute (5.12) into (5.34c), which leads to:

$$2^{\varphi_k} - 1 \leq \frac{\left|(\boldsymbol{u}_k \boldsymbol{\Phi} \boldsymbol{G}_{\text{AR}}) \mathbf{w}_k\right|^2}{\left\|(\boldsymbol{u}_k \boldsymbol{\Phi} \boldsymbol{G}_{\text{AR}}) \mathbf{W}_{-k}\right\|^2 + \sigma_k^2}, \quad \forall k. \tag{5.35}$$

By introducing the auxiliary variables $\boldsymbol{\beta} = [\beta_1, \ldots, \beta_K]$ to represent the interference plus noise power, (5.35) can be equivalently reformulated as:

$$\left|(\boldsymbol{u}_k \boldsymbol{\Phi} \boldsymbol{G}_{\text{AR}}) \mathbf{w}_k\right|^2 \geq (2^{\varphi_k} - 1)\beta_k, \quad \forall k, \tag{5.36a}$$

$$\left\|(\boldsymbol{u}_k \boldsymbol{\Phi} \boldsymbol{G}_{\text{AR}}) \mathbf{W}_{-k}\right\|^2 + \sigma_k^2 \leq \beta_k, \quad \forall k. \tag{5.36b}$$

To handle the nonconvexity of the semi-infinite inequalities in (5.36a), we replace the left-hand side by its linear lower bound using the following lemma.

Lemma 9. *At iteration* (ι)*, given the current solutions* $\mathbf{w}^{(\iota)}$ *and* $\boldsymbol{\theta}^{(\iota)}$*, the linear lower bound of* (5.36a) *at the point* $(\mathbf{w}^{(\iota)}, \boldsymbol{\theta}^{(\iota)})$ *is given by:*

$$|(\boldsymbol{u}_k \boldsymbol{\Phi} \boldsymbol{G}_{_{AR}}) \boldsymbol{w}_k|^2 = \boldsymbol{u}_k \mathbf{X}_k \boldsymbol{u}_k^H, \tag{5.37}$$

where,

$$\begin{aligned}\mathbf{X}_k \triangleq & \boldsymbol{\Phi} \boldsymbol{G}_{_{AR}} \boldsymbol{w}_k \boldsymbol{w}_k^{(\iota),H} \boldsymbol{G}_{_{AR}}^H \boldsymbol{\Phi}^{(\iota),H} + \boldsymbol{\Phi}^{(\iota)} \boldsymbol{G}_{_{AR}} \boldsymbol{w}_k^{(\iota)} \boldsymbol{w}_k^H \boldsymbol{G}_{_{AR}}^H \boldsymbol{\Phi}^{(\iota),H} \\ & - \boldsymbol{\Phi}^{(\iota)} \boldsymbol{G}_{_{AR}} \boldsymbol{w}_k^{(\iota)} \boldsymbol{w}_k^{(\iota),H} \boldsymbol{G}_{_{AR}}^H \boldsymbol{\Phi}^{(\iota),H}.\end{aligned}$$

Proof: Refer to Appendix D.1.

Next, by substituting (5.37) into (5.36a), and applying (5.5a) along with Lemma 9, the inequality in (5.36a) can be reformulated as:

$$\Delta \boldsymbol{u}_k \mathbf{X}_k \Delta \boldsymbol{u}_k^H + 2\Re\left\{\widehat{\boldsymbol{u}}_k^H \mathbf{X}_k \Delta \boldsymbol{u}_k\right\} + d_k \geq (2^{\varphi_k} - 1)\beta_k, \ \forall \|\Delta \boldsymbol{u}_k\|_2 \leq \xi_k, \ \forall k, \tag{5.38}$$

where,

$$d_k \triangleq \widehat{\boldsymbol{u}}_k \mathbf{X}_k \widehat{\boldsymbol{u}}_k^H.$$

To handle the uncertainty in $\{\Delta \boldsymbol{u}_k\}$ in (5.38), we use the $\mathcal{S}$-procedure [75].

Lemma 10. ***($\mathcal{S}$-procedure)*** *For any Hermitian matrix* $\mathbf{U}_i \in \mathbb{C}^{L \times L}$*, vector* $\mathbf{u}_i \in \mathbb{C}^{L \times 1}$*, and scalar* u_i*, for* $i = 0, \ldots, Q$*, define a quadratic function in variable* x *as:*

$$f_i(x) \triangleq x^H \mathbf{U}_i x + 2\Re\{\mathbf{u}_i^H x\} + u_i. \tag{5.39}$$

The implication

$$f_i(x) \geq 0, \quad i = 1, \ldots, Q \implies f_0(x) \geq 0,$$

holds if and only if there exist scalars $\mathfrak{n}_i \geq 0$*,* $i = 1, \ldots, Q$*, such that*

$$\begin{bmatrix} \mathbf{U}_0 & \mathbf{u}_0 \\ \mathbf{u}_0^H & u_0 \end{bmatrix} - \sum_{i=1}^{Q} \mathfrak{n}_i \begin{bmatrix} \mathbf{U}_i & \mathbf{u}_i \\ \mathbf{u}_i^H & u_i \end{bmatrix} \succeq 0. \tag{5.40}$$

By applying Lemma 10, the semi-infinite constraint in (5.38) can be equivalently reformulated as the LMI:

$$\begin{bmatrix} \varpi_k \mathbf{I}_M + \mathbf{X}_k & (\widehat{\boldsymbol{u}}_k \mathbf{X}_k)^H \\ \widehat{\boldsymbol{u}}_k \mathbf{X}_k & d_k - (2^{\varphi_k} - 1)\beta_k - \eta_k \Omega_k^2 \end{bmatrix} \succeq 0, \quad \forall k, \tag{5.41}$$

where $\boldsymbol{\eta} = [\eta_1, \ldots, \eta_K]^T \geq \mathbf{0}$ denotes a vector of slack variables.

Despite the conversion of (5.38) to an LMI (5.41), the constraint remains non-convex owing to the bilinear term $2^{\varphi_k}\beta_k$. To address this challenge, the SCA technique [74] is employed to obtain a convex upper bound of this term. Specifically, by utilising the first-order Taylor expansion around the point $(\varphi_k^{(\iota)}, \beta_k^{(\iota)})$ at iteration ι, the product $2^{\varphi_k}\beta_k$ is upper bounded as follows:

$$(\beta_k 2^{\varphi_k})^{ub} \triangleq \left((\varphi_k - \varphi_k^{(\iota)})\beta_k^{(\iota)} \ln 2 + \beta_k\right) 2^{\varphi_k^{(\iota)}}. \tag{5.42}$$

Substituting the above convex upper bound into (5.41) yields the following LMI representation:

$$\begin{bmatrix} \varpi_k \mathbf{I}_M + \mathbf{X}_k & (\widehat{\boldsymbol{u}}_k \mathbf{X}_k)^H \\ \widehat{\boldsymbol{u}}_k \mathbf{X}_k & d_k - (\beta_k 2^{\varphi_k})^{ub} + \beta_k - \varpi_k \Omega_k^2 \end{bmatrix} \succeq 0, \quad \forall k. \tag{5.43}$$

Next, we address constraint (5.36b) by employing Schur's complement [96].

Lemma 11. *(**Schur's Complement**) For given matrices* $\mathbf{U} \succeq 0$, $\mathbf{Y}$, *and* $\mathbf{Z}$, *define the Hermitian matrix,*

$$\mathbf{X} \triangleq \begin{bmatrix} \mathbf{Z} & \mathbf{Y}^H \\ \mathbf{Y} & \mathbf{U} \end{bmatrix}. \tag{5.44}$$

Then, $\mathbf{X} \succeq 0$ *if and only if the Schur complement* $\Delta\mathbf{U} \triangleq \mathbf{Z} - \mathbf{Y}^H\mathbf{U}^{-1}\mathbf{Y} \succeq 0$.

Utilising Lemma 11, the constraint (5.36b) can be equivalently expressed as the

following LMI:

$$\begin{bmatrix} \beta_k & \mathbf{t}_k^H \\ \mathbf{t}_k & \mathbf{I}_{\mathcal{K}-1} \end{bmatrix} \succeq 0, \quad \forall \|\Delta \boldsymbol{u}_k\|_2 \leq \Omega_k, \quad \forall k, \tag{5.45}$$

where

$$\mathbf{t}_k \triangleq \left((\widehat{\boldsymbol{u}}_k^H \boldsymbol{\Phi} \boldsymbol{G}_{\text{AR}}) \mathbf{W}_{-k} \right)^H,$$

and

$$\mathbf{W}_{-k} \triangleq [\mathbf{w}_1, \ldots, \mathbf{w}_{k-1}, \mathbf{w}_{k+1}, \ldots, \mathbf{w}_{\mathcal{K}}] \in \mathbb{C}^{M \times (\mathcal{K}-1)}.$$

Subsequently, we employ the Nemirovski's Lemma [97], to further handle the constraint in (5.45).

Lemma 12. *(**Nemirovski's Lemma**) For any Hermitian matrix* $\mathbf{A}$*, matrices* $\mathbf{B}$*,* $\mathbf{C}$*, and* $\mathbf{X}$*, and scalar* $t > 0$*, the following inequality holds:*

$$\mathbf{A} \succeq \mathbf{B}^H \mathbf{X} \mathbf{C} + \mathbf{C}^H \mathbf{X}^H \mathbf{B}, \quad \textit{for } \|\mathbf{X}\| \leq t, \tag{5.46}$$

if and only if there exists $a \geq 0$ *such that*

$$\begin{bmatrix} \mathbf{A} - a\mathbf{C}^H \mathbf{C} & -t\mathbf{B}^H \\ -t\mathbf{B} & a\mathbf{I} \end{bmatrix} \succeq 0. \tag{5.47}$$

By applying Lemma 12 and introducing the slack variables $\boldsymbol{\varkappa} \triangleq [\varkappa_1, \ldots, \varkappa_K]^T \succeq \mathbf{0}$, the constraint (5.45) can be equivalently reformulated as:

$$\begin{bmatrix} B_{11,k} & \widehat{\mathbf{t}}_k^H & \mathbf{0}_{1\times M} \\ \widehat{\mathbf{t}}_k & \mathbf{I}_{\mathcal{K}-1} & \Omega_k \left(\boldsymbol{\Phi} \boldsymbol{G}_{\text{AR}} \mathbf{W}_{-k} \right)^H \\ \mathbf{0}_{M\times 1} & \Omega_k \left(\boldsymbol{\Phi} \boldsymbol{G}_{\text{AR}} \mathbf{W}_{-k} \right) & \varkappa_k \mathbf{I}_M \end{bmatrix} \succeq 0, \quad \forall k, \tag{5.48}$$

where $B_{11,k} \triangleq \beta_k - \sigma_k^2 - \varkappa_k$, and $\widehat{\mathbf{t}}_k \triangleq \left((\widehat{\boldsymbol{u}}_k \boldsymbol{\Phi} \boldsymbol{G}_{\text{AR}}) \mathbf{W}_{-k} \right)^H$.

To this end, we address the constraint (5.34d) by first substituting (5.12) into it, and then treating the interference plus noise term in (5.34d) as an auxiliary variable

$\boldsymbol{\beta}_{e_k} \triangleq [\beta_{e_1}, \ldots, \beta_{e_k}]$. Consequently, constraint (5.34d) can be reformulated as

$$\left|(\boldsymbol{u}_e \boldsymbol{\Phi} \boldsymbol{G}_{\text{AR}}) \mathbf{w}_k\right|^2 \leq (2^{\mu_{k_e}} - 1)\beta_{ke}, \quad \forall k, \tag{5.49a}$$

$$\left\|(\boldsymbol{u}_e \boldsymbol{\Phi} \boldsymbol{G}_{\text{AR}}) \mathbf{W}_{-k}\right\|^2 + \sigma_e^2 \geq \beta_{ke}, \quad \forall k. \tag{5.49b}$$

To manage the uncertainties associated with $\{\Delta \boldsymbol{u}_e\}$ in constraints (5.49a) and (5.49b), we adopt an approach analogous to that employed in (5.36b). Accordingly, the equivalent LMIs corresponding to (5.49a) and (5.49b) are expressed as:

$$\begin{bmatrix} C_{e,k} & \widehat{c}_{ke}^H & \mathbf{0}_{1\times M} \\ \widehat{c}_{ke} & 1 & \Omega_e(\boldsymbol{\Phi} \boldsymbol{G}_{\text{AR}} \mathbf{w}_k)^H \\ \mathbf{0}_{M\times 1} & \Omega_e(\boldsymbol{\Phi} \boldsymbol{G}_{\text{AR}} \mathbf{w}_k) & \vartheta_k \mathbf{I}_M \end{bmatrix} \succeq 0, \quad \forall k, \tag{5.50}$$

$$\begin{bmatrix} C_{11,k} & -\widehat{c}_{ke}^H & \mathbf{0}_{1\times M} \\ -\widehat{c}_{ke} & \mathbf{I}_{K-1} & -\Omega_e(\boldsymbol{\Phi} \boldsymbol{G}_{\text{AR}} \mathbf{W}_{-k})^H \\ \mathbf{0}_{M\times 1} & -\Omega_e(\boldsymbol{\Phi} \boldsymbol{G}_{\text{AR}} \mathbf{W}_{-k}) & \varrho_k \mathbf{I}_M \end{bmatrix} \succeq 0, \quad \forall k, \tag{5.51}$$

where $\boldsymbol{\vartheta} \triangleq [\vartheta_1, \ldots, \vartheta_K] \geq 0$ and $\boldsymbol{\varrho} \triangleq [\varrho_1, \ldots, \varrho_K] \geq 0$ denote slack variables, and

$$\begin{aligned} C_{e,k} &\triangleq (\beta_{ke}(2^{\mu_{k_e}}))^{ub} - \beta_{ke} - \vartheta_k, \\ (\beta_{ke}(2^{\mu_{k_e}}))^{ub} &\triangleq \big((\mu_{k_e} - \mu_{k_e}^{(\iota)})\beta_{ke}^{(\iota)} \ln 2 + \beta_{ke}\big) 2^{\mu_{k_e}^{(\iota)}}, \\ \widehat{c}_{ke} &\triangleq \big((\widehat{\boldsymbol{u}}_e^H \boldsymbol{\Phi} \boldsymbol{G}_{\text{AR}}) \mathbf{W}_{-k}\big)^H, \\ C_{11,k} &\triangleq \beta_{ke} - \sigma_e^2 - \varrho_k. \end{aligned}$$

Subsequently, we present the derivation steps for the LMIs corresponding to constraints (5.34e) and (5.34f). Utilising (5.14), together with inequalities (A.4) and (A.5) in Appendix A, and by defining the variables $x \triangleq V_i$, $\mathbf{A} \triangleq \rho_i$, and $B \triangleq \varsigma_i$, the dispersion factors for $i \in \{k, e\}$ can be expressed as:

$$\xi_i \sqrt{V_i} \leq \frac{\xi_i \sqrt{V_i^{(\iota)}}}{2} + \frac{\xi_i |(\boldsymbol{u}_i \boldsymbol{\Phi} \boldsymbol{G}_{\text{AR}}) \mathbf{w}_k|^2}{\sqrt{V_i^{(\iota)}} \left(\|(\boldsymbol{u}_i \boldsymbol{\Phi} \boldsymbol{G}_{\text{AR}}) \mathbf{W}_k\|_2^2 + \sigma_i^2\right)}, \tag{5.52}$$

where $\mathbf{W}_k \triangleq [\mathbf{w}_1, \ldots, \mathbf{w}_{\mathcal{K}}] \in \mathbb{C}^{M \times \mathcal{K}}$.

Therefore, constraints (5.34e) and (5.34f) can be equivalently reformulated as:

$$\frac{\tilde{\varphi}_i - \mathfrak{L}}{\mathfrak{Y}} \geq \frac{|(\boldsymbol{u}_i \boldsymbol{\Phi} \boldsymbol{G}_{\text{AR}}) \mathbf{w}_k|^2}{\|(\boldsymbol{u}_i \boldsymbol{\Phi} \boldsymbol{G}_{\text{AR}}) \mathbf{W}_k\|_2^2 + \sigma_i^2}, \quad i \in \{k, e\}, \tag{5.53}$$

where $\mathfrak{L} \triangleq \frac{\xi_i \sqrt{V_i^{(\iota)}}}{2}$ and $\mathfrak{Y} \triangleq \frac{\xi_i}{\sqrt{V_i^{(\iota)}}}$.

Analogous to the approach to linearise (5.35), by introducing the auxiliary variables $\boldsymbol{\zeta} \triangleq [\zeta_1, \ldots, \zeta_K]$ to represent the interference plus noise terms, the inequality (5.53) can be decomposed as follows:

$$|(\boldsymbol{u}_i \boldsymbol{\Phi} \boldsymbol{G}_{\text{AR}}) \mathbf{w}_k|^2 \leq \left(\frac{\tilde{\varphi}_i - \mathfrak{L}}{\mathfrak{Y}} \right) \zeta_i, \quad \forall k, \quad i \in \{k, e\}, \tag{5.54a}$$

$$\|(\boldsymbol{u}_i \boldsymbol{\Phi} \boldsymbol{G}_{\text{AR}}) \mathbf{W}_k\|^2 + \sigma_i^2 \geq \zeta_i, \quad \forall k, \quad i \in \{k, e\}. \tag{5.54b}$$

Similarly to (5.51), the constraint (5.54b) can be equivalently expressed as the following LMI:

$$\begin{bmatrix} \widetilde{C}_{11,i} & -\tilde{c}_i^H & \mathbf{0}_{1\times M} \\ -\tilde{c}_i & \mathbf{I}_K & -\Omega_i \left(\boldsymbol{\Phi} \boldsymbol{G}_{\text{AR}} \mathbf{W}_k \right)^H \\ \mathbf{0}_{M\times 1} & -\Omega_i \left(\boldsymbol{\Phi} \boldsymbol{G}_{\text{AR}} \mathbf{W}_k \right) & \mathfrak{u}_i \mathbf{I}_M \end{bmatrix} \succeq 0, \quad j \neq k, \tag{5.55}$$

where $\widetilde{C}_{11,i} \triangleq \zeta_k - \sigma_k^2 - \mathfrak{u}_i$, $\mathbf{u} \triangleq [\mathfrak{u}_1, \mathfrak{u}_2, \ldots, \mathfrak{u}_i] \geq \mathbf{0}$ is a slack variable vector, and $\tilde{c}_i \triangleq \left((\widehat{\boldsymbol{u}}_i^H \boldsymbol{\Phi} \boldsymbol{G}_{\text{AR}}) \mathbf{W}_k \right)^H$.

Subsequently, the constraint (5.54a) can be reformulated as the following LMI:

$$\begin{bmatrix} C_{k_f} & \tilde{c}_{ke}^H & \mathbf{0}_{1\times M} \\ \tilde{d}_i & 1 & \Omega_e \left(\boldsymbol{\Phi} \boldsymbol{G}_{\text{AR}} \mathbf{w}_k \right)^H \\ \mathbf{0}_{M\times 1} & \Omega_e \left(\boldsymbol{\Phi} \boldsymbol{G}_{\text{AR}} \mathbf{w}_k \right) & \tilde{\mathfrak{u}}_i \mathbf{I}_M \end{bmatrix} \succeq 0, \quad j \neq k, \tag{5.56}$$

where $C_{k_f} \triangleq \frac{\tilde{\varphi}_k \zeta_k}{\mathfrak{Y}} - \frac{\mathfrak{L} \zeta_k}{\mathfrak{Y}} - \tilde{\mathfrak{u}}_i$, $\tilde{\mathbf{u}} \triangleq [\tilde{\mathfrak{u}}_1, \ldots, \tilde{\mathfrak{u}}_K] \geq \mathbf{0}$ denotes a slack variable vector, and $\tilde{d}_i \triangleq ((\widehat{\boldsymbol{u}}_e \boldsymbol{\Phi} \boldsymbol{G}_{\text{AR}}) \mathbf{w}_k)^H$.

Note that (5.56) remains nonconvex due to the bilinear term $\tilde{\varphi} \zeta_k$. To address this, we apply the SCA method to linearise its nonconvexity as follows:

$$(\tilde{\varphi} \zeta_i)^{ub} \triangleq \tilde{\varphi}^{(\iota)} \zeta_i + \left(\tilde{\varphi} - \tilde{\varphi}^{(\iota)} \right) \zeta_i^{(\iota)}, \tag{5.57}$$

where $\tilde{\varphi}^{(\iota)}$ and $\zeta_i^{(\iota)}$ denote the values of $\tilde{\varphi}_i$ and ζ_i at iteration (ι) of the SCA algorithm, respectively.

By substituting (5.57) into (5.56), the resulting LMI is given by:

$$\begin{bmatrix} \widetilde{C}_{k_f} & \tilde{c}_{ke}^H & \mathbf{0}_{1\times M} \\ \tilde{d}_i & 1 & \Omega_e\left(\boldsymbol{\Phi}\boldsymbol{G}_{\text{AR}}\mathbf{w}_k\right)^H \\ \mathbf{0}_{M\times 1} & \Omega_e\left(\boldsymbol{\Phi}\boldsymbol{G}_{\text{AR}}\mathbf{w}_k\right) & \tilde{\mathfrak{u}}_i\mathbf{I}_M \end{bmatrix} \succeq 0, \quad j \neq k, \tag{5.58}$$

where

$$\widetilde{C}_{k_f} \triangleq \frac{\left(\tilde{\varphi}\zeta_k\right)^{ub}}{\mathfrak{Y}} - \frac{\mathfrak{L}\zeta_k}{\mathfrak{Y}} - \tilde{\mathfrak{u}}_i. \tag{5.59}$$

Eventually, by reformulating problem $(\mathcal{P}2.1)$ with constraints (5.43), (5.48), (5.50), (5.51), (5.55), and (5.58), we obtain the following optimization problem:

$$(\mathcal{P}2.2): \max_{\mathbf{w}} \; z, \tag{5.60a}$$

$$\text{s.t.} \quad z \leq \varphi_k - \mu_{k_e} - \tilde{\varphi}_k - \tilde{\varphi}_{k_e}, \quad \forall k, \tag{5.60b}$$

$$(5.43), (5.48), (5.50), (5.51), (5.55), (5.58), \quad i \in \{k, e\}, \tag{5.60c}$$

$$\boldsymbol{\varpi} \geq \mathbf{0}, \quad \boldsymbol{\varkappa} \geq \mathbf{0}, \quad \boldsymbol{\vartheta} \geq \mathbf{0}, \quad \boldsymbol{\varrho} \geq \mathbf{0}, \quad \mathfrak{u} \geq \mathbf{0}, \quad \tilde{\mathfrak{u}} \geq \mathbf{0}, \tag{5.60d}$$

$$(5.33\text{b}), \quad (5.33\text{e}). \tag{5.60e}$$

At this stage, all nonlinear constraints (5.34c), (5.34d), (5.34e), and (5.34f) have been equivalently transformed into LMIs (5.43), (5.48), (5.50), (5.51), (5.55), and (5.58). Therefore, problem $(\mathcal{P}2.2)$ is an SDP problem that can be efficiently solved using standard convex optimisation solvers, such as the interior-point method or the CVX toolbox [93].

5.3.2 Sub-Problem for Optimising the PREs

Given a fixed $\mathbf{w}$, our goal is to determine $\boldsymbol{\theta}^{(\iota+1)}$ such that:

$$\mathcal{S}_k^{\mathcal{F}}(\mathbf{w}_k^{(\iota+1)}, \boldsymbol{\theta}^{(\iota+1)}) \geq \mathcal{S}_k^{\mathcal{F}}(\mathbf{w}_k^{(\iota+1)}, \boldsymbol{\theta}^{(\iota)}). \tag{5.61}$$

Consistent with the approach presented in the previous section, the constraints (5.34c) and (5.34d) can be equivalently represented by their corresponding LMIs (5.43), (5.48), (5.50), and (5.51). To handle the UMC (5.33c), we PCCP [76]. This method introduces slack variables to relax the original constraint, allowing violations to be penalised in the objective function. The resulting solution upon convergence is an approximate first-order stationary point of the original problem [76].

To facilitate the PCCP method, we introduce an auxiliary variable set $\mathbf{b} \triangleq \{b_n \mid n \in N\}$, where, $b_n \triangleq |e^{j\theta_n}|^*|e^{j\theta_n}|$. Thus, the nonconvex constraint (5.33c) is reformulated as:

$$b_n \leq |e^{j\theta_n}|^*|e^{j\theta_n}| \leq b_n. \tag{5.62}$$

The nonconvex lower bound can be approximated at the (ι)-th iteration by a first-order Taylor expansion as:

$$b_n \leq 2\Re\left\{(e^{j\theta_n})^* e^{j\theta_n^{(\iota)}}\right\} - |e^{j\theta_n^{(\iota)}}|^*|e^{j\theta_n^{(\iota)}}|. \tag{5.63}$$

Incorporating this approximation into the PCCP framework, we penalise the objective function (5.34a) and rewrite problem $(\mathcal{P}2.1)$ as:

$$(\mathcal{P}2.3): \max_{\boldsymbol{\theta}} \quad z - oQ, \tag{5.64a}$$

$$\text{s.t.} \quad (5.43), (5.48), (5.50), (5.51), (5.55), (5.58), \tag{5.64b}$$

$$|e^{j\theta_n}|^*|e^{j\theta_n}| \leq b_n + c_n, \tag{5.64c}$$

$$b_n - \hat{c}_n \leq 2\Re\left\{(e^{j\theta_n})^* e^{j\theta_n^{(\iota)}}\right\} - |e^{j\theta_n^{(\iota)}}|^*|e^{j\theta_n^{(\iota)}}|, \tag{5.64d}$$

$$b_n \geq 0, \quad \forall n \in N, \tag{5.64e}$$

where $o > 0$ denotes the penalty coefficient, and Q quantifies the aggregate constraint violations, defined as:

$$Q \triangleq \sum_{n=1}^{N} (c_n + \hat{c}_n), \tag{5.65}$$

Algorithm 5.2 Compressed PCCP-Based Algorithm for ($\mathcal{P}$2.3)

Input: $(\boldsymbol{w}^{(1)}, \boldsymbol{\theta}^{(1)})$, $o_{\max}$, $\nu \geq 1$, ϵ_{t_1}, ϵ_{t_2}, $\iota_{\max}$

Initialise: $\iota = 1$

repeat

  Solve ($\mathcal{P}$2.3) to get $\boldsymbol{\theta}^{(\iota)}$

  if $\left\| e^{(j\boldsymbol{\theta}^{(\iota)})} - e^{(j\boldsymbol{\theta}^{(\iota-1)})} \right\|_1 \leq \epsilon_{t_1}$ **and** $Q \leq \epsilon_{t_2}$ **then**

    Output: $\boldsymbol{\theta}^* = \boldsymbol{\theta}^{(\iota)}$; **return**

  else $o^{(\iota+1)} \leftarrow \min\{\nu o^{(\iota)}, o_{\max}\}$; $\iota \leftarrow \iota + 1$

  end if

until $\iota > \iota_{\max}$

Restart: Reset $\boldsymbol{\theta}^{(1)}$, choose $\nu > 1$, set $\iota = 1$, repeat

Output: Final $\boldsymbol{\theta}^* = \boldsymbol{\theta}^{(\iota)}$

with $\mathbf{c} \triangleq \{c_n, \hat{c}_n\}$ representing the slack variables introduced to relax the UMC (5.33c). The regularisation factor o serves to control the enforcement of the UMC (5.33c) by appropriately scaling the penalty term Q.

Problem ($\mathcal{P}$2.3) constitutes an SDP problem. In contrast to the conventional semidefinite relaxation (SDR) approach for handling the UMC, the PCCP method, summarised in Algorithm 5.2, is guaranteed to identify a feasible solution to problem ($\mathcal{P}$2.3) [98].

The following considerations are pertinent for the numerical implementation of Algorithm 5.2:

(a) A maximum penalty coefficient $o_{\max}$ is enforced to prevent numerical instability when o becomes excessively large [99];

(b) The stopping criterion $Q \leq \epsilon_{t_2}$ ensures satisfaction of the UMC (5.33c) for sufficiently small ϵ_{t_2} [52];

Algorithm 5.3 AO Algorithm for Solving Problem ($\mathcal{P}2$)

1: **Input:** $(\boldsymbol{w}^{(1)} = \mathbf{w}^*, \boldsymbol{\theta}^{(1)} = \boldsymbol{\theta}^*, \varsigma_{\max}, \varsigma_{e_{\max}}, t_{\max})$, tolerance $\epsilon_t > 0$, $\iota = 1$

2: **repeat**

3: Solve ($\mathcal{P}2.2$) to get $\boldsymbol{w}^{(\iota+1)}$, and ($\mathcal{P}2.3$) to get $\boldsymbol{\theta}^{(\iota+1)}$

4: **if** $\dfrac{|R_s(\boldsymbol{w}^{(\iota+1)}, \boldsymbol{\theta}^{(\iota+1)}) - R_s(\boldsymbol{w}^{(\iota)}, \boldsymbol{\theta}^{(\iota)})|}{R_s(\boldsymbol{w}^{(\iota)}, \boldsymbol{\theta}^{(\iota)})} \leq \epsilon_t$ **then**

5: **Output:** $\boldsymbol{w}^* = \boldsymbol{w}^{(\iota+1)}, \boldsymbol{\theta}^* = \boldsymbol{\theta}^{(\iota+1)}$; **return**

6: **else** $\iota \leftarrow \iota + 1$

7: **end if**

8: **until** convergence

(c) The convergence of Algorithm 5.2 is monitored via the condition

$$\left\| e^{j\boldsymbol{\theta}^{(\iota+1)}} - e^{j\boldsymbol{\theta}^{(\iota)}} \right\|_1 \leq \epsilon_{t_1}.$$

Finally, the pseudocode for the AO algorithm designed to solve problem ($\mathcal{P}2$) is presented in Algorithm 5.3. This algorithm converges to a locally optimal solution of ($\mathcal{P}2$), as formally stated in the following theorem.

Theorem 5.2. *Algorithm 5.3 generates a locally optimal solution to problem* ($\mathcal{P}2$).

Proof: See Appendix D.3.

Complexity Analysis

Since the convex problems ($\mathcal{P}2.2$) and ($\mathcal{P}2.3$) involve linear constraints and LMIs, given in (5.43), (5.48), (5.50), (5.51), (5.55), and (5.58), they can be efficiently solved by the interior-point method [93].

The computational complexity of the algorithm is characterised by its worst-case runtime and the number of floating-point operations required [52]. To efficiently measure the complexity if Algorithm 5.3, we start by defining the following parameters: the number of variables as $c \triangleq 2M$, the dimension of the LMI in (5.43)

Table 5.2 : FBR-IRS Maximising SSR Simulation Parameters

Parameter	**Numerical Value**
Noise power density, σ_i^2	-174 dBm/Hz
Alice transmission power, P	20 dBm
Antenna gains, G_{A} and G_{IRS}	5 dBi
Convergence tolerances, ϵ_t, ϵ_{t_1}, ϵ_{t_2}	10^{-3}
Simulation initial settings	$\beta_k^{(\iota)} = 1$, $\beta_{ke}^{(\iota)} = 1$, $o^{(1)} = 10$, $o_{\max} = 30$

as $a_1 \triangleq MN + M + 1$, and the dimensions of the LMIs in (5.48) and (5.51) as $a_2 \triangleq 2M + 1$, and the size of the LMI in (5.50) as $a_3 \triangleq 2M + 1$. Accordingly, the complexity of solving problems ($\mathcal{P}2.2$) and ($\mathcal{P}2.3$) can be approximated by:

$$\mathcal{O}_{\mathbf{w}} \triangleq \mathcal{O}\left\{\sqrt{b_1 + 2}\, c\left(c^2 + cb_2 + b_3 + (c+1)^2\right)\right\}, \tag{5.66}$$

$$\mathcal{O}_{\mathbf{\Phi}} \triangleq \mathcal{O}\left\{\sqrt{b_1 + 4N}\,(2N)\left(4N^2 + 2Nb_2 + b_3 + 4NM\right)\right\}, \tag{5.67}$$

where,

$$b_1 \triangleq \sum_{k=1}^{\mathcal{K}} (a_1 + a_2) + 2k\,(a_2 + a_3) + (k-2)\,(a_1 + a_3)\,,$$

$$b_2 \triangleq \sum_{k=1}^{\mathcal{K}} \left(a_1^2 + a_2^2\right) + 2k\left(a_2^2 + a_3^2\right) + (k-2)\left(a_1^2 + a_3^2\right),$$

$$b_3 \triangleq \sum_{k=1}^{\mathcal{K}} \left(a_1^3 + a_2^3\right) + 2k\left(a_2^3 + a_3^3\right) + (k-2)\left(a_1^3 + a_3^3\right).$$

5.4 Numerical Results

5.4.1 Parameter Setting

In this section, we conduct extensive simulations to evaluate the performance of the proposed algorithms. The simulations are implemented using MATLAB and the CVX toolbox. In this setup, Alice is positioned at coordinates $(15, 0, 15)$, the IRS is

located at $(0, 25, 40)$, and the users are randomly distributed within a 60 m $\times$ 60 m area to the right of Alice. The eavesdropper (Eve), modelled as a compromised legitimate user, is randomly placed within a 100 m $\times$ 100 m area outside the users' region. It is important to note that if Eve is located very close to any legitimate user, guaranteeing a positive SR for the users becomes practically impossible [102]. In such scenarios, alternative methods such as encryption or friendly jamming may be employed to ensure secrecy [50].

The path loss factor for the Alice-to-IRS link is given by:

$$\beta_{\text{AR}} \triangleq \boldsymbol{G}_{\text{A}} + \boldsymbol{G}_{\text{IRS}} - 35.9 - 22\log_{10}(d_{\text{AR}}) \quad \text{(dB)}, \tag{5.68}$$

where d_{AR} denotes the distance between Alice and the IRS in meters, $\boldsymbol{G}_{\text{A}}$ is the antenna gain at Alice, and $\boldsymbol{G}_{\text{IRS}}$ corresponds to the antenna gain of the IRS elements [70, 86]. Similarly, the path loss factor from the IRS to the users and Eve is modeled as:

$$\beta_{\text{R}i} \triangleq \boldsymbol{G}_{\text{IRS}} - 33.05 - 30\log_{10}(d_{\text{R}i}) \quad \text{(dB)}, \quad i \in \{k, e\}, \tag{5.69}$$

where $d_{\text{R}i}$ is the distance between the IRS and user k or Eve, measured in meters [70, 86].

The spatial correlation matrix for the IRS-to-user/Eve channels is defined as:

$$[\boldsymbol{R}_{Ri}]_{l,\bar{l}} \triangleq \exp\left(j\pi(l-\bar{l})\sin\hat{\vartheta}\sin\hat{\aleph}\right), \quad i \in \{k, e\}, \tag{5.70}$$

where $\hat{\aleph}$ and $\hat{\vartheta}$ denote the elevation and azimuth angles, respectively [86].

The entries of the Alice-to-IRS channel matrix $\boldsymbol{G}_{\text{AR}}$ are generated as:

$$[\boldsymbol{G}_{\text{AR}}]_{a,b} \triangleq \exp\left(j\pi\left((b-1)\sin\overline{\Theta}_b\sin\overline{\vartheta}_b + (a-1)\sin\Theta_n\sin\vartheta_b\right)\right), \tag{5.71}$$

where $\Theta_n, \vartheta_n \in (0, 2\pi)$, and $\overline{\Theta}_n \triangleq \pi - \Theta_n$, $\overline{\vartheta}_n \triangleq \pi + \vartheta_n$ [86]. The small-scale fading $\widehat{\boldsymbol{u}}_i$ for $i \in \{k, e\}$ are modelled as Rician fading channels with a Rician K-factor equal to 3. The CSI error bounds are characterised by:

$$\Omega_i \triangleq \delta_i \|\widehat{\boldsymbol{u}}_i\|_2, \quad \forall i \in \{k, e\}, \tag{5.72}$$

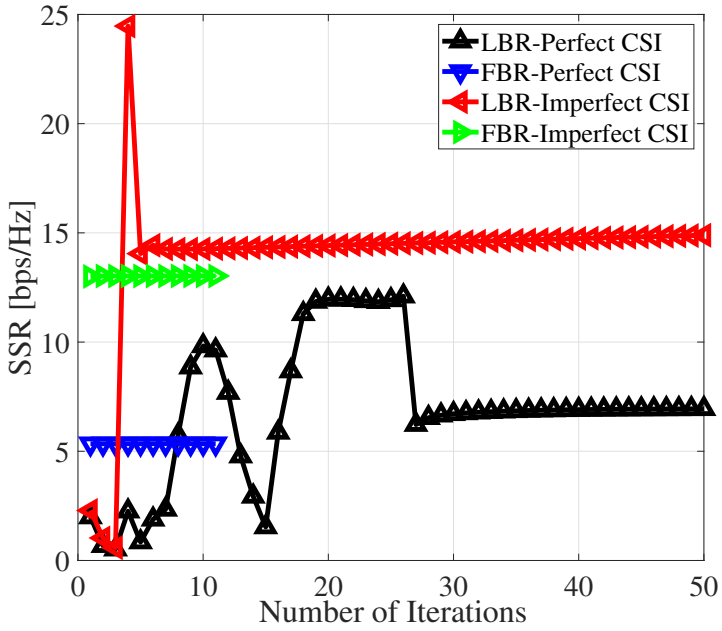

Figure 5.2 : Convergence rate of the SSR algorithms under perfect and Imperfect CSI with $M = 10$, $\mathcal{K} = 6$, $N = 16$.

where $\delta_i \in [0, 1)$ quantifies the relative CSI uncertainty. The case $\delta_i = 0$ corresponds to perfect CSI knowledge of the IRS-to-user/Eve reflected channels at Alice.

For the FBR scenario, the maximum allowable error probabilities are set as $\varsigma_{\max} = \varsigma_{e_{\max}} = 10^{-5}$. The packet length N_t is determined by the product of transmission duration t_t and bandwidth $\mathcal{B}$. Unless stated otherwise, the transmission duration is fixed at $t_t = 0.1$ ms, which is consistent with typical FBR transmission requirements [2]. This short delay ensures quasi-static channel conditions over the packet duration [85]. The system bandwidth is set to $\mathcal{B} = 1$ MHz. The simulation parameters follow those listed in Table 5.2. Finally, all spectral efficiency results are scaled by $\log_2(e)$ to convert natural logarithm units to bits per second per Hertz (bps/Hz).

5.4.2 Performance Evaluation

Fig. 5.2 illustrates the convergence rate of the SSR algorithms under perfect CSI and Imperfect CSI for the FBR and the LBR systems. It can be noticed that the FBR needs fewer iterations to converge since the local optimal solution obtained in the LBR case is used as the initial feasible point for the FBR counterparts. Such a choice highlights the importance of choosing the best initial feasible points in the FBR case.

One way to evaluate the system performance in the proposed algorithms is by using the arithmetic mean. The arithmetic mean is defined as, arithmetic mean = $\frac{1}{\mathcal{K}}\sum_{k=1}^{\mathcal{K}}\mathcal{S}_k^{\mathcal{F}}(\mathbf{w},\boldsymbol{\theta})$. Fig. 5.3 plots the achieved arithmetic mean while varying the number of Alice's antennas M, with $\mathcal{K} = 7$, $N = 10$, and $\delta_k = \delta_e = 0.02$. As expected, the proposed SSR algorithms' achieved arithmetic mean increases with M, since increasing M provides more degrees of freedom, hence it increases the users' SINR. The SSR-FBR algorithms achieve a lower arithmetic mean than their LBR-SSR counterpart due to the FBR constraints, namely, the transmission duration and the latency.

Fig. 5.4 portrays the arithmetic mean against the number of users $\mathcal{K}$, with $M = 10$, $N = 16$, and $\delta_k = \delta_e = 0.02$. From this figure, one can notice that the achieved arithmetic mean obtained by all algorithms decreases with $\mathcal{K}$. This is mainly due to the fact that the inter-user interference increases with $\mathcal{K}$, hence the arithmetic mean decreases. In addition, the FBR counterparts suffer from the same effect as the LBR parts, since the FBR initial feasible point is generated from the optimal solution obtained by solving its LBR counterparts. It can be noticed that the imperfect CSI SSR algorithms achieve a lower arithmetic mean than their perfect CSI counterparts. This is because the imperfect CSI lowers the users' SINR, thus the arithmetic mean tends to decrease.

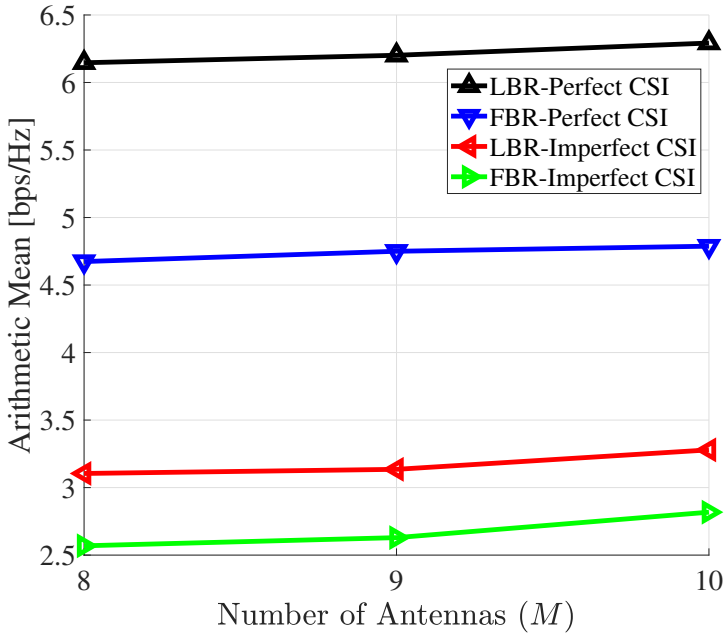

Figure 5.3 : SR Arithmetic mean Vs the number of Alice's antennas M with $\mathcal{K} = 7, N = 10$, and $\delta_k = \delta_e = 0.02$.

Fig. 5.5 illustrates the arithmetic mean against the transmission power budget P with $M = 10$, $\mathcal{K} = 7$, $N = 16$, and $\delta_k = \delta_e = 0.02$. The achieved arithmetic mean obtained by all algorithms increases with P. As we can see, increasing P improves the users' SINR; hence, the arithmetic mean increases. The FBR algorithms illustrate a similar behaviour to that of their LBR counterparts, as expected.

The arithmetic mean is illustrated against the relative amount of CSI uncertainty δ in Fig. 5.6. The achieved arithmetic mean in the LBR and the FBR algorithm decreases with δ. This is expected since, as the uncertainty increases, the users' SINR decreases. However, even under high uncertainty, the proposed algorithms achieve system secrecy, even under the strict constraints of the FBR case. The obtained results demonstrate the robustness of the proposed LBR/FBR algorithm.

Lastly, the minimum SR and the SSR arithmetic mean are illustrated against the transmission duration t_t in Fig. 5.7 and Fig. 5.8, respectively. Both the minimum

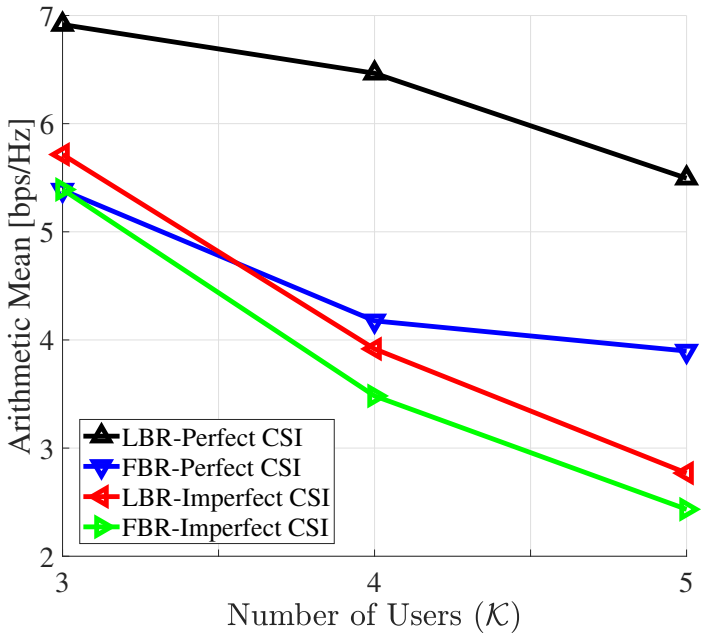

Figure 5.4 : SR Arithmetic mean against the number of users $\mathcal{K}$ with $M = 10$, $N = 16$, and $\delta_k = \delta_e = 0.02$.

SR and the SSR arithmetic mean increase with t_t. Even at low t_t, our proposed algorithms can provide system secrecy, which demonstrates the advantages of our algorithms. Finally, it can be noticed that the achieved LBR-SR serves as an upper bound for the SR-FBR counterpart, since the LBR assumes that the transmission duration $t_t = \infty$.

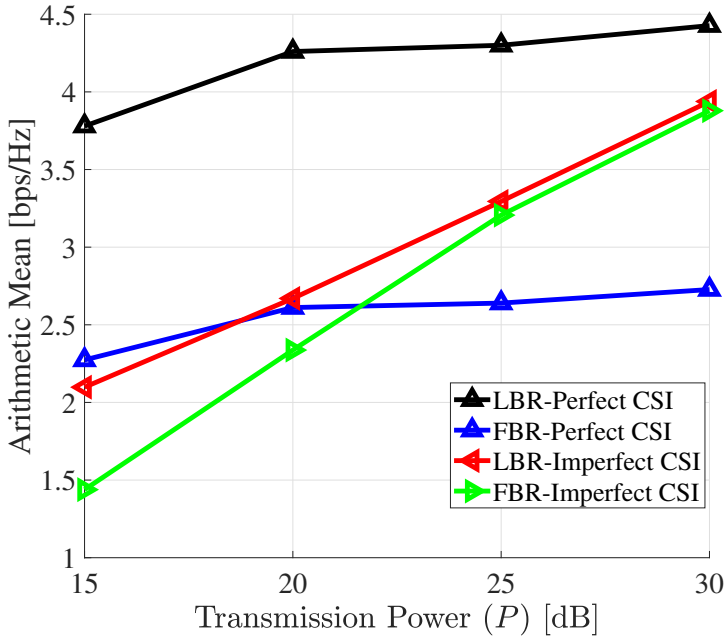

Figure 5.5 : SR Arithmetic mean against the transmission power budget P with $M = 10$, $\mathcal{K} = 7$, $N = 16$, and $\delta_k = \delta_e = 0.02$.

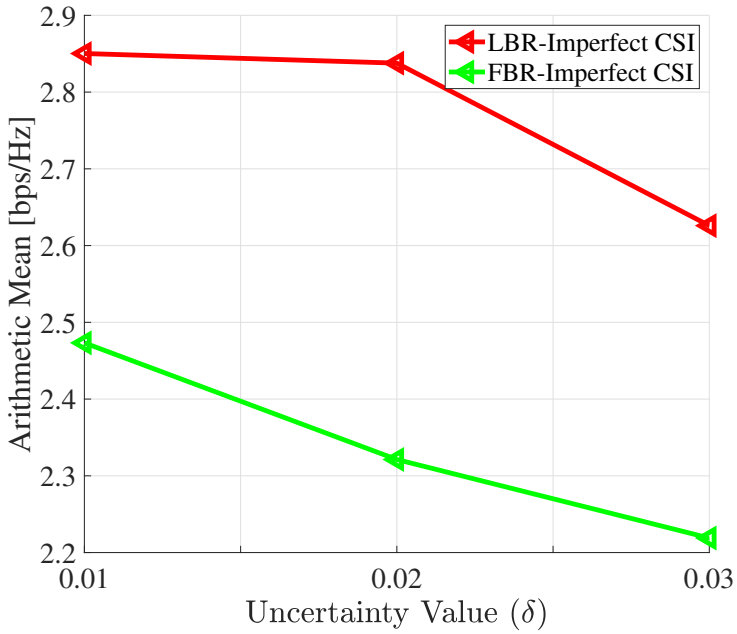

Figure 5.6 : SR Arithmetic mean Vs. the uncertainty level $\delta_k = \delta_e$ with $M = 10$, $\mathcal{K} = 7$, and $N = 10$.

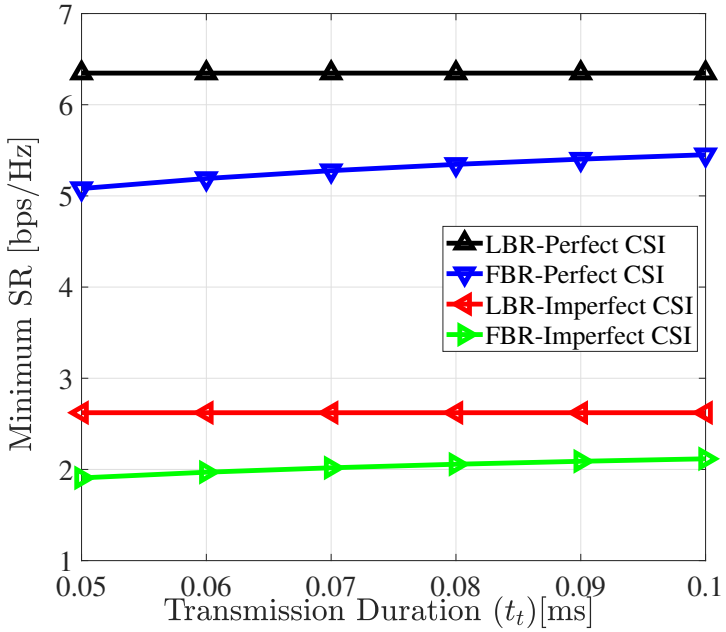

Figure 5.7 : user's min SR Vs. Transmission Duration t_t with $M = 10$, $\mathcal{K} = 6$ $N = 16$, and $\delta_k = \delta_e = 0.02$.

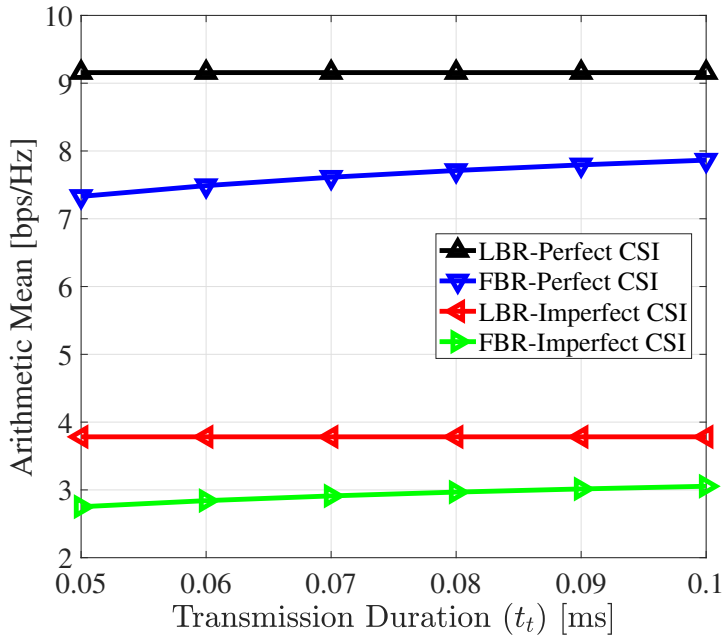

Figure 5.8 : SR Arithmetic mean Vs. Transmission Duration t_t with $M = 10$, $\mathcal{K} = 6$ $N = 16$, and $\delta_k = \delta_e = 0.02$.

5.5 CONCLUSION

In this paper, we proposed a framework to achieve system secure communications under the FBR constraints for IoT settings in URLLC/mMTC applications aided by IRS. Specifically, through linearization and different nonconvex optimisation techniques, we designed a computationally efficient algorithm to maximise the SSR under both perfect and imperfect CSI from the IRS to the users and the eavesdropper. Extensive simulation results showed that maximising the SSR algorithm can provide secure communications under FBR constraints even with only imperfect CSI. Note that if Eve is too close to one user, it is infeasible to guarantee secrecy for all the users, and other solutions like cryptography-based or friendly jamming-based methods should be in place.

Chapter 6

Conclusions and Future Work

This thesis focuses on designing solutions to deal with the challenges of enhancing users' data rate and physical layer security (PLS) in 6G networks, focusing on the challenges raised by intelligent reflective surfaces (IRS). We presented various methods to enhance users' data and secrecy in 6G-IRS-aided systems, where the problems were tackled in long blocklength (LBR), and finite blocklength regime (FBR), under various conditions such as low-resolution IRS, perfect/Imperfect/Unknown IRS-to-users/eavesdropper CSI. These methods vary from ensuring secrecy among all users under the strict conditions of the FBR system, or when the CSI from the IRS to users/Eve is imperfect or unknown. These conditions are challenging and provide more realistic scenarios, which we presented in this thesis. In this chapter, we will summarise the innovations of this thesis in Section 6.1 and provide some potential future research directions in Section 6.2.

6.1 Conclusions

This thesis first addressed the problem of maximising users' data rates in a multi-user IRS-aided downlink system by optimising the geometric mean of the users' rates. The proposed algorithm is mathematically tractable and low-complexity, enabling efficient operation even with a large number of IRS programmable reflective elements (PREs). Simulation results demonstrated significant rate improvements as the number of IRS PREs increased.

Next, we investigated physical layer security (PLS) in IRS-aided systems. We

considered secrecy rate (SR) maximisation in low-resolution IRS systems under perfect, imperfect, and unknown IRS-to-users CSI. The problem was approached by maximising the minimum SR through joint optimisation of transmitter beamforming vectors and IRS PREs, with comparisons to sum secrecy rate (SSR) maximisation. The challenges are more pronounced under imperfect or unknown CSI and with low-resolution IRSs. Simulation results confirmed that the proposed algorithms maintain user and system secrecy even with low-resolution IRSs.

Finally, the framework was extended to the finite blocklength regime (FBR), enabling ultra-reliable and low-latency communication (URLLC). Unlike traditional long blocklength systems, FBR imposes strict constraints on transmission duration and latency. Both minimum SR and SSR maximisation were studied through joint optimisation of the transmitter and IRS PREs. Numerical results show that minimum SR maximisation ensures secure communication for all users, whereas SSR maximisation yields higher SR for some users at the expense of fairness. Both approaches provide valuable trade-offs and can be applied depending on system-specific SR requirements.

6.2 Future Research Directions

Despite the advancements presented in this thesis, several challenges in PLS for IRS-aided systems remain open. This section outlines potential directions for future research.

6.2.1 Secrecy Rate in Multi-IRS Environments

Future work will investigate SR enhancement in multi-IRS-assisted wireless systems. Deploying multiple IRSs across buildings offers opportunities to improve user performance, but requires strategic optimisation of their phase shifts [91]. While prior studies have explored multi-IRS deployment for data rate improvement [91]

and some have considered SR enhancement through joint beamforming and IRS phase shift optimisation [113], the integration of multiple IRSs specifically for PLS remains underexplored. We aim to extend our proposed algorithms to evaluate the impact of multiple IRS deployments on users' SR, accounting for practical considerations such as multiple eavesdroppers, imperfect CSI, and low-resolution IRS elements. This study will provide deeper insights into the feasibility and limitations of secure communication in next-generation networks supported by distributed intelligent surfaces.

6.2.2 Real World IRS Scenarios: Using Ray Tracing Model (Sionna) to Improve Secrecy Rate

A further direction is to leverage ray-tracing-based modelling to capture realistic wireless environments and evaluate the proposed algorithms for enhancing SR. The Sionna RT framework [114] enables high-fidelity simulation of IRS deployments in complex scenarios. Previous work [115] has used Sionna to improve IRS performance by optimising reflection amplitudes beyond conventional phase gradient approaches. Integrating our secrecy enhancement algorithms within such a realistic framework will demonstrate their practical feasibility and effectiveness, bridging the gap between theoretical models and real-world IRS-aided secure communication systems for 6G networks.

6.2.3 IRS-Aided Physical Layer Key Generation

Physical Layer Key Generation (PLKG) exploits the inherent randomness and reciprocity of wireless channels to establish secure cryptographic keys [116]. IRS can introduce controlled variations in the propagation environment, providing additional entropy for key generation between users [117]. Future research should investigate the deployment of multiple IRSs to exploit secondary reflections, enhancing channel randomness, spatial diversity, and key generation rates, particularly in environments

with severe blockage or limited line-of-sight. The emergence of STAR-IRS offers further opportunities by supporting both reflection and transmission functionalities, enabling more flexible control over the medium. While recent studies highlight STAR-IRS potential for robust key generation, this area remains underexplored. Future work should address phase configuration, system synchronisation, security guarantees, and efficient adaptive algorithms suitable for dynamic next-generation wireless networks.

6.2.4 Intelligent Jamming and Friendly Interference in IRS-aided Systems

Cooperative jamming using multiple IRSs or mobile relays is a promising strategy to enhance PLS. By exploiting the spatial diversity and adaptability of distributed IRSs, artificial noise can be directed toward eavesdroppers, while coordination among IRSs allows constructive and destructive interference to be tailored across space, improving SR performance in complex propagation environments [118]. These schemes require joint optimisation of beamforming, IRS phase configurations, and relay trajectories, introducing new challenges in algorithm design and system modelling. The integration of cooperative jamming in IRS-aided systems remains underexplored, particularly for PLS.

Appendix A

Inequalities

For any $\mathbf{A}$ and $\boldsymbol{F}$ with $\hat{\Lambda}$ and $\hat{F}$ are fixed point, the following inequality holds [95],

$$\ln\left|I_n + [\boldsymbol{\Lambda}]^2(\boldsymbol{F})^{-1}\right| \geq \ln\left|I_n + [\hat{\Lambda}]^2(\hat{F})^{-1}\right| - \langle[\hat{\Lambda}]^2(\hat{F})^{-1}\rangle + 2\Re\{\langle\hat{\Lambda}^H(\hat{F})^{-1}\mathbf{A}\rangle\} - \langle(\hat{F})^{-1} - (\hat{F} + [\hat{\Lambda}]^2)^{-1}, [\mathbf{A}]^2 + \boldsymbol{F}\rangle. \tag{A.1}$$

Next, for any z_i with $i = 1, \ldots, l$ and $\bar{z}_i$ is a fixed point, the following inequality holds [92]:

$$\ln(1 + \sum_{i=1}^{l}|z_i|^2) \geq \ln(1 + \sum_{i=1}^{l}|\bar{z}_i|^2) - \sum_{i=1}^{l}|\bar{z}_i|^2 + \sum_{i=1}^{l}2\Re\{\bar{z}_i^* z_i\} - \frac{\sum_{i=1}^{l}|\bar{z}_i|^2\left(1 + \sum_{i=1}^{l}|z_i|^2\right)}{1 + \sum_{i=1}^{l}|\bar{z}_i|^2}. \tag{A.2}$$

The logarithmic function is a concave function and can be written as [92, Eq. 15]:

$$-\ln(1 + \boldsymbol{\Upsilon}) \geq -\ln(1 + \bar{\Upsilon}) - \frac{1 + \boldsymbol{\Upsilon}}{1 + \bar{\Upsilon}} + 1. \tag{A.3}$$

The following inequality follows from the concavity of the function $\sqrt{x}$ [71]:

$$\sqrt{x} \leq \sqrt{\bar{x}}/2\left(1 + x/\bar{x}\right), \ \forall x > 0, \bar{x} > 0. \tag{A.4}$$

Lastly, for a any vector $\mathbf{A} \in \mathbb{C}^n$, $\bar{\mathbf{A}} \in \mathbb{C}^n$, scalar $B > 0$, $\bar{B} > 0$, $\sigma > 0$, The following inequality (A.5) holds [71]:

$$\frac{||\mathbf{A}||^2}{B + \sigma} \geq \frac{||\bar{\mathbf{A}}||^2}{\bar{B} + \sigma}\left(2\frac{\Re\{\bar{\mathbf{A}}^H\mathbf{A}\}}{||\bar{\mathbf{A}}||^2} - \frac{B + \sigma}{\bar{B} + \sigma}\right). \tag{A.5}$$

Appendix B

Proofs in Chapters 3

B.1 Proof of Theorem 1

First we prove that the sequence $\mathrm{SR}_k(\boldsymbol{w}^{(\iota+1)}, \lfloor\boldsymbol{\theta}_n^{(\iota+1)}\rceil_b + \epsilon_R)$ is non decreasing for all k, i.e. $\mathrm{SR}_k(\boldsymbol{w}^{(\iota+1)}, \lfloor\boldsymbol{\theta}_n^{(\iota+1)}\rceil_b) \geq \mathrm{SR}_k(\boldsymbol{w}^{(\iota)}, \boldsymbol{\theta}^{(\iota)})$ for all $\iota > 0$. To that end, with the aid of the CVX solver, we obtain $\boldsymbol{w}^{(\iota+1)}$ by solving problem ($\mathcal{P}1.2$). CVX solver is guaranteed to find the optimal solution. Thus, we have $\mathrm{SR}_k(\boldsymbol{w}^{(\iota+1)}, \lfloor\boldsymbol{\theta}\rceil_b + \epsilon_R) > \mathrm{SR}_k(\boldsymbol{w}^{(\iota)}, \boldsymbol{\theta})$ for all k. Next, from ($\mathcal{P}1.3$), we obtain $\lfloor\boldsymbol{\theta}_n^{(\iota+1)}\rceil_b + \epsilon_R$, where we have $\mathrm{SR}_k(\mathbf{w}, \lfloor\boldsymbol{\theta}_n^{(\iota+1)}\rceil_b + \epsilon_R) > \mathrm{SR}_k(\mathbf{w}, \lfloor\boldsymbol{\theta}^{(\iota)}\rceil_b + \epsilon_R)$ as stated before.

Hence, by combining the solutions, we obtain

$$\mathrm{SR}_k(\boldsymbol{w}^{(\iota+1)}, \lfloor\boldsymbol{\theta}_n^{(\iota+1)}\rceil_b + \epsilon_R) > \mathrm{SR}_k(\boldsymbol{w}^{(\iota)}, \lfloor\boldsymbol{\theta}^{(\iota)}\rceil_b + \epsilon_R), \tag{B.1}$$

hence, the optimal sequence $\{(\boldsymbol{w}^{(\iota+1)}, \lfloor\boldsymbol{\theta}_n^{(\iota+1)}\rceil_b + \epsilon_R)\}$ converge to a point $\{(\mathbf{w}^*, \lfloor\boldsymbol{\theta}^*\rceil_b + \epsilon_R)\}$ which is the solution obtained from solving ($\mathcal{P}2$) and ($\mathcal{P}1.1$).

Next, we prove that the converged point $\hat{X}^* \triangleq \{\mathbf{w}^*, \boldsymbol{\theta}^*\}$ is a locally optimal solution of problem $\mathcal{P}1$. For that, we show that the converged point satisfies the Karush-Kuhn-Tucker (KKT) condition of the problem. The KKT condition for problem ($\mathcal{P}1.1$) is satisfied at $\boldsymbol{\theta}^*$. Let $\boldsymbol{Y}(\boldsymbol{\theta})$ is the objective function of ($\mathcal{P}3$) and $\boldsymbol{T}(\boldsymbol{X}) \triangleq [\boldsymbol{T}_1(\boldsymbol{X}), \boldsymbol{T}_2(\boldsymbol{X}), \ldots, \boldsymbol{T}_I(\boldsymbol{X})]$ be the set of constraints of problem $\mathcal{P}3$. Then, we can write

$$\begin{aligned} &\nabla_{\boldsymbol{\theta}^*}\boldsymbol{Y}(\boldsymbol{X}^*) + \boldsymbol{Z}^T\nabla_{\boldsymbol{\theta}^*}\boldsymbol{T}(\boldsymbol{X}^*) = 0 \\ &z_i \geq 0, z_i\boldsymbol{T}(\boldsymbol{X}^*) = 0, \forall i. \end{aligned} \tag{B.2}$$

where ∇_s is the gradient with respect to s, and $\boldsymbol{Z} \triangleq [z_1, z_2, \ldots, z_I]$ is the optimal Lagrangian variable set. Similarly, the obtained ($\mathcal{P}2$) solution is locally optimal. Hence its KKT is satisfied with respect to $\mathbf{W} = \mathbf{w}_k^*$, which is

$$\begin{aligned} &\nabla_{\mathbf{W}^*} \boldsymbol{Y}(\boldsymbol{X}^*) + Z^T \nabla_{\mathbf{W}^*} \boldsymbol{T}(\boldsymbol{X}^*) = 0 \\ &z_i \geq 0, t_i \boldsymbol{T}(\boldsymbol{X}^*) = 0, \forall i. \end{aligned} \tag{B.3}$$

Combining (B.2) and (B.3), we get

$$\begin{aligned} &\nabla_{\boldsymbol{X}^*} \boldsymbol{Y}(\boldsymbol{X}^*) + Z^T \nabla_{\boldsymbol{X}^*} \boldsymbol{T}(\boldsymbol{X}^*) = 0 \\ &t_i \geq 0, t_i \boldsymbol{T}(\boldsymbol{X}^*) = 0, \forall i, \end{aligned} \tag{B.4}$$

which is the KKT condition for ($\mathcal{P}1$). ■

B.2 Proof of Lemma 1

Let a be a scalar complex variable, and $a^{(\iota)}$ is the fixed point obtained at iteration (ι), then the following inequality holds [77]

$$|a|^2 \geq a^{*,(\iota)} a + a^* a^{(\iota)} - a^{*,(\iota)} a^{(\iota)}, \tag{B.5}$$

By replacing a with $(\boldsymbol{u}_k \boldsymbol{\Phi} \boldsymbol{G}_{\text{AR}}) \mathbf{w}_k$ we obtain (3.36), (4.36), and (5.38). Thus, this concludes the proof. ■

B.3 Proof of Theorem 2, and 3

Similar to the proof of Theorem 3.1, it can be shown the sequence $\text{SR}_k(\boldsymbol{w}^{(\iota+1)}, \lfloor \boldsymbol{\theta}_n^{(\iota+1)} \rceil_b)$ is non-decreasing for all k, i.e. $\text{SR}_k(\boldsymbol{w}^{(\iota+1)}, \lfloor \boldsymbol{\theta}_n^{(\iota+1)} \rceil_b) \geq \text{SR}_k(\boldsymbol{w}^{(\iota)}, \lfloor \boldsymbol{\theta}^{(\iota)} \rceil_b)$ for all $(\iota) > 0$, and the converged point is a locally optimal solution for problems. ■.

Appendix C

Proofs in Chapter 4

C.1 Proof of Theorem 1

First we prove that the sequence $\mathcal{S}_k^{\mathcal{F}}(\boldsymbol{w}^{(n+1)}, \boldsymbol{\theta}^{(n+1)})$ is non decreasing for all k, i.e. $\mathcal{S}_k^{\mathcal{F}}(\boldsymbol{w}^{(n+1)}, \boldsymbol{\theta}^{(n+1)}) \geq \mathcal{S}_k^{\mathcal{F}}(\boldsymbol{w}^{(n)}, \boldsymbol{\theta}^{(n)})$ for all $n > 0$. To that end, with the aid of the CVX solver, we obtain $\boldsymbol{w}^{(n+1)}$ by solving problem ($\mathcal{P}$1.3). CVX solver is guaranteed to find the optimal solution. Thus, we have $\mathcal{S}_k^{\mathcal{F}}(\boldsymbol{w}^{(n+1)}, \boldsymbol{\theta}) > \mathcal{S}_k^{\mathcal{F}}(\boldsymbol{w}^{(n)}, \boldsymbol{\theta})$ for all k. Next, from ($\mathcal{P}$2), we obtain $\boldsymbol{\theta}^{(n+1)}$ by solving (4.29), where we have $\mathcal{S}_k^{\mathcal{F}}(\mathbf{w}, \boldsymbol{\theta}^{(n+1)}) > \mathcal{S}_k^{\mathcal{F}}(\mathbf{w}, \boldsymbol{\theta}^{(n)})$ as stated before.

Hence, by combining the solutions obtained by solving problem ($\mathcal{P}$1.3) and problem ($\mathcal{P}$1.4), we obtain:

$$\mathcal{S}_k^{\mathcal{F}}(\boldsymbol{w}^{(n+1)}, \boldsymbol{\theta}^{(n+1)}) > \mathcal{S}_k^{\mathcal{F}}(\boldsymbol{w}^{(n)}, \boldsymbol{\theta}^{(n)}), \tag{C.1}$$

the optimal sequence $\{(\boldsymbol{w}^{(n+1)}, \boldsymbol{\theta}^{(n+1)})\}$ thus converge to a point $\{(\mathbf{w}^*, \boldsymbol{\theta}^*)\}$ which is the solution obtained from solving ($\mathcal{P}$1.3) and ($\mathcal{P}$1.4).

Next, we prove that the converged point $\hat{X}^* \triangleq \{\mathbf{w}^*, \boldsymbol{\theta}^*\}$ is a locally optimal solution of problem ($\mathcal{P}$1). For that, we show that the converged point satisfies the Karush-Kuhn-Tucker (KKT) condition of the problem. The KKT condition for problem ($\mathcal{P}$1.3) is satisfied at $\boldsymbol{\theta}^*$. Let $\boldsymbol{Y}(\boldsymbol{\theta})$ be the objective function of ($\mathcal{P}$2) and $\boldsymbol{T}(\boldsymbol{X}) = [\boldsymbol{T}_1(\boldsymbol{X}), \boldsymbol{T}_2(\boldsymbol{X}), \ldots, \boldsymbol{T}_I(\boldsymbol{X})]$ be the set of constraint of problem ($\mathcal{P}$2). Then, we can write:

$$\nabla_{\boldsymbol{\theta}^*} \boldsymbol{Y}(\boldsymbol{X}^*) + \boldsymbol{Z}^T \nabla_{\boldsymbol{\theta}^*} \boldsymbol{T}(\boldsymbol{X}^*) = 0, \tag{C.2}$$

$$z_i \geq 0, z_i \boldsymbol{T}(\boldsymbol{X}^*) = 0, \forall i.$$

where ∇_s is the gradient with respect to s, and $\boldsymbol{Z} = [z_1, z_2, \ldots, z_I]$ is the optimal Lagrangian variable set. Similarly, the obtained $(\mathcal{P}2)$ solution is locally optimal. Hence, its KKT is satisfied with respect to $\mathbf{W} = \mathbf{w}_k^*$, which is:

$$\begin{aligned} &\nabla_{\mathbf{W}^*} \boldsymbol{Y}(\boldsymbol{X}^*) + Z^T \nabla_{\mathbf{W}^*} \boldsymbol{T}(\boldsymbol{X}^*) = 0, \\ &z_i \geq 0, z_i \boldsymbol{T}(\boldsymbol{X}^*) = 0, \forall i. \end{aligned} \tag{C.3}$$

Combining (C.2) and (C.3), we get:

$$\begin{aligned} &\nabla_{\boldsymbol{X}^*} \boldsymbol{Y}(\boldsymbol{X}^*) + Z^T \nabla_{\boldsymbol{X}^*} \boldsymbol{T}(\boldsymbol{X}^*) = 0, \\ &z_i \geq 0, z_i \boldsymbol{T}(\boldsymbol{X}^*) = 0, \forall i, \end{aligned} \tag{C.4}$$

which is the KKT condition for $(\mathcal{P}1)$ in (4.15a), i.e., $\hat{\boldsymbol{X}}^*$ is the local optimal point for (4.15a). ■

C.2 Proof of Lemma 1

Let q be a scalar complex variable, and $q^{(n)}$ is the fixed point obtained at iteration (n), then the following inequality holds [77]:

$$|q|^2 \geq q^{*,(n)} q + q^* q^{(n)} - q^{*,(n)} q^{(n)}. \tag{C.5}$$

By replacing q with $(\boldsymbol{l}_k \boldsymbol{\Phi} \boldsymbol{L}_{\mathrm{AR}}) \mathbf{w}_k$ we obtain (4.35). Thus, this concludes the proof. ■

C.3 Proof of Theorem 2

Similar to the proof of Theorem 4.1, it can be shown the sequence $\mathcal{S}_k^{\mathcal{F}}(\boldsymbol{w}^{(n+1)}, \boldsymbol{\theta}^{(n+1)})$ is non-decreasing for all k, i.e. $\mathcal{S}_k^{\mathcal{F}}(\boldsymbol{w}^{(n+1)}, \boldsymbol{\theta}^{(n+1)}) \geq \mathcal{S}_k^{\mathcal{F}}(\boldsymbol{w}^{(n)}, \boldsymbol{\theta}^{(n)})$ for all $n > 0$, and the converged point is a locally optimal solution for problems. ■.

Appendix D

Proofs in Chapter 5

D.1 Convergence and Optimality Analysis

We begin by showing that the sequence $R_s(\boldsymbol{w}^{(\iota+1)}, \boldsymbol{\theta}^{(\iota+1)})$ is non-decreasing, i.e.,

$$R_s(\boldsymbol{w}^{(\iota+1)}, \boldsymbol{\theta}^{(\iota+1)}) \geq R_s(\boldsymbol{w}^{(\iota)}, \boldsymbol{\theta}^{(\iota)}),\ \forall \iota > 0. \tag{D.1}$$

To establish this, we first compute $\boldsymbol{w}^{(\iota+1)}$ by solving problem ($\mathcal{P}1.3$) using the CVX solver. Since CVX yields the optimal solution, it follows that:

$$R_s(\boldsymbol{w}^{(\iota+1)}, \boldsymbol{\theta}^{(\iota)}) \geq R_s(\boldsymbol{w}^{(\iota)}, \boldsymbol{\theta}^{(\iota)}). \tag{D.2}$$

Then, by solving problem ($\mathcal{P}1.4$) using equation (5.31), we obtain $\boldsymbol{\theta}^{(\iota+1)}$, which guarantees:

$$R_s(\boldsymbol{w}^{(\iota+1)}, \boldsymbol{\theta}^{(\iota+1)}) \geq R_s(\boldsymbol{w}^{(\iota+1)}, \boldsymbol{\theta}^{(\iota)}). \tag{D.3}$$

Combining the two inequalities, we conclude that:

$$R_s(\boldsymbol{w}^{(\iota+1)}, \boldsymbol{\theta}^{(\iota+1)}) \geq R_s(\boldsymbol{w}^{(\iota)}, \boldsymbol{\theta}^{(\iota)}), \tag{D.4}$$

demonstrating that the sequence $\{(\boldsymbol{w}^{(\iota+1)}, \boldsymbol{\theta}^{(\iota+1)})\}$ is non-decreasing and converges to a point $(\mathbf{w}^*, \boldsymbol{\theta}^*)$, which corresponds to the solution obtained by jointly solving ($\mathcal{P}1.3$) and ($\mathcal{P}1.4$).

Next, we show that the converged point $\hat{X}^* \triangleq \{\mathbf{w}^*, \boldsymbol{\theta}^*\}$ is a locally optimal solution to problem ($\mathcal{P}1$). To verify this, we demonstrate that $\hat{X}^*$ satisfies the KKT conditions for the problem.

Let $\boldsymbol{Y}(\boldsymbol{X})$ denote the objective function of $(\mathcal{P}1)$, and let the constraints be represented by $\boldsymbol{T}(\boldsymbol{X}) = [\boldsymbol{T}_1(\boldsymbol{X}), \ldots, \boldsymbol{T}_I(\boldsymbol{X})]$. The KKT condition with respect to $\boldsymbol{\theta}^*$ is then given by:

$$\begin{aligned} \nabla_{\boldsymbol{\theta}^*} \boldsymbol{Y}(\boldsymbol{X}^*) + \boldsymbol{Z}^T \nabla_{\boldsymbol{\theta}^*} \boldsymbol{T}(\boldsymbol{X}^*) = 0, \\ z_i \geq 0,\ z_i \boldsymbol{T}_i(\boldsymbol{X}^*) = 0,\ \forall i. \end{aligned} \tag{D.5}$$

where $\boldsymbol{Z} = [z_1, z_2, \ldots, z_I]$ is the vector of Lagrange multipliers and ∇_s denotes the gradient with respect to s.

Similarly, for the solution $\mathbf{w}^* = \boldsymbol{w}^{(\iota+1)}$, the KKT condition from problem $(\mathcal{P}1.4)$ is:

$$\begin{aligned} \nabla_{\boldsymbol{W}^*} \boldsymbol{Y}(\boldsymbol{X}^*) + \boldsymbol{Z}^T \nabla_{\boldsymbol{W}^*} \boldsymbol{T}(\boldsymbol{X}^*) = 0, \\ z_i \geq 0,\ z_i \boldsymbol{T}_i(\boldsymbol{X}^*) = 0,\ \forall i. \end{aligned} \tag{D.6}$$

By combining (D.5) and (D.6), we obtain the unified KKT conditions for the overall problem $(\mathcal{P}1)$:

$$\begin{aligned} \nabla_{\boldsymbol{X}^*} \boldsymbol{Y}(\boldsymbol{X}^*) + \boldsymbol{Z}^T \nabla_{\boldsymbol{X}^*} \boldsymbol{T}(\boldsymbol{X}^*) = 0, \\ z_i \geq 0,\ z_i \boldsymbol{T}_i(\boldsymbol{X}^*) = 0,\ \forall i. \end{aligned} \tag{D.7}$$

Thus, the point $\hat{\boldsymbol{X}}^* = (\boldsymbol{w}^{(\iota+1)}, \boldsymbol{\theta}^{(\iota+1)})$ satisfies the KKT conditions and is therefore a locally optimal solution to problem (5.17a). ■

D.2 Proof of Lemma 1

Let $s \in \mathbb{C}$ be a scalar complex variable, and denote by $s^{(\iota)}$ its value at iteration ι. According to [77], the following inequality holds:

$$|s|^2 \geq a^{*,(\iota)} s + s^* s^{(\iota)} - s^{*,(\iota)} s^{(\iota)}. \tag{D.8}$$

By substituting $s = (\boldsymbol{u}_k\ \boldsymbol{\Phi}\ \boldsymbol{G}_{\text{AR}})\ \mathbf{w}_k$ into the expression above, we recover inequality (5.37), which concludes the proof. ■

D.3 Proof of Theorem 2

By following steps analogous to those in the proof of Theorem 5.1, it can be shown that the sequence $\widehat{R}_s(\boldsymbol{w}^{(\iota+1)}, \boldsymbol{\theta}^{(\iota+1)})$ is non-decreasing, i.e.,

$$\widehat{R}_s(\boldsymbol{w}^{(\iota+1)}, \boldsymbol{\theta}^{(\iota+1)}) \geq \widehat{R}_s(\boldsymbol{w}^{(\iota)}, \boldsymbol{\theta}^{(\iota)}), \ \forall \ \iota > 0, \tag{D.9}$$

and that it converges to a point which constitutes a locally optimal solution to the associated optimization problems. ■

Bibliography

[1] G. Brown, "Ultra-reliable low-latency 5G for industrial automation," Technol. Rep. 2, Qualcomm, 2018.

[2] M. Bennis, M. Debbah, and H. V. Poor, "Ultrareliable and low-latency wireless communication: Tail, risk, and scale," *Proc. IEEE*, vol. 106, no. 10, pp. 1834–1853, 2018.

[3] H. Pennanen, T. Hänninen, O. Tervo, A. Tölli, and M. Latva-Aho, "6G: The intelligent network of everything," *IEEE Access*, vol. 13, pp. 1319–1421, 2025.

[4] M. Giordani, M. Polese, M. Mezzavilla, S. Rangan, and M. Zorzi, "Toward 6G networks: Use cases and technologies," *IEEE Communications Magazine*, vol. 58, no. 3, pp. 55–61, 2020.

[5] V.-L. Nguyen, P.-C. Lin, B.-C. Cheng, R.-H. Hwang, and Y.-D. Lin, "Security and privacy for 6G: A survey on prospective technologies and challenges," *IEEE Communications Surveys & Tutorials*, vol. 23, no. 4, pp. 2384–2428, 2021.

[6] C.-X. Wang, X. You, X. Gao, X. Zhu, Z. Li, C. Zhang, H. Wang, Y. Huang, Y. Chen, H. Haas, J. S. Thompson, E. G. Larsson, M. D. Renzo, W. Tong, P. Zhu, X. Shen, H. V. Poor, and L. Hanzo, "On the road to 6G: Visions, requirements, key technologies, and testbeds," *IEEE Communications Surveys & Tutorials*, vol. 25, no. 2, pp. 905–974, 2023.

[7] G. Durisi, T. Koch, and P. Popovski, "Toward massive, ultrareliable, and low-

latency wireless communication with short packets," *Proceedings of the IEEE*, vol. 104, no. 9, pp. 1711–1726, 2016.

[8] G. Brown and H. Reading, "Ultra-reliable low-latency 5G for industrial automation," *Technol. Rep. Qualcomm*, vol. 2, p. 52065394, 2018.

[9] M. Bennis, M. Debbah, and H. V. Poor, "Ultrareliable and low-latency wireless communication: Tail, risk, and scale," *Proceedings of the IEEE*, vol. 106, no. 10, pp. 1834–1853, 2018.

[10] Y. Wang, W. Chen, and H. V. Poor, "Ultra-reliable and low-latency wireless communications in the high snr regime: A cross-layer tradeoff," *IEEE Transactions on Communications*, vol. 70, no. 1, pp. 149–162, 2021.

[11] P. Schulz, M. Matthe, H. Klessig, M. Simsek, G. Fettweis, J. Ansari, S. A. Ashraf, B. Almeroth, J. Voigt, I. Riedel, *et al.*, "Latency critical IoT applications in 5G: Perspective on the design of radio interface and network architecture," *IEEE Communications Magazine*, vol. 55, no. 2, pp. 70–78, 2017.

[12] T. Jacobsen, R. Abreu, G. Berardinelli, K. Pedersen, P. Mogensen, I. Z. Kovács, and T. K. Madsen, "System level analysis of uplink grant-free transmission for urllc," in *2017 IEEE Globecom Workshops (GC Wkshps)*, pp. 1–6, IEEE, 2017.

[13] B. Soret, P. Mogensen, K. I. Pedersen, and M. C. Aguayo-Torres, "Fundamental tradeoffs among reliability, latency and throughput in cellular networks," in *2014 IEEE Globecom Workshops (GC Wkshps)*, pp. 1391–1396, IEEE, 2014.

[14] J. Sachs, G. Wikstrom, T. Dudda, R. Baldemair, and K. Kittichokechai, "5G radio network design for ultra-reliable low-latency communication," *IEEE network*, vol. 32, no. 2, pp. 24–31, 2018.

[15] C. She, C. Yang, and T. Q. Quek, "Radio resource management for ultra-reliable and low-latency communications," *IEEE Communications Magazine*, vol. 55, no. 6, pp. 72–78, 2017.

[16] W. Yang, G. Durisi, T. Koch, and Y. Polyanskiy, "Quasi-static multiple-antenna fading channels at finite blocklength," *IEEE Transactions on Information Theory*, vol. 60, no. 7, pp. 4232–4265, 2014.

[17] C. She, C. Yang, and T. Q. Quek, "Cross-layer optimization for ultra-reliable and low-latency radio access networks," *IEEE Transactions on Wireless Communications*, vol. 17, no. 1, pp. 127–141, 2017.

[18] G. Berardinelli, N. H. Mahmood, R. Abreu, T. Jacobsen, K. Pedersen, I. Z. Kovács, and P. Mogensen, "Reliability analysis of uplink grant-free transmission over shared resources," *Ieee Access*, vol. 6, pp. 23602–23611, 2018.

[19] C. She, C. Yang, and T. Q. Quek, "Joint uplink and downlink resource configuration for ultra-reliable and low-latency communications," *IEEE Transactions on Communications*, vol. 66, no. 5, pp. 2266–2280, 2018.

[20] C. Sun, C. She, C. Yang, T. Q. Quek, Y. Li, and B. Vucetic, "Optimizing resource allocation in the short blocklength regime for ultra-reliable and low-latency communications," *IEEE Transactions on Wireless Communications*, vol. 18, no. 1, pp. 402–415, 2018.

[21] J. Jalali, A. Khalili, A. Rezaei, R. Berkvens, M. Weyn, and J. Famaey, "IRS-based energy efficiency and admission control maximization for IoT users with short packet lengths," *IEEE Transactions on Vehicular Technology*, vol. 72, no. 9, pp. 12379–12384, 2023.

[22] L. Zhang, X. Q. Chen, S. Liu, Q. Zhang, J. Zhao, J. Y. Dai, G. D. Bai,

X. Wan, Q. Cheng, G. Castaldi, *et al.*, "Space-time-coding digital metasurfaces," *Nature communications*, vol. 9, no. 1, pp. 1–11, 2018.

[23] M. Di Renzo, A. Zappone, M. Debbah, M.-S. Alouini, C. Yuen, J. De Rosny, and S. Tretyakov, "Smart radio environments empowered by reconfigurable intelligent surfaces: How it works, state of research, and the road ahead," *IEEE Journal on Selected Areas in Communications*, vol. 38, no. 11, pp. 2450–2525, 2020.

[24] E. Basar, M. Di Renzo, J. De Rosny, M. Debbah, M.-S. Alouini, and R. Zhang, "Wireless communications through reconfigurable intelligent surfaces," *IEEE access*, vol. 7, pp. 116753–116773, 2019.

[25] C. Huang, A. Zappone, G. C. Alexandropoulos, M. Debbah, and C. Yuen, "Reconfigurable intelligent surfaces for energy efficiency in wireless communication," *IEEE Transactions on Wireless Communications*, vol. 18, no. 8, pp. 4157–4170, 2019.

[26] S. Tretyakov, V. Asadchy, and A. Díaz-rubio, "Metasurfaces for general control of reflection and transmission," in *World Scientific Handbook of Metamaterials and Plasmonics: Volume 1: Electromagnetic Metamaterials*, pp. 249–293, World Scientific, 2018.

[27] Q. Wu and R. Zhang, "Towards smart and reconfigurable environment: Intelligent reflecting surface aided wireless network," *IEEE Communications Magazine*, vol. 58, no. 1, pp. 106–112, 2019.

[28] M. Di Renzo, M. Debbah, D.-T. Phan-Huy, A. Zappone, M.-S. Alouini, C. Yuen, V. Sciancalepore, G. C. Alexandropoulos, J. Hoydis, H. Gacanin, *et al.*, "Smart radio environments empowered by reconfigurable AI metasurfaces: An idea whose time has come," *EURASIP Journal on Wireless*

Communications and Networking, vol. 2019, no. 1, pp. 1–20, 2019.

[29] C. Huang, S. Hu, G. C. Alexandropoulos, A. Zappone, C. Yuen, R. Zhang, M. Di Renzo, and M. Debbah, "Holographic MIMO surfaces for 6G wireless networks: Opportunities, challenges, and trends," *IEEE Wireless Communications*, vol. 27, no. 5, pp. 118–125, 2020.

[30] Q. Wu and R. Zhang, "Intelligent reflecting surface enhanced wireless network: Joint active and passive beamforming design," in *2018 IEEE Global Communications Conference (GLOBECOM)*, pp. 1–6, IEEE, 2018.

[31] E. Björnson and L. Sanguinetti, "Demystifying the power scaling law of intelligent reflecting surfaces and metasurfaces," in *2019 IEEE 8th International Workshop on Computational Advances in Multi-Sensor Adaptive Processing (CAMSAP)*, pp. 549–553, IEEE, 2019.

[32] X. Yu, D. Xu, and R. Schober, "MISO wireless communication systems via intelligent reflecting surfaces," in *2019 IEEE/CIC International Conference on Communications in China (ICCC)*, pp. 735–740, IEEE, 2019.

[33] H.-M. Wang, J. Bai, and L. Dong, "Intelligent reflecting surfaces assisted secure transmission without eavesdropper's CSI," *IEEE Signal Processing Letters*, vol. 27, pp. 1300–1304, 2020.

[34] S. Zhang and R. Zhang, "Capacity characterization for intelligent reflecting surface aided MIMO communication," *IEEE Journal on Selected Areas in Communications*, vol. 38, no. 8, pp. 1823–1838, 2020.

[35] K. Ying, Z. Gao, S. Lyu, Y. Wu, H. Wang, and M.-S. Alouini, "Gmd-based hybrid beamforming for large reconfigurable intelligent surface assisted millimeter-wave massive MIMO," *IEEE Access*, vol. 8, pp. 19530–19539, 2020.

[36] B. Ning, Z. Chen, W. Chen, and J. Fang, "Beamforming optimization for intelligent reflecting surface assisted MIMO: A sum-path-gain maximization approach," *IEEE Wireless Communications Letters*, vol. 9, no. 7, pp. 1105–1109, 2020.

[37] S. Abeywickrama, R. Zhang, Q. Wu, and C. Yuen, "Intelligent reflecting surface: Practical phase shift model and beamforming optimization," *IEEE Transactions on Communications*, vol. 68, no. 9, pp. 5849–5863, 2020.

[38] Y. Han, W. Tang, S. Jin, C.-K. Wen, and X. Ma, "Large intelligent surface-assisted wireless communication exploiting statistical CSI," *IEEE Transactions on Vehicular Technology*, vol. 68, no. 8, pp. 8238–8242, 2019.

[39] J. Xu, W. Xu, and A. L. Swindlehurst, "Discrete phase shift design for practical large intelligent surface communication," in *2019 IEEE Pacific Rim Conference on Communications, Computers and Signal Processing (PACRIM)*, pp. 1–5, IEEE, 2019.

[40] M. Di Renzo, A. Zappone, M. Debbah, M.-S. Alouini, C. Yuen, J. de Rosny, and S. Tretyakov, "Smart radio environments empowered by reconfigurable intelligent surfaces: How it works, state of research, and the road ahead," *IEEE Journal on Selected Areas in Communications*, vol. 38, no. 11, pp. 2450–2525, 2020.

[41] Z. Zhang and L. Dai, "A joint precoding framework for wideband reconfigurable intelligent surface-aided cell-free network," *IEEE Transactions on Signal Processing*, vol. 69, pp. 4085–4101, 2021.

[42] M. Ahmed, S. Raza, A. Amin Soofi, F. Khan, W. Ullah Khan, S. Zain Ul Abideen, F. Xu, and Z. Han, "Active reconfigurable intelligent surfaces:

Expanding the frontiers of wireless communication-a survey," *IEEE Communications Surveys and Tutorials*, vol. 27, no. 2, pp. 839–869, 2025.

[43] X. Yu, D. Xu, and R. Schober, "Enabling secure wireless communications via intelligent reflecting surfaces," in *2019 IEEE Global Communications Conference (GLOBECOM)*, pp. 1–6, IEEE, 2019.

[44] M. Cui, G. Zhang, and R. Zhang, "Secure wireless communication via intelligent reflecting surface," *IEEE Wireless Communications Letters*, vol. 8, no. 5, pp. 1410–1414, 2019.

[45] X. Guan, Q. Wu, and R. Zhang, "Intelligent reflecting surface assisted secrecy communication: Is artificial noise helpful or not?," *IEEE Wireless Communications Letters*, vol. 9, no. 6, pp. 778–782, 2020.

[46] X. Yu, D. Xu, Y. Sun, D. W. K. Ng, and R. Schober, "Robust and Secure Wireless Communications via Intelligent Reflecting Surfaces," *IEEE Journal on Selected Areas in Communications*, vol. 38, no. 11, pp. 2637–2652, 2020.

[47] W. Hao, J. Li, G. Sun, M. Zeng, and O. A. Dobre, "Securing reconfigurable intelligent surface-aided cell-free networks," *IEEE Transactions on Information Forensics and Security*, vol. 17, pp. 3720–3733, 2022.

[48] W. Shi, Q. Wu, F. Xiao, F. Shu, and J. Wang, "Secrecy throughput maximization for IRS-aided MIMO wireless powered communication networks," *IEEE Transactions on Communications*, vol. 70, no. 11, pp. 7520–7535, 2022.

[49] W. Li, W. Yu, H. Liu, and H. Hou, "Robust secrecy rate maximization for IRS-aided MISO communication systems," in *2023 IEEE 13th International Conference on CYBER Technology in Automation, Control, and Intelligent Systems (CYBER)*, pp. 604–609, 2023.

[50] L. Dong, H.-M. Wang, and H. Xiao, "Secure cognitive radio communication via intelligent reflecting surface," *IEEE Transactions on Communications*, vol. 69, no. 7, pp. 4678–4690, 2021.

[51] G. Zhou, C. Pan, H. Ren, K. Wang, and Z. Peng, "Secure wireless communication in RIS-aided MISO system with hardware impairments," *IEEE Wireless Communications Letters*, vol. 10, no. 6, pp. 1309–1313, 2021.

[52] G. Zhou, C. Pan, H. Ren, K. Wang, and A. Nallanathan, "A framework of robust transmission design for IRS-aided MISO communications with imperfect cascaded channels," *IEEE Transactions on Signal Processing*, vol. 68, pp. 5092–5106, 2020.

[53] X. Tan, Z. Sun, J. M. Jornet, and D. Pados, "Increasing indoor spectrum sharing capacity using smart reflect-array," in *2016 IEEE International Conference on Communications (ICC)*, pp. 1–6, 2016.

[54] Q. Wu and R. Zhang, "Beamforming optimization for intelligent reflecting surface with discrete phase shifts," in *ICASSP 2019 - 2019 IEEE International Conference on Acoustics, Speech and Signal Processing ()*, pp. 7830–7833, 2019.

[55] Y. Han, W. Tang, S. Jin, C.-K. Wen, and X. Ma, "Large intelligent surface-assisted wireless communication exploiting statistical CSI," *IEEE Transactions on Vehicular Technology*, vol. 68, no. 8, pp. 8238–8242, 2019.

[56] M.-A. Badiu and J. P. Coon, "Communication through a large reflecting surface with phase errors," *IEEE Wireless Communications Letters*, vol. 9, no. 2, pp. 184–188, 2020.

[57] M. Di Renzo *et al.*, "Smart radio environments empowered by reconfigurable intelligent surfaces: how it works, state of research, and road ahead," *IEEE*

J. Sel. Areas Commun, vol. 38, pp. 2450–2525, Nov. 2020.

[58] C. Huang *et al.*, "Holographic MIMO surfaces for 6G wireless networks: Opportunities, challenges, and trends," *IEEE Wirel. Commun.*, vol. 27, no. 5, pp. 118–125, 2200.

[59] Z. Cui, K. Guan, J. Zhang, and Z. Zhong, "SNR coverage probability analysis of RIS-aided communication systems," *IEEE Trans. Veh. Technol.*, vol. 70, pp. 3914–3919, Apr. 2021.

[60] Y. Han *et al.*, "Large intelligent surface-assisted wireless communication exploiting statistical CSI," *IEEE Trans. Veh. Technol.*, vol. 68, p. 8238–8242, Aug. 2019.

[61] C. Huang, R. Mo, and C. Yuen, "Reconfigurable intelligent surface assisted multiuser MISO systems exploiting deep reinforcement learning," *IEEE J. Select. Areas Commun.*, vol. 38, no. 8, pp. 1839–1850, 2020.

[62] H. Yu, H. D. Tuan, A. A. Nasir, T. Q. Duong, and H. V. Poor, "Joint design of reconfigurable intelligent surfaces and transmit beamforming under proper and improper Gaussian signaling," *IEEE J. Sel. Areas Commun.*, vol. 38, pp. 2589–2603, Nov. 2020.

[63] H. Yu, H. D. Tuan, E. Dutkiewicz, H. V. Poor, and L. Hanzo, "Maximizing the geometric mean of user-rates to improve rate-fairness: Proper vs. improper Gaussian signaling," *IEEE Trans. Wirel. Commun.*, vol. 21, pp. 295–306, Jan. 2022.

[64] Y. Polyanskiy, H. V. Poor, and S. Verdú, "Channel coding rate in the finite blocklength regime," *IEEE Trans. Inf. Theory*, vol. 56, pp. 2307–2359, May 2010.

[65] A. A. Nasir, H. D. Tuan, H. H. Nguyen, M. Debbah, and H. V. Poor, "Resource allocation and beamforming design in the short blocklength regime for URLLC," *IEEE Trans. Wirel. Commun.*, vol. 20, pp. 1321–1335, Feb. 2021.

[66] A. A. Nasir, H. D. Tuan, H. Q. Ngo, T. Q. Duong, and H. V. Poor, "Cell-free massive MIMO in the short blocklength regime for URLLC," *IEEE Trans. Wirel. Commun.*, vol. 20, pp. 5861–5871, Sept. 2021.

[67] R. Hashemi, S. Ali, N. H. Mahmood, and M. Latva-aho, "Average rate and error probability analysis in short packet communications over RIS-aided URLLC systems," *IEEE Trans. Veh. Techn.*, vol. 70, pp. 10320–10334, Oct. 2021.

[68] H. Ren, K. Wang, and C. Pan, "Intelligent reflecting surface-aided URLLC in a factory automation scenario," Tech. Rep. arXiv:2103.09323, arXiv, 2021.

[69] W. R. Ghanem, V. Jamali, and R. Schober, "Joint beamforming and phase shift optimization for multicell IRS-aided OFDMA-URLLC systems," in *Proc. IEEE Wirel. Commun. Network. Conf.*, pp. 1–7, 2021.

[70] E. Bjornson, O. Ozdogan, and E. G. Larsson, "Intelligent reflecting surface vs. decode-and-forward: How large surfaces are needed to beat relaying?," *IEEE Wirel. Commun. Lett.*, vol. 9, pp. 244–248, Feb. 2020.

[71] M. Abughalwa, H. D. Tuan, D. N. Nguyen, H. V. Poor, and L. Hanzo, "Finite-blocklength RIS-aided transmit beamforming," *IEEE Transactions on Vehicular Technology*, vol. 71, no. 11, pp. 12374–12379, 2022.

[72] G. Chen, Q. Wu, C. He, W. Chen, J. Tang, and S. Jin, "Active IRS aided multiple access for energy-constrained IoT systems," *IEEE Transactions on Wireless Communications*, vol. 22, no. 3, pp. 1677–1694, 2023.

[73] S. Hong, C. Pan, H. Ren, K. Wang, K. K. Chai, and A. Nallanathan, "Robust transmission design for intelligent reflecting surface-aided secure communication systems with imperfect cascaded CSI," *IEEE Transactions on Wireless Communications*, vol. 20, no. 4, pp. 2487–2501, 2020.

[74] F. Fang, Y. Xu, Q.-V. Pham, and Z. Ding, "Energy-efficient design of IRS-NOMA networks," *IEEE Transactions on Vehicular Technology*, vol. 69, no. 11, pp. 14088–14092, 2020.

[75] S. Boyd, L. El Ghaoui, E. Feron, and V. Balakrishnan, *Linear matrix inequalities in system and control theory*. SIAM, 1994.

[76] H. Niu, Z. Chu, F. Zhou, and Z. Zhu, "Simultaneous transmission and reflection reconfigurable intelligent surface assisted secrecy MISO networks," *IEEE Communications Letters*, vol. 25, no. 11, pp. 3498–3502, 2021.

[77] G. Zhou, C. Pan, H. Ren, K. Wang, M. D. Renzo, and A. Nallanathan, "Robust beamforming design for intelligent reflecting surface aided MISO communication systems," *IEEE Wireless Communications Letters*, vol. 9, no. 10, pp. 1658–1662, 2020.

[78] W. Zhao, J. Ni, S. Hao, B. Li, and T. Zhang, "Joint physical layer security and information freshness of RIS-assisted SPC system: Analysis and optimization," *IEEE Transactions on Vehicular Technology*, pp. 1–13, 2025.

[79] G. Xie, C. Yang, Y. Feng, G. Liu, and B. Dai, "Secure finite blocklength coding schemes for reconfigurable intelligent surface aided wireless channels with feedback," *IEEE Transactions on Communications*, vol. 71, no. 5, pp. 2931–2946, 2023.

[80] W. Yang, G. Durisi, T. Koch, and Y. Polyanskiy, "Quasi-static multiple-antenna fading channels at finite blocklength," *IEEE Transactions on Inform-*

ation Theory, vol. 60, no. 7, pp. 4232–4265, 2014.

[81] K. Singh, S. K. Singh, and C.-P. Li, "On the performance analysis of RIS-assisted infinite and finite blocklength communication in presence of an eavesdropper," *IEEE Open Journal of the Communications Society*, vol. 4, pp. 854–872, 2023.

[82] G. Durisi, T. Koch, and P. Popovski, "Toward massive, ultrareliable, and low-latency wireless communication with short packets," *Proceedings of the IEEE*, vol. 104, no. 9, pp. 1711–1726, 2016.

[83] Q.-U.-A. Nadeem, A. Kammoun, A. Chaaban, M. Debbah, and M.-S. Alouini, "Asymptotic max-min SINR analysis of reconfigurable intelligent surface assisted MISO systems," *IEEE Trans. Wirel. Commun.*, vol. 19, Dec. 2020.

[84] J. Scarlett, V. Y. F. Tan, and G. Durisi, "The dispersion of nearest-neighbor decoding for additive non-Gaussian channels," *IEEE Trans. Infor. Theory*, vol. 63, pp. 81–92, Jan. 2017.

[85] C. She, C. Yang, and T. Q. Quek, "Cross-layer optimization for ultra-reliable and low-latency radio access networks," *IEEE Trans. Wirel. Commun.*, vol. 17, no. 1, pp. 127–141, 2017.

[86] Q.-U.-A. Nadeem, A. Kammoun, A. Chaaban, M. Debbah, and M.-S. Alouini, "Asymptotic Max-Min SINR analysis of reconfigurable intelligent surface assisted MISO systems," *IEEE Transactions on Wireless Communications*, vol. 19, no. 12, pp. 7748–7764, 2020.

[87] B. Zheng, C. You, and R. Zhang, "Uplink channel estimation for double-IRS assisted multi-user MIMO," in *ICC 2021 - IEEE International Conference on Communications*, pp. 1–6, 2021.

[88] B. Zheng, C. You, and R. Zhang, "Efficient channel estimation for double-irs aided multi-user mimo system," *IEEE Transactions on Communications*, vol. 69, no. 6, pp. 3818–3832, 2021.

[89] C. Pan, H. Ren, M. Elkashlan, A. Nallanathan, and L. Hanzo, "Robust beamforming design for ultra-dense user-centric C-RAN in the face of realistic pilot contamination and limited feedback," *IEEE Transactions on Wireless Communications*, vol. 18, no. 2, pp. 780–795, 2019.

[90] M. Bloch, J. Barros, M. R. D. Rodrigues, and S. W. McLaughlin, "Wireless information-theoretic security," *IEEE Transactions on Information Theory*, vol. 54, no. 6, pp. 2515–2534, 2008.

[91] T. V. Nguyen, D. N. Nguyen, M. D. Renzo, and R. Zhang, "Leveraging secondary reflections and mitigating interference in multi-IRS/RIS aided wireless networks," *IEEE Transactions on Wireless Communications*, vol. 22, no. 1, pp. 502–517, 2023.

[92] H. Niu, Z. Lin, Z. Chu, Z. Zhu, P. Xiao, H. X. Nguyen, I. Lee, and N. Al-Dhahir, "Joint beamforming design for secure RIS-assisted IoT networks," *IEEE Internet of Things Journal*, vol. 10, no. 2, pp. 1628–1641, 2023.

[93] M. Grant and S. Boyd, "CVX: Matlab software for disciplined convex programming, version 2.1," 2014.

[94] Y. Labit, D. Peaucelle, and D. Henrion, "SeDuMi interface 1.02: a tool for solving LMI problems with sedumi," in *Proceedings. IEEE International Symposium on Computer Aided Control System Design*, pp. 272–277, 2002.

[95] H. H. M. Tam, H. D. Tuan, and D. T. Ngo, "Successive convex quadratic programming for quality-of-service management in full-duplex MU-MIMO

multicell networks," *IEEE Transactions on Communications*, vol. 64, no. 6, pp. 2340–2353, 2016.

[96] S. Boyd and L. Vandenberghe, *Convex optimization*. Cambridge university press, 2004.

[97] Y. Eldar, A. Ben-Tal, and A. Nemirovski, "Robust mean-squared error estimation in the presence of model uncertainties," *IEEE Transactions on Signal Processing*, vol. 53, no. 1, pp. 168–181, 2005.

[98] W. Wang, W. Ni, H. Tian, Z. Yang, C. Huang, and K.-K. Wong, "Safeguarding NOMA networks via reconfigurable dual-functional surface under imperfect CSI," *IEEE Journal of Selected Topics in Signal Processing*, vol. 16, no. 5, pp. 950–966, 2022.

[99] Y. Chen, Y. Wang, and L. Jiao, "Robust transmission for reconfigurable intelligent surface aided millimeter wave vehicular communications with statistical CSI," *IEEE Transactions on Wireless Communications*, vol. 21, no. 2, pp. 928–944, 2022.

[100] H.-M. Wang, J. Bai, and L. Dong, "Intelligent reflecting surfaces assisted secure transmission without eavesdropper's csi," *IEEE Signal Processing Letters*, vol. 27, pp. 1300–1304, 2020.

[101] H. Niu, X. Lei, Y. Xiao, M. Xiao, and S. Mumtaz, "On the efficient design of RIS-assisted secure MISO transmission," *IEEE Wireless Communications Letters*, vol. 11, no. 8, pp. 1664–1668, 2022.

[102] A. D. Wyner, "The wire-tap channel," *The Bell System Technical Journal*, vol. 54, no. 8, pp. 1355–1387, 1975.

[103] R. K. Jain, D.-M. W. Chiu, W. R. Hawe, *et al.*, "A quantitative measure of

fairness and discrimination," *Eastern Research Laboratory, Digital Equipment Corporation, Hudson, MA*, vol. 21, 1984.

[104] D. N. Nguyen and M. Krunz, "A cooperative MIMO framework for wireless sensor networks," *ACM Trans. Sen. Netw.*, vol. 10, May 2014.

[105] A. Al-Rimawi and A. Al-Dweik, "On the performance of RIS-assisted communications with direct link over κ-μ shadowed fading," *IEEE Open Journal of the Communications Society*, vol. 3, pp. 2314–2328, 2022.

[106] Z. Zhang, L. Lv, Q. Wu, H. Deng, and J. Chen, "Robust and secure communications in intelligent reflecting surface assisted NOMA networks," *IEEE Communications Letters*, vol. 25, no. 3, pp. 739–743, 2021.

[107] H. Niu, Z. Chu, F. Zhou, Z. Zhu, M. Zhang, and K.-K. Wong, "Weighted sum secrecy rate maximization using intelligent reflecting surface," *IEEE Transactions on Communications*, vol. 69, no. 9, pp. 6170–6184, 2021.

[108] Z. Chu, W. Hao, P. Xiao, D. Mi, Z. Liu, M. Khalily, J. R. Kelly, and A. P. Feresidis, "Secrecy rate optimization for intelligent reflecting surface assisted MIMO system," *IEEE Transactions on Information Forensics and Security*, vol. 16, pp. 1655–1669, 2021.

[109] X. Guan, Q. Wu, and R. Zhang, "Anchor-assisted channel estimation for intelligent reflecting surface aided multiuser communication," *IEEE Transactions on Wireless Communications*, vol. 21, no. 6, pp. 3764–3778, 2022.

[110] W. Yang, R. F. Schaefer, and H. V. Poor, "Wiretap channels: Nonasymptotic fundamental limits," *IEEE Transactions on Information Theory*, vol. 65, no. 7, pp. 4069–4093, 2019.

[111] C. Feng, H.-M. Wang, and H. V. Poor, "Reliable and secure short-packet

communications," *IEEE Transactions on Wireless Communications*, vol. 21, no. 3, pp. 1913–1926, 2021.

[112] T. Lipp and S. Boyd, "Variations and extension of the convex–concave procedure," *Optimization and Engineering*, vol. 17, pp. 263–287, 2016.

[113] J. Li, L. Zhang, K. Xue, Y. Fang, and Q. Sun, "Secure transmission by leveraging multiple intelligent reflecting surfaces in MISO systems," *IEEE Transactions on Mobile Computing*, vol. 22, no. 4, pp. 2387–2401, 2023.

[114] J. Hoydis, F. Aït Aoudia, S. Cammerer, M. Nimier-David, N. Binder, G. Marcus, and A. Keller, "Sionna rt: Differentiable ray tracing for radio propagation modeling," in *2023 IEEE Globecom Workshops (GC Wkshps)*, pp. 317–321, IEEE, 2023.

[115] J. Shabanpour, C. Simovski, and G. Geraci, "Physically consistent ris: From reradiation mode optimization to practical realization," *arXiv preprint arXiv:2409.17738*, 2024.

[116] J. Zhang, G. Li, A. Marshall, A. Hu, and L. Hanzo, "A new frontier for IoT security emerging from three decades of key generation relying on wireless channels," *IEEE Access*, vol. 8, pp. 138406–138446, 2020.

[117] Y. Song, L. Chen, J. Shen, P. Zhang, and Q. Gu, "Phase-shift matrices optimization in star-ris-aided physical-layer key generation," *IEEE Internet of Things Journal*, vol. 11, no. 23, pp. 38778–38789, 2024.

[118] Y. Wen, F. Wang, H.-M. Wang, J. Li, J. Qian, K. Wang, and H. Wang, "Cooperative jamming aided secure communication for ris enabled symbiotic radio systems," *IEEE Transactions on Communications*, vol. 73, no. 5, pp. 2936–2949, 2025.